CANADIAN THESES ON MICROFICHE

THÈSES CANADIENNES SUR MICROFICHE

National Library of Canada
Collections Development Branch

Canadian Theses on
Microfiche Service

Ottawa, Canada
K1A 0N4

Bibliothèque nationale du Canada
Direction du développement des collections

Service des thèses canadiennes
sur microfiche

NOTICE

The quality of this microfiche is heavily dependent upon the quality of the original thesis submitted for microfilming. Every effort has been made to ensure the highest quality of reproduction possible.

If pages are missing, contact the university which granted the degree.

Some pages may have indistinct print especially if the original pages were typed with a poor typewriter ribbon or if the university sent us an inferior photocopy.

Previously copyrighted materials (journal articles, published tests, etc.) are not filmed.

Reproduction in full or in part of this film is governed by the Canadian Copyright Act, R.S.C. 1970, c. C-30. Please read the authorization forms which accompany this thesis.

AVIS

La qualité de cette microfiche dépend grandement de la qualité de la thèse soumise au microfilmage. Nous avons tout fait pour assurer une qualité supérieure de reproduction.

S'il manque des pages, veuillez communiquer avec l'université qui a conféré le grade.

La qualité d'impression de certaines pages peut laisser à désirer, surtout si les pages originales ont été dactylographiées à l'aide d'un ruban usé ou si l'université nous a fait parvenir une photocopie de qualité inférieure.

Les documents qui font déjà l'objet d'un droit d'auteur (articles de revue, examens publiés, etc.) ne sont pas microfilmés.

La reproduction, même partielle, de ce microfilm est soumise à la Loi canadienne sur le droit d'auteur, SRC 1970, c. C-30. Veuillez prendre connaissance des formules d'autorisation qui accompagnent cette thèse.

THIS DISSERTATION
HAS BEEN MICROFILMED
EXACTLY AS RECEIVED

LA THÈSE A ÉTÉ
MICROFILMÉE TELLE QUE
NOUS L'AVONS REÇUE

NL 339 (r. 86/09)

Canada

0-315-19468-5

124

National Library of Canada
Canadian Theses Division
Ottawa, Canada
K1A 0N4

Bibliothèque nationale du Canada
Division des thèses canadiennes

67376

PERMISSION TO MICROFILM — AUTORISATION DE MICROFILMER

- Please print or type — Écrire en lettres moulées ou dactylographier

Full Name of Author — Nom complet de l'auteur

Bruce Robert Sutherland

Date of Birth — Date de naissance

April 29 1959

Country of Birth — Lieu de naissance

Canada

Permanent Address — Résidence fixe

101 Ross Glen Way SE, Medicine Hat, Alberta

Title of Thesis — Titre de la thèse

Binuclear DPM-Bridged Complexes of Iridium: Structure, Reactivity and Models for Catalysis

University — Université

University of Alberta

Degree for which thesis was presented — Grade pour lequel cette thèse fut présentée

Ph. D

Year this degree conferred — Année d'obtention de ce grade

1984

Name of Supervisor — Nom du directeur de thèse

Dr. Martin Cowie.

Permission is hereby granted to the NATIONAL LIBRARY OF CANADA to microfilm this thesis and to lend or sell copies of the film.

The author reserves other publication rights, and neither the thesis nor extensive extracts from it may be printed or otherwise reproduced without the author's written permission.

L'autorisation est, par la présente, accordée à la BIBLIOTHÈQUE NATIONALE DU CANADA de microfilmer cette thèse et de prêter ou de vendre des exemplaires du film.

L'auteur se réserve les autres droits de publication; ni la thèse ni de longs extraits de celle-ci ne doivent être imprimés ou autrement reproduits sans l'autorisation écrite de l'auteur.

Date

October 12, 1984

Signature

Bruce Sutherland

NL-91 (4/77)

THE UNIVERSITY OF ALBERTA

Binuclear DPM-Bridged Complexes of Iridium: Structure, Reactivity and Models for Catalysis

by

© Bruce Robert Sutherland

A THESIS
SUBMITTED TO THE FACULTY OF GRADUATE STUDIES AND RESEARCH
IN PARTIAL FULFILMENT OF THE REQUIREMENTS FOR THE DEGREE
OF DOCTOR OF PHILOSOPHY

DEPARTMENT OF CHEMISTRY

EDMONTON, ALBERTA
FALL, 1984

THE UNIVERSITY OF ALBERTA

RELEASE FORM

NAME OF AUTHOR Bruce Robert Sutherland

TITLE OF THESIS Binuclear DPM-Bridged Complexes of Iridium: Structure, Reactivity and Models for Catalysis

DEGREE FOR WHICH THESIS WAS PRESENTED Ph.D.

YEAR THIS DEGREE GRANTED 1984

Permission is hereby granted to THE UNIVERSITY OF ALBERTA LIBRARY to reproduce single copies of this thesis and to lend or sell such copies for private, scholarly or scientific research purposes only.

The author reserves other publication rights, and neither the thesis nor extensive extracts from it may be printed or otherwise reproduced without the author's written permission.

(Signed)..Bruce Sutherland..

PERMANENT ADDRESS:

101 Ross Glen Way SE
Medicine Hat, Alberta, Canada

Dated...October 10...1984

THE UNIVERSITY OF ALBERTA

FACULTY OF GRADUATE STUDIES AND RESEARCH

The undersigned certify that they have read, and recommend to the Faculty of Graduate Studies and Research, for acceptance, a thesis entitled Binuclear DPM-Bridged Complexes of Iridium: Structure, Reactivity and Models for Catalysis submitted by Bruce Robert Sutherland in partial fulfilment of the requirements for the degree of Doctor of Philosophy.

Martin Cowie
Supervisor

Robert B Jordan

W.A.G. Graham

R Puddephatt

George Kotovych

Murray R. Gray

Date.....October 10 1984.........

ABSTRACT

The reaction of DPM (DPM = bis(diphenylphosphino)methane = $Ph_2PCH_2PPh_2$) with $[IrCl(C_8H_{14})_2]_2$ under CO yields the binuclear complex $[Ir_2Cl(CO)_3(\mu\text{-}CO)(DPM)_2][Cl]$ from which the BF_4^- salt can readily be prepared. Carbonyl-loss from the chloro salt first yields a mixture of two isomers of $[Ir_2Cl_2(CO)_2(\mu\text{-}CO)(DPM)_2]$ and finally trans-$[IrCl(CO)(DPM)]_2$, whereas CO-loss from the BF_4^- salt gives $[Ir_2(CO)_2(\mu\text{-}Cl)(\mu\text{-}CO)(DPM_2)][BF_4]$. The dicarbonyl A-frame complex $[Ir_2(CO)_2(\mu\text{-}Cl)(DPM)_2]^+$ is obtained by the reaction of trans-$[IrCl(CO)(DPM)]_2$ with $AgBF_4$. The two isomers of $[Ir_2Cl_2(CO)_2(\mu\text{-}CO)(DPM)_2]$ rapidly interconvert in solution and co-crystallize in the solid state. An X-ray structural determination shows that the terminal chloro and carbonyl ligands are disordered.

The reactions of trans-$[IrCl(CO)(DPM)]_2$ with dimethylacetylene dicarboxylate (DMA), hexafluoro-2-butyne (HFB) and acetylene yields the complexes $[Ir_2Cl_2(CO)_2(\mu\text{-}RC_2R)(DPM)_2]$ ($R = CO_2CH_3$, CF_3, H). An X-ray structural determination of the DMA adduct shows that the alkyne bridges the metals as a cis-dimetallated olefin. Refluxing the DMA and HFB adducts in toluene results in the loss of one CO per dimer. Reaction of the DMA and HFB adducts with $AgBF_4$ produces $[Ir_2Cl(CO)_2(\mu\text{-}RC_2R)(DPM)_2][BF_4]$ ($R = CO_2CH_3$, CF_3) which are observed to

be fluxional in solution. Isomers of these latter two compounds are prepared by the reaction of DMA and HFB with $[Ir_2(CO)_2(\mu\text{-}Cl)(DPM)_2][BF_4]$. Both isomers react with CO to give $[Ir_2Cl(CO)_3(\mu\text{-}RC_2R)(DPM)_2][BF_4]$.

The reaction of trans-$[IrCl(CO)(DPM)]_2$ with H_2 yields $[Ir_2(H)_2Cl_2(CO)_2(DPM)_2]$ in which the hydride ligands are mutually cis on adjacent metals. This complex reacts with one equivalent of DMA to give $[Ir_2(H)(CH_3CO_2C{=}CHCO_2CH_3)(CO)_2(DPM)_2]$, where the alkyne has inserted into one of the Ir-H bonds. The reaction of $[Ir_2(CO)_2(\mu\text{-}Cl)(DPM)_2][BF_4]$ with H_2 initially yields $[Ir_2(H)_4Cl(CO)_2(DPM)_2][BF_4]$ which upon heating produces $[Ir_2(H)_2(CO)_2(\mu\text{-}Cl)(DPM)_2][BF_4]$. This compound reacts with an excess of DMA in CH_2Cl_2 to give $[Ir_2(CH_3CO_2C{=}CHCO_2CH_3)_2Cl_2(CO)_2(DPM)_2]$ as the major product. An X-ray structural determination shows that alkyne insertion has occurred into both Ir-H bonds.

The reaction of trans-$[IrCl(CO)(DPM)]_2$ with excess NaOH yields $[Ir_2(CO)_2(\mu\text{-}OH{\cdot}Cl)(DPM)_2]$ which upon treatment with $HBF_4{\cdot}Et_2O$ gives $[Ir_2(CO)_2(\mu\text{-}OH)(DPM)_2][BF_4]$. An X-ray structural determination was done on the former. Reaction of the former product with CO produces the binuclear Ir(0) complex $[Ir_2(CO)_4(DPM)_2]$ which after flushing with N_2 yields $[Ir_2(CO)_2(\mu\text{-}CO)(DPM)_2]$. Reaction of $[Ir_2(CO)_2(\mu\text{-}OH)(DPM)_2][BF_4]$ with CO produces $[Ir_2(CO)_2(\mu\text{-}H)(\mu\text{-}CO)(DPM)_2][BF_4]$. This latter complex reacts with $HBF_4{\cdot}Et_2O$ to give $[Ir_2(H)(CO)_2(\mu\text{-}H)(\mu\text{-}CO)(DPM)_2][BF_4]$ which rearranges with time yielding the isomeric complex $[Ir_2(H)_2(CO)_3(DPM)_2][BF_4]_2$. Reaction of either of these dihydrides with CO produces $[Ir_2(CO)_4(\mu\text{-}H)_2(DPM)_2][BF_4]_2$ and $[Ir_2(CO)_4(\mu\text{-}CO)(DPM)_2][BF_4]_2$ in the ratio 9:1, the latter product resulting from reductive elimination of H_2. Refluxing $[Ir_2(H)_2(CO)_3(DPM)_2][BF_4]_2$ in CH_3CN also produces some H_2 elimination and the formation of $[Ir_2(CO)_2(CH_3CN)_2(\mu\text{-}CO)(DPM)_2][BF_4]_2$. Reaction of $[Ir_2(CO)_4(\mu\text{-}CO)(DPM)_2][BF_4]_2$ with OH^- yields $[Ir_2(CO)_2(\mu\text{-}H)(\mu\text{-}CO)(DPM)_2][BF_4]$ whereas reaction of $[Ir_2(CO)_2(CH_3CN)_2(\mu\text{-}CO)(DPM)_2][BF_4]_2$ with OH^- gives a mixture of this hydride and the bridging hydroxide complex $[Ir_2(CO)_2(\mu\text{-}OH)(DPM)_2][BF_4]$.

The reaction of trans-$[IrCl(CO)(DPM)]_2$ with $NaBH_4$ under a H_2 atmosphere yields the hydride complex, $[Ir(H)_4(CO)_2(DPM)_2]$. Addition of acid to this complex under H_2 produces the pentahydride $[Ir_2(H)_3(CO)_2(\mu\text{-}H)_2(DPM)_2][X]$ ($X = BF_4^-$, Cl^-, OMe^-). In solution this species loses a proton to give $[Ir_2(H)_2(CO)_2(\mu\text{-}H)_2(DPM)_2]$. If the addition of acid is performed under an N_2 atmosphere, the trihydride $[Ir_2(H)(CO)_2(\mu\text{-}H)_2(DPM)_2][X]$ is isolated. An X-ray structural determination was performed on the chloride salt. The addition of $HBF_4{\cdot}Et_2O$ to this trihydride yields the complex $[Ir_2(H)_2(CO)_2(\mu\text{-}H)_2(DPM)_2][BF_4]_2$.

ACKNOWLEDGEMENTS

I wish to express my gratitude and appreciation to the following people:

Professor Martin Cowie for his expert guidance and assistance during the course of this work.

Dr. R.G. Ball for collecting the data sets for the compounds described in Chapter 2, 5 and 6.

My family and friends for their support.

The University of Alberta and the National Sciences and Engineering Research Council for financial support.

Jacki Jorgensen for her expert preparation of this manuscript.

TABLE OF CONTENTS

Chapter 1..1

- Introduction.....................................1

Chapter 2..11

- The Preparation and Characterization of Some Binuclear DPM-Bridged Complexes of Iridium and the Structure of One Product, $[Ir_2Cl_2(CO)_2(\mu\text{-}CO)(Ph_2PCH_2PPh_2)_2]\cdot 3C_4H_8O$........11
- Introduction.....................................11
- Experimental Section.............................12
- Preparation of Compounds.........................14
- X-ray Data Collection............................20
- Solution Structure and Refinement................23
- Discussion.......................................30
- Description of Structure.........................45
- Conclusions......................................53

Chapter 3..54

- Neutral and Cationic Alkyne-Bridged Complexes of Iridium and the Structure of $[Ir_2Cl_2(CO)_2(\mu\text{-}CH_3O_2CC_2CO_2CH_3)(Ph_2PCH_2PPh_2)_2]$..............54
- Introduction.....................................54
- Experimental Section.............................56
- Preparation of Compounds.........................56
- Attempted Reactions..............................65
- X-ray Data Collection............................67

Structure Solution and Refinement....................70

Discussion of Results....................83

Conclusions....................97

Chapter 4....................100

Binuclear DPM-Bridged Complexes of Iridium as Models for the Catalytic Hydrogenation of Alkynes in the Presence of Two Metal Centres. The Structure of $[Ir_2(CH_3CO_2C{=}CHCO_2CH_3)_2Cl_2(CO)_2(DPM)_2]$........100

Introduction....................100

Experimental Section....................102

Preparation of Compounds....................102

X-ray Data Collection....................107

Structure Solution and Refinement....................109

Description of Structure....................116

Discussion of Results....................123

Conclusions....................134

Chapter 5....................137

Hydroxy and Hydrido-Bridged Binuclear Complexes of Iridium as Models for Water-Gas Shift Catalysts and the Structure of One Model Catalyst Precursor, $[Ir_2(CO)_2(\mu\text{-}OH\cdot Cl)(Ph_2PCH_2PPh_2)_2]$...137

Introduction....................137

Experimental Section....................140

Preparation of Compounds....................141

X-ray Data Collection....................152

Structure Solution and Refinement................155

Description of Structure..........................161

Results and Discussion............................167

Chapter 6..193

The Preparation and Characterization of Some DPM-Bridged Iridium Polyhydride Complexes and the Structure of $[Ir_2(H)(CO)_2(\mu\text{-}H)_2(DPM)_2]$-$[Cl]\cdot 1.2CH_2Cl_2$..............................193

Introduction.......................................193

Preparation of Compounds..........................194

X-ray Data Collection..............................201

Structure Solution and Refinement................204

Description of Structure..........................206

Results and Discussion............................216

Summary..226

Chapter 7..229

Conclusions.......................................229

References and Footnotes..........................233

Appendix I..253

LIST OF TABLES

Table 1 Acid Dissociation Constants of Some Transition Metal Hydrides....................................4

Table 2 Spectral Data for the Compounds of Chapter 2...19

Table 3 Summary of Crystal Data and Details of Intensity Collection for $[Ir_2Cl_2(CO)_2(\mu\text{-}CO)\text{-}(DPM)_2]\cdot 3C_4H_8O$....................................22

Table 4 Positional and Thermal Parameters for the Non-Group Atoms of $[Ir_2Cl_2(CO)_3(DPM)_2]\cdot 3C_4H_8O$.......27

Table 5 Derived Parameters for the Rigid Groups of $[Ir_2Cl_2(CO)_3(DPM)_2]\cdot 3C_4H_8O$....................29

Table 6 Derived Hydrogen Positions and Thermal Parameters of $[Ir_2Cl_2(CO)_3(DPM)_2]$.............30

Table 7 Selected Interatomic Distances (Å) in $[Ir_2Cl_2(CO)_3(DPM)_2]\cdot 3C_4H_8O$....................48

Table 8 Selected Angles (Deg) in $[Ir_2Cl_2(CO)_3\text{-}(DPM)_2]\cdot 3C_4H_8O$....................................49

Table 9 Infrared Stretching Frequencies for the Compounds of Chapter Three....................58

Table 10 NMR Spectral Results for the Compound of Chapter Three....................................59

Table 11 Summary of Crystal Data and Intensity Collection Details for $[Ir_2Cl_2(CO)_2(\mu\text{-}DMA)\text{-}(DPM)_2]\cdot 2CH_2Cl_2$....................................69

Table 12 Positional and Anisotropic Thermal Parameters for the Non-group Atoms of $[Ir_2Cl_2(CO)_2(\mu\text{-DMA})(DPM)_2]\cdot 2CH_2Cl_2$.............73

Table 13 Derived Parameters for the Rigid-Group Atoms of $[Ir_2Cl_2(CO)_2(\mu\text{-DMA})(DPM)_2]\cdot 2CH_2Cl_2$..........74

Table 14 Derived Hydrogen Positions for $[Ir_2Cl_2(CO)_2(\mu\text{-DMA})(DPM)_2]\cdot 2CH_2Cl_2$.............75

Table 15 Selected Distances (Å) in $[Ir_2Cl_2(CO)_2(\mu\text{-DMA})(DPM)_2]\cdot 2CH_2Cl_2$..............................78

Table 16 Selected Angles (Deg) in $[Ir_2Cl_2(CO)_2(\mu\text{-DMA})(DPM)_2]\cdot 2CH_2Cl_2$.............79

Table 17 Spectral Data for the Compound of Chapter Four.......................................106

Table 18 Summary of Crystal Data and Details of Intensity Collection for $[Ir_2(CH_3CO_2C{=}CHCO_2CH_3)_2Cl_2(CO)_2(DPM)_2]$........109

Table 19 Positional and Thermal Parameters for the Non-group Atoms of $[Ir_2(CH_3CO_2C{=}CHCO_2CH_3)_2Cl_2(CO)_2(DPM)_2]$........112

Table 20 Derived Parameters for the Rigid-Group Atoms of $[Ir_2(CH_3CO_2C{=}CHCO_2CH_3)_2Cl_2(CO)_2(DPM)_2]$.....115

Table 21 Derived Hydrogen Positions for $[Ir_2(CH_3CO_2C{=}CHCO_2CH_3)_2Cl_2(CO)_2(DPM)_2]$........116

Table 22 Selected Distances (Å) in $[Ir_2(CH_3CO_2C{=}CHCO_2CH_3)_2Cl_2(CO)_2(DPM)_2]$........117

Table 23 Selected Angles (Deg) in $[Ir_2(CH_3CO_2C{=}CHCO_2CH_3)_2Cl_2(CO)_2(DPM)_2]$........118

Table 24 Infrared Spectral Data for the Compounds of Chapter Five................................148

Table 25 NMR Spectral Data for the Compounds of Chapter Five..................................149

Table 26 Summary of Crystal Data and Details of Intensity Collection for $[Ir_2(CO)_2(\mu\text{-}OH{\cdot}Cl)(DPM)_2]$.....................153

Table 27 Positional and Thermal Parameters for the Non-group Atoms of $[Ir_2(CO)_2(\mu\text{-}OH{\cdot}Cl)(DPM)_2]$..157

Table 28 Derived Parameters for the Rigid Groups of $[Ir_2(OH{\cdot}Cl)(CO)_2(DPM)_2]$.......................159

Table 29 Derived Hydrogen Positions for $[Ir_2(CO)_2(\mu\text{-}OH{\cdot}Cl)(DPM)_2]$.....................160

Table 30 Selected Distances (Å) in $[Ir_2(CO)_2(\mu\text{-}OH{\cdot}Cl)(DPM)_2]$.....................162

Table 31 Selected Angles (deg) in $[Ir_2(CO)_2(\mu\text{-}OH{\cdot}Cl)(DPM)_2]$.....................163

Table 32 Spectral Data for the Compound of Chapter Six.......................................199

Table 33 Summary of Crystal Data and Details of Intensity Collection for $[Ir_2(H)(CO)_2(\mu\text{-}H)_2(DPM)_2][Cl]{\cdot}1.2CH_2Cl_2$.......203

Table 34 Positional and Thermal Parameters of the Nongroup Atoms of $[Ir_2(H)(CO)_2(\mu\text{-}H)_2(DPM)_2]$-$[Cl]\cdot1.2CH_2Cl_2$....206

Table 35 Derived Parameters for the Rigid Groups of $[Ir_2(H)(CO)_2(\mu\text{-}H)(DPM)_2][Cl]$....208

Table 36 Derived Hydrogen Positions for $[Ir_2(H)(CO)_2(\mu\text{-}H)_2(DPM)_2][Cl]\cdot1.2CH_2Cl_2$....209

Table 37 Selected Distances (Å) in $[Ir_2(H)(CO)_2(\mu\text{-}H)_2(DPM)_2][Cl]$....210

Table 38 Selected Angles (deg) in $[Ir_2(H)(CO)_2(\mu\text{-}H)_2(DPM)_2][Cl]$....211

LIST OF FIGURES

Figure 1 $^{31}P\{^1H\}$ NMR spectrum of $[Ir_2Cl(CO)_3(\mu\text{-}CO)(DPM)_2][Cl]$ (**1a**) obtained at 36.4 MHz.........31

Figure 2 Perspective View of Isomer **2a**, $[Ir_2Cl_2(CO)_2(\mu\text{-}CO)(DPM)_2]$ (25% abundance)................46

Figure 3 Perspective View of the 75% Isomer **2b**, $[Ir_2Cl_2(CO)_2(\mu\text{-}CO)(DPM)_2]$....................47

Figure 4 Perspective view of $[Ir_2Cl_2(CO)_2(\mu\text{-}DMA)(DPM)_2]$, showing the numbering scheme.........76

Figure 5 Representation of the inner coordination sphere of the complex in the approximate plane of the metal atoms and the alkyne molecules.................................77

Figure 6 $^{31}P\{^1H\}$ NMR spectra of $[Ir_2Cl(CO)_3(\mu\text{-}DMA)(DPM)_2][BF_4]$ as a function of temperature.....92

Figure 7 Perspective view of **21**, $[Ir_2(CH_3CO_2C{=}CHCO_2CH_3)_2Cl_2(CO)_2(DPM)_2]$ (Dimer A)................................119

Figure 8 Representation of the inner coordination sphere of the complex in the plane of the metal atoms and metallated olefin ligands....120

Figure 9 Perspective view of $[Ir_2(CO)_2(\mu\text{-}OH\cdot Cl)(DPM)_2]$ showing the numbering scheme................165

Figure 10 The inner coordination sphere of the title complex along with some relevant bond lengths and angles....................................166

Figure 11 Perspective view of $[Ir_2H(CO)_2(\mu\text{-}H)_2(DPM)_2]$-[Cl]....................................213

List of Abbreviations and Symbols

Chemical Abbreviations and Symbols

av	average
ca.	approximately
CNMe	methyl isocyanide
DMA	dimethylacetylene dicarboxylate
DPM	bis(diphenylphosphino)methane
Et	ethyl
h	hour
HFB	hexafluoro-2-butyne
I.R.	infrared
Me	methyl
MeCN, CH_3CN	acetonitrile
min	minutes
NMR	nuclear magnetic resonance
Ph	phenyl
PPh_3	triphenylphosphine
ppm	parts per million
^{t}Bu	tertiary butyl
sec	seconds
THF	tetrahydrofuran

Crystallographic Abbreviations and Symbols

a,b,c	respective lengths of x, y and z axes of the unit cell
B	isotropic thermal parameter
F_c	calculated structure factor
F_o	observed structure factor
p	ignorance factor, accounting for equipment inaccuracies in intensity measurement
R	agreement index
R_w	weighted agreement index
U_{ij}	anisotropic thermal parameter
w	weighting factor applied to structure factor
Z	number of fomula weights per unit cell
Å	Angstrom units, 10^{-10} m
° or deg	degrees
α	angle between b and c of unit cell
β	angle between a and c of unit cell
γ	angle between a and b of unit cell
2θ	diffraction angle, related to Bragg's Law $n\lambda = 2d\sin\theta$
σ	standard deviation
ω	the angle between the incident beam and the diffracting plane, $\omega = \theta$

CHAPTER 1

Introduction

Transition metal hydrides, defined as complexes in which a hydrogen atom is bound to one or more transition metals, are among the most extensively studied groups of compounds in inorganic chemistry[1,2] and have been shown to play an important role in many stoichiometric and catalytic reactions.[3] Historically, the nature of the metal-hydrogen interaction has been a controversial subject. In 1939, Ewens and Lister carried out electron diffraction studies on gaseous $HCo(CO)_4$ and $H_2Fe(CO)_4$ and concluded that the metal atoms were surrounded by a tetrahedron of carbonyl groups.[4] They concluded that the hydrogen atoms exerted no stereochemical influence and were likely attached to the oxygen atoms of the carbonyl groups. Later, Hieber proposed that the hydrogen atoms were buried in the metal orbitals making FeH_2 and CoH into pseudo nickel atoms.[5] This idea was further promoted by the very large upfield shifts observed in the ^1H NMR spectrum of $HCo(CO)_4$.[6] An LCAO calculation performed by Cotton in 1958, which suggested that the Co-H bond distance was no longer than 1.2 Å, provided additional support for this view.[7] In the period 1939-59, transition metal hydride complexes were studied using I.R., N.M.R. and electron diffraction techniques with the general conclusion being that the H atom exerted no stereochemical influence and lay buried in the electronic core of the metal atom. This view changed with the first X-ray diffraction studies of hydrides and in particular with the structure of $HRh(CO)(PPh_3)_3$ by LaPlaca and Ibers in 1963.[8] In this structure the hydride was located and observed to occupy a normal coordination site with a bond length of 1.72(15) Å, implying normal covalent bonding between the hydrogen atom and the metal.

As this and the many X-ray and neutron diffraction studies done since confirm,[9] a terminal metal-hydride bond is best considered as a simple two electron covalent bond. However, when the hydride interacts with two or more metals the bonding picture is not so clear. For example, in complexes which contain a M-H-M unit, it has been found in all cases that the M-H-M framework is nonlinear and that the two metals are close enough to have significant interaction.[9] This type of bonding is best described as a 3-centre 2-electron bond as proposed by Mason and Mingos.[10] The orbital combinations as shown below, using the d_{z^2} orbitals of the metals and the 1s of the hydrogen atom, are reminiscent of those used to explain the B-H-B bridged bonding in B_2H_6. This type of scheme explains both the bent framework and the significant metal-metal interaction.

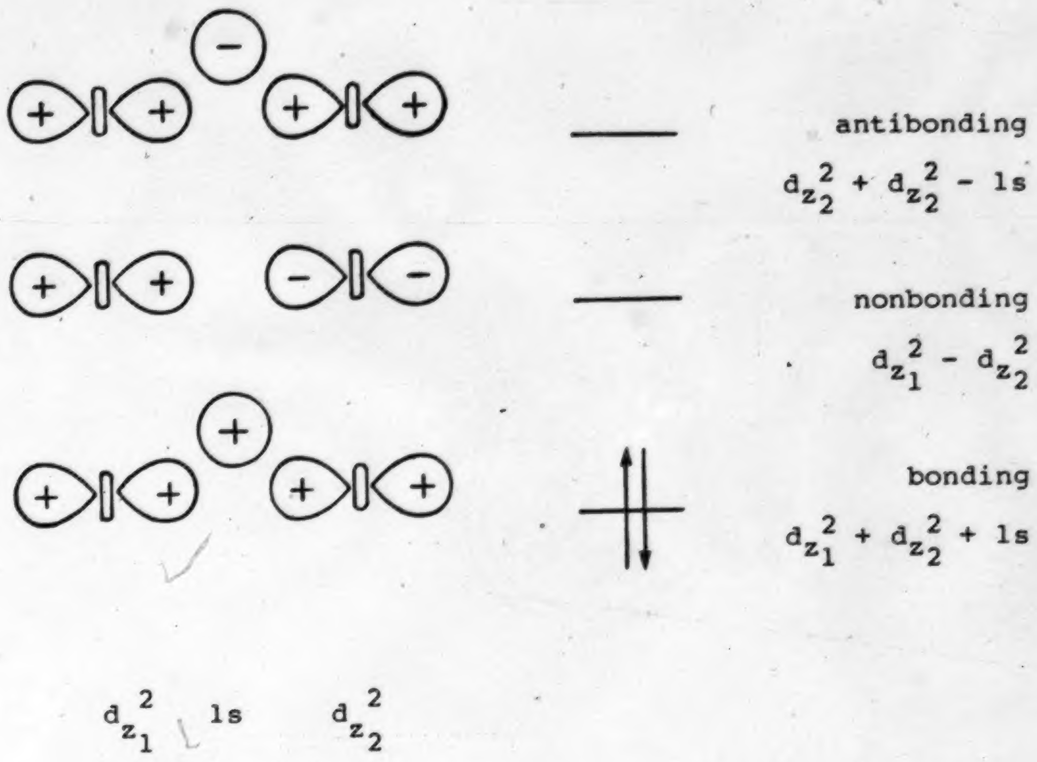
antibonding
$d_{z_2}^2 + d_{z_2}^2 - 1s$
nonbonding
$d_{z_1}^2 - d_{z_2}^2$
bonding
$d_{z_1}^2 + d_{z_2}^2 + 1s$
$d_{z_1}^2$
1s
$d_{z_2}^2$

The term hydride is actually a misnomer since a wide range of metal-hydrogen bond polarities is observed throughout the transition series, ranging from the hydridic nature of Cp_2ZrHCl [11] to the strongly acidic nature of $HCo(CO)_4$.[12] As the following table demonstrates, changing the metal and/or the ligands can have a significant effect on the acidity of the metal hydride.

Table 1. Acid Dissociation Constants of Some Transition Metal Hydrides.[13]

Complex	K_a (H_2O)
$HCo(CO)_4$	<2
$HCo(CO)_3PPh_3$	1.1×10^{-7}
$HMn(CO)_5$	8×10^{-8}
$HRe(CO)_5$	very weak acid
$H_2Fe(CO)_4$	3.6×10^{-5} (K_1)
	1×10^{-14} (K_2)

As mentioned previously, transition metal hydrides play an important role in many homogeneous catalytic reactions. The most widely studied and perhaps best known of these is the hydrogenation of olefins. In order to demonstrate why catalysts are needed, it is useful to first consider the uncatalyzed addition of hydrogen to an olefin. This process could theoretically occur by either of the two paths shown below. The first, a concerted process, is forbidden by Woodward-Hoffman[14] orbital symmetry rules and thus has a high activation barrier, while the second, a stepwise process, is also highly unfavoured because it involves the formation of hydrogen

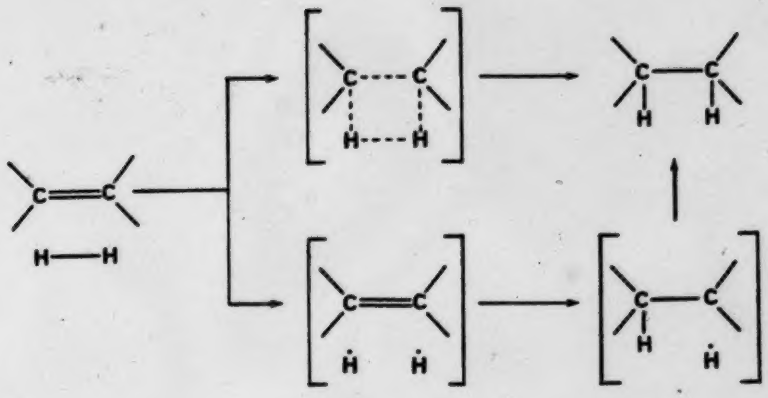

atoms, a high energy process. Thus the role of the catalyst is to accomplish the transfer of hydrogen to the olefin by a relatively low energy pathway. To see how a transition metal hydride can accomplish the task, it is instructive to look at an actual example, the hydrogenation of olefins by Wilkinson's catalyst, $RhCl(PPh_3)_3$. The mechanism of this reaction has been studied in depth and the basic steps involved are representative of those proposed for most other hydrogenation catalysts.[3,15-19]

The first step is believed to involve phosphine dissociation from the trisphosphine complex to give a highly reactive intermediate, which rapidly oxidatively adds a molecule of hydrogen to give a bisphosphine dihydride complex (see below). Since this dihydrido intermediate is a coordinatively unsaturated 16e species, an olefin can coordinate to it and subsequently insert into a metal-hydrogen bond yielding an alkyl hydride complex.

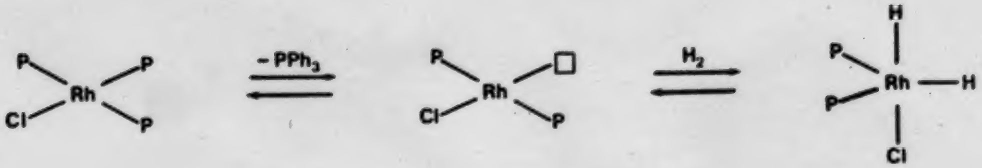
P
P
Cl
Rh
P
- PPh$_3$
P
Rh
Cl
P
H$_2$
H
P
Rh
H
P
Cl

P = PPh$_3$

Rapid reductive elimination follows yielding an alkane and the parent unsaturated bisphosphine species. Addition of hydrogen to this latter species reinitiates the process as shown below.

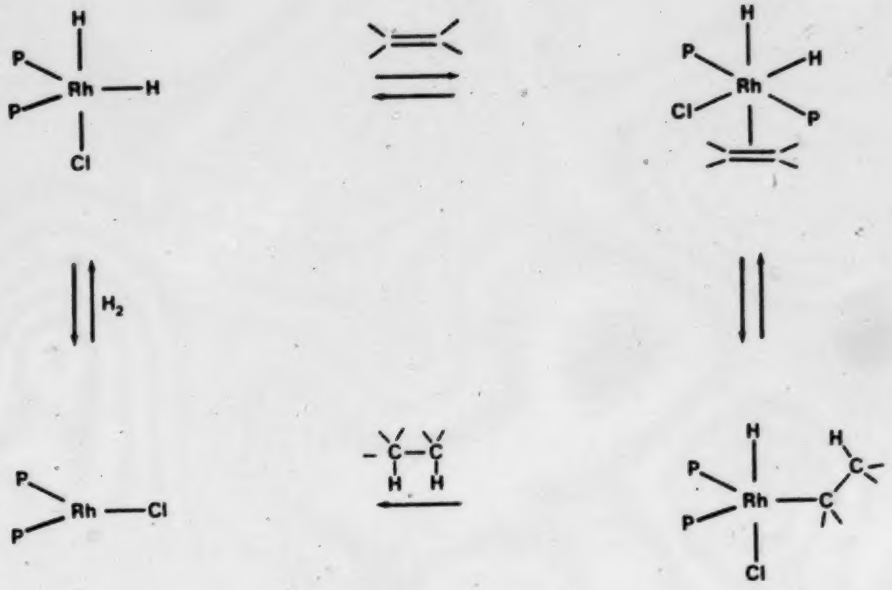
H
P
Rh
H
P
Cl
H
P
Rh
H
Cl
P
H$_2$
P
Rh
Cl
P
H H
H
P
Rh
C
H
C
P
Cl

Another hydrogenation catalyst, HRh(CO)(PPh$_3$)$_3$,[20-23] operates by a similar mechanism but with the significant difference that hydrogen addition is not the first step in the catalytic cycle. As the scheme below shows, transition metal hydrides can act as catalyst precursors owing to the presence of chemically active H ligand.

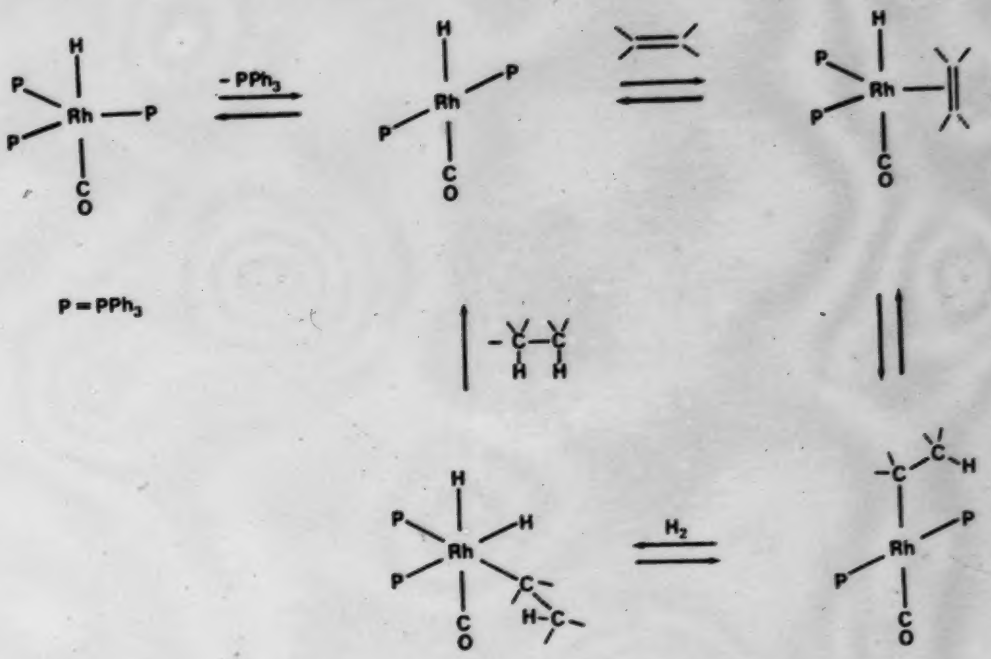

It can be seen from these examples that the net transfer of hydrogen to the unsaturated olefin is based on the ability of the metal to cleave the H-H bond with the simultaneous formation of two M-H bonds and to subsequently coordinate the olefin such that transfer of the hydrogen atoms from the metal to the olefin can occur. One point relevant to this latter step is that the metal-hydrogen bonds must not be too strong or no transfer of hydrogen to the olefin will take place. Another prerequisite for the reaction is that the unsaturated molecule, in this case the olefin, be able to coordinate to the catalyst. This is an important step and often determines which substrates can successfully be hydrogenated.[19]

The use of hydrides in catalytic systems is not limited to olefin hydrogenation. Other reactions catalyzed by transition metal hydrides include olefin isomerization,[23] hydroformylation[24] and the water gas shift reaction.[25]

Although the preceding examples dealt with complexes containing only one metal atom, this is not a fundamental requirement of catalytic systems. On the contrary, there has been increasing interest of late in the corresponding chemistry of polynuclear transition metal complexes.[26-28] In principle, polynuclear complexes have the added feature that more than one metal atom can interact with the incoming substrate molecule. This can result in new bonding modes not available in mononuclear chemistry and in increased activation of the substrate towards further reaction. Furthermore, polynuclear species also have the capability of redistributing their ligands by allowing them to migrate from one centre to another, creating a vacant coordination site for either an incoming ligand or one that is already coordinated.[29] In contrast, as was pointed out in the previous examples, ligand dissociation is often required for the generation of an open site in mononuclear species. This latter process depends highly on the nature of the ligands and is not always feasible.

One of the major problems encountered in studying polynuclear systems is their tendency to fragment into mononuclear species under the conditions employed.[30] One of the ways currently employed to circumvent this problem is the use of multidentate bridging ligands which hold the metals in close proximity throughout the course of the reaction but are still flexible enough to allow for the breaking and formation of bonds between the metals.[31,32] One such ligand which fulfills these requirements is bis(diphenylphosphino)methane (DPM). This ligand has displayed the ability to form a large variety of stable binuclear complexes with group VIII metals and is flexible enough to allow wide range of metal-metal separations to occur.[33] Two particular DPM-bridged complexes of Rh are shown below. Of relevance to this thesis is the fact that both complexes have been reported to act as acetylene hydrogenation catalysts under mild conditions and II was also shown to be a catalyst for the water gas shift reaction.[34,35] In none of these reactions was information available concerning the nature of the intermediates involved. For example, although I acts as a hydrogenation catalyst, no evidence for any hydride or alkyl species was observed. It is important to understand the mechanisms involved with these reactions in order to determine what

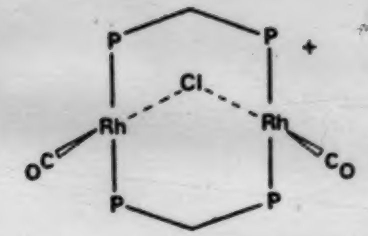

I

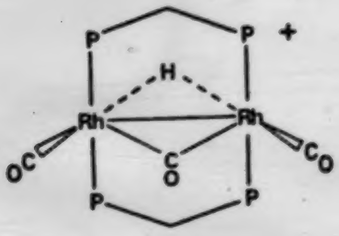

II

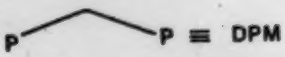

effect, if any, the presence of the second metal centre has on the observed chemistry, and in particular on the catalytic reactions of interest. One way of finding out more about unstable intermediates is to examine model complexes which resemble these intermediate but are stable and more readily characterized. Owing to the generally greater stability of iridium hydrides and alkyls compared to rhodium, binuclear Ir-DPM complexes should function as useful models for probing the observed Rh chemistry.

With the above ideas in mind, the aim of the studies described in these thesis are two fold: 1) to prepare binuclear DPM-bridged compounds analogous to those known for Rh and 2) to examine these compounds as potential model systems for the Rh chemistry, particularly examining what role binuclear DPM hydrides play in catalysis.

CHAPTER 2

THE PREPARATION AND CHARACTERIZATION OF SOME BINUCLEAR DPM-BRIDGED COMPLEXES OF IRIDIUM AND THE STRUCTURE OF ONE PRODUCT, $[Ir_2Cl_2(CO)_2(\mu\text{-}CO)(Ph_2PCH_2PPh_2)_2]\cdot 3C_4H_8O$.

Introduction

There is considerable current interest in multinuclear metal complexes and in their reactions with small molecules, especially with regards to their potential catalytic activity and their relationship to reactions at metal surfaces.[26,36] The prototype multinuclear system is the binuclear one in which the two metals are in close proximity to one another. In such systems it is common to use bridging groups to hold the metals together in order to maintain the integrity of the complex during the course of reactions. One class of binuclear compounds which has been shown to display a rather diverse chemistry utilizes bidentate ligands, such as bis(diphenylphosphino) methane (DPM) or related groups, to bind the two metals. Binuclear complexes bridged by such groups have been extensively studied for rhodium,[34,35,37-73] palladium[74-93] and platinum[94-138] and more recently for mixed metal systems involving one or more of these metals.[139-149]

A major area of research in this group has centred on the reaction of small molecules with binuclear Rh-DPM complexes.[24,48,60-69] It was decided to extend this work to include analogous complexes of iridium with the intention of isolating and characterizing iridium complexes which bore a strong resemblance to potential intermediates in the rhodium chemistry and by so doing, obtain information about these labile rhodium intermediates. In order to fully develop this chemistry, it was necessary to prepare some useful iridium carbonyl precursors since very little work had been done with iridium at the time this study was begun.[41,150,151] Very early in this study it became apparent that significant differences existed between the related rhodium and iridium carbonyl complexes. This chapter describes the preparation of these Ir starting complexes and provides a comparison between them and their Rh analogues.

Experimental Section

All solvents were appropriately dried and distilled prior to use and were stored under dinitrogen (See Appendix 1). Reactions were performed under standard Schlenk conditions (using dinitrogen which had previously been passed through columns containing Ridox and 4 A molecular sieves to remove traces of oxygen and water, respectively). Hydrated iridium (III) chloride was obtained from Johnson-Matthey and bis(diphenylphosphino) methane (DPM) was purchased from Strem Chemicals. Carbon monoxide was obtained from Matheson and used as received. $[IrCl(C_8H_{14})_2]_2$ was prepared by the reported procedure.[152] Variable temperature $^{31}P\{^1H\}$ NMR spectra were run on a Bruker HFX-90 spectrometer with Fourier transform capability operating at 36.43 MHz; the temperature was measured with a thermocouple inserted directly into the probe. NMR spectra were measured using an external d_6-acetone lock and chemical shifts are referenced to 85% H_3PO_4. ^1H NMR spectra were run on a Bruker WH-200 or WH-400 spectrometer at room temperature unless otherwise stated. Infrared spectra were run on a Nicolet 7199 Fourier Transform interferometer either as solids in Nujol mulls on KBr plates or as solutions in NaCl cells with 0.5 mm window pathlengths. Analyses were performed within the department or by Canadian Microanalytical Service Ltd., Vancouver. Conductivity measurements were performed with a Yellow Springs Instrument Model 31 using 1×10^{-3} M solutions in CH_2Cl_2.

Preparation of Compounds

a) $[Ir_2Cl(CO)_3(\mu\text{-}CO)(DPM)_2][Cl]$ (**1a**).

Bis(diphenylphosphino) methane (171.1 mg, 0.445 mmol) was dissolved in 2 mL of CH_2Cl_2 under a slow stream of carbon monoxide. A solution of $[IrCl(C_8H_{14})_2]_2$ (200.0 mg 0.222 mmol) in 10 mL of CH_2Cl_2 was then added dropwise from a syringe while the solution was rapidly stirred. The solution initially turned black but over a period of five minutes changed to red-orange and then to red, after which time the carbon monoxide flow was shut off and the solution allowed to stir under the CO atmosphere for an additional 15 min. During this time the colour changed to pale yellow. The addition of 30 mL of diethyl ether, saturated with carbon monoxide, to the solution resulted in the precipitation of a pale yellow solid which was collected and dried under a slow stream of CO. If THF was used as the solvent instead of CH_2Cl_2, the precipitate appeared after approximately 30 min without the addition of the ether. Compound 1 was determined to be a 1:1 electrolyte in CH_2Cl_2 solutions ($\Lambda(10^{-3}\ M) = 38.6\ \Omega^{-1}\ cm^2\ mole^{-1}$).[168] Typical isolated yields were 90-95%. Spectroscopic parameters for this and all subsequent products are given in Table 2.

Anal. Calcd for $Ir_2Cl_2P_4O_4C_{54}H_{44}$: C, 48.54%; H, 3.32%; Cl, 5.31%. Found: C, 48.83%; H, 3.18%; Cl, 5.37%.

b) $[Ir_2Cl_2(CO)_2(\mu\text{-}CO)(DPM)_2]$ (**2**).

A CH_2Cl_2 solution of $[Ir_2Cl(CO)_3(\mu\text{-}CO)(DPM)_2][Cl]$ was refluxed under a slow stream of N_2 until the colour changed from light yellow to dark orange (approximately 20 min). The addition of 30 mL of degassed diethyl ether to the solution, after it had been allowed to cool to room temperature, resulted in the precipitation of a bright yellow microcrystalline product. The solid was collected and dried initially under a slow N_2 stream and finally by storing the sample under a slight vacuum for several hours. Recrystallization from a mixture of warm THF and diethyl ether yielded golden yellow crystals which contained both the cis and trans isomers (vide infra); attempts to separate the two by fractional crystallization and chromatography proved unsuccessful. Conductivity measurements on a CH_2Cl_2 solution of the crystalline material indicated the mixture was non-conducting ($\Lambda(10^{-3}$ M) = 2.2 Ω^{-1} cm^2 mole^{-1}). Typical combined yields of both isomers were 90-95%.

Anal. Calcd for $Ir_2Cl_2P_4O_3C_{53}H_{44}$: C, 48.66%; H, 3.39%; Cl, 5.42%. Found: C, 49.22%; H, 4.39%; Cl, 5.62%.

c) trans-$[IrCl(CO)(DPM)]_2$ (**3**).

Method A: $[Ir_2Cl_2(CO)_2(\mu\text{-}CO)(DPM)_2]$ (200 mg, 0.153 mmol) was dissolved in 20 mL of THF and refluxed while a slow stream of dinitrogen was bubbled through the solution. The solution was heated for 1.5 h during which time the colour changed from orange to dark red-purple. A red-purple solid precipitated after approximately 1 h. 10 mL of degassed diethyl ether was added to ensure complete precipitation and the solution was cooled for 20 min in an icebath. The pale yellow mother liquor was removed, the solid collected and washed with several portions of ice-cold THF and then dried in vacuo for 2 h. A CH_2Cl_2 solution of the red-purple solid showed that it was a non-electrolyte ($\Lambda(10^{-3}$ M) = 3.1 Ω^{-1} cm^2 $mole^{-1}$). Typical yields were 80-85%.

Anal. Calcd for $Ir_2Cl_2P_4O_2C_{52}H_{44}$: C, 48.79%; H, 3.46%; Cl, 5.54%. Found: C, 48.51%; H, 3.40%; Cl, 5.53%.

Method B: If toluene was used instead of THF and the refluxing continued for 6 h, a maroon microcrystalline solid precipitated. This solid was collected, washed with diethyl ether and dried in vacuo. Typical yields were 90 to 95%. In its spectroscopic properties and subsequent reactions with small molecules this product proved to be identical to the red-purple solid isolated in Method A. Preliminary X-ray photographs indicated that this species crystallized in the space group $P2_1/n$; a = 11.05 Å, b = 13.85 Å, c = 18.50 Å, β = 93.16°. This unit cell volume of 2827.0 $Å^3$ and the measured density of 1.658 g/cm^3

corresponded to approximately Z = 2 and therefore suggested that the molecule had crystallographic $\bar{1}$ symmetry.

Anal. Calcd for $Ir_2Cl_2P_4O_2C_{52}H_{44}$: C, 48.79%; H, 3.46%; Cl, 5.54%. Found: C, 49.45%; H, 3.44%; Cl, 5.57%.

d) $[Ir_2(CO)_2(\mu\text{-}Cl)(\mu\text{-}CO)(DPM)_2][BF_4]$ (**4b**).

Method A: $[Ir_2Cl(CO)_3(\mu\text{-}CO)(DPM)_2][BF_4]$ (**1b**) was prepared and isolated according to literature procedure[41] using $NaBF_4$ instead of $NaBPh_4$. 200 mg (0.144 mmol) was then dissolved in 20 mL of CH_2Cl_2 under an N_2 atmosphere. The solution was refluxed for 45 min under a slow N_2 stream during which time the colour changed from pale yellow to orange-yellow to golden-orange. After cooling the solution to room temperature, 30 mL of degassed diethyl ether was added to the solution resulting in the precipitation of a golden-orange solid. This solid was identical in all spectral and physical properties to that previously reported for the compound. Typical yields were 90-95%.

Method B: 200 mg (0.153 mmol) of $[Ir_2Cl_2(CO)_2\text{-}(\mu\text{-}CO)(DPM)_2]$ was dissolved in 10 mL of THF. To this solution was added a solution of 29.8 mg (0.153 mmol) of $AgBF_4$ in 2 mL THF. The colour immediately changed to golden-orange and a precipitate slowly appeared. This solution was stirred for 1 h, afer which time 30 mL of degassed diethyl ether was added to complete the precipitation. The solid was collected and dried under a stream of N_2. The golden-orange product was then redissolved in CH_2Cl_2, filtered under N_2, reprecipitated by adding diethyl ether, and then collected and dried *in vacuo* for several hours. The product was identical in all spectroscopic properties to that obtained for the product from method A.

e) $[Ir_2(CO)_2(\mu\text{-}Cl)(DPM)_2][BF_4]$ (**5b**).

$[IrCl(CO)(DPM)]_2$(200 mg 0.156 mmol) was suspended in 10 mL of THF. To this slurry a solution of $AgBF_4$ (28.6 mg, 0.156 mmol) in 2 mL of THF was added. The colour immediately changed to dark red and after stirring for 30 min, a coral-orange precipitate appeared. Addition of 30 mL of diethyl ether caused complete precipitation. After removing the solvent and drying the solid under an N_2 stream, the product was redissolved in 10 mL of CH_2Cl_2, filtered under dinitrogen and reprecipitated by the addition of diethyl ether to give a dark red solid. Compound **5** was determined to be a 1:1 electrolyte in CH_2Cl_2 solutions ($\Lambda(10^{-3}\ M) = 47.2\ \Omega^{-1}\ cm^2\ mole^{-1}$). Typical yields were 90 to 95%.

Anal. Calcd for $Ir_2ClP_4F_4O_2C_{52}BH_{44}$: C, 46.91%; H, 3.53%; Cl, 2.82%. Found: C, 46.27%; H, 3.42%; Cl, 2.63%.

Table 2. Spectral Data for the Compounds of Chapter 2.

Compound	Infrared ν(CO), cm^{-1} solid[a]	Infrared ν(CO), cm^{-1} solution[b]	$^{31}P\{^1H\}$NMR δ, ppm[c]	
(1a) $[Ir_2Cl(CO)_3(\mu\text{-}CO)(DPM)_2][Cl]$	2036(m) 2001(vs) 1979(vs) 1764(m)	2054(s) 1999(s) 1971(vs) 1767(m)	-6.32,-15.49	mult.[d]
(1b) $[Ir_2Cl(CO)_3(\mu\text{-}CO)(DPM)_2][BF_4]$	2034(m) 2001(s) 1981(vs) 1761(m)	2039(m) 1999(s) 1987(vs) 1759(m)	-6.32,-15.49	mult.
(2) $[Ir_2Cl_2(CO)_2(\mu\text{-}CO)(DPM)_2]$	1980(s) 1955(vs,br) 1938(sh) 1728(s) 1704(m)	1962(vs,br) 1731(m) 1717(m)	-5.72	sing.
(3) $[IrCl(CO)(DPM)]_2$	1953(vs)	1954(vs,br) (1999(w)[e])	1.85,(8.69[e])	sing.
(4) $[Ir_2(CO)_2(\mu\text{-}Cl)(\mu\text{-}CO)(DPM)_2][BF_4]$	1971(s) 1946(vs) 1809(s)	1973(vs) 1941(s) 1822(m)	1.96	sing.
(5) $[Ir_2(CO)_2(\mu\text{-}Cl)(DPM)_2][BF_4]$	1989(s) 1964(vs)	1999(s) 1976(vs)	17.26 15.80[f] 12.07[g]	sing. sing. sing.

(a) Nujol mulls. (b) In CH_2Cl_2 solution. (c) In CH_2Cl_2 solution unless otherwise noted, vs. 85% H_3PO_4. (d) See reference 41 for assignment of coupling constants. (e) Due to $[Ir_2(\mu\text{-}Cl)(CO)_2)DPM)_2][Cl]$. (f) In acetone. (g) In THF.

X-Ray Data Collection

Bright yellow crystals of $[Ir_2Cl_2(CO)_2(\mu\text{-}CO)(DPM)_2]\cdot 3C_4H_8O$ were obtained by slow cooling of a saturated THF/ether solution of **2**. A suitable crystal was mounted in the air on a glass fibre, immediately coated in a layer of epoxy and then cooled to -40°C to minimize CO-loss. Unit cell parameters (at -40°C) were obtained from a least-squares refinement of the setting angles of 23 reflections, in the range $16.3° \leq 2\theta \leq 30.6°$, which were accurately centred on an Enraf-Nonius CAD4 diffractometer using Mo Kα radiation. The systematic absences ($h0\ell$: ℓ = odd, $0k0$: k = odd) were consistent with the space group $P2_1/c$.

Intensity data were collected at -40°C on a CAD4 diffractometer in the bisecting mode employing the ω-2θ scan technique up to $2\theta = 57.0°$ with graphite monochromated Mo Kα radiation. Backgrounds were scanned for 25% of the peak width on either end of the peak scan. The intensities of three standard reflections were measured every 1 h of exposure to assess possible crystal decomposition or movement. No significant variation in these standards was noted so no correction was applied to the data. 8968 unique reflections were measured and processed in the usual way using a value of 0.04 for p;[153] of these 5303 were considered to be observed and were used in subsequent calculations. Since the crystal faces were obscured by the epoxy coating, an empirical absorption correction based on phi scans was used.[154] See Table 3 for pertinent crystal data and the details of data collection.

Solution Structure and Refinement.

The structure was solved in the space group $P2_1/c$ using standard Patterson and Fourier techniques. Atomic scattering factors for non-hydrogen atoms[155] and hydrogen[156] were taken from the usual sources. Anomalous dispersion terms for Ir, Cl, and P were included in Fc.[157] The carbon atoms of the DPM phenyl groups were refined as rigid groups having idealized D_{6h} symmetry, C-C distances of 1.392 Å and independent isotropic thermal parameters. All hydrogen atoms were input as fixed contributions; their idealized positions were calculated after each cycle of refinement from the geometries of their attached carbon atoms using a C-H distance of 0.95 Å. These hydrogen atoms were assigned isotropic thermal parameters of 1Å^2 greater than the B (or equivalent isotropic B) of their attached carbon atom.

Although location of most atoms was straightforward, the chlorines and terminal carbonyl groups were found to be disordered such that only essentially spherical electron

Table 3. Summary of Crystal Data and Details of Intensity Collection for $[Ir_2Cl_2(CO)_2(\mu\text{-}CO)(DPM)_2]\cdot 3C_4H_8O$.

cmpd	$[Ir_2Cl_2(CO)_2(\mu\text{-}CO)(DPM)_2]\cdot 3C_4H_8O$
fw	1524.49
formula	$Ir_2Cl_2P_4O_6C_{65}H_{68}$
cell parameters	a = 22.890(6) Å b = 13.152(4) Å c = 22.129(5) Å β = 114.39(3)° V = 6075.61 $Å^3$
ρ(calcd), g/cm^3	1.666
space group	$P2_1/c$
temp., °C	-40
radiation	Mo, Kα (λ 0.71069 Å), graphite monochromated
receiving	2.00 + 0.500 x tan(θ) wide x 4.0 high
aperture, mm	173 from crystal
take-off angle, deg	1.7
scan speed, deg/min	variable between 10.058 and 1.804
scan width, deg	0.75 + 0.350 x tan(θ) in ω
2θ limits, deg	$3.0 \leq 2\theta \leq 57.0$
unique data collected	8968 ±h, k, -ℓ

(continued...)

Table 3. (continued)

unique data used ($Fo^2 \geq 3\sigma(Fo^2)$)	5303
range of transmission factors	0.792-0.999
final no. of parameters refined	268
error in observation of unit weight	1.007
R	0.043
Rw	0.054

densities were located at distances from the Ir atoms corresponding to the approximate positions of the chlorine atoms and the mid-points of the CO groups. In attempts to resolve this disorder, the chlorine atoms were placed at the positions of the peak maxima and assigned occupancy factors based on the relative intensities of these peaks such that the total chlorine occupancy in the dimer equalled two. A difference Fourier map phased on all other atoms and these chlorine positions showed electron density in the approximate positions for carbonyl groups. However, subsequent attempts to refine the carbon and oxygen positions failed; these atoms invariably moved together towards the chlorine positions resulting in unreasonably short C-O distances. For this reason, the carbon and oxygen positions were idealized on either side of the Fourier peak corresponding to the chlorine position such that the Ir-C-O group was linear with Ir-C and C-O distances of 1.82 Å and 1.15 Å, respectively. Many refinements were carried out in which the occupancy factors were correlated in a variety of ways and all resulted in essentially the same result, i.e., that Cl(1) and C(1)O(1) had occupancies near 50% (corresponding to 50% for Cl(1)' and C(1)'O(1)') while Cl(2) and C(2)O(2) had occupancies near 75% (corresponding to 25% for Cl(2)' and C(2)'O(2)'). These occupancies proved to be consistent with the infrared spectrum which could readily be explained based on this information (vide infra) and so were fixed to these values in the remaining cycles. The thermal parameters of Cl(2)' and C(2)' and O(2)' did not behave well so these were fixed at the average values observed for the other atoms of the same type. In the final refinements, the chlorine atom positions and isotropic thermal parameters were refined isotropically (apart from Cl(2)' whose positional parameters were refined only) and the carbonyl thermal parameters were refined (apart from C(2)' and O(2)' which were not refined). In spite of the difficulty in resolving this disorder all other parts of the molecule are well defined. The chlorine atoms refined to acceptable values and the positions of these and the CO groups with respect to other groups in the molecule are chemically reasonable (vide infra). Furthermore, it is encouraging that the occupancy factors offer an explanation of the infrared data (vide infra).

In the final refinements the non-disordered atoms of the complex were refined anisotropically except for hydrogens which were included as fixed contributions; the C and O atoms of the THF molecules were refined isotropically. The hydrogen atoms of these solvent molecules were not included owing to the relatively high thermal parameters of the C and O atoms.

The final model with 268 parameters refined converged to R = 0.043 and Rw = 0.054.[158] On the final difference Fourier map the highest 20 peaks (2.52 - 1.56 $eÅ^{-3}$) were in the vicinities of the disordered atoms, the phenyl groups and the Ir and P atoms. A typical carbon atom on earlier syntheses had a peak intensity of about 9.5 $eÅ^{-3}$.

The final positional parameters of the individual non-hydrogen atoms and the phenyl groups are given in Tables 4 and 5, respectively. The derived hydrogen positions, their thermal parameters are listed in Table 6. A listing of observed and calculated structure amplitudes used in the refinements are available.[159]

Discussion

The reaction of $[IrCl(C_8H_{14})_2]_2$ with DPM and CO results in a series of colour changes of the initial orange solution to black, red and finally to pale yellow. The black species initially formed is probably $[IrCl(CO)_3]_n$[160] which then rapidly reacts with DPM to give the DPM-containing complexes, the final species of which is the pale-yellow product 1. $^{31}P\{^1H\}$ NMR (see Figure 1) and infrared spectra of this final species are essentially identical to those reported for $[Ir_2Cl(CO)_4(DPM)_2]$-$[BPh_4]$[41,50] (apart from the absence of any infrared

Table 4. Positional and Thermal Parameters for the Non-Group Atoms of $[Ir_2Cl_2(CO)_3(DPM)_2]\cdot 3C_4H_8O$

a) Anisotropic Atoms.

Atom	x	y	z	U_{11}[b]	U_{22}	U_{33}	U_{12}	U_{13}	U_{23}
Ir(1)	0.25048(3)	0.13450(4)	0.04861(3)	2.20(3)	1.13(3)	1.47(3)	0.01(2)	0.82(2)	0.07(2)
Ir(2)	0.22651(3)	0.33550(4)	0.00698(3)	1.99(3)	1.28(3)	1.32(3)	0.10(2)	0.73(2)	0.04(2)
P(1)	0.3320(2)	0.1816(2)	0.1506(2)	2.4(2)	1.5(2)	1.6(2)	0.1(1)	0.8(2)	0.2(1)
P(2)	0.3129(2)	0.3951(2)	0.0997(2)	2.4(2)	1.3(2)	1.6(2)	0.1(1)	0.8(2)	0.0(1)
P(3)	0.1587(2)	0.0783(2)	-0.0403(2)	2.8(2)	1.2(2)	1.5(2)	0.2(2)	0.9(2)	0.0(1)
P(4)	0.1276(2)	0.2969(3)	-0.0796(2)	1.9(2)	1.6(2)	1.6(2)	0.1(1)	0.8(2)	0.1(2)
O(3)	0.3096(4)	0.2136(6)	-0.0424(5)	2.2(5)	2.4(5)	2.7(6)	0.4(4)	1.4(5)	0.6(4)
C(3)	0.2782(6)	0.224(10)	-0.0108(7)	1.9(8)	3.6(9)	1.8(8)	-1.0(6)	1.2(7)	0.7(7)
C(4)	0.3258(7)	0.3140(10)	-0.1707(6)	4.3	1.8(8)	0.9(7)	0.0(6)	1.0(7)	0.1(6)
C(5)	0.0969(6)	0.1783(10)	-0.0630(6)	3.0	3.1(8)	1.3(7)	0.2(7)	1.1(7)	0.2(6)

---

[a] Estimated standard deviations in this and other tables are given in parentheses and correspond to the least significant digits.

[b] The thermal parameters have been multiplied by 10^2. The form of the thermal ellipsoid is: $\exp[-2\pi^2(a^{*2}U_{11}h^2 + b^{*2}U_{22}k^2 + c^{*2}U_{33}l^2 + 2a^*b^*U_{12}hk + 2a^*c^*U_{13}hl + 2b^*c^*U_{23}kl)]$.

(continued...)

Table 4. (continued)

b) Isotropic Atoms

Atom	x	y	z	B(Å^2)^a	Atom	x	y	z	B(Å^2)
Cl(1)	0.1784(4)	0.1255(6)	0.1074(4)	2.5(2)	C(2')	0.1814	0.3717	0.0549	2.5
Cl(1')	0.3160(4)	-0.0239(8)	0.0506(3)	2.1(2)	C(T1)	0.247(1)	-0.254(2)	-0.146(1)	5.9(5)
Cl(2)	0.1637(2)	0.3760(4)	0.0745(3)	2.8(2)	C(T2)	0.3034(8)	-0.2310(11)	-0.1510(8)	3.1(3)
Cl(2')	0.2428	0.4750	-0.0650	1.8(4)	C(T3)	0.356(1)	-0.218(2)	-0.094(1)	5.7(5)
O(1)	0.3259	-0.0487	0.0476	5.7(1)	C(T4)	0.3388(8)	-0.2659(12)	-0.0390(9)	3.8(4)
O(1')	0.1666	0.1095	0.1204	4.6(8)	C(T5)	0.3960(8)	-0.0860(16)	-0.1372(11)	5.4(5)
O(2)	0.2430	0.5085	-0.0707	3.8(3)	C(T6)	0.441(1)	0.112(2)	-0.067(2)	9.3(8)
O(2')	0.1528	0.3946	0.0851	4.5	C(T7)	0.0502(2)	0.145(3)	-0.071(2)	12.3(8)
O(T1)^b	0.2646(9)	-0.2446(14)	-0.0676(9)	9.7(5)	C(T8)	0.496(1)	0.124(2)	-0.143(1)	6.5(5)
O(T2)	0.4288(7)	0.1155(11)	-0.178(8)	6.5(4)	C(T9)	0.074(1)	-0.093(3)	0.246(1)	8.4(7)
O(T3)	0.0480(7)	-0.1286(11)	0.1771(8)	6.4(3)	C(T10)	0.138(1)	-0.047(2)	0.248(1)	7.9(6)
C(1)	0.2967	0.0222	0.0480	1.8(6)	C(T11)	0.159(1)	-0.112(2)	0.205(1)	6.8(6)
C(1')	0.1990	0.1192	0.0926	3.9(8)	C(T12)	0.099(2)	-0.148(3)	0.156(2)	14.3(13)
C(2)	0.2366	0.4415	-0.0406	2.4(4)					

---

[a] $B = 8\pi^2 \bar{U}^2$

[b] The THF solvent molecules are labelled as follows - THF(1): O(T1), C(T1), C(T2), C(T3), C(T4); THF(2): O(T2), C(T5), C(T6), C(T7), C(T8); THF(3): O(T3), C(T9), C(T10), C(T11), C(T12).

Table 5. Derived Parameters for the Rigid Groups of $[Ir_2Cl_2(CO)_3(DPM)_2]\cdot 3C_4H_8O$.

Atom	x	y	z	B,Å^2	Atom	x	y	z	B,Å^2
C(11)	0.3282(4)	0.1135(6)	0.2212(4)	1.4(2)	C(51)	0.1617(4)	0.0409(7)	-0.1182(4)	1.5(2)
C(12)	0.3279(5)	0.1651(5)	0.2760(5)	2.3(3)	C(52)	0.2197(3)	0.03302(7)	-0.1242(4)	1.9(3)
C(13)	0.3260(5)	0.1109(7)	0.3292(4)	2.7(3)	C(53)	0.2205(4)	0.0046(8)	-0.1845(5)	2.5(3)
C(14)	0.3244(5)	0.0051(7)	0.3276(4)	2.8(4)	C(54)	0.1632(5)	-0.0159(8)	-0.2388(4)	2.9(3)
C(15)	0.3246(5)	-0.0464(5)	0.2728(5)	2.6(3)	C(55)	0.1052(4)	-0.0080(8)	-0.2328(4)	2.8(4)
C(16)	0.3266(5)	0.0078(6)	0.2196(4)	2.2(3)	C(56)	0.1044(3)	0.0204(8)	-0.1726(5)	2.2(3)
C(21)	0.4325(4)	0.1621(8)	0.1112(3)	1.9(3)	C(61)	0.1189(4)	-0.0323(6)	-0.0242(5)	1.8(2)
C(22)	0.4156(3)	0.1664(7)	0.1648(4)	1.5(2)	C(62)	0.0527(4)	-0.0360(7)	-0.0452(5)	2.8(3)
C(23)	0.4632(5)	0.1686(8)	0.2292(4)	2.5(3)	C(63)	0.0233(3)	-0.1259(8)	-0.0394(6)	3.4(4)
C(24)	0.5275(4)	0.1665(9)	0.2400(4)	3.0(4)	C(64)	0.0602(5)	-0.2121(7)	-0.0126(6)	3.6(4)
C(25)	0.5444(3)	0.1621(9)	0.1864(5)	3.3(4)	C(65)	0.1264(5)	-0.2084(6)	0.0084(6)	3.6(4)
C(26)	0.4968(5)	0.1599(9)	0.1220(4)	2.9(4)	C(66)	0.1558(3)	-0.1185(8)	0.0026(5)	2.6(3)
C(31)	0.3014(5)	0.5228(5)	0.1261(5)	1.4(2)	C(71)	0.0668(4)	0.3896(6)	-0.0846(5)	1.4(2)
C(32)	0.3112(5)	0.6045(7)	0.0914(4)	3.0(4)	C(72)	0.0113(5)	0.3646(6)	-0.0765(5)	2.3(3)
C(33)	0.3014(5)	0.7034(6)	0.1077(5)	2.8(4)	C(73)	-0.0336(4)	0.4395(8)	-0.0822(6)	3.8(4)
C(34)	0.2819(5)	0.7206(5)	0.1586(5)	2.5(3)	C(74)	-0.0231(5)	0.5394(7)	-0.0961(6)	3.6(4)
C(35)	0.2721(5)	0.6389(8)	0.1933(5)	3.2(4)	C(75)	0.0323(5)	0.5643(5)	-0.1042(6)	2.8(4)
C(36)	0.2819(5)	0.5399(6)	0.1771(5)	2.4(3)	C(76)	0.0772(4)	0.4894(7)	-0.0985(5)	2.3(3)
C(41)	0.3909(3)	0.4090(7)	0.0970(5)	1.7(2)	C(81)	0.1186(4)	0.2889(7)	-0.1642(3)	1.8(2)
C(42)	0.4450(5)	0.4298(8)	0.1548(4)	2.2(3)	C(82)	0.0570(3)	0.2903(7)	-0.2147(5)	1.8(3)
C(43)	0.5044(4)	0.4423(9)	0.1523(4)	3.3(4)	C(83)	0.0483(3)	0.2811(8)	-0.2806(4)	2.2(3)
C(44)	0.5097(4)	0.4340(9)	0.0920(6)	3.3(4)	C(84)	0.1011(5)	0.2705(8)	-0.2960(3)	2.9(4)
C(45)	0.4555(5)	0.4133(9)	0.0342(4)	3.2(4)	C(85)	0.1627(4)	0.2691(8)	-0.2455(5)	2.7(4)
C(46)	0.3962(4)	0.4008(8)	0.0368(4)	1.6(3)	C(86)	0.1715(3)	0.2783(7)	-0.1796(4)	1.8(3)

Rigid Group Parameters

	Xc[a]	Yc	Zc	phi[b]	theta	rho
Ring 1	0.3263(3)	0.0593(5)	0.2744(3)	3.127(8)	2.603(5)	1.549(7)
Ring 2	0.4800(3)	0.1643(5)	0.1756(3)	-1.621(9)	2.351(5)	1.628(9)
Ring 3	0.2917(3)	0.6217(5)	0.1424(3)	2.517(14)	-2.019(6)	0.844(14)
Ring 4	0.4503(3)	0.4215(5)	0.0945(3)	1.929(15)	2.039(5)	-1.773(15)
Ring 5	0.1624(3)	0.0125(5)	-0.1785(3)	1.639(6)	-3.135(5)	-1.843(6)
Ring 6	0.0896(3)	-0.1222(5)	-0.0184(3)	-2.038(6)	-3.106(7)	0.296(7)
Ring 7	0.0218(3)	0.4645(5)	-0.0904(3)	-0.697(6)	2.664(7)	2.899(7)
Ring 8	0.1099(3)	0.2797(4)	-0.2301(3)	-1.637(6)	3.015(5)	-1.475(6)

a) Xc, Yc and Zc are the fractional coordinates of the centroid of the rigid group.

b) The rigid group orientation angles phi, theta and rho (radians) are the angles by which the rigid body is rotated with respect to a set of axes x, y, z. See: LaPlaca, S.J.; Ibers, J.A. Acta Crystallogr. 1965, **18**, 511.

Table 6. Derived Hydrogen Positions and Thermal Parameters of $[Ir_2Cl_2(CO)_3(DPM)_2]$.

Atom	x	y	z	B, Å^2	Atom	x	y	z	B, Å^2
H(1)C(4)	0.2907	0.3223	0.1841	2.8	H(45)	0.4589	0.4082	-0.0070	4.3
H(2)C(4)	0.3642	0.3346	0.2082	2.8	H(46)	0.3590	0.3874	-0.0028	2.6
H(1)C(5)	0.0591	0.1586	-0.1024	2.8	H(52)	0.2588	0.0466	-0.0871	2.9
H(2)C(5)	0.0819	0.1876	-0.0282	2.8	H(53)	0.2602	-0.0018	-0.1884	3.5
H(12)	0.3296	0.2369	0.2775	3.2	H(54)	0.1638	-0.0362	-0.2799	3.9
H(13)	0.3259	0.1458	0.3668	3.7	H(55)	0.0660	-0.0222	-0.2701	3.8
H(14)	0.3226	-0.0321	0.3639	3.7	H(56)	0.0646	0.0262	-0.1688	3.2
H(15)	0.3230	-0.1189	0.2717	3.5	H(62)	0.0274	0.0232	-0.0637	3.8
H(16)	0.3267	-0.0278	0.1824	3.2	H(63)	-0.0224	-0.1276	-0.0539	4.4
H(22)	0.4004	0.1599	0.0673	2.9	H(64)	0.0393	-0.2729	-0.0087	4.6
H(23)	0.5088	0.1569	0.0857	4.2	H(65)	0.1508	-0.2674	0.0267	4.6
H(24)	0.5886	0.1610	0.1942	4.3	H(66)	0.2006	-0.1166	0.0169	3.6
H(25)	0.5599	0.1681	0.2843	4.1	H(72)	0.0035	0.2967	-0.0672	3.2
H(26)	0.4516	0.1711	0.2659	3.7	H(73)	-0.0719	0.4227	-0.0761	4.8
H(32)	0.3239	0.5927	0.0559	4.0	H(74)	-0.0543	0.5908	-0.0992	4.6
H(33)	0.3079	0.7592	0.0835	3.8	H(75)	0.0387	0.6329	-0.1134	3.8
H(34)	0.2760	0.7884	0.1699	3.5	H(76)	0.1141	0.5069	-0.1045	3.3
H(35)	0.2601	0.6511	0.2288	4.2	H(82)	0.0207	0.2979	-0.2043	2.8
H(36)	0.2761	0.4846	0.2013	3.4	H(83)	0.0058	0.2825	-0.3151	3.2
H(42)	0.4415	0.4344	0.1960	3.2	H(84)	0.0946	0.2638	-0.3412	3.9
H(43)	0.5414	0.4552	0.1918	4.3	H(85)	0.1983	0.2605	-0.2563	3.8
H(44)	0.5501	0.4421	0.0903	4.3	H(86)	0.2132	0.2759	-0.1455	2.8

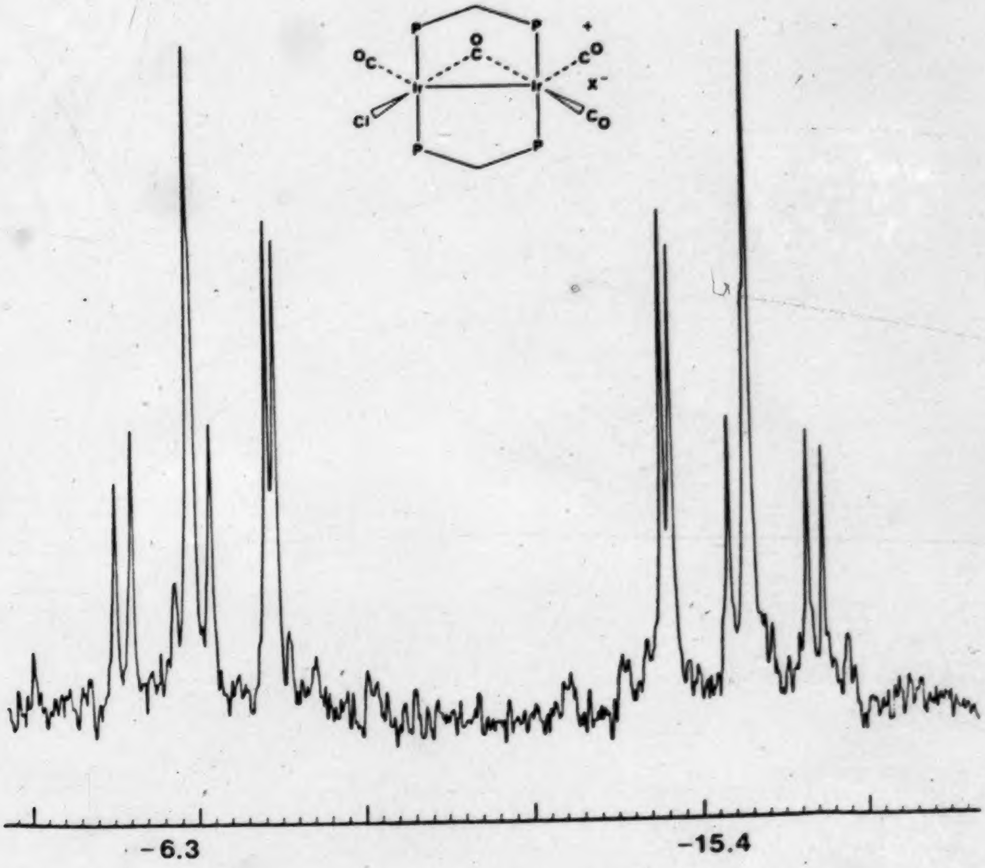

Figure 1: $^{31}P\{^{1}H\}$ NMR spectrum of $[Ir_2Cl(CO)_3(\mu\text{-}CO)(DPM)_2][Cl]$ (**1a**) obtained at 36.4 MHz.

stretches due to BPh_4^-). This, together with its conductivity, which indicates that it is a 1:1 electrolyte, and the elemental analysis, which shows the presence of two Cl atoms per dimer, suggests the fomulation $[Ir_2Cl(CO)_4(DPM)_2][Cl]$ (**1a**). Although two structures have been suggested[41,50] for this cation, the one shown below, as proposed by Mague and De Vries[41] for the arsine analogue based on a careful ^{13}CO labelling study, is most probably correct. In further support of this fomulation for the chloro salt (**1a**), the analogous compounds (**1b** and **1c**) containing the non-coordinating anions, BF_4^- and BPh_4^- can be readily prepared from **1a** by inducing precipitation in the presence of these larger anions, although the BF_4^- salt is best prepared by reacting **1a** with $AgBF_4$. Furthermore, carbonyl-loss from **1a** yields the dichloro tricarbonyl species $[Ir_2Cl_2(CO)_3(DPM)_2]$, which has been completely characterized and has been shown by an X-ray structure analysis to display a geometry very similar to that

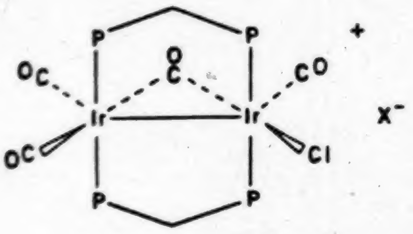

(1)

X = Cl(**1a**), BF_4(**1b**), BPh_4 (**1c**) proposed for **1** (vide infra). Compound **1a** presents an interesting contrast to the analogous DPM-bridged, rhodium carbonyl compounds where the highest carbonyl-containing species is the tricarbonyl cation, $[Rh_2(CO)_2(\mu\text{-}Cl)(\mu\text{-}CO)(DPM)_2]^+$.[48,60] The formation of **1** is also in contrast to the reaction of $[RhCl(C_8H_{12})]_2$ with DPM under CO which leads to a neutral dicarbonyl complex, trans-$[RhCl(CO)(DPM)]_2$.[38] In the present case it is apparent that the more basic Ir centres allow the coordination of more π-acid carbonyl groups than the analogous Rh compounds.

Previous studies have usually utilized the above tetracarbonyl species with non-coordinating anions as a precursor for the preparation of DPM-bridged binuclear iridium complexes.[41,151] However, this study shows that **1a**, with the chloride counter ion, proves to be a more versatile starting material in the preparation of both neutral and charged binuclear carbonyl products (vide infra). Like its BPh_4^- analogue, **1a** readily loses CO even in the solid state and must be stored under an atmosphere of CO. However, CO-loss from the solid is usually inefficient, leaving some of the tetracarbonyl starting material. Carbonyl-loss is more conveniently carried out in refluxing CH_2Cl_2. After heating the solution for 20 min the colour changes to dark orange, indicating the formation of a new compound, **2**. The $^{31}P\{^1H\}$ NMR spectrum of this sample shows only one peak, a singlet at -5.72 ppm. An infrared spectrum of this solution shows a very broad band at 1962 cm^{-1} and two bands at 1731 and 1717 cm^{-1}. The solid precipitate obtained from this solution displays three bands in the terminal carbonyl region, at 1980 (s), 1955 (br, vs) and 1938 (sh) cm^{-1}, and two bridging carbonyl bands at 1728 and 1704 cm^{-1}. Some insight into the origin of these bands, when only one species is observed in the $^{31}P\{^{1}H\}$ NMR spectrum, is obtained from the X-ray structure of **2** which shows that each metal has one chloro and one terminal ligand and that both metals share a bridging carbonyl group. The terminal Cl and CO groups are disordered such that the two species present in the solid (**2a** and **2b**) are those shown below. The infrared spectra can then be readily explained as arising from a mixture of these two isomers. In solution, the bands in the terminal CO region are broad and coalesce to a single wide peak but the bridging bands remain resolved. In the solid state, however, all bands are resolved. The two isomers would be expected to give rise to different infrared spectra; in **2a** all carbonyls are cis whereas in **2b** the bridging CO is almost trans to one terminal CO but cis to the other.

In the solid the infrared stretches for the bridging carbonyl groups can readily be assigned based on their relative intensities and on the relative abundance of the two isomers **2a** and **2b**, as determined from the X-ray study. The band at 1728 cm^{-1} is several times more intense than that at 1704 cm^{-1} so can be attributed to **2b**, the more abundant isomer in the crystal (see discussion of structure). Unfortunately, we are unable to unambiguously assign the terminal carbonyl bands. Only three terminal carbonyl stretches are observed although four are expected, arising from the two terminal CO groups on each isomer; presumably the broad intense band at 1955 cm^{-1} conceals two stretches. Attempts to correlate these terminal carbonyl bands with the bridging ones by varying the isomer ratios by crystallizing the mixture at different temperatures (-80° to 40°C) did not succeed. Although slight variations in band intensities were observed, we were unable to correlate the changes in a satisfactory manner.

In THF solution the bridging carbonyl bands of redissolved samples of **2** are of comparable intensity suggesting essentially equal concentrations of **2a** and **2b**. It appears that in solution species **2a** and **2b** readily interconvert through the ionic intermediate **4a**, by chloride loss and subsequent recoordination. Chloride recoordination in the proposed ionic intermediate can occur adjacent to either the bridging CO or to the bridging Cl; the former

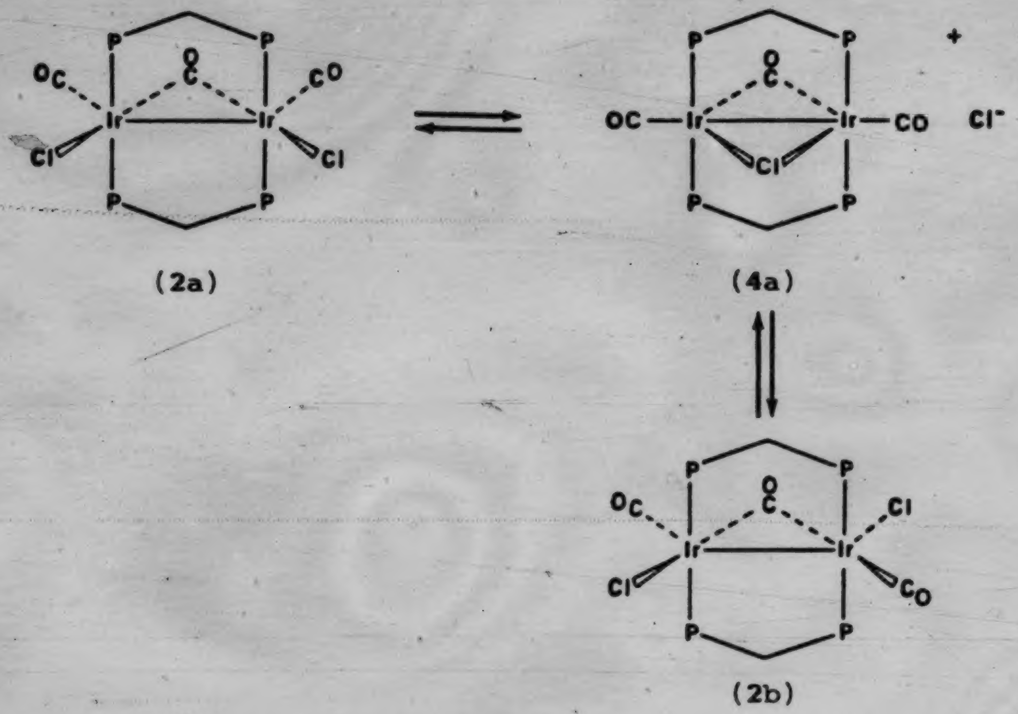

will yield **2b** and the latter will yield **2a**. Compound **4** with non-coordinating anions has been prepared by ourselves and others[41,150] and has a bridging carbonyl band at ca. 1811 cm^{-1}. This band is not observed in the solution infrared spectrum of **2** suggesting that the species is present in quantities too small to be detected. Consistent with this, solutions of **2** are non-conducting. The $^{31}P\{^1H\}$ NMR data suggest that **2a** and **2b** are interconverting rapidly on the NMR time scale; even at -80°C there is no obvious change in the spectrum from that run at 20°C. Support for the postulation of **4a** as the intermediate in this exchange comes from the addition of a solution of $Me_4N^+Cl^-$ to an acetone solution of the BF_4^- salt of **4**; a rapid reaction occurs to produce a mixture of **2a** and **2b** as identified by ^{31}P NMR and infrared spectroscopy. Additional support for this isomerism is found in the work of Mague[41] where the reaction of **4** (as the BPh_4^- salt) with CN^tBu yields $[Ir_2Cl(CN^tBu)(CO)_2(\mu\text{-}CO)(DPM)_2]^+$ in which the infrared band due to the bridging CO group is reported to be somewhat asymmetric suggesting two isomers of the type that we propose for **2a** and **2b**. The rapid interconversion of the two isomers (**2a** and **2b**) in solution also explains our inability to separate them either by chromatography or fractional crystallization.

Compound **2** is very moisture and air sensitive in solution and even the solid decomposes after several hours in air. This species also loses CO quite readily and crystals left overnight under a recirculating N_2 atmosphere in a glove box turned red on their surface due to CO-loss (vide infra).

Refluxing compound **2** in THF results in the formation of a red-purple solid whereas refluxing in toluene yields a maroon solid. Although these two differ in appearance and in solubility (the red-purple solid is slightly soluble in CH_2Cl_2 and the maroon solid is very insoluble in solvents such as $CHCl_3$, CH_2Cl_2, acetone, THF and toluene) they both appear to be the same species, trans-$[IrCl(CO)(DPM)]_2$

(3). The analogous rhodium dicarbonyl species also has been observed to crystallize in different crystal modifications in which the solubilities of the different forms differ.[38,63,161-163] Both forms of 3 react with small molecules to give identical products, offering further confirmation that they are the same compound. Although there is an earlier report of this compound,[164] it does not seem to have been obtained in a pure form. It was reported to have been obtained as a yellow solid from the reaction of $[IrCl(C_8H_{12})]_2$ and DPM in 1:2 stoichiometries under an atmosphere of CO. On drying in vacuo it was reported that this species lost benzene of crystallization to become a red-orange product. Based on our results it seems more likely that the initial product was the tetracarbonyl complex or a mixture of it and the tricarbonyl species which then lost CO in vacuo to give a mixture of these species and compound 3. The mixture would explain the red-orange colour instead of the bright red-purple or maroon colours we observe. In all of these studies the reactions were carefully monitored by $^{31}P\{^1H\}$ NMR and infrared spectroscopy so it is clear in all cases how many phosphorus-containing species are present.

Both samples of 3 show a single broad carbonyl band at 1953 cm^{-1} in the infrared spectra of the solids, however dichloromethane solutions of the red-purple product show a band at 1954 cm^{-1} and a smaller peak at 1999 cm^{-1}. This smaller band was observed in the original report[164] and was attributed to distortions of the compound from the ideal C_{2h} symmetry such that both carbonyl bands (B_u and A_g) became infrared active. It is found instead that this smaller band is due to small amounts of an additional species **5a**. In the $^{31}P\{^1H\}$ NMR spectrum both species are clearly observed, the major one at $\delta = 1.85$ ppm and the minor one (in approximately 10% abundance) at $\delta = 8.69$ ppm. It appears that this minor species is $[Ir_2(CO)_2(\mu\text{-}Cl)(DPM)_2][Cl]$ (**5a**) which is in equilibrium with (**3**) in solution. The analogous BF_4^- salt (**5b**) has infrared bands at 1999 and 1976 cm^{-1} in CH_2Cl_2 (see Table I) so that the lower frequency band of **5a** in CH_2Cl_2 solutions of **3** could easily be obscured by the broad band arising due to **3** at 1954 cm^{-1} (in fact, the band at 1954 cm^{-1} is unsymmetrical suggesting the presence of a weak shoulder at _ca_. 1970 cm^{-1}). Although the $^{31}P\{^1H\}$ NMR chemical shift of **5a** with the chloro counter ion is different from that observed with BF_4^- (**5b**) ($\delta = 8.69$ and 17.26 ppm, respectively), such shift differences have been previously observed on changing from coordinating to non-coordinating anions.[165] Furthermore, the chemical shift of **5b** is found to be extremely solvent dependent (vide infra), so it is not surprising that the presence of a coordinating anion has a significant effect. In support of this formulation for 5a, we have observed that significant quantities of the analogous rhodium compound, $[Rh_2(CO)_2(\mu\text{-}Cl)(DPM)_2][Cl]$, occur in solutions of trans-$[RhCl(CO)(DPM)]_2$.[166] Although in solution it appears that species 3 and 5a are in equilibrium, an infrared spectrum of the solid obtained from the solution shows only a single band at 1953 cm^{-1} due to 3, indicating that Cl^- recoordination has occurred in 5a. Furthermore, the reaction mixtures of 3 and 5a with small molecules such as acetylenes results in the formation of only one product (see Chapter 3).

In theory, compound 3 could have either of the two possible geometries shown below: a trans form (3a) or a cis form (3b).

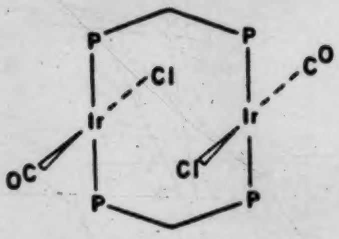

(3a)

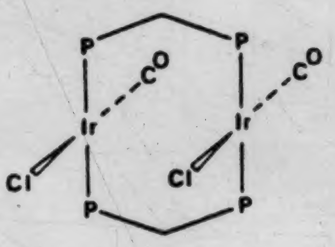

(3b)

The spectral data does not rule out either possibility since without an Ir-Ir bond the carbonyl stretches need not be coupled, in which case there would be only one carbonyl stretch for both isomers. Preliminary X-ray photos of 3 indicate that it crystallizes in the space group $P2_1/n$ with

Z $\simeq$ 2 so the molecules are required to have $\bar{1}$ crystallographic symmetry.[167] This is the symmetry found for the molecules in all determinations of $[RhCl(CO)(L_2)]_2$ (L_2 = DPM or $Ph_2AsCH_2AsPh_2$).[63,161-163] Although compound 3 could have cis carbonyl groups and be disordered in the solid we feel that the cis isomer is unlikely. In principle, it should be simple to distinguish between **3a** and **3b** by examining the methylene region of the ^1H NMR spectrum. As shown below, in **3a** there are only two types of methylene hydrogen, labelled H_a and H_b. At room temperature these two should become equivalent, giving rise to only one signal. However, in the cis case **3b**, where the four original methylene hydrogens are labelled H_a , H_b , $H_{a'}$, and $H_{b'}$, there are two inequivalent sets of hydrogens, (H_a, $H_{b'}$ and $H_{a'}$, H_b) which are never interchanged. Therefore two distinct resonances would be expected in the ^1H NMR. The latter case is the one more commonly observed for DPM-bridged complexes. Unfortunately, the limited solubility of **3** makes the distinction between **3a** and **3b** on this basis, impossible.

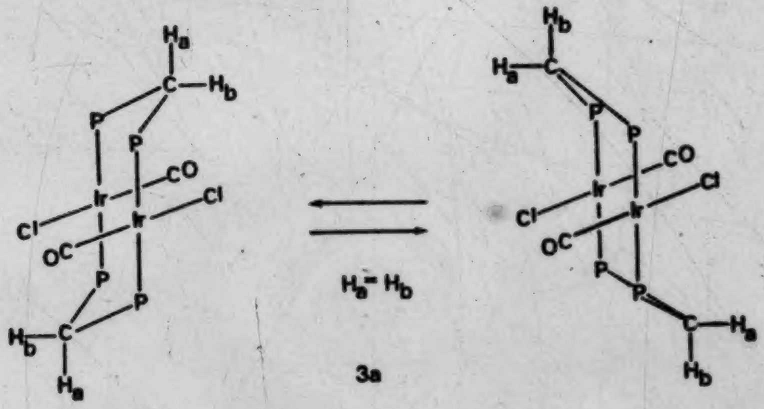

3a

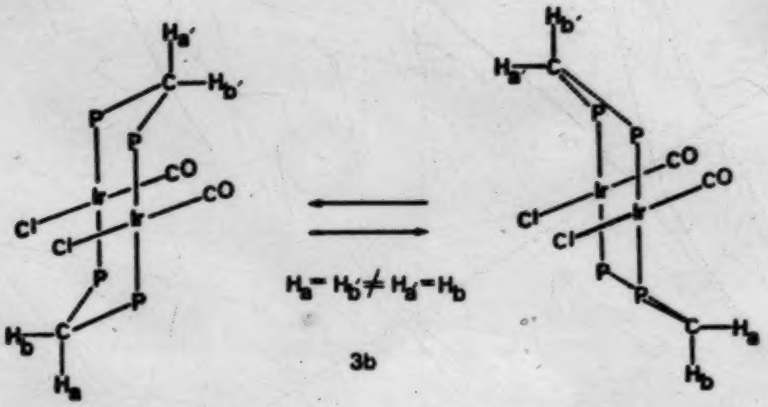

3b

Compound 3 is air sensitive in solution and turns from purple to yellow-green within 1-2 h upon exposure to air. A $^{31}P\{^1H\}$ NMR spectrum of this green-yellow solution shows that major species appears as a singlet at $\delta = -16.1$ ppm and its I.R. spectrum displays a new carbonyl stretch at 2020 cm^{-1}. It is likely that this species results from O_2 addition to 3, although this has not yet been verified.

This study shows that successive carbonyl-loss can be effected from $[Ir_2Cl(CO)_4(DPM)_2][Cl]$ yielding first $[Ir_2Cl_2(CO)_2(\mu\text{-}CO)(DPM)_2]$ then $[IrCl(CO)(DPM)]_2$. Based on the analogous Rh-DPM system[64] it might be expected that further CO-loss should occur to produce $[Ir_2Cl_2(\mu\text{-}CO)(DPM)_2]$. However, all attempts to prepare this complex have failed; it appears that the basic iridium centres are more reluctant to lose carbonyl groups than are the rhodium centres in the analogous rhodium complexes. Carbonyl-loss from the above tetracarbonyl and tricarbonyl species is reversible, so under CO compound 3 yields 2 and ultimately 1a.

Starting with $[Ir_2Cl(CO)_4(DPM)_2][X]$, having non-coordinating anions ($X^- = BF_4^-$, BPh_4^-), we might also expect to obtain the cationic tricarbonyl and dicarbonyl complexes analogous to the known rhodium species.[48,60,61] Although CO-loss from the tetracarbonyl species occurs to give the tricarbonyl complex **4** (see Experimental), loss of a second CO to give the dicarbonyl A-frame does not occur readily; under refluxing conditions a mixture of products is obtained, one of which is the desired dicarbonyl compound. This again contrasts the behaviour of the analogous Rh tricarbonyl species which loses CO readily to give the dicarbonyl A-frame. However, $[Ir_2(CO)_2(\mu\text{-}Cl)(DPM)_2][BF_4]$ (**5b**) can easily be obtained by chloride abstraction from $[IrCl(CO)(DPM)]_2$ (**3**) using one equivalent of $AgBF_4$. All evidence suggests an A-frame formulation for **5b** analogous to that of $[Rh_2(CO)_2(\mu\text{-}Cl)(DPM)_2][BF_4]$;[48,61] its infrared spectrum has two terminal carbonyl bands at 1989 and 1964 cm^{-1}, it is a 1:1 electrolyte and its $^{31}P\{^1H\}$ NMR spectrum indicates that all phosphorus atoms are chemically equivalent. In addition, the stepwise addition of CO to compound **5b** yields the corresponding tricarbonyl complex **4b** and finally the tetracarbonyl species **1b**.

As noted earlier, the $^{31}P\{^1H\}$ NMR chemical shift of **5b** is highly solvent dependent; in CH_2Cl_2 $\delta = 17.26$ ppm, in acetone δ = 15.80 ppm and in THF δ = 12.07 ppm. Also, the addition of THF to a CH_2Cl_2 solution of **5b** causes a shift from the CH_2Cl_2-only value to the THF-only value at THF:CH_2Cl_2 volume ratios of 3:2; at no time during these additions are any new peaks observed. Similarly, the addition of acetone caused a shift in the position of the $^{31}P\{^1H\}$ NMR peak at **5b**. With the stronger donor solvent, acetonitrile, the addition of only 100 µL of acetonitrile to a CH_2Cl_2 solution of **5b** (75 mg in 1 mL) caused a shift by approximately 15 ppm to δ = 2.40 ppm. The solution infrared spectrum, however, showed no band attributable to coordinated acetonitrile and similarly no obvious change in the carbonyl stretches was observed in any of the above additions, suggesting a weak interaction between **5b** and solvent. Solid samples isolated from acetonitrile solutions of **5b** contained no acetonitrile, further indicating only weak interaction between CH_3CN and **5b** in solution. It seems therefore that in coordinating solvents compound 5 interacts with the solvent molecules; however, the number of molecules involved and the site(s) of solvent coordination are not known.

Description of Structure

$[Ir_2Cl_2(CO)_2(\mu-CO)(DPM)_2]$ crystallized from a THF/ether mixture along with three molecules of THF in the space group $P2_1/c$. Two of the solvent molecules have twist conformations while the other has an envelope geometry and higher thermal parameters, suggesting a slight disorder of this group. The presence of the two conformations of THF molecules is not unusual and both have been observed before.[168] Significantly, in a report by Hodgson and Raymond,[168] in which both THF conformations were observed in the same structure, the thermal parameters involving the envelope conformation were significantly higher than those in the planar one, as is observed in our structure. Nevertheless, even the worst THF molecule in the present structure has a geometry typically observed for such a group.[157] There are no unusual contacts between the THF molecules and the Ir-DPM complex.

The complex has essentially the geometry expected for a binuclear DPM-bridged compound (see Figures 2 and 3). All Ir-P distances (range 2.321(3) - 2.341(3) Å) are in agreement with the analogous distances found in other structurally characterized DPM-bridged Ir complexes.[151,173] All P-C distances (see Table 7) are normal as are the angles associted with the DPM ligands

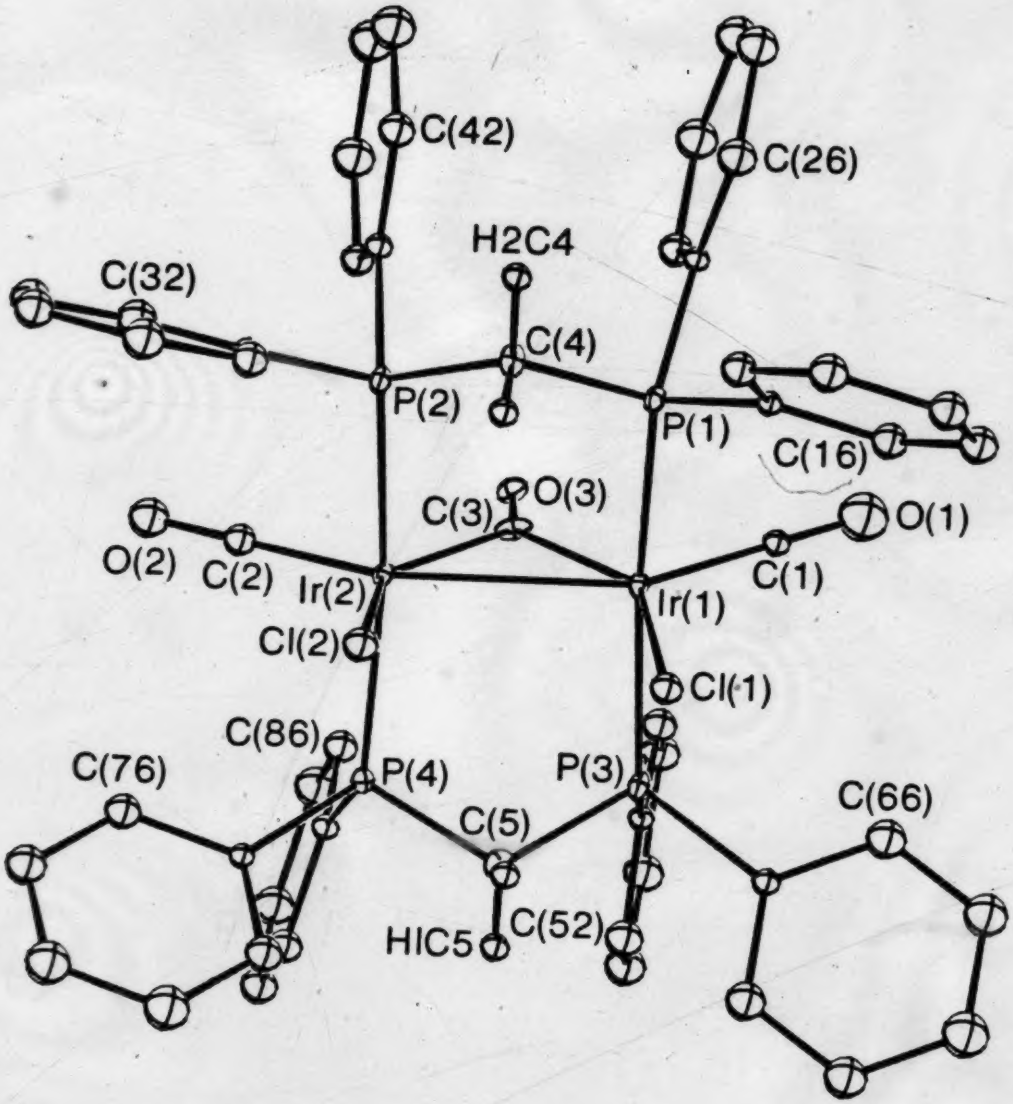
C(42)
C(26)
H2C4
C(32)
C(4)
P(2)
P(1)
C(16)
C(3)
O(3)
O(1)
O(2)
C(2)
Ir(2)
C(1)
Ir(1)
Cl(2)
Cl(1)
C(86)
C(76)
P(4)
P(3)
C(66)
C(5)
HIC5
C(52)

Figure 2. Perspective View of Isomer **2a**, $[Ir_2Cl_2(CO)_2(\mu\text{-}CO)\text{-}(DPM)_2]$ (25% abundance). Thermal ellipsoids are drawn at the 20% level except for methylene hydrogens which are drawn artificially small on both figures. Phenyl hydrogens have the same number as their attached carbon atoms.

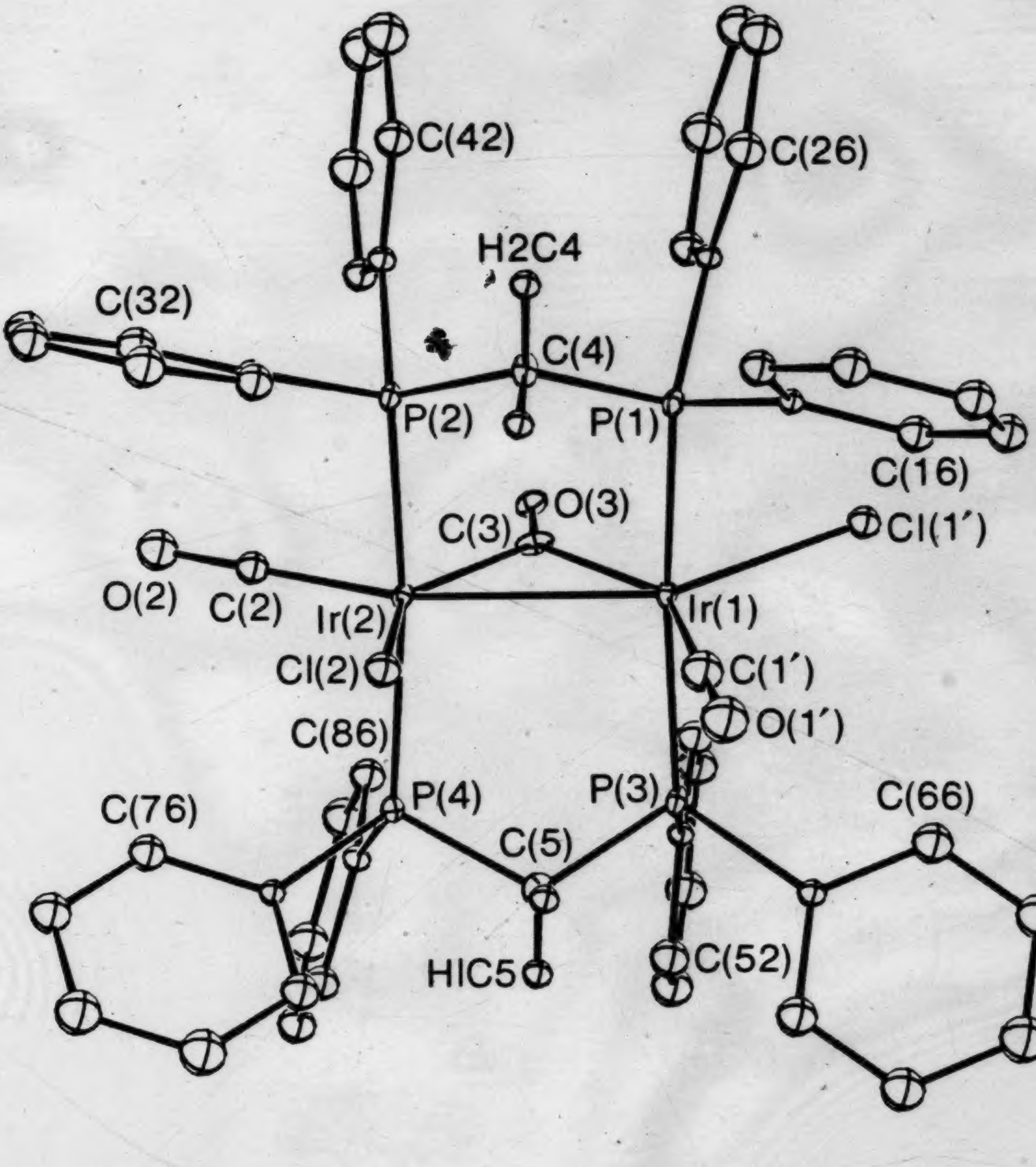
C(42)
C(26)
H2C4
C(32)
C(4)
P(2)
P(1)
C(16)
O(3)
C(3)
Cl(1′)
O(2)
C(2)
Ir(2)
Ir(1)
Cl(2)
C(1′)
O(1′)
C(86)
P(4)
P(3)
C(66)
C(76)
C(5)
HIC5
C(52)

Figure 3. Perspective View of the 75% Isomer **2b**, $[Ir_2Cl_2(CO)_2(\mu\text{-}CO)(DPM)_2]$.

Table 7. Selected Interatomic Distances (Å) in $[Ir_2Cl_2(CO)_3(DPM)_2]\cdot 3C_4H_8O^{a,b}$

Ir(1) - Ir(2)	2.779(1)	P(1) - C(4)	1.82(2)
Ir(1) - C(3)	2.04(3)	P(2) - C(4)	1.82(3)
Ir(2) - C(3)	2.04(2)	P(3) - C(5)	1.84(3)
Ir(1) - Cl(1)	2.489(7)	P(4) - C(5)	1.80(3)
Ir(1) - Cl(1')	2.557(9)	P(1) - C(11)	1.834(10)
Ir(2) - Cl(2)	2.520(5)	P(1) - C(21)	1.817(9)
Ir(2) - Cl(2')	2.556(1)	P(2) - C(31)	1.833(9)
Ir(1) - P(1)	2.341(3)	P(2) - C(41)	1.819(10)
Ir(1) - P(3)	2.329(3)	P(3) - C(51)	1.821(10)
Ir(2) - P(2)	2.321(3)	P(3) - C(61)	1.826(10)
Ir(2) - P(4)	2.331(8)	P(4) - C(71)	1.813(13)
C(3) - O(3)	1.20(4)	P(4) - C(81)	1.823(13)

a) All terminal carbonyl groups were input in their idealized positions with distances of Ir-C = 1.82 Å and C-O = 1.15 Å, and with Ir-C-O angles of 180°.

b) Interatomic Distances (Å) for the THF solvent molecules are listed in the supplementary data.[159]

Table 8. Selected Angles (Deg) in $[Ir_2Cl_2(CO)_3(DPM)_2]\cdot 3C_4H_8O$.

Ir(2) - Ir(1) - Cl(1)	97.8(1)	Ir(1) - Ir(2) - Cl(2')	146.11(2)	Ir(1) - C(1') - O(1')	idealized 180°	C(11) - P(1) - C(21)	102.4(4)
Ir(2) - Ir(1) - Cl(1')	144.6(2)	Ir(1) - Ir(2) - C(2)	150.08(2)	Ir(2) - C(2) - O(2)	idealized 180°	C(31) - P(2) - C(41)	101.0(5)
Ir(2) - Ir(1) - C(1)	143.67(2)	Ir(1) - Ir(2) - C(2')	97.91(2)	Ir(2) - C(2') - O(2')	idealized 180°	C(51) - P(3) - C(61)	100.7(4)
Ir(2) - Ir(1) - Cl(1')	101.50(2)	Ir(1) - Ir(2) - C(3)	47.0(7)	Ir(1) - C(3) - O(3)	138.0(9)	C(71) - P(3) - C(81)	102.0(4)
Ir(2) - Ir(1) - C(3)	47.0(7)	Ir(1) - Ir(2) - P(2)	92.78(8)	Ir(2) - C(3) - O(3)	136.0(9)	P(1) - C(4) - P(2)	110.6(2)
Ir(2) - Ir(1) - P(1)	92.15(8)	Ir(1) - Ir(2) - P(4)	93.1(2)	Ir(1) - P(1) - C(4)	112.2(6)	P(3) - C(4) - P(4)	110.9(3)
Ir(2) - Ir(1) - P(3)	92.08(9)	Cl(2) - Ir(2) - C(2)	114.86(8)	Ir(2) - P(2) - C(4)	109.9(7)	P(1) - C(11)- C(12)	121.6(3)
Cl(1) - Ir(1) - C(1)	118.5(1)	Cl(2')- Ir(2) - C(2')	115.98(2)	Ir(1) - P(3) - C(5)	109.1(8)	P(1) - C(11)- C(16)	118.5(4)
Cl(1) - Ir(1) - C(1')	113.8(2)	Cl(2) - Ir(2) - C(3)	141.9(7)	Ir(2) - P(4) - C(5)	111.0(7)	P(1) - C(21)- C(22)	119.9(3)
Cl(1) - Ir(1) - C(3)	144.5(7)	Cl(2')- Ir(2) - C(3)	99.1(7)	Ir(1) - P(1) - C(11)	113.1(2)	P(1) - C(21)- C(26)	119.8(5)
Cl(1')- Ir(1) - C(3)	97.9(7)	C(2) - Ir(2) - C(3)	103.0(7)	Ir(1) - P(1) - C(21)	120.1(3)	P(2) - C(31)- C(32)	117.0(5)
C(1) - Ir(1) - C(3)	96.8(7)	C(2') - Ir(2) - C(3)	144.8(7)	Ir(2) - P(2) - C(31)	114.1(3)	P(2) - C(31)- C(36)	122.9(4)
C(1') - Ir(1) - C(3)	148.1(6)	P(2) - Ir(2) - P(4)	168.4(3)	Ir(2) - P(2) - C(41)	119.7(3)	P(2) - C(41)- C(42)	120.2(5)
P(1) - Ir(1) - P(3)	168.8(2)	P(2) - Ir(2) - Cl(2)	83.7(1)	Ir(1) - P(3) - C(51)	120.8(3)	P(2) - C(41)- C(46)	119.8(3)
P(1) - Ir(1) - Cl(1)	86.9(2)	P(2) - Ir(2) - Cl(2')	91.1(1)	Ir(1) - P(3) - C(61)	115.9(3)	P(3) - C(51)- C(52)	121.3(3)
P(1) - Ir(1) - Cl(1')	88.3(2)	P(4) - Ir(2) - Cl(2)	85.8(3)	Ir(2) - P(4) - C(71)	111.8(2)	P(3) - C(51)- C(56)	118.7(5)
P(3) - Ir(1) - Cl(1)	82.2(2)	P(4) - Ir(2) - Cl(2')	89.6(2)	Ir(2) - P(4) - C(81)	120.8(3)	P(3) - C(61)- C(62)	121.6(4)
P(3) - Ir(1) - Cl(1')	94.3(2)	P(2) - Ir(2) - C(2)	89.3(1)	C(4) - P(1) - C(11)	102.9(9)	P(3) - C(61)- C(66)	118.0(4)
P(1) - Ir(1) - C(1)	89.27(9)	P(2) - Ir(2) - C(2')	83.0(1)	C(4) - P(1) - C(21)	104.2(8)	P(4) - C(71)- C(72)	123.0(4)
P(1) - Ir(1) - C(1')	87.1(1)	P(4) - Ir(2) - C(2)	90.6(2)	C(4) - P(2) - C(31)	104.8(9)	P(4) - C(71)- C(76)	117.0(5)
P(3) - Ir(1) - C(1)	93.5(1)	P(4) - Ir(2) - C(2')	86.3(3)	C(4) - P(2) - C(41)	106.0(8)	P(4) - C(81)- C(82)	118.4(5)
P(3) - Ir(1) - C(1')	81.9(1)	P(2) - Ir(2) - C(3)	93.8(5)	C(5) - P(3) - C(51)	104.9(11)	P(4) - C(81)- C(86)	121.6(40
P(1) - Ir(1) - C(3)	97.8(5)	P(4) - Ir(2) - C(3)	97.5(6)	C(5) - P(3) - C(61)	103.6(10)		
P(3) - Ir(1) - C(3)	92.7(5)	Ir(1) - C(3) - Ir(2)	85.95(3)	C(5) - P(4) - C(71)	104.5(10)		
Ir(1) - Ir(2) - Cl(2)	95.03(8)	Ir(1) - C(1) - O(1)	idealized 180°	C(5) - P(4) - C(81)	105.3(10)		

(Table 8). Both methylene groups of the DPM ligands are bent away from the bridging CO. The orientation of these CH_2 groups is dictated by the positions of the phenyl groups which are situated such as to minimize contacts with the CO and Cl ligands in the equatorial plane. As noted earlier, the terminal CO positions were idealized while the Cl positions were allowed to vary. All of the resulting Ir-Cl distances (range 2.489(7) - 2.557(9) Å) are reasonable and these, together with the refined occupancy factors and thermal parameters of the CO and Cl ligands, suggest that the positioning of the CO groups was fairly accurate. The bridging carbonyl group is quite typical although the slight elongation of the C(3) thermal ellipsoid parallel to the Ir-Ir vector probably disguises a slight disorder of this group. It is to be expected that the CO parameters trans to another CO should differ slightly compared to those when it is trans to a Cl ligand. It is not unexpected then that the disorder of the terminal CO and Cl groups should result in a slight disorder of the bridging CO group. Nevertheless, only one atom position was observed for each of C(3) and O(3). The Ir-C(3) distances (2.04(3) Å) and the C(3)-O(3) distance (1.20(4)) are normal for such groups and are, as expected, longer than those involving terminal CO groups. The acute Ir(1)-C(3)-Ir(2) angle of 85.95(3)° is typical of bridging CO's when accompanied by a metal-metal bond.[60]

The Ir(1)-Ir(2) distance (2.779(1) Å) is typical for a single bond and is significantly less than that observed in the similar compound $[Ir_2(CO)_2(\mu\text{-}S)(\mu\text{-}CO)(DPM)_2]^{151}$ in which the large bridging sulfide group forces the metals apart somewhat. The metal-metal distance in the present compound is substantially less than the intra ligand P-P distances (av. 2.996(5) Å) indicating compression along the Ir-Ir axis due to the metal-metal interaction.

As indicated, the present structure is disordered in the solid state such that there are two chemically distinct species in approximately a 75:25 ratio, with the minor isomer having all carbonyls mutually cis while in the major isomer one of the terminal carbonyls is trans to the bridging CO and the other is cis to it (see Figures 2 and 3 for views of the two isomers). In the solid state the major isomer is further disordered such that the three contributing structures in the solid state with their percent occupancies are shown below. These structures clearly explain the 50% occupancies of C(1)O(1), C(1)'O(1)', Cl(1) and Cl(1)' and the 75:25 occupancies of C(2)O(2), Cl(2) and their primed counterparts. Chemically, the second and third structures (IV and V) are identical so

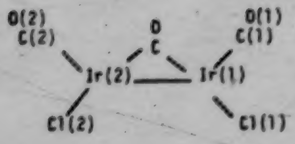

III(25%)

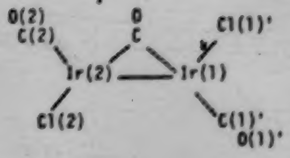

IV(50%)

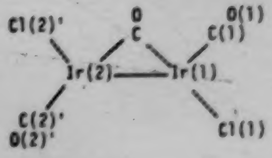

V(25%)

that only two sets of carbonyl bands are observed, one for each isomer. In the infrared spectrum of the solid these are observed in approximately the correct intensity ratios with the CO bands due to the trans isomer more intense than those of the cis isomer, while in CH_2Cl_2 solution their intensities are approximately the same, indicating an equal abundance (vide supra).

Although the terminal carbonyl and chloro ligands are disordered in this structure, this X-ray determination is nevertheless a significant one. It clearly establishes the geometry of the complex and demonstrates in these DPM-bridged complexes the higher coordination that is favoured for Ir over that for Rh. The analogous compound for Rh has only one of the chloride ligands coordinated in the bridging position with the other acts as a Cl^- counter ion. This structure also represents the first reported for which the $Ir_2(DPM)_2$ framework has a bridging equatorial ligand and two terminal ligands on each metal and therefore supports the formulation proposed for the tetracarbonyl complex **1**[41,150] and also those proposed for a series of analogous isocyanide adducts.[41] In addition, the disorder which plagued the structural determination did prove beneficial in explaining the spectral parameters observed for compounds **2a** and **2b**.

Conclusions

We have now clearly established the identities of a series of neutral and cationic binuclear chloro-carbonyl complexes of iridium and have developed reasonable synthetic routes to these complexes. Although there are many close analogies to the Rh-DPM chemistry, there are also significant differences related to the higher basicity of the Ir atoms compared to Rh, causing the Ir complexes to bind CO more strongly. This latter tendency suggests an even richer chemistry of these complexes with small molecules than was observed for the Rh system, the study of which will be dealt with further in subsequent chapters.

CHAPTER 3

NEUTRAL AND CATIONIC ALKYNE-BRIDGED COMPLEXES OF IRIDIUM AND THE STRUCTURE OF $[Ir_2Cl_2(CO)_2(\mu\text{-}CH_3O_2CC_2CO_2CH_3)(Ph_2PCH_2PPh_2)_2]$.

Introduction

As described previously in Chapter 1, one of the important steps in olefin and acetylene hydrogenation by transition metal complexes involves coordination of the unsaturated molecule to the metal centre. In order to develop the analogous chemistry with binuclear complexes, it is important to examine how such molecules interact with two metal centres. Alkynes were chosen for this study because of their well established chemistry with binuclear DPM complexes of other metals.[42,44,66,68,69] The chemistry of DPM-bridged binuclear complexes of rhodium had previously been thoroughly investigated in this group. In all cases, the alkyne molecule was found to bridge the two metal centres parallel to the metal-metal axis, in what is often referred to as a cis-dimetallated olefin geometry (see equations (1) and (2), below). This in contrast to an

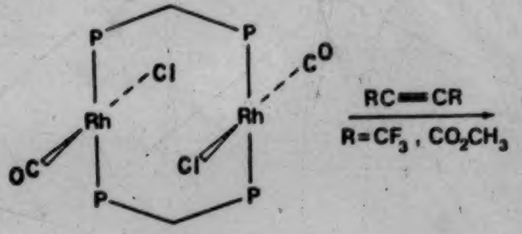
RC≡CR
R=CF$_3$, CO$_2$CH$_3$

(1)

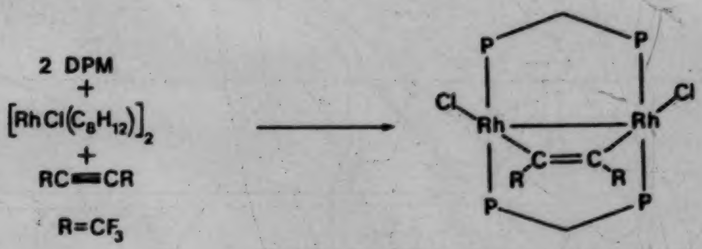
2 DPM
[RhCl(C$_8$H$_{12}$)]$_2$
RC≡CR
R=CF$_3$

(2)

analogous DAM-bridged cobalt species (DAM = $Ph_2AsCH_2AsPh_2$)[169] in which the alkyne molecule binds perpendicular to the Co-Co bond in a pseudo-tetrahedral geometry (see equation (3) below).

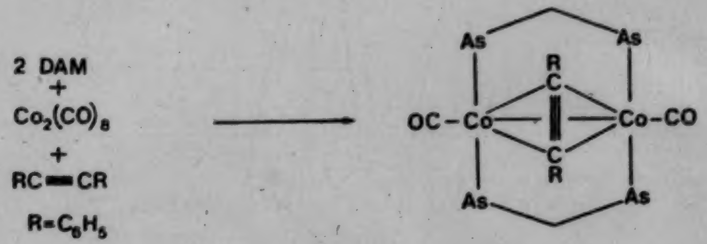
2 DAM
Co$_2$(CO)$_8$
RC≡CR
R=C$_6$H$_5$

(3)

It was of interest to establish whether the same bonding patterns would be observed for Ir or whether new bonding modes might be observed. It was also of interest to see what relevance, if any, these complexes might have to alkyne hydrogenation.

Experimental Section

The general experimental conditions and techniques are given in Chapter Two. Hexafluoro-2-butyne (HFB) was purchased from PCR and used as received. Dimethylacetylene dicarboxylate (DMA) was purchased from Aldrich and used without further purification.

Preparation of Compounds

(a) $[Ir_2Cl_2(CO)_2(\mu\text{-DMA})(DPM)_2].2CH_2Cl_2$ (**6**).

The addition of 15.2 μL (0.16 mmol) of dimethylacetylene dicarboxylate (DMA) to 200 mg (0.16 mmol) of $[IrCl(CO)(DPM)]_2$ (**3**), dissolved in 20 mL of CH_2Cl_2, produced an immediate colour change from purple to light yellow. The solution was stirred for an additional ½ h during which time no further changes were observed. The volume was reduced to 10 mL under N_2 and 10 mL of diethyl ether was slowly added. The solution was placed in the freezer overnight resulting in the precipitation of **6** as a crop of pale yellow prisms. The solid was collected and washed with two 10 mL portions of ether and then dried in vacuo for 2 h. Typical isolated yields were 90%. Compound **6** was determined to be a non-electrolyte in CH_2Cl_2 solutions. ($\Lambda(10^{-3}M) < 0.5\ \Omega^{-1}\ cm^2\ mole^{-1}$).[170]

Spectroscopic parameters for this and all subsequent compounds are given in Tables 9 and 10.

Anal. Calcd for $Ir_2Cl_6P_4O_6C_{60}H_{54}$: C, 45.27%; H, 3.42%; Cl, 13.36%. Found: C, 45.17%; H, 2.89%; Cl,13.16%.

(b) $[Ir_2Cl_2(CO)_2(\mu\text{-HFB})(DPM)_2] \cdot 2CH_2Cl_2$ (7).

200 mg(0.16 mmol) of $[IrCl(CO)(DPM)]_2$ was placed in a 100 mL 3 neck flask which was evacuated and then charged with one atmosphere of hexafluoro-2-butyne (HFB). 15 mL of CH_2Cl_2 was added to the flask and the resulting solution was stirred under the HFB atmosphere for ½ h during which time the colour changed from purple to yellow. The volume was concentrated to ca. 5 mL under N_2 and the flask was placed in the freezer for 48 h during which time a light yellow crystalline solid separated from the solution. The precipitate was collected and washed with two 10 mL portions of ether and dried in vacuo for 2 h. Typical isolated yields were 75-80%. Essentially quantitative yields were obtained when the solution was taken completely to dryness under N_2, however this gave (7) as a glassy yellow solid. Conductivity measurements on a CH_2Cl_2 solution of the crystalline material showed it to be non-conducting ($\Lambda(10^{-3}M) < 0.5\Omega^{-1}\ cm^2\ mole^{-1}$).

Anal. Calcd for $Ir_2Cl_6P_4F_6O_2C_{58}H_{48}$: C, 43.21%; H, 3.00%. Found: C, 43.21%; H, 3.02%. The presence and amounts of

Table 9. Infrared Stretching Frequencies for the Compounds of Chapter Three.

		ν(CO), cm^{-1}		
	Compound	solid[a]	solution[b]	other, cm^{-1}
6	$[Ir_2Cl_2(CO)_2(\mu\text{-DMA})(DPM)_2]$	2023(s),1999(s)	2044(s),2005(m)	1549(w)[c];1653(m),1674(m)[d]
7	$[Ir_2Cl_2(CO)_2(\mu\text{-HFB})(DPM)_2]$	2024(s)	2021(s)	1549(w)[c]
8	$[Ir_2Cl_2(CO)_2(\mu\text{-HC}_2\text{H})(DPM)_2]$	1977(s),1968(s)	1982(br,s)	1533(w)[c]
9	$[Ir_2Cl_2(CO)(\mu\text{-DMA})(DPM)_2]$	2004(s)	2009(s)	1554(w)[c];1696(m),1674(m)[d]
10	$[Ir_2Cl_2(CO)(\mu\text{-HFB})(DPM)_2]$	2009(s),1988(m)	e	
11	$[Ir_2Cl(CO)_2(\mu\text{-DMA})(DPM)_2][BF_4]$	2025(s),1982(s)	2039(s,br)	1538(w)[c];1708(m),1691(m)[d]
12	$[Ir_2Cl(CO)_2(\mu\text{-HFB})(DPM)_2][BF_4]$	2045(s),2033(s)	2048(m),2036(s),2004(m)	1565(w)[c]
13	$[Ir_2Cl(CO)_3(\mu\text{-DMA})(DPM)_2][BF_4]$	2085(s),2040(sh),2038(s)	2070(s),2057(s),2029(s)	1572(w)[c];1699(m),1712[d]
14	$[Ir_2Cl(CO)_3(\mu\text{-HFB})(DPM)_2][BF_4]$	2075(m),2049(s),2038(s)	2091(m),2053(br,s)	1562(w)[c]
15	$[Ir_2Cl(CO)_2(\mu\text{-DMA})(DPM)_2][BF_4]$	2095(s),2055(s)	f	1559(w)[c];1702(m),1679(m)[d]
16	$[Ir_2Cl(CO)_2(\mu\text{-HFB})(DPM)_2][BF_4]$	2091(s),2054(s)	f	1573(w)[c]

---

a) Nujol mull. b) CH_2Cl_2 solution. c) ν(C=C) of coordinated alkyne. d) ν(C=O) of CO_2CH_3. e) insoluble in CH_2Cl_2. f) reacted with NaCl cells. g) Abbreviations used: s = strong, m = medium, w = weak, sh = shoulder, br = broad.

Table 10. NMR Spectral Results for the Compounds of Chapter Three.

	Compound	$^{31}P(^{1}H)$[a] δ,ppm	^{1}H[b] δ,ppm(CH_3)	^{19}F[c] δ,ppm
6	$[Ir_2Cl_2(CO)_2(\mu\text{-DMA})(DPM)_2]$	-27.4(m),-29.5(m)[h]	2.80(s),3.24(s)	
7	$[Ir_2Cl_2(CO)_2(\mu\text{-HFB})(DPM)_2]$	-26.9(m),-34.7(m)		-48.23(q),-54.42(q)
8	$[Ir_2Cl_2(CO)_2(\mu\text{-HC}_2\text{H})(DPM)_2]$	-22.4(m),-25.4(m)	6.13(s),6.52(s)	
9	$[Ir_2Cl_2(CO)(\mu\text{-DMA})(DPM)_2]$	+6.1(m), -29.8(m)	2.18(s),2.75(s)	
10	$[Ir_2Cl_2(CO)(\mu\text{-HFB})(DPM)_2]$	g		
11	$[Ir_2Cl(CO)_2(\mu\text{-DMA})(DPM)_2][BF_4]$	+ 9.6(m),-22.7(m)	2.19(s),2.65(s)[e]	
12	$[Ir_2Cl(CO)_2(\mu\text{-HFB})(DPM)_2][BF_4]$	+ 5.4(m),-28.1(m),-14.9(s)		-48.16(q),-52.47(q)[f] -51.24(s)
13	$[Ir_2Cl(CO)_3(\mu\text{-DMA})(DPM)_2][BF_4]$	-29.9(m)[d]	2.67(s),3.52(s)[d] 2.27(s),3.47(s)[c]	
14	$[Ir_2Cl(CO)_3(\mu\text{-HFB})(DPM)_2][BF_4]$	-34.5(m),-37.5(m)		-51.50(q), -54.55(q)
15	$[Ir_2(CO)_2Cl(\mu\text{-DMA})(DPM)_2][BF_4]$	+ 1.9(m),-29.9(m)	2.96(s),2.28(s)[e]	
16	$[Ir_2(CO)_2Cl(\mu\text{-HFB})(DPM)_2][BF_4]$	+ 5.4(m),-28.1(m)		-46.60(q),-47.61(q)

---

a) *vs* 85% H_3PO_4, -40°C. b) phenyl H's typically occurred from δ = 6.5 to 7.5 ppm and DPM methylene H's typically occurred from δ = 3.5 to 5.0 ppm. c) *vs* external $CFCl_3$, room temp. d) room temperature. e) -60°C. f) -40°C. g) insoluble. h) Abbreviations used: m = multiplet, s = singlet, q = quartet.

solvent molecules in this and other complexes were verified by ^1H NMR spectroscopy whenever possible.

(c) $[Ir_2Cl_2(CO)_2(\mu\text{-}HC_2H)(DPM)_2] \cdot 0.5\ CH_2Cl_2$ **(8)**.

The preparation of compound **8** was carried out as described above for **7** except that acetylene (C_2H_2) was used instead of HFB. The initial crude product obtained in this manner was purified (as determined by $^{31}P\{^1H\}$ NMR) by several recrystallizations from CH_2Cl_2/ether. Typical isolated yields were 70-75% of a pale yellow microcrystalline solid. A CH_2Cl_2 solution of the solid proved to be a non-conducting ($\Lambda(10^{-3}\ M) < 0.5\ \Omega^{-1}\ cm^2\ mole^{-1}$). Anal. Calcd for $Ir_2Cl_3P_4O_2C_{54.5}H_{47}$: C, 48.54%; H, 3.51%; Cl, 7.89%. Found: C, 48.08%; H, 3.64%; Cl: 7.75%.

(d) $[Ir_2Cl_2(CO)(\mu\text{-}DMA)(\mu\text{-}DPM)_2].2CH_2Cl_2$ **(9)**.

200 mg (0.13 mmol) of compound **6** was suspended in 10 mL toluene and refluxed under a slow N_2 stream for 12 h during which time a light purple powder precipitated from solution. The resulting suspension was cooled in an ice bath and the colourless mother liquor was removed. The residue was dried first under an N_2 stream and then under vacuum. Recrystallization from CH_2Cl_2 and ether yielded a crop of dark purple needles. Typical isolated yields were 90-95%. When dissolved in CH_2Cl_2, compound **9** proved to be non-conducting ($\Lambda_m(10^{-3}M) < 0.5\ \Omega^{-1}\ cm^2\ mole^{-1}$).

Anal. Calcd for $Ir_2Cl_6P_4OC_{59}H_{54}$: C, 45.31%; H, 3.48%. Found: C, 45.53%; H, 3.50%.

(e) $[Ir_2Cl_2(CO)(\mu\text{-HFB})_2(DPM)_2]\cdot\frac{1}{2}\,C_7H_8$ (10).

The reaction was carried out the same as described for **9** except that **7** was used instead of **6**. The purple solid obtained from the refluxed toluene solution proved to be highly insoluble in all common solvents making purification and subsequent characteriztion difficult. Typical isolated yields were about 80%.

Anal. Calcd for $Ir_2Cl_2P_4OC_{58.5}H_{48}$: C, 48.10%; H, 3.35%. Found: C, 48.44%; H, 3.27%.

(f) $[Ir_2Cl(CO)_2(\mu\text{-DMA})(DPM)_2][BF_4]$ (isomer 1) (11).

To a slurry of 250 mg (0.16 mmol) of **6** in 10 mL of THF was added dropwise one equivalent of $AgBF_4$ (34.2 mg, 0.16 mmol) dissolved in 2 mL THF. The solution immediately changed from light yellow to dark orange and an orange precipitate appeared. Complete precipitation was induced by the addition of 30 mL of diethyl ether. The solid was collected and dried under an N_2 stream. The resulting residue was redissolved in 10 mL of CH_2Cl_2 and filtered under dinitrogen. The addition of ether yielded a red-orange microcrystalline product in approximately 90% yield. Compound **11** was determined to be 1:1 electrolyte in CH_2Cl_2 solutions ($\Lambda(10^{-3}M) = 56.6\ \Omega^{-1}\ cm^2\ mole^{-1}$).

Anal. Calcd for $Ir_2ClP_4F_4O_2C_{58}BH_{50}$: C, 47.27%; H, 3.42%; Cl, 2.41%. Found: C, 46.78%; H, 3.44%; Cl, 2.39%.

(g) $[Ir_2Cl(CO)_2(\mu\text{-HFB})(DPM)_2][BF_4]$ (isomer 1) (**12**).

The reaction was carried out as described above for **11**, except that 180 mg (0.11 mmol) of **7** was used along with 24.7 mg (0.11 mmol) of $AgBF_4$. The resulting light orange microcrystalline product was obtained in approximately 90-95% yield. Conductivity measurements of this solid in CH_2Cl_2 indicated that it was a 1:1 electrolyte ($\Lambda(10^{-3}M) = 44.2\ \Omega^{-1}\ cm^2\ mole^{-1}$). Anal. Calcd. for $Ir_2ClP_4F_{10}O_2C_{56}BH_{52}$: C, 45.04%; H, 2.97%. Found: C, 44.98%; H, 3.11%.

(h) $[Ir_2Cl(CO)_3(\mu\text{-DMA})(DPM)_2][BF_4].CH_2Cl_2$ (**13**).

Method A: An atmosphere of carbon monoxide was placed over a solution of 200 mg (0.14 mmol) of **11** in 10 mL of CH_2Cl_2 resulting in an immediate colour change from dark orange to pale yellow. The addition of 20 mL of diethyl ether resulted in the precipitation of a white microcrystalline solid which was collected and dried under a stream of CO. Typical isolated yields were 90-95%. Conductivity measurements on a CH_2Cl_2 solution of this solid showed it to be a 1:1 electrolyte ($\Lambda(10^{-3}M) = 55.7\ \Omega^{-1}\ cm^2\ mole^{-1}$).

Anal. Calcd for $Ir_2Cl_3P_4F_4O_3C_{60}BH_{52}$: C, 45.42%; H, 3.30%; Cl, 6.70%. Found: C, 45.32%; H, 3.31%; Cl, 6.69%.

(i) $[Ir_2Cl(CO)_3(\mu\text{-}HFB)(DPM)_2][BF_4]$ (14).

Method A: Compound **14** was prepared by the same procedure described for **13** except that **12** was used instead of **11**. The reaction produced a white microcrystalline solid in 90-95% yield. Compound **14** was determined to be a 1:1 electrolyte in CH_2Cl_2 solutions ($\Lambda(10^{-3}M) = 47.7\ \Omega^{-1}\ cm^2\ mole^{-1}$).

Anal. Calcd for $Ir_2ClP_4F_{10}O_3C_{57}BH_{44}$: C, 44.99%; H, 2.91%. Found: C, 44.71%; H, 2.95%.

(j) $[Ir_2Cl(CO)_2(\mu\text{-}DMA)(DPM)_2][BF_4]$ (isomer 2) (15).

To a solution of 100 mg of $[Ir_2(CO)_2(\mu\text{-}Cl)(DPM)_2][BF_4]$ (0.075 mmol) in 10 mL of CH_2Cl_2 at -78°C, was added one equivalent of DMA (7.4 μL, 0.075 mmol) producing a rapid colour change from dark red-orange to purple. The solution was stirred for 5 min and then 30 mL of diethyl ether was added resulting in the precipitation of a dark purple solid. The solid was collected and washed with two 10 mL portions of ether at room temperature and then dried in vacuo for 2 h. Typical isolated yields were 90-95%. Compound **15** was shown to be a 1:1 electrolyte in CH_2Cl_2 solutions ($\Lambda(10^{-3}M) = 49.8\ \Omega^{-1}\ cm^2\ mole^{-1}$).

Anal. Calcd for $Ir_2ClP_4F_4O_2C_{58}BH_{50}$: C, 47.27%; H, 3.42%; Cl, 2.41%. Found: C, 47.52%; H, 3.44%; Cl, 2.50%.

(k) $[Ir_2Cl(CO)_2(\mu\text{-HFB})(DPM)_2][BF_4]$ (isomer 2) (**16**).

100 mg $[Ir_2(CO)_2(\mu\text{-Cl})(DPM)_2][BF_4]$ (0.075 mmol) was placed in a 3-neck flask which was evacuated and then filled with one atmosphere of HFB. 10 mL of CH_2Cl_2 was then added and the resulting solution stirred under the HFB atmosphere for 15 min during which time the solution colour changed from dark red-orange to purple. The HFB atmosphere was replaced with N_2 and the volume reduced to 5 mL. 20 mL of diethyl ether was added resulting in the precipitation of a dark purple solid in 90-95% yield. The solid was collected and washed with diethyl ether and dried in vacuo for 2h. Conductivity measurements on a CH_2Cl_2 solution of **16** showed it to be a 1:1 electrolyte ($\Lambda_m(10^{-3}M) = 52.3\ \Omega^{-1}$ cm^2 $mole^{-1}$).

Anal. Calcd for $Ir_2ClP_4O_2F_{10}C_{56}BH_{44}$: C, 45.04%; H, 2.97%. Found: C, 45.01%; H, 3.15%.

(l) $[Ir_2Cl(CO)_3(\mu\text{-DMA})(DPM)_2][BF_4]\cdot CH_2Cl_2$ (**10**)

Method B: An atmosphere of carbon monoxide was placed over a solution of 200 mg (0.14 mmol) of **15** in 10 mL of CH_2Cl_2 resulting in an immediate colour change from dark purple to pale yellow. The addition of 20 mL of diethyl ether resulted in the precipitation of a white microcrystalline solid. The solid was collected and dried under a stream of CO. The product obtained from this reaction was indistinguishable in all of its physical properties to that obtained from Method A. Typical yields were 90-95%.

(m) $[Ir_2Cl(CO)_3(\mu\text{-HFB})(DPM)_2][BF_4]$ (**14**)

Method B: The procedure used was identical to that described above for **13** except that **16** was used instead of **15**. The reaction produced a white microcrystalline solid in 90-95% yield which was indistinguishable in all of its physical properties to that obtained from Method A.

Attempted Reactions

Attempted Reactions of $[IrCl(CO)(DPM)]_2$ (3) and $[Ir_2(CO)_2(\mu\text{-}Cl)(DPM)_2][BF_4]$ (5) with $CH_3C{\equiv}CCH_3$.

To a solution of $[IrCl(CO)(DPM)]_2$ (3) (200 mg, 0.16 mmol) in 15 mL of CH_2Cl_2 was added an excess of 2-butyne (50 μL, mmol). The resulting solution was stirred for 3 h with no apparent colour change. Examination of the infrared and $^{31}P\{^1H\}$ NMR spectra indicated that no reaction had taken place. The solution was then refluxed for 2 h after which time the infrared and $^{31}P\{^1H\}$ NMR spectra showed only starting material. Similar results were obtained using $[Ir_2(CO)_2(\mu\text{-}Cl)(DPM)_2][BF_4]$ (5) instead of (3).

Attempted Reaction of $[Ir_2(CO)_2(\mu\text{-}Cl)(DPM)_2][BF_4]$ (5) with HC_2H.

200 mg (0.15 mmol) was placed in a 100 mL 3 neck flask which was evacuated and then charged with one atmosphere of acetylene. 15 mL of CH_2Cl_2 was added to the flask and immediately produced a dark brown-black solution. This solution was stirred under the acetylene atmosphere for ½ h during which time no further changes were observed. The solvent was removed under vacuum leaving a dark brown glassy solid. A $^{31}P\{^1H\}$ NMR spectrum of this solid showed it to contain at least 3 major species and a number of minor ones. No attempts were made to separate and identify these products.

Attempted Reactions of Alkyne Complexes with H_2.

In a typical reaction 200 mg of compound was placed in a 100 mL 3 neck flask which was evacuated and then charged with one atmosphere of H_2. 10 mL of CH_2Cl_2 was then added to the flask. The reaction mixture was allowed to stir for 24 h and then the solution was analyzed by $^{31}P\{^1H\}$ NMR. The results can be broken down into two categories:

1) with the saturated complexes 3 and 4 no reaction was

observed; 2) with the coordinatively unsaturated species 8 and 9 complex mixtures occurred containing at least 5 major species including starting material. Attempts to separate and isolate these compounds were unsuccessful and so no further effort was made to identify these products.

X-Ray Data Collection

Crystals of $[Ir_2Cl_2(CO)_2(\mu\text{-DMA})(DPM)_2].2CH_2Cl_2$ (**6**) of suitable quality for an X-ray study, were obtained by the slow diffusion of diethyl ether into a saturated CH_2Cl_2 solution of the title complex. A light yellow prism was mounted on a glass fibre in the air and coated with shellac.

Preliminary film data showed $\bar{1}$ Laue symmetry and no systematic absences, consistent with the space groups P1 and $P\bar{1}$. The centrosymmetric space group was chosen and later verified by the successful refinement of the structure with acceptable positional parameters, thermal parameters and agreement indices. Accurate cell parameters were obtained by a least-squares refinement of the setting angles of 12 carefully centred reflections chosen from diverse regions of reciprocal space ($50° < 2\theta < 60°$, CuKα radiation) and obtained by using a narrow X-ray source. A cell reduction[171] failed to show the presence of higher symmetry. The reduced cell is reported.

Data were collected on a Picker four-circle automated diffractometer equipped with a scintillation counter and pulse-height analyzer, tuned to accept 90% of the CuKα peak. Background counts were measured at both ends of the scan range with stationary crystal and counter. The intensities of three standard reflections were measured every 100 reflections and four additional standards were measured three times a day. No significant variation in the intensities of the standards was noted during data collection so no corrections were applied.

The intensities of 9864 reflections ($3° < 2\theta < 121°$) were measured by using Ni-filtered CuKα radiation. Data were processed in the usual manner with a value of 0.04 for p^{153}. Of these, 7796 were unique and had $F_o^2 > 3\sigma(F_o^2)$; these were used in subsequent calculations. Absorption corrections were applied to the data by using Gaussian integration.[172] See Table 11 for pertinent crystal data and details of data collection.

Structure Solution and Refinement

The positions of the two independent Ir atoms were obtained from a sharpened Patterson synthesis. Subsequent refinements and difference Fourier calculations led to the location of all other atoms. Atomic scattering factors were taken from Cromer and Waber's tabulation[155] for all

Table 11. Summary of Crystal Data and Intensity Collection Details for $[Ir_2Cl_2(CO)_2(\mu\text{-DMA})(DPM)_2]\cdot 2CH_2Cl_2$.

compd	$[Ir_2Cl_2(CO)_2(\mu\text{-DMA})(DPM)_2].2CH_2Cl_2$
formula	$Ir_2Cl_6P_4O_6C_{60}H_{54}$
formula wt	1580.07 g/mole
cell parameters	
a, Å	11.880(2)
b, Å	23.514(3)
c, Å	11.689(1)
α, deg	95.429(9)
β, deg	110.389(9)
γ, deg	77.999(10)
Z	2
V, $Å^3$	2992.93
space group	C_i^1 - $P\bar{1}$
crystal shape	triclinic prism with faces of the form {100}, {010} , $\{11\bar{3}\}$, {011}
crystal dimens, mm	0.356 x 0.096 x 0.396
crystal vol, mm^3	6.55×10^{-3}
temp, °C	23
radiation	CuKα (λ 1.540562 Å) filtered with 0.5 mil nickel foil
μ, cm^{-1}	122.914
range in abs corr factors (as applied to Fo^2)	0.116 to 0.383
receiving aperature	4mm x 4 mm, 30 cm from crystal
takeoff angle, deg	3.4°
scan speed	2° in 2θ/min
scan range	0.6° below $K\alpha_1$ to 0.6° above $K\alpha_2$
bkgd counting time, s	10 ($3° < 2\theta \le 99.4°$), 20($99.4° < 2\theta \le 121.0°$)
2θ limits	$3.0° < 2\theta \le 121.0°$

(continued...)

Table 11. (continued)

final no. of variables	367
data collected	$\pm h, \pm k, \ell$; 9868
unique data used $(Fo^2 \geq 3\sigma (Fo^2)$	7796
error in observn of unit wt	1.588
R	0.037
R_ω	0.067

atoms except hydrogen, for which the values of Stewart et al[156] were used. Anomalous dispersion[157] terms for Ir, Cl and P were included in F_c. The carbon atoms of all phenyl rings were refined as rigid groups having D_{6h} symmetry, C-C distances of 1.392 Å, and independent isotropic thermal parameters. All hydrogen atoms of the DPM ligands were located and included as fixed contributions in the least-squares refinements but were not themselves refined. Their idealized positions were calculated from the geometries about their attached carbon atoms using C-H distances of 0.95 Å. Hydrogen atoms were assigned isotropic thermal parameters of 1 $Å^2$ greater than the isotropic thermal parameter (or equivalent isotropic thermal parameter of anisotropic atoms) of their attached carbons. The positions of the methylcarboxylate hydrogen atoms were not clearly defined; only a smear of electron density was observed in their approximate locations. No attempt was made to resolve these atom positions.

The final model in the space group $P\bar{1}$ with 367 parameters refined converged to R = 0.037 and R_w = 0.067[158]. In the final difference Fourier map, the 20 highest residuals (0.72 - 0.36 e/$Å^3$) were in the vicinity of the iridium atoms and the alkyne methyl carbons. A typical carbon on an earlier synthesis had an electron density of about 7-8 e/$Å^3$. The final positional parameters of the group and non-hydrogen atoms are given in Tables 12 and 13. The derived hydrogen position and thermal parameters are listed in Table 14. A listing of the observed and calculated structure amplitudes are available.[159]

Description of Structure of $[Ir_2Cl_2(CO)_2(\mu\text{-DMA})(DPM)_2].2CH_2Cl_2$ (6)

The title complex crystallizes in the space group $P\bar{1}$ with two complex molecules and four solvent CH_2Cl_2 molecules in the unit cell; all are well separated with no unusually short contacts between them. Both independent solvent molecules are crystallographically well behaved and display the expected geometry. A perspective view of the complex, including the numbering scheme is shown in Figure 4 (phenyl hydrogens have the same number as their attached carbon atom). A view of the approximate plane of the metals and the bridging alkyne group is shown in Figure 5 along with some relevent bond lengths and angles.

The overall geometry of the complex is essentially as expected for a binuclear species bridged by two mutually trans DPM ligands. Within the DPM framework, the bond lengths and angles are all normal (Tables 15 and 16, respectively) and similar to those found in other DPM-

Table 12. Positional and Anisotropic Thermal Parameters for the Non-group Atoms of $[Ir_2Cl_2(CO)_2(\mu\text{-DMA})(DPM)_2]\cdot 2CH_2Cl_2$.

Atom	x[a]	y	z	U11[b]	U22	U33	U12	U13	U23
Ir(1)	0.17707(2)	0.228630(10)	0.34596(2)	2.937(14)	3.136(15)	2.597(15)	-0.043(10)	0.963(11)	0.366(10)
Ir(2)	-0.06276(2)	0.261175(10)	0.19192(2)	2.852(14)	2.840(14)	2.457(15)	-0.448(10)	0.876(10)	0.105(10)
Cl(1)	0.12724(16)	0.20209(7)	0.51861(14)	6.07(10)	5.56(9)	3.30(8)	-1.54(8)	1.95(7)	0.46(7)
Cl(2)	-0.26575(13)	0.30123(7)	0.03732(15)	3.54(7)	4.74(9)	4.32(9)	-0.62(7)	-0.00(7)	0.46(7)
Cl(3)	0.4026(3)	0.45110(13)	0.8755(3)	8.58(18)	9.55(19)	18.0(3)	-0.69(15)	5.7(2)	-1.9(2)
Cl(4)	0.5735(4)	0.43022(15)	0.7488(4)	15.2(3)	11.7(3)	17.0(3)	-2.9(2)	8.7(3)	2.5(2)
Cl(5)	0.4678(4)	0.1277(2)	0.7418(3)	17.1(4)	21.7(4)	10.3(3)	-7.0(3)	3.3(3)	1.9(3)
Cl(6)	0.3057(4)	0.08954(15)	0.8380(4)	17.5(4)	10.0(2)	16.1(3)	-1.7(2)	8.2(3)	-0.2(2)
P(1)	0.18086(15)	0.13363(7)	0.26449(15)	4.72(9)	3.18(8)	3.79(9)	-0.02(7)	1.92(7)	0.40(7)
P(2)	-0.04915(14)	0.17884(6)	0.06282(14)	4.54(8)	3.15(8)	2.99(8)	-0.80(7)	1.55(7)	-0.24(6)
P(3)	0.17675(13)	0.32093(6)	0.44948(14)	2.79(7)	3.74(8)	2.99(8)	-0.44(6)	0.88(6)	-0.05(6)
P(4)	-0.09078(13)	0.34796(6)	0.30325(13)	2.81(7)	3.12(7)	3.11(8)	-0.26(6)	1.01(6)	-0.00(6)
O(1)	0.4518(4)	0.2058(2)	0.4581(5)	3.8(3)	7.1(3)	6.3(4)	0.4(2)	1.1(2)	0.1(3)
O(2)	-0.1870(5)	0.2115(2)	0.3356(5)	6.9(3)	6.0(3)	5.0(3)	-1.7(3)	3.4(3)	0.3(2)
O(3)	0.2957(4)	0.2170(2)	0.0646(4)	5.4(3)	6.6(3)	4.7(3)	-1.4(2)	2.8(2)	-1.2(3)
O(4)	0.1208(4)	0.3386(2)	-0.0050(5)	5.1(3)	6.8(3)	6.0(3)	-1.4(3)	1.9(3)	2.6(3)
O(5)	0.3754(4)	0.2738(2)	0.2243(4)	3.9(3)	6.7(3)	5.5(3)	-1.5(2)	2.3(2)	-1.7(3)
O(6)	-0.0649(4)	0.31519(19)	-0.0801(4)	4.9(3)	5.8(3)	2.8(2)	-1.2(2)	0.5(2)	1.1(2)
C(1)	0.3490(6)	0.2133(3)	0.4196(6)	4.8(4)	3.9(3)	2.7(3)	-0.2(3)	1.4(3)	0.4(3)
C(2)	-0.1401(5)	0.2301(3)	0.2807(6)	3.6(3)	3.5(3)	3.5(4)	-0.2(3)	1.1(3)	-0.0(3)
C(3)	0.1061(6)	0.1367(3)	0.1010(6)	5.5(4)	3.4(3)	4.0(4)	-0.9(3)	2.4(3)	-0.5(3)
C(4)	0.0235(5)	0.3467(3)	0.4554(5)	3.3(3)	3.8(3)	3.5(3)	-0.1(3)	1.6(3)	-0.0(3)
C(5)	0.1745(5)	0.2591(2)	0.1861(5)	3.5(3)	3.0(3)	2.7(3)	-0.6(2)	1.1(3)	0.0(2)
C(6)	0.0613(5)	0.2834(2)	0.1160(5)	3.6(3)	3.3(3)	3.4(3)	-1.2(3)	1.6(3)	-0.5(3)
C(7)	0.2849(5)	0.2489(3)	0.1502(6)	3.7(3)	3.9(3)	3.9(4)	-0.1(3)	2.0(3)	0.7(3)
C(8)	0.0448(6)	0.3143(3)	0.0064(6)	4.2(3)	4.1(3)	3.3(3)	-0.4(3)	1.5(3)	0.9(3)
C(9)	0.4917(7)	0.2582(4)	0.2018(10)	4.4(5)	11.1(7)	11.4(8)	-2.5(5)	4.7(5)	-2.6(6)
C(10)	-0.0871(8)	0.3446(4)	-0.1905(7)	7.6(6)	9.2(6)	3.5(4)	-0.5(5)	0.4(4)	2.7(4)
C(D1)	0.5540(9)	0.4306(4)	0.8891(10)	7.6(6)	7.1(6)	11.4(9)	-0.3(5)	2.2(6)	0.3(6)
C(D2)	0.3456(12)	0.1475(5)	0.8011(11)	11.9(9)	10.7(9)	9.1(8)	-0.9(7)	1.5(7)	1.5(7)

[a] Estimated standard deviations in the least signicant figure(s) are given in parentheses in this and all subsequent tables.

[b] The form of the thermal ellipsoid is: exp[-2*PI'(a*'U11h'+b*'U22k'+c*'U33l'+2a*b*U12hk+2a*c*U13hl+2b*c*U23kl)]. The quantities given in the table are the thermal coefficients x 10'.

Table 13. Derived Parameters for the Rigid-Group Atoms of $[Ir_2Cl_2(CO)_2(\mu\text{-DMA})(DPM)_2]\cdot 2CH_2Cl_2$.

Atom	x[a]	y	z	B(A^2)	Atom	x	y	z	B(A^2)
C(11)	0.3364(4)	0.0960(5)	0.292(3)	3.92(13)	C(51)	0.274(3)	0.3139(3)	0.610(3)	2.75(10)
C(12)	0.390(2)	0.0845(5)	0.2014(16)	6.1(2)	C(52)	0.2271(9)	0.3113(3)	0.7025(5)	3.58(12)
C(13)	0.513(2)	0.0582(5)	0.2313(14)	9.0(3)	C(53)	0.306(3)	0.3018(5)	0.822(3)	4.78(16)
C(14)	0.5816(4)	0.0433(5)	0.351(3)	8.2(3)	C(54)	0.432(3)	0.2949(3)	0.849(3)	4.81(15)
C(15)	0.528(2)	0.0548(5)	0.4417(16)	7.0(2)	C(55)	0.4785(9)	0.2974(3)	0.7558(5)	4.26(14)
C(16)	0.405(2)	0.0811(5)	0.4119(14)	5.19(17)	C(56)	0.400(3)	0.3069(5)	0.636(3)	3.51(12)
C(21)	0.1169(5)	0.07750(19)	0.3066(5)	3.44(12)	C(61)	0.2162(4)	0.38545(16)	0.4086(4)	2.74(10)
C(22)	0.0194(5)	0.09122(16)	0.3506(5)	4.24(14)	C(62)	0.2073(4)	0.39423(16)	0.2894(4)	3.31(11)
C(23)	-0.0369(4)	0.0474(2)	0.3653(3)	5.74(19)	C(63)	0.2243(4)	0.44685(18)	0.2588(3)	4.40(14)
C(24)	0.0042(5)	-0.01006(19)	0.3361(5)	6.4(2)	C(64)	0.2501(4)	0.49070(16)	0.3474(4)	4.58(15)
C(25)	0.1017(5)	-0.02377(16)	0.2921(5)	6.4(2)	C(65)	0.2590(4)	0.48193(16)	0.4666(4)	4.72(15)
C(26)	0.1580(4)	0.0200(2)	0.2774(3)	4.88(16)	C(66)	0.2420(4)	0.42931(18)	0.4972(3)	3.56(12)
C(31)	-0.1491(4)	0.12787(19)	0.0590(4)	3.23(11)	C(71)	-0.2322(4)	0.3631(2)	0.3418(6)	2.66(10)
C(32)	-0.2641(4)	0.15062(15)	0.0671(5)	3.96(13)	C(72)	-0.2347(5)	0.3409(3)	0.4470(5)	3.72(13)
C(33)	-0.3466(3)	0.1141(2)	0.0529(3)	5.02(16)	C(73)	-0.3416(8)	0.3533(3)	0.4760(6)	4.66(15)
C(34)	-0.3142(4)	0.05478(19)	0.0307(4)	5.58(18)	C(74)	-0.4459(4)	0.3878(2)	0.3998(6)	4.98(16)
C(35)	-0.1892(4)	0.03204(15)	0.0226(5)	5.57(18)	C(75)	-0.4434(5)	0.4100(3)	0.2947(5)	4.83(15)
C(36)	-0.1167(3)	0.0686(2)	0.0367(3)	4.51(15)	C(76)	-0.3365(8)	0.3976(3)	0.2657(6)	3.75(12)
C(41)	-0.091(4)	0.1878(4)	-0.1026(13)	3.42(12)	C(81)	-0.0960(4)	0.41649(14)	0.2375(4)	2.89(11)
C(42)	-0.0028(15)	0.1859(4)	-0.156(4)	4.42(15)	C(82)	-0.0786(4)	0.46653(18)	0.3103(3)	3.63(12)
C(43)	-0.037(3)	0.1892(5)	-0.283(4)	6.02(19)	C(83)	-0.0848(4)	0.51835(15)	0.2585(4)	4.55(15)
C(44)	-0.160(4)	0.1944(4)	-0.3549(13)	5.86(19)	C(84)	-0.1064(4)	0.52012(14)	0.1338(4)	4.61(15)
C(45)	-0.2480(15)	0.1864(4)	-0.301(4)	5.35(17)	C(85)	-0.1228(4)	0.47007(18)	0.0610(3)	4.25(14)
C(46)	-0.214(3)	0.1831(5)	-0.175(4)	4.00(13)	C(86)	-0.1176(4)	0.41826(15)	0.1128(4)	3.52(12)

Rigid Group Parameters

	Xc[a]	Yc	Zc	Delta[b]	Epsilon	Eta
Ring1	0.4590(4)	0.06964(17)	0.3216(4)	1.834(4)	1.566(15)	4.636(15)
Ring2	0.0606(3)	0.03372(15)	0.3213(3)	0.006(3)	0.693(3)	0.863(3)
Ring3	-0.2317(3)	0.09133(14)	0.0448(3)	0.087(3)	0.373(3)	0.835(3)
Ring4	-0.1254(3)	0.19113(13)	-0.2287(3)	4.599(3)	1.88(3)	3.10(3)
Ring5	0.3528(3)	0.30437(12)	0.7292(3)	4.598(3)	2.61(2)	5.91(2)
Ring6	0.2331(3)	0.43808(12)	0.3780(3)	0.185(3)	1.666(3)	4.326(2)
Ring7	-0.3391(3)	0.37545(12)	0.3708(3)	2.055(3)	0.663(6)	0.102(6)
Ring8	-0.1012(3)	0.46830(12)	0.1857(3)	3.194(3)	1.741(3)	2.097(2)

[a] Xc,Yc and Zc are the fractional coordinates of the centroid of the rigid group.

[b] The rigid group orientation angles Delta,Epsilon and Eta(radians) are the angles by which the rigid body is rotated with respect to a set of axes X,Y and Z. The origin is the centre of the ring; X is parallel to a* , Z is parallel to c and Y is parallel to the line defined by the intersection of the plane containing a* and b* with the plane containing b and c.

Table 14. Derived Hydrogen Positions for $[Ir_2Cl_2(CO)_2(\mu\text{-DMA})(DPM)_2]\cdot 2CH_2Cl_2$.

Atom	x	y	z	B(A')	Atom	x	y	z	B(A')
H(1C3)	0.1027	0.0979	0.0671	4.07	H(43)	0.0231	0.1873	-0.3209	6.77
H(2C3)	0.1517	0.1536	0.0647	4.07	H(44)	-0.1837	0.1965	-0.4412	7.40
H(1C4)	0.0176	0.3856	0.4898	3.68	H(45)	-0.3314	0.2003	-0.3490	6.06
H(2C4)	0.0069	0.3226	0.5062	3.68	H(46)	-0.2724	0.1948	-0.1365	5.05
H(1)	0.5799	0.3933	0.9305	7.66	H(52)	0.1419	0.3167	0.6844	4.76
H(2)	0.5951	0.4576	0.9513	7.66	H(53)	0.2739	0.3006	0.8856	5.65
H(3)	0.2816	0.1672	0.7395	8.19	H(54)	0.4856	0.2878	0.9309	5.46
H(4)	0.3725	0.1788	0.8692	8.19	H(55)	0.5654	0.2910	0.7750	5.23
H(12)	0.3458	0.0939	0.1212	7.30	H(56)	0.4334	0.3071	0.5738	4.78
H(13)	0.5535	0.0519	0.1745	9.93	H(62)	0.1880	0.3646	0.2280	4.23
H(14)	0.6681	0.0283	0.3777	9.35	H(63)	0.2179	0.4529	0.1766	5.33
H(15)	0.5751	0.0468	0.5276	7.49	H(64)	0.2624	0.5266	-0.3258	5.63
H(16)	0.3674	0.0888	0.4743	6.16	H(65)	0.2769	0.5120	0.5263	5.61
H(22)	-0.0093	0.1301	0.3697	5.14	H(66)	0.2470	0.4237	0.5776	4.34
H(23)	-0.1047	0.0566	0.3940	6.75	H(72)	-0.1645	0.3165	0.4979	4.73
H(24)	-0.0352	-0.0403	0.3456	7.45	H(73)	-0.3437	0.3381	0.5476	5.62
H(25)	0.1296	-0.0636	0.2728	7.54	H(74)	-0.5187	0.3969	0.4202	5.92
H(26)	0.2250	0.0100	0.2485	6.28	H(75)	-0.5145	0.4340	0.2431	5.67
H(32)	-0.2866	0.1903	0.0808	4.99	H(76)	-0.3353	0.4124	0.1934	4.55
H(33)	-0.4232	0.1280	0.0607	6.49	H(82)	-0.0663	0.4656	0.3952	4.69
H(34)	-0.3662	0.0281	0.0267	7.09	H(83)	-0.0763	0.5530	0.3081	5.85
H(35)	-0.1727	-0.0096	0.0128	6.79	H(84)	-0.1117	0.5560	0.0985	5.43
H(36)	-0.0361	0.0526	0.0329	5.61	H(85)	-0.1372	0.4716	-0.0239	5.02
H(42)	0.0820	0.1817	-0.1084	5.50	H(86)	-0.1272	0.3842	0.0632	4.54

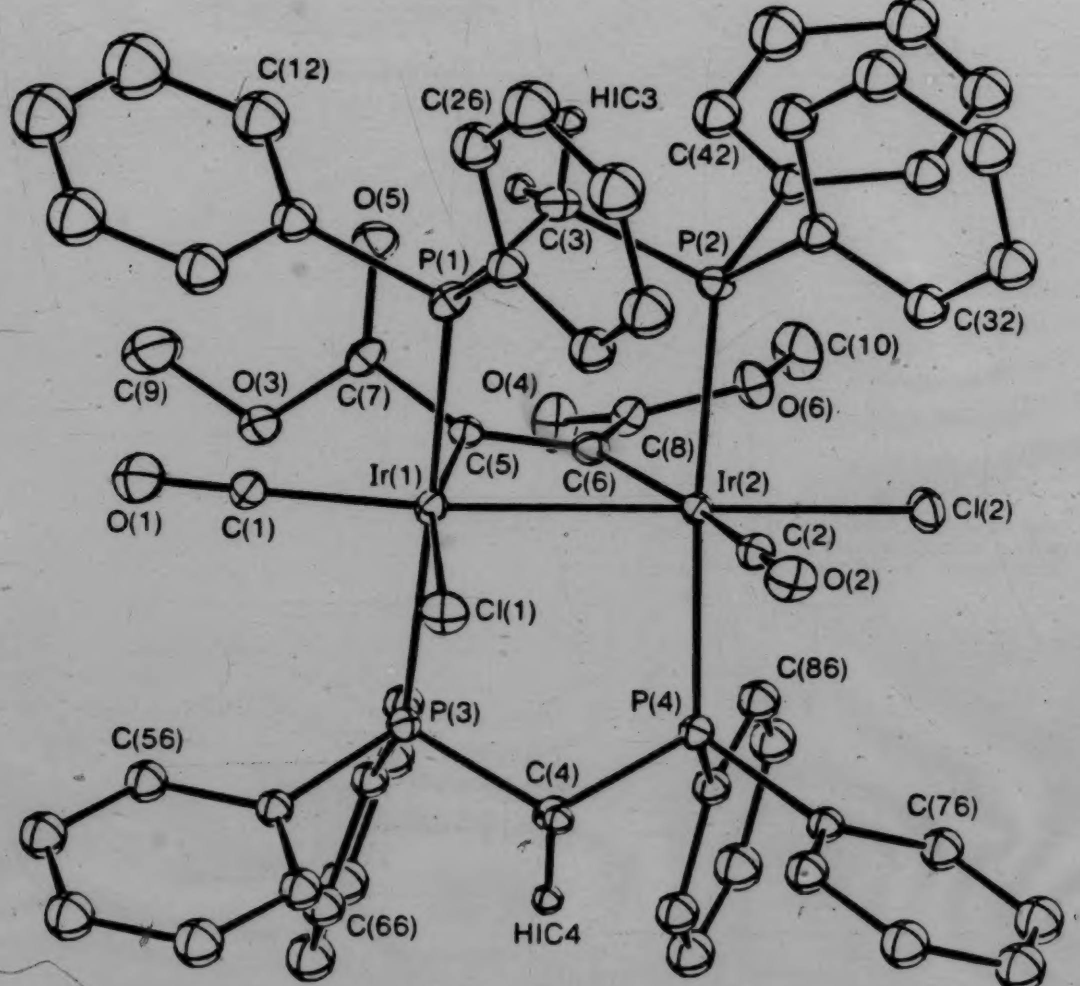
C(12)
C(26)
HIC3
C(42)
O(5)
P(1)
C(3)
P(2)
C(32)
C(10)
C(9)
O(3)
C(7)
O(4)
O(6)
C(8)
C(5)
C(6)
Ir(1)
Ir(2)
Cl(2)
O(1)
C(1)
C(2)
O(2)
Cl(1)
C(86)
P(3)
P(4)
C(56)
C(4)
C(76)
C(66)
HIC4

Figure 4. Perspective view of $[Ir_2Cl_2(CO)_2(\mu\text{-DMA})(DPM)_2]$, showing the numbering scheme. The numbering on the phenyl carbon atoms starts at the carbon bonded to phosphorus and increases sequentially around the ring. Twenty percent thermal ellipsoids are shown.

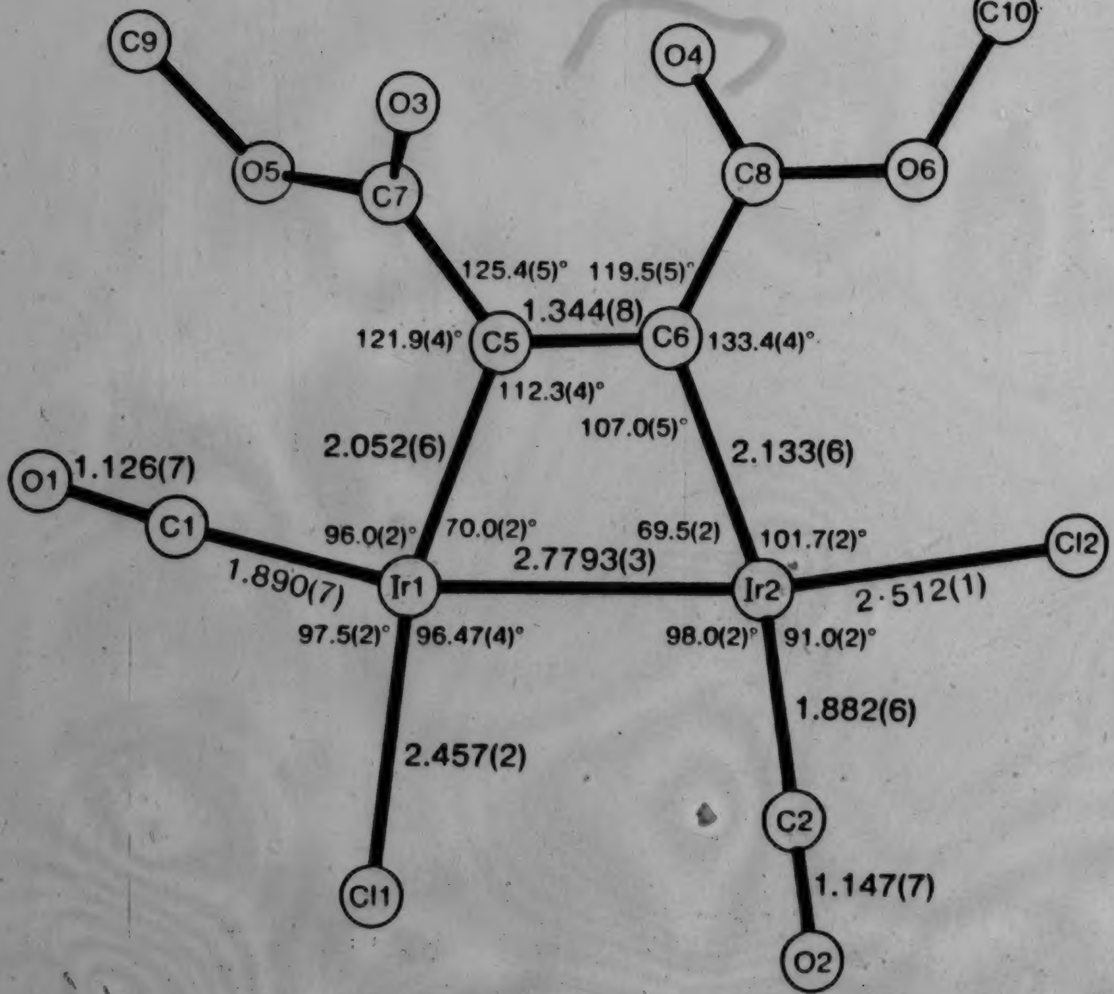
C9
O3
O4
C10
O5
C7
C8
O6
125.4(5)°
119.5(5)°
1.344(8)
121.9(4)°
C5
C6
133.4(4)°
112.3(4)°
107.0(5)°
2.052(6)
2.133(6)
O1
1.126(7)
C1
96.0(2)°
70.0(2)°
69.5(2)
101.7(2)°
Cl2
2.7793(3)
1.890(7)
Ir1
Ir2
2·512(1)
97.5(2)°
96.47(4)°
98.0(2)°
91.0(2)°
1.882(6)
2.457(2)
C2
Cl1
1.147(7)
O2

Figure 5. Representation of the inner coordination sphere of the complex in the approximate plane of the metal atoms and the alkyne molecules. Some relevant bond lengths and angles are shown.

Table 15. Selected Distance (Å) in

$[Ir_2Cl_2(CO)_2(\mu\text{-DMA})(DPM)_2]\cdot 2CH_2Cl_2$.

Bonding Distances

Ir(1)-Ir(2)	2.7793(3)	C(8)-O(6)	1.340(7)
Ir(1)-Cl(1)	2.457 (2)	C(9)-O(5)	1.462(8)
Ir(2)-Cl(2)	2.512 (1)	C(10)-O(6)	1.438(8)
Ir(1)-P(1)	2.342 (2)	P(1)-C(3)	1.807(7)
Ir(1)-P(3)	2.383(2)	P(2)-C(3)	1.825(7)
Ir(2)-P(2)	2.354(2)	P(3)-C(4)	1.819(6)
Ir(2)-P(4)	2.342(2)	P(4)-C(4)	1.821(6)
Ir(1)-C(1)	1.890(7)	P(1)-C(11)	1.807(4)
Ir(2)-C(2)	1.882(6)	P(1)-C(21)	1.834(4)
Ir(1)-C(5)	2.052(6)	P(2)-P(31)	1.842(4)
Ir(2)-C(6)	2.133(6)	P(2)-C(41)	1.842(4)
C(1)-O(1)	1.126(7)	P(3)-C(51)	1.828(3)
C(2)-O(2)	1.147(7)	P(3)-C(61)	1.827(3)
C(5)-C(6)	1.344(8)	P(4)-C(71)	1.845(3)
C(5)-C(7)	1.479(8)	P(4)-C(81)	1.830(3)
C(6)-C(8)	1.467(8)	C(D1)-Cl(3)[a]	1.72(1)
C(7)-O(3)	1.219(7)	C(D1)-Cl(4)	1.73(1)
C(8)-O(4)	1.215(7)	C(D2)-Cl(5)[a]	1.78(1)
C(7)-O(5)	1.330(7)	C(D2)-Cl(6)	1.67(1)

---

a) The dichloromethane molecules of solvation consist of C(D1), Cl(3), Cl(4) and C(D2), Cl(5), Cl(6).

Table 16. Selected Angles (Deg) in $[Ir_2Cl_2(CO)_2(\mu\text{-DMA})(DPM)_2]\cdot 2CH_2Cl_2$.

P(1)-Ir(1)-Ir(2)	90.18(4)	C1(1)-Ir(1)-C(5)	166.2(2)	P(1)-C(3)-P(2)	110.7(3)	C(61)-P(3)-C(4)	103.5(2)
P(3)-Ir(1)-Ir(2)	92.71(4)	C1(2)-Ir(2)-C(6)	101.7(2)	P(3)-C(4)-P(4)	111.0(3)	C(71)-P(4)-C(81)	102.3(2)
P(2)-Ir(2)-Ir(1)	92.90(4)	C(1)-Ir(1)-C(5)	96.0(2)	Ir(1)-P(1)-C(3)	108.9(2)	C(71)-P(4)-C(4)	100.4(2)
P(4)-Ir(2)-Ir(1)	92.12(3)	C(2)-Ir(2)-C(6)	166.8(2)	Ir(1)-P(1)-C(11)	110.6(2)	C(81)-P(4)-C(4)	105.9(2)
P(1)-Ir(1)-P(3)	173.81(5)	C(5)-Ir(1)-Ir(2)	70.0(2)	Ir(1)-P(1)-C(21)	125.8(2)	P(1)-C(11)-C(12)	123.6(3)
P(2)-Ir(2)-P(4)	174.27(5)	C(6)-Ir(2)-Ir(1)	69.5(2)	Ir(2)-P(2)-C(3)	112.6(2)	P(1)-C(11)-C(16)	116.4(3)
C1(1)-Ir(1)-Ir(2)	96.47(4)	Ir(1)-C(1)-O(1)	176.0(6)	Ir(2)-P(2)-C(31)	115.0(2)	P(1)-C(21)-C(22)	122.1(3)
C1(2)-Ir(2)-Ir(1)	170.65(4)	Ir(2)-C(2)-O(2)	179.4(5)	Ir(2)-P(2)-C(41)	119.9(2)	P(1)-C(21)-C(26)	117.3(3)
P(1)-Ir(1)-C1(1)	91.43(6)	Ir(1)-C(5)-C(6)	112.3(4)	Ir(1)-P(3)-C(4)	107.0(2)	P(2)-C(31)-C(32)	118.3(3)
P(3)-Ir(1)-C1(1)	82.81(5)	Ir(2)-C(6)-C(5)	107.0(4)	Ir(1)-P(3)-C(51)	111.2(1)	P(2)-C(31)-C(36)	121.4(3)
P(2)-Ir(2)-C1(2)	88.51(5)	Ir(1)-C(5)-C(7)	122.0(4)	Ir(1)-P(3)-C(61)	127.5(1)	P(2)-C(41)-C(42)	121.4(3)
P(4)-Ir(2)-C1(2)	86.09(5)	Ir(2)-C(6)-C(8)	133.4(4)	Ir(2)-P(4)-C(4)	112.5(2)	P(2)-C(41)-C(46)	118.5(3)
P(1)-Ir(1)-C(1)	90.8(2)	C(6)-C(5)-C(7)	125.4(5)	Ir(2)-P(4)-C(71)	114.9(1)	P(3)-C(51)-C(52)	122.2(2)
P(3)-Ir(1)-C(1)	87.7(2)	C(5)-C(6)-C(8)	119.5(5)	Ir(2)-P(4)-C(81)	118.7(1)	P(3)-C(51)-C(56)	117.6(2)
P(2)-Ir(2)-C(2)	95.3(2)	C(5)-C(7)-O(3)	123.0(6)	C(11)-P(1)-C(21)	100.4(2)	P(3)-C(61)-C(62)	121.7(2)
P(4)-Ir(2)-C(2)	86.7(2)	C(6)-C(8)-O(4)	124.0(6)	C(11)-P(1)-C(3)	107.0(3)	P(3)-C(61)-C(66)	117.9(2)
P(1)-Ir(1)-C(5)	91.3(2)	C(5)-C(7)-O(5)	114.5(5)	C(21)-P(1)-C(3)	102.6(3)	P(4)-C(71)-C(72)	120.5(2)
P(3)-Ir(1)-C(5)	94.8(2)	C(6)-C(8)-O(6)	113.7(5)	C(31)-P(2)-C(41)	98.9(2)	P(4)-C(71)-C(76)	119.5(2)
P(2)-Ir(2)-C(6)	81.7(2)	O(5)-C(7)-O(6)	122.3(5)	C(31)-P(2)-C(3)	106.9(2)	P(4)-C(81)-C(82)	120.8(2)
P(4)-Ir(2)-C(6)	97.5(2)	O(4)-C(8)-O(6)	122.3(6)	C(41)-P(2)-C(3)	101.7(3)	P(4)-C(81)-C(86)	119.2(2)
C1(1)-Ir(1)-C(1)	97.5(2)	C(7)-O(5)-C(9)	116.1(6)	C(51)-P(3)-C(61)	101.2(2)	C1(3)-C(01)-C1(4)	111.2(6)
C1(2)-Ir(2)-C(2)	91.0(2)	C(8)-O(6)-C(10)	116.7(5)	C(51)-P(3)-C(4)	104.1(2)	C1(5)-C(02)-C1(6)	112.1(7)

bridged complexes of iridium.[151,173] Each metal has a slightly distorted octahedral geometry in which the coordination sites are occupied by the two trans phosphorus atoms, mutually cis terminal carbonyl and chloride ligands, one end of the bridging alkyne group, bound as a cis-dimetallated olefin, and by an Ir-Ir bond. The major distortions from octahedral geometry about each metal result from the strain imposed by the bridging alkyne ligand (vide infra) accompanying the Ir-Ir bond, and as a consequence the Ir-Ir-alkyne angles (av. 69.8°) are rather acute. The respective carbonyl and chloride ligands on each metal are chemically inequivalent; on Ir(1), the Cl atom is pseudo-trans to the alkyne group and the carbonyl is opposite the Ir-Ir bond; on Ir(2) the positions are reversed.

The iridium-iridium distance of 2.7793(3) Å is typical of that observed for an Ir-Ir single bond and is comparable to the values found in analogous Ir-DPM systems.[151,173] This distance is significantly shorter than the intraligand P-P distances (2.989(2) Å and 3.001(2) Å indicating a compression along the Ir-Ir axis as expected for a metal-metal bonded system. Both Ir-Cl distances are somewhat long. The Ir(1)-Cl(1) distance (2.457(2) Å) can be explained based on the high trans influence of the σ-bonded alkenyl carbon of the cis-dimetallated olefin, however, the

Ir(2)-Cl(2) length is even longer (2.512(1) Å and must be attributed to an even higher trans influence of the Ir-Ir interaction. Although trans lengthening by a metal-metal bond does not seem to be widely examined phenomenon, several reports alluding to such an effect have appeared recently.[62,174,175] The parameters involving the carbonyl groups are quite normal with no significant differences between the two ligands, in spite of their different environments.

As noted earlier, the alkyne molecule is bound parallel to the metal-metal axis in a cis-dimetallated olefin geometry. Consistent with this, the geometries of the metallated carbons are reminiscent of sp^2 hybridization and the C(5)-C(6) distance (1.344(8)) Å is close to that of a normal carbon-carbon double bond. The methoxycarbonyl substituents are twisted by an angle of ca. 116° with respect to each other such that one group (attached to C(6)) lies close to the metal-metal-alkyne plane, while the other (attached to C(5)) is almost perpendicular to this plane. The twisting most likely occurs in order to minimize unfavourable non-bonded contacts with the phenyl groups. Although most of the parameters concerning this bridging alkyne group are comparable to those of related structures[45,66], the DMA ligand in the present case is rather unsymmetrically bonded; not only is the Ir(1)-C(5) bond length (2.052(6) A) significantly shorter than that of Ir(2)-C(6) (2.133(6) A) but the angles about C(5) and C(6) also differ appreciably (see Figure 5). We suggest that this latter asymmetry results from an attempt to minimize the above non-bonded contacts. Since, as noted earlier, these groups are oriented essentially at right angles, their interactions with the phenyl groups should differ appreciably leading to the observed asymmetry in the orientation of the ligand with respect to the metals. This results in a slight twist of the alkyne group from the Ir-Ir axis (ca. 5.7(2)°) as can be seen in Figure 4. C(5) lies above the plane defined by the iridium atoms and the centre of the C(5)-C(6) bond, most likely because of the interactions involving C(5) and its attached substituents with phenyl ring 6. A similar skewing of the alkyne group was obseved in $[Rh_2Cl_2(\mu\text{-}CO)(\mu\text{-}DMA)(DPM)_2]$; however in this case the alkyne was symmetrically bonded to each metal[66]. The difference in the metal-carbon bond lengths may result from the above steric interactions but may also be a result of the differing trans influence of the chloride and carbonyl groups opposite this alkyne ligand. A similar asymmetry was observed for another alkyne-bridged complex, $[Rh_2Cl(CNMe)_2(\mu\text{-}HFB)(DPM)_2]^+$ where the ligands on each metal differ significantly.[176]

Discussion of Results.

(i) Neutral Complexes. The addition of dimethylacetylene dicarboxylate (DMA) to a solution of *trans*-$[IrCl(CO)(DPM)]_2$ (**3**) produces an immediate reaction as evidenced by a colour change from purple to light yellow. The solid isolated, formulated as $[Ir_2Cl_2(CO)_2(\mu\text{-}DMA)(DPM)_2]$ (**6**) displays carbonyl stretches in the I.R. spectrum at 2023 and 1999 cm^{-1}, as well as stretches at 1674 and 1653 cm^{-1} due to the carboxylate groups and one at 1549 cm^{-1} due to the coordinated acetylenic moiety. The low acetylenic stretch is consistent with either of two binding modes for this group; when the alkyne is bound perpendicular to the metal-metal axis (μ_2-η^2 binding mode) this stretch has been observed in the range from 1491 to 1595 cm^{-1},[177,178] whereas when it binds parallel to the metal-metal axis (as a cis-dimetallated olefin) a range in stretches from 1639 to 1643 cm^{-1} has been reported.[179,180] Although the observed stretch is more consistent with the perpendicular binding mode, the X-ray structure determination, described earlier, establishes that the alkyne is bound as a cis-dimetallated olefin, as shown below in structure VI (see also Figures 4 and 5). As such, this is one of the lowest acetylenic stretches observed for this geometry and is certainly lower than related rhodium complexes that have been studied in this group.[66,68,69,176] This is probably a reflection of the

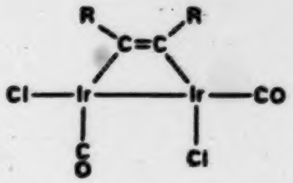

R = CO_2Me (6)
= CF_3 (7)
= H (8)

VI

more basic metal centre in the case of iridium and the concomitant greater π back donation to the alkyne group. The strong Ir-alkyne bond is also evidenced by the fact that refluxing **6** in toluene leads to carbonyl loss but no loss of the alkyne ligand (vide infra). The solution characteristics suggest that the same structure is maintained in solution; a $^{31}P\{^1H\}$ NMR spectrum shows an AA'BB' pattern[183] (see Table 10) indicating that both iridium centres are chemically inequivalent and the solution I.R. spectrum is quite similar to that in the solid (see Table 9). Furthermore, compound **6** is a non-electrolyte suggesting that no significant chloride dissociation occurs.

With hexafluoro-2-butyne (HFB), reaction with compound **3** yields a single species which we formulate as $[Ir_2Cl_2(CO)_2(\mu\text{-HFB})(DPM)_2]$ (**7**), having a similar structure to that of **6**. Unlike compound **6**, however, this HFB adduct displays only one carbonyl stretch at 2024 cm^{-1}. Nevertheless **7** is formulated as a dicarbonyl species based on its subsequent reactions (vide infra); in particular removal of Cl^- by the addition of Ag^+ quantitatively yields a cationic dicarbonyl complex. It would seem that in compound **7** both carbonyl bands are accidentally coincident. Changing the bridging group from DMA to HFB might be expected to have relatively little effect on the carbonyl ligand which is cis to these bridging groups but a greater effect on the trans carbonyl. This suggests that the higher carbonyl stretch in compound **6** (2023 cm^{-1}), which is close to that observed in **7** (2024 cm^{-1}), corresponds to the carbonyl ligand which is opposite the Ir-Ir bond, and the lower stretch of 1999 cm^{-1} in **6** is due to the carbonyl which is trans to the Ir-alkyne linkage. Based on the greater group electronegativity of CF_3 compared to CO_2Me,[181] HFB should be a better π-acceptor ligand than DMA which should result in a higher CO stretching frequency for the carbonyl trans to HFB. Presumably, in **7** this increase in CO frequency is sufficient to bring it into coincidence with the one opposite the Ir-Ir bond, giving rise to only one observed carbonyl stretch. These arguments are consistent with our findings in related complexes of rhodium where CO and SO_2

groups were found to be more labile for HFB-bridged complexes than for the DMA analogues.[176]

Compound **3** also reacts with acetylene (HC≡CH) to give a species having carbonyl stretches at 1977 and 1968 cm^{-1} and a stretch for the coordinated alkyne group at 1533 cm^{-1}. This species has a $^{31}P\{^1H\}$ NMR spectrum which is very similar to those of **6** and **7** and shows two ^1H resonances (6.13 and 6.52 ppm) in the region typical for olefin hydrogens. Based on this data, on the conductivity measurements, which indicate that it is a non-electrolyte, and on its elemental analysis, we formulate this alkyne adduct as $[Ir_2Cl_2(CO)_2(\mu\text{-}C_2H_2)(DPM)_2]$ (**8**), having a structure similar to those of **6** and **7**. The carbonyl stretches for this species are both much lower than those of **6** and **7**, consistent with the substitution of the very electron withdrawing CO_2Me and CF_3 groups by hydrogen atoms. Formation of the acetylene adduct **8** confirms that strongly electron withdrawing groups are not required for complex formation. However, it is to be noted that substituting H for the slightly electron donating methyl group in 2-butyne results in no adduct formation (see experimental section).

Loss of one of the carbonyl groups in compound **6** can be effected by refluxing the species in toluene. The new species, $[Ir_2Cl_2(CO)(\mu\text{-}DMA)(DPM)_2]$ (**9**), displays a complex pattern in the $^{31}P\{^{1}H\}$ NMR spectrum and displays only one carbonyl band (2004 cm^{-1}) in the I.R. spectrum. If the carbonyl group trans to the acetylenic moiety in **6** is lost, either species VII or VIII, shown below, could result, whereas loss of the CO trans to the Ir-Ir bond would yield IX. It is expected that the carbonyl group in **6** having

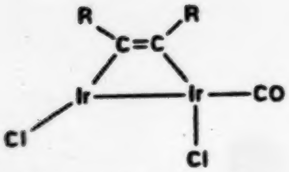
VII

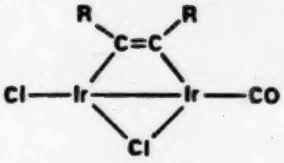
VIII

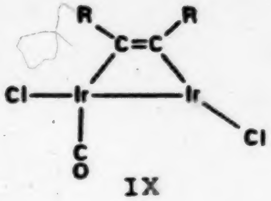
IX

the higher stretching frequency should be less tightly bound, and based on our assignment of these carbonyl bands we suggest that it is the CO trans to the Ir-Ir bond which is labile, yielding structure IX. A similar product, $[Ir_2Cl_2(CO)(\mu\text{-}HFB)(DPM)_2]$ (**10**), is obtained upon refluxing compound **7** in toluene, however its lack of solubility in all solvents tried precludes its characterization in solution. An I.R. spectrum of **10** displays two carbonyl bands at 2009 and 1988 cm^{-1} suggesting that two different products are formed. Such an interpretation is not inconsistent with the I.R. spectrum of the precursor **7**, which showed that both carbonyl stretches are coincident, suggesting similar binding abilities of these groups. The two isomers observed would then result from CO-loss from opposite the Ir-alkyne linkage to give either structure VII or VIII, or from opposite the Ir-Ir bond to give IX.

(ii) Cationic Complexes. This study shows that the most direct routes to cationic alkyne adducts utilizes either chloride abstraction from the neutral alkyne adducts, or direct reaction of the alkynes with the cationic A-frame complex, $[Ir_2(CO)_2(\mu\text{-}Cl)(DPM)_2]^+$ (**5**). Another route, used by Mague and coworkers, involves alkyne addition to and subsequent CO loss from $[Ir_2Cl(CO)_4(DPM)_2]$-$[BPh_4]$.[182] Looking first at chloride removal from the neutral species, it is found that the reactions of compounds **6** and **7** with $AgBF_4$ yield $[Ir_2Cl(CO)_2(\mu\text{-}RC{\equiv}CR)$-$(DPM)_2][BF_4]$ (R = CO_2CH_3 (**11**), CF_3 (**12**)). Although the precursor to compound **12** (compound **7**) displays only one carbonyl stretch, both species **11** and **12** show the two expected CO stretches (see Table 9). At -40°C both compounds display sharp, well resolved patterns in the $^{31}P\{^1H\}$ NMR spectra which appear as a pair of pseudo-triplets[183]. In addition, a small singlet appears in the spectrum of **12**. However, upon warming, the peaks of the "triplets" begin to broaden and at ambient temperature have begun to collapse into the baseline; the singlet in the spectrum of **12** collapses into the baseline along with the other signals. The ^1H and ^{19}F resonances due to the CH_3 and CF_3 groups in compounds **11** and **12**, respectively, behave in an analogous manner. This temperature dependence is consistent with a fluxional process as diagrammed below. Structures X and XII are chemically equivalent and give rise to the two pseudo-triplets in the $^{31}P\{^1H\}$ NMR spectrum, one for each of the two inequivalent ends of the dimer. The singlet observed in the spectrum of **12** is due to the symmetrical chloro-bridged intermediate XI. At higher temperatures the fluxional process, which interchanges the two different phosphorus environments by chloride transfer from one metal to the other, is facilitated and the high temperature limiting spectrum (which was not obtained) should appear as a singlet. Although a resonance for XI is observed in the $^{31}P\{^1H\}$ NMR spectra of **12** (in approximately 8% abundance), no evidence for an analogous species is observed in the spectra of compound **11**. It is not clear why the unsymmetrical species (X or XII) should predominate

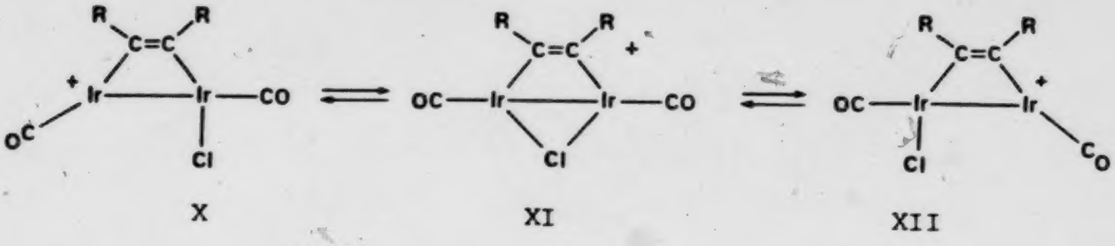

over the chloro-bridged isomer XI, since the somewhat analogous tricarbonyl species, $[Ir_2(CO)_2(\mu\text{-}Cl)(\mu\text{-}CO)(DPM)_2]^+$, exists only as the symmetric species. However, it is conceivable that the strain involved in bridging the Ir-Ir bond by the alkyne (bound as a cis-dimetallated olefin) and the chloro ligand, both of which favour larger metal-metal separations, is enough to destabilize the symmetric structure. It is also not clear why none of the symmetric species is observed for compound **11**. The unsymmetrical forms, X and XII, are obtained from the neutral parent compounds (**6** and **7**) by removal of the chloride ligand which is trans to the Ir-Ir bond. Removal of this chloride ligand, rather than the one which is cis to the Ir-Ir bond is consistent with the much longer Ir-Cl distance found for the former in the structure determination of **6**, suggesting that this chloro ligand is more weakly bound.

Compounds **11** and **12** react rapidly with carbon monoxide to give pale yellow, almost colourless solutions from which white microcrystalline solids are obtained. The I.R. spectra of these solids display three terminal carbonyl bands and, based on the structures suggested for the precursors **11** and **12**, are formulated as shown below. These geometries are consistent with the observed NMR spectra (^1H, ^{19}F and $^{31}P\{^1H\}$) and have been confirmed by X-ray structural determinations for both R = CO_2Me[182] and R = CF_3.[166] Although no temperature dependence was observed in the $^{31}P\{^1H\}$ NMR spectrum of **14**, the DMA analogue **13**, displays unusual temperature dependence, as shown in Figure 6. At room temperature the $^{31}P\{^1H\}$ NMR spectrum of **13** appears as a normal AA'BB' pattern, however as the temperature is lowered the pattern compresses and eventually appears as a sharp singlet at -60°C. At no time during this process is any line broadening observed, strongly arguing against a dynamic process which averages the phosphorus environments. Instead, it appears that the chemical shift for each chemically inequivalent phosphorus nucleus is temperature dependent; but rather than moving in the same direction at roughly the same rate, as normally occurs, the chemical shifts move together, becoming equivalent at -60°C. At lower temperatures, the AA'BB' pattern should reemerge, however we were unable to obtain

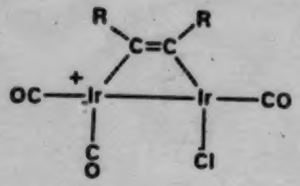

R = CO_2Me(**13**)
= CF_3(**14**)

XIII

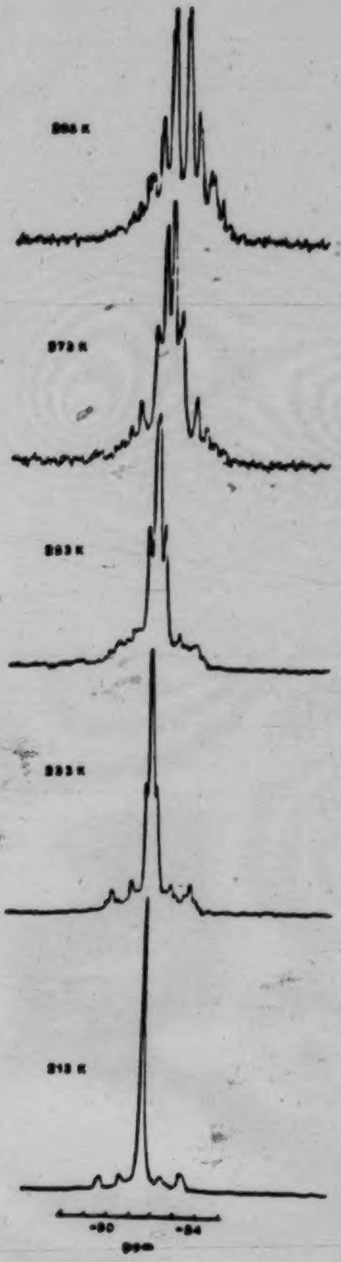

Figure 6. $^{31}P\{^1H\}$ NMR spectra of $[Ir_2Cl(CO)_3(\mu\text{-}DMA)(DPM)_2]$-$[BF_4]$ as a function of temperature in CH_2Cl_2.

these spectra due to instrumental limitations. In the ^1H NMR spectra, a similar phenomenon is observed in which the chemical shift of one methyl group changes from 2.67 to 2.27 ppm over the temperature range from 0 to -60°C, while the other methyl resonance remains essentially fixed at -3.5 ppm (see Table 10); again no broadening is observed. An analogous temperature dependence in the $^{31}P\{^1H\}$ NMR spectrum of $[Pd_2ClI(DPM)_2]$, has previously been reported,[88] except that in this case the crossover of the two sets of resonances occurred at a much higher temperature (35°C). Refluxing compounds **13** and **14** in toluene for 6h regenerates the parent dicarbonyl species **11** and **12**.

A second route to cationic dicarbonyl alkyne complexes, involving the reactions of alkynes with the A-frame complex $[Ir_2(CO)_2(\mu\text{-}Cl)(DPM)_2][BF_4]$ (**5**), has also been studied. Addition of DMA or HFB to solutions of **5** produces an immediate colour change from red to dark purple-brown, and purple solids can be obtained. These species each show two carbonyl stretches at ca. 2093 and 2055 cm^{-1}, which together with the other spectral information suggests that they be formulated as isomers of **11** and **12**, $[Ir_2Cl(CO)_2(\mu\text{-}RC{\equiv}CR)(DPM)_2][BF_4]$ (R = CO_2CH_3 (**15**), CF_3 (**16**)). Compounds **15** and **16** are clearly different from their respective isomers **11** and **12**, described earlier (see Tables 9 and 10). In particular, compounds **15** and **16** do not show fluxional behaviour in the NMR spectra, as was observed for **11** and **12**. Therefore the structures of compounds **15** and **16** are likely as shown below, with the Cl ligand trans to the Ir-Ir bond instead of cis to it.

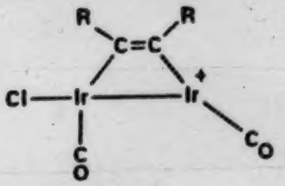

R = CO_2Me(**15**)
= CF_3 (**16**)

XIV

Clearly, facile fluxionality via a symmetric intermediate, as was described for **11** and **12**, is not possible for these species since significant rearrangement would be required in order to obtain the chloro-bridged intermediate (Structure XI). Why structure XIV is obtained for compounds **15** and **16**, instead of the isomeric structure X or XII, is readily understood when one considers the site of alkyne attack in compound **5**. If attack were to occur between the metals, in the enclosed bridging site, one would expect species X or XII to result, however attack at one of the terminal vacant sites, as diagrammed below, would, after migration of the ligands around the framework,

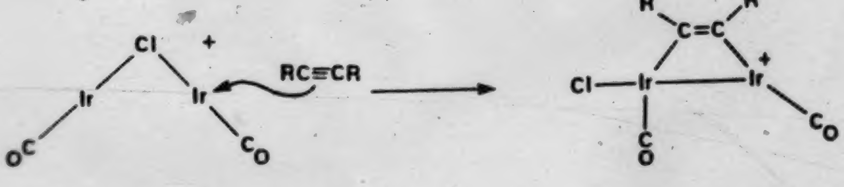

yield structure XIV. In the analogous rhodium A-frame, $[Rh_2(CO)_2(\mu-Cl)(DPM)_2]^+$, attack by CO has been demonstrated to occur at this terminal site.[39,40] In addition, the reaction of a related acetate-bridged rhodium A-frame, $[Rh_2(CO)_2(\mu-O_2CCH_3)(DPM)_2]^+$, with HFB has also been shown to yield a product having a geometry much as that proposed for structure XIV, except that for the rhodium species one carbonyl group bridges the two metals with no accompanying metal-metal bond.[42,44]

Although compounds **15** and **16** are not fluxional in solution, they do with time in CH_2Cl_2 solution convert to their isomers **11** and **12**. At present, it is not clear how this rearrangement occurs since no intermediate has been observed. However, two routes seem likely, involving either loss of CO or Cl^- from the iridium atom which is coordinatively saturated followed by recoordination. Attempts to trap the intermediates in the above dissociations, by flushing the system with N_2 to remove CO or by addition of Ag^+, failed, and had no significant affect on the rate of isomerization, although the latter gives rise to small amounts of two unidentified species. It is also interesting that the rate of isomerization of **15** is much faster than that of **16**; the former is complete within one hour whereas the latter requires approximately two weeks at room temperature. This rate difference can be rationalized based on stabilization of the electron deficient intermediate, which results from either CO or Cl^- dissociation, by coordination of one of the carboxylate oxygen atoms as shown for structure XV. That **11** and **12** are favoured over **10** and **11** may reflect the preference for a π-acceptor versus a π-donor ligand in the sites trans the Ir-Ir bond (cf. the long Ir-Cl bond in **6**).

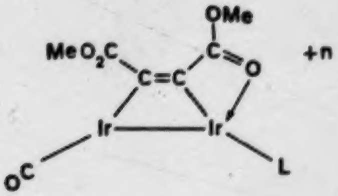

L = CO, n = 2
= Cl, n = 1

XV

$[Ir_2(CO)_2(\mu\text{-}Cl)(DPM)_2][BF_4]$ also reacts readily with acetylene (HC≡CH), however a mixture of products is obtained and none has yet been characterized. As was the case for trans-$[IrCl(CO)(DPM)]_2$ (**3**), no reaction of compound **5** with 2-butyne was observed.

Compounds **15** and **16** react rapidly with CO to give the previously observed tricarbonyl species **13** and **14**. Our initial expectation was that the isomeric structure XVI would result, however, no species other than **13** and **14** is observed. This is perhaps not surprising, considering that compounds **15** and **16** were shown to isomerize, and this

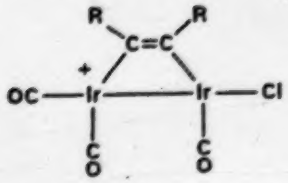

XVI

isomerization may be accelerated in the presence of excess CO. Again, the preferred geometry has the chloro ligand opposite the metal-alkyne linkage instead of trans to the Ir-Ir bond

Conclusions

The syntheses outlined, involving the reactions of trans-$[IrCl(CO)(DPM)]_2$ and $[Ir_2(CO)_2(\mu\text{-}Cl)(DPM)_2][BF_4]$ with alkynes, present convenient routes to both neutral and cationic iridium complexes containing bridging alkyne groups. Not surprisingly, these iridium complexes have the alkyne ligands bound as cis- dimetallated olefins as was observed in the analogous rhodium compounds [1-6] and as has been discussed by Hoffmann and coworkers.[184-185]

In many respects the iridium chemistry parallels that of rhodium but there are significant differences that are consistent with the differences between second and third row metals. For example, in several of the rhodium complexes the bridging alkyne groups are accompanied by bridging carbonyl ligands, and in fact these compounds are some of the few examples of bridging carbonyl complexes with no accompanying metal-metal bonds.[42,44,66,74,145,187] On the other hand, no bridging carbonyls are observed in the iridium complexes described, which is consistent with the lower tendency of the third row transition metals to have bridging carbonyl groups. This study also demonstrates a much greater tendency for the more basic iridium complexes to bind CO compared with their rhodium counterparts. For example, when trans-$[RhCl(CO)(DPM)]_2$ reacts with DMA or HFB one carbonyl group is very labile and only the monocarbonyl complexes, $[Rh_2Cl_2(\mu\text{-}CO)(\mu\text{-}RC_2R)(DPM)_2]$, are isolated.[66] However, with iridium the dicarbonyl alkyne adducts are obtained and removal of both carbonyl groups can be effected only with difficulty.[186] Similarly, a series of tricarbonyl alkyne complexes has been prepared and isolated with iridium, whereas with rhodium these analogues are not obtained.[187]

Owing to the lower lability of third row metal complexes compared to their second row analogues, we had hoped to observe examples of alkyne attack and coordination at one of the terminal sites in these complexes. However, rearrangement to complexes having bridging alkynes is very facile, even with iridium, so although the initial products probably have the alkynes coordinated at only one metal, such species are never observed.

It is apparent from these studies that the bonding between the alkyne ligand and the metals is very strong. In several of the complexes there is a cis positioning of a carbonyl ligand and one end of the Ir-alkyne linkage, yet no evidence of insertion is observed even when the system is left stirring under CO pressure (> 1 atmosphere) for extended periods of time. This is also apparent from the reaction of these complexes with hydrogen where either no reaction is observed or the reactions follow a very complex pathway resulting in the formation of several species (see Experimental). It is therefore unlikely that these cis-dimetallated olefin species play any significant role in alkyne hydrogenation.

CHAPTER 4

Binuclear DPM-Bridged Complexes of Iridium as Models for the Catalytic Hydrogenation of Alkynes in the Presence of Two Metal Centres. The Structure of $[Ir_2(CH_3CO_2C{=}CHCO_2CH_3)_2Cl_2(CO)_2(DPM)_2]$.

Introduction

As described in Chapter 1, much of the present understanding of the mechanisms of homogeneous hydrogenation of unsaturated organic substrates comes from studies on mononuclear rhodium-phosphine complexes.[3,15-21] More recent studies have focussed on complexes containing more than one metal centre as catalysts because of the potentially new modes of reactivity not available with mononuclear systems.[188,189] Understanding the functions of the different metal centres in these polynuclear complexes is especially important in designing new catalysts. Reports of alkyne hydrogenation under mild conditions by the binuclear complexes $[Rh_2(CO)_2(\mu\text{-}Cl)(DPM)_2][BPh_4]$[34] (I) and $[Rh_2(CO)_2(\mu\text{-}H)(\mu\text{-}CO)(DPM)_2)[BF_4]$[35] (II) raise the question as to how the two metal centres in each complex are involved in the catalysis. Although it is attractive to consider that both metals are participating, perhaps in a cooperative manner, it is not clear from these studies that this is the case. In neither case were any intermediate species observed. Because of this group's ongoing interest in binuclear, DPM-bridged complexes as models for multicentre catalysts, it was decided to use the Ir-DPM system at hand in an attempt to model the catalytic behaviour of the Rh systems. It was felt that with iridium we might be able to isolate complexes which would be analogous to intermediates in the rhodium-catalyzed reactions and thereby define the role of the metal centres during the course of the catalytic cycle. This chapter deals with studies using the Ir analogue of I, $[Ir_2(CO)_2(\mu\text{-}Cl)(DPM)_2][BF_4]$, ~~**5**~~ 7, and its close relative, *trans*-$[IrCl(CO)(DPM)]_2$, **3**.

Experimental Section

The general experimental conditions and techniques are given in Chapter Two.

Preparation of Compounds

(a) $[Ir_2(H)_2Cl_2(CO)_2(DPM)_2]$ (**17**).

An atmosphere of hydrogen was placed over a solution of trans-$[IrCl(CO)(DPM)]_2$ (**3**), (200 mg, 0.156 mmole) in 10 mL of CH_2Cl_2 and the mixture was stirred for 15 min during which time the colour changed from dark purple to light yellow. The solution was concentrated to a volume of 5 mL under hydrogen and 30 mL of hexanes was added resulting in the precipitation of a pale yellow powder. The solid was collected and dried under a stream of hydrogen. Recrystallization from toluene/hexanes yielded **17** as a colourless microcrystalline solid in 90% yield. Compound **17** was determined to be non-conducting in CH_2Cl_2 solutions ($\Lambda(10^{-3}M) < 0.5\ \Omega^{-1}\ cm^2\ mole^{-1}$)[170]. Spectroscopic parameters for this and all subsequent compounds is given in Table 17.

Anal. Calcd for $Ir_2Cl_2P_4O_2C_{59}H_{54}$: C, 51.57%; H, 3.96%, Found: C, 51.64%; H, 4.05%.

b) $[Ir_2(H)_4Cl(CO)_4(DPM)_2][BF_4]$ (**18**).

An atmosphere of hydrogen was placed over a solution of $[Ir_2(CO)_2(\mu\text{-}Cl)(DPM)_2][BF_4]$, (**5**), (200 mg, 0.150 mmole) in 5 mL of CH_2Cl_2 and the mixture was stirred for 15 min during which time the colour changed from dark red to light yellow. The solution was taken to dryness under a rapid flow of hydrogen leaving a pale yellow powder which proved to be susceptible to decomposition except when kept sealed under an atmosphere of hydrogen. For this reason no elemental analyses could be obtained.

c) $[Ir_2(H)_2(CO)_2(\mu\text{-}Cl)(DPM)_2][BF_4]$ (**19**).

Method A. An atmosphere of hydrogen was placed over a slurry of $[Ir_2(CO)_2(\mu\text{-}Cl)(DPM)_2][BF_4]$, (**5**), (200 mg, 0.150 mmole) in 10 mL of THF and the mixture stirred for 15 min. during which time all of the solid disappeared leaving a clear light yellow solution of **18**. The hydrogen atmosphere was replaced by one of dinitrogen and the solution was refluxed for 20 min during which time the colour changed to a very intense yellow and a bright yellow flocculent precipitate appeared. The mixture was taken to dryness under an N_2 stream giving **19** as a bright yellow powder. Recrystallization from CH_2Cl_2/diethyl ether gave **19** as a bright yellow microcrystalline solid in 90% yield. A CH_2Cl_2 solution of this solid proved to be a 1:1 electrolyte ($\Lambda(10^{-3}M) = 54.2\ \Omega^{-1}\ cm^2\ mole^{-1}$).

Anal. Calcd for $Ir_2ClP_4F_4O_2C_{52}BH_{46}$: C, 46.84%; H, 3.48%. Found: C, 46.76%; H, 3.54%.

Method B. To a slurry of **17** (200 mg, 0.156 mmol) in 10 mL THF under dinitrogen was added dropwise one equivalent of $AgBF_4$ (30.4 mg, mmol) in 2 mL of THF. The colour immediately changed to bright yellow and upon continued stirring a yellow precipitate appeared. The solution was taken to dryness under a stream of dinitrogen. The product was extracted from the silver-containing products by adding 10 mL of CH_2Cl_2 and filtering under dinitrogen to give a clear bright yellow solution. Product precipitation was induced by the addition of 30 mL of diethyl ether. The resulting bright yellow solid, obtained in 85% yield, was identical in all spectroscopic properties to the product obtained from Method A.

d) $[Ir_2(H)(CH_3CO_2C{=}CHCO_2CH_3)Cl_2(CO)_2(DPM)_2]\cdot CH_2Cl_2$ (**20**).

To a solution of **3** (200 mg, 0.156 mmol) in 10 mL CH_2Cl_2 under dinitrogen was added one equivalent of dimethylacetylene dicarboxylate (DMA) (15.2 µl, 0.156 mmol) which produced an immediate colour change from pale yellow to bright yellow. The solution was allowed to stir for 12 h, during which time a yellow solid precipitated from solution. 30 mL of diethyl ether was added to ensure complete precipitation and the resulting solid was collected and washed with two 10 mL portions of diethyl ether and finally dried under an N_2 stream giving **20** as a yellow microcrystalline solid in 90% yield. Compound **20** was determined to be non-conducting in CH_2Cl_2 solutions ($\Lambda(10^{-3}M) < 0.5\ \Omega^{-1}\ cm^2\ mole^{-1}$).

Anal. Calcd for $Ir_2Cl_4P_4O_6C_{59}H_{54}$: C, 46.96%; H, 3.61%. Found: C, 46.97%; H, 3.69%. The presence and amount of solvent of crystallization was confirmed by ^1H NMR.

e) $[Ir_2(CH_3CO_2C{=}CHCO_2CH_3)_2Cl_2(CO)_2(DPM)_2]$ (**21**).

To a solution of 4 (200 mg, 0.150 mmol) in 10 mL CH_2Cl_2 under dinitrogen was added an excess of DMA (50.0 µl, 0.513 mmol) which produced an immediate colour change from yellow to orange. The solution was allowed to stir for 12 h after which time 30 mL of diethyl ether was added resulting in the precipitation of a bright yellow flocculent solid. The solid was dissolved in acetone and placed on a chromatography column containing 100 mesh Florisil. Elution with acetone gave one bright yellow band which was collected as a yellow solution. The solution was taken to dryness under vacuum giving a bright yellow solid. Recrystallization from CH_2Cl_2/diethyl ether gave **21** a bright yellow crystals in 50% yield. Compound **21** was determined to be a nonelectrolyte in CH_2Cl_2 solutions ($\Lambda(10^{-3}M) < 0.5\ \Omega^{-1}\ cm^2\ mole^{-1}$).

Table 17. Spectral Data for the Compounds of Chapter Four.

	Compound	Infrared cm^{-1}		NMR	
		solid^b	solution^c	$^{31}P\{^1H\}$ δ, ppm^d	^1H δ, ppm
(17)	$[Ir_2(H)_2Cl_2(CO)_2(DPM)_2]$	2012(vs), 1972(st)^e 2091(m), 2222(w)^f	2009(s), 1971(m)^e 2073(w)^f, 2098(w), 2232(w)^f	-1.4, -8.6(m), -5.2(s)^i, -7.6(m)^j	7.6-7.1(m,40H), 5.0(br,4H),-5.76, -14.86(t,$^2J_{P-H}$ = 14.4 Hz) -15.10(t,$^2J_{P-H}$ = 12.5 Hz)^i
(18)	$[Ir_2(H)_4Cl(CO)_2(DPM)_2][BF_4]$		2038(s), 2073(vs)^e 1964(w)^f, 2147(m), 2221(w)^f	-9.6(m)	7.7-7.2(m,40H),5.04(m,2H), 4.97(m,2H),-10.00(br,1H) -14.02(br,1H),-14.46(br,1H) -16.59(t,1H,$^2P_{P-H}$ = 11,1Hz)
(19)	$[Ir_2(H)_2(CO)_2(\mu-Cl)(DPM)_2][BF_4]$	1934(vs)^e, 2067(st)^f		-1.3(s)	7.55-7.34(m,40H),4.17(s,4H) -13.50(br,t,2H)
(20)	$[Ir_2(H)(CH_3CO_2C{=}CHCO_2CH_3)Cl_2(CO)_2(DPM)_2]$	1982(vs)^e, 2131(w)^e 1712(st)^g, 1623(w)^h	1987(vs), 2004(vs)^e 2148(w)^f	-2.8,-16.5(m)	7.05-7.81(m,40H), 5.19(m,2H),4.47(m,2H), 3.85(s,1H),3.21(s,3H), 2.97(s,3H)
(21)	$[Ir_2(CH_3CO_2C{=}CHCO_2CH_3)_2Cl_2(CO)_2(DPM)_2)]$	1987(vs), 1947(m)^e 1706(vs)^g, 1632(m)^h	2002(st), 1963(m)^e	-12.5,-16.5(m)	7.43-6.92(m,40H),5.74(m,2H) 4.81(m,2H),4.49(s,1H), 4.75(s,1H),3.19(s,3H), 3.28(s,3H),3.46(s,3H) 3.48(s,3H),

a) Abbreviations used: st = strong, vs = very strong, med = medium, w = weak, s = singlet, m = multiplet, br = broad, t = triplet.

b) Nujol mull. c) CH_2Cl_2 solution d) vs 85% H_3PO_4. e) v(CO). f) v(Ir-H) g) v(C=O) of CO_2CH_3.

h) v(C=C). i) -40°C j) -100°C.

Anal. Calcd for $Ir_2Cl_2P_4O_{10}C_{64}H_{58}$: C, 49.07%; H, 3.73%. Found: C, 48.78%; H, 3.91%.

X-Ray Data Collection

Crystals of $[Ir_2(CH_3CO_2C{=}CHCO_2CH_3)_2Cl_2(CO)_2(DPM)_2]$ (**21**) of suitable quality for an X-ray study were obtained by the slow diffusion of diethyl ether into a saturated acetone solution of the complex. The crystals proved to be air stable so one was mounted on a glass fibre in the air and no special precautions were taken. Unit cell parameters were obtained from a least-squares refinement of the setting angles of 25 reflections, in the range $18.0° \leq 2\theta \leq 24.0°$, which were accurately centred on an Enraf-Nonius CAD4 diffractometer using MoKα radiation. The lack of systematic absences and the $\bar{1}$ diffraction symmetry were consistent with the space groups P1 and $P\bar{1}$. The centrosymmetric space group was chosen and later verified by the successful refinement of the structure with acceptable positional parameters, thermal parameters and agreement indices. A cell reduction failed to show the presence of a higher symmetry cell.[171]

Intensity data were collected on a CAD4 diffractometer in the bisecting mode employing the ω-2θ scan technique up to $2\theta = 46.0°$ with graphite monochromated MoKα radiation.

Backgrounds were scanned for 25% of the peak width on either end of the peak scan. The intensities of three standard reflections were measured every 1 h of exposure to assess possible crystal decomposition or movement. No significant variation in these standards was observed so no correction was applied to the data. 17756 unique reflections were measured and processed in the usual way using a value of 0.04 for p[153]; of these 11275 were considered to be observed and were used in subsequent calculations. Absorption corrections were applied to the data by using Gaussian integration.[154] See Table 18 for pertinent crystal data and details of data collection.

Structure Solution and Refinement

The structure was solved in the space group $P\bar{1}$ with two individual dimers per asymmetric unit. The positions of the four independent Ir atoms were obtained by using a combination of direct methods and Patterson techniques. Subsequent refinements and difference Fourier calculations led to the location of the other atoms. Atomic scattering factors were taken from Cromer and Waber's tabulation[155] for all atoms except hydrogen, for which the values of Stewart et al[156] were used. Anomalous dispersion terms[157] for Ir, Cl and P were included in F_c. The carbon atoms of

Table 18. Summary of Crystal Data and Details of Intensity Collection for $[Ir_2(CH_3CO_2C{=}CHCl_2CH_3)_2Cl_2(CO)_2(DPM)_2]$

compd	$[Ir_2(CH_3CO_2C{=}CHCO_2CH_3)_2Cl_2(CO)_2(DPM)_2]$
f_ω	1566.35
formula	$Ir_2Cl_2P_4O_{10}C_{64}H_{58}$
cell parameters	a = 15.983(2) Å b = 20.458(6) Å c = 21.502(5) Å α = 107.88(2)° β = 90.40(1)° γ = 106.20(2)° V = 6392.08 $Å^3$
d(calcd)g/cm^3	1.628
space group	$P\bar{1}$ (Z = 4)
temp, °C	22
radiation (λ, Å)	graphite-monchromated MoKα (0.71069)
receiving aperture, mm	2.00 + (1.00 tanθ)wide x 4.0 high 173 from crystal
take-off angle, deg	3.0
scan speed, deg/min	variable between 6.705 and 1.059
scan width	0.75 + (0.347 tanθ) in ω
2θ limits, deg	$0.6 < 2\theta < 46.0$
no. of unique data collected	17756 (+h, ±k, ±ℓ)
no. of unique data used	11275
range of transmission factors	0.32906 - 0.44765
final no. of parameters refined	545
error in observation of unit weight	2.9598
R	0.061
R_ω	0.090

all phenyl rings were refined as rigid groups having D_{6h} symmetry, C-C distances of 1.392 Å and independent isotropic thermal parameters. All hydrogen atoms of the DPM ligands were located and included as fixed contributions in the least-squares refinements but were not themselves refined. Their idealized positions were calculated from the geometries about their attached carbon atoms using C-H distances of 0.95 Å. Hydrogen atoms were assigned isotropic thermal parameters of 1 $Å^2$ greater than the isotropic thermal parameter of their attached carbons. The olefinic hydrogens attached to carbons C(5A), C(5B), C(6A), and C(6B) were located and were included as fixed contributions as described above. No attempt was made to locate the methyl hydrogens of the methyl carboxylate substituents. In the final refinements only the Ir, Cl and P atoms were refined anisotropically owing to the large number of variables and the resulting high cost of the least-squares calculations.

The final model with 545 parameters varied refined to $R = 0.060$ and R_ω 0.090[158]. On the final difference Fourier map, the 20 highest peaks (1.01-0.34 $eÅ^{-3}$) were in the vicinities of the iridium and chlorine atoms. A typical carbon on earlier synthesis had a peak intensity of about 4.0 $eÅ^{-3}$. The final positional parameters of the individual non-hydrogen atoms and the phenyl groups are given in Tables 19 and 20, respectively. The derived hydrogen positions and their thermal parameters are listed in Table 21. A listing of observed and calculated structure amplitudes used in the refinements is available.[159]

Description of Structure

The title complex crystallizes in the space group $P\bar{1}$ with two independent dimers per asymmetric unit. Although the dimers differ on their relative orientations, all the analogous bond lengths and angles (see Tables 22 and 23) associated with each are virtually identical confirming that there is no major difference between them. A perspective view of molecule A, including the numbering scheme, is shown in Figure 7. A view of the approximate equatorial plane of the metals is shown in Figure 8 along with some relevent average bond lengths and angles.

The overall geometry of the complex is essentially as expected for a binuclear species bridged by two mutually trans DPM ligands. Within the DPM framework, the bond lengths and angles are all normal (Tables 22 and 23) and similar to those found in other DPM-bridged complexes of iridium[151-166,173]. Each metal has a slightly distorted octahedral geometry in which the coordination sites are

Table 19. Positional and Thermal Parameters for the Non-group Atoms of $[Ir_2(CH_3CO_2C{=}CHCO_2CH_3)_2Cl_2(CO)_2(DPM)_2]$.

a) Anisotropic Atoms

Atom	x[a]	y	z	U11[b]	U22	U33	U12	U13	U23
Ir(1A)	0.43271(5)	0.24036(4)	-0.15032(3)	3.64 (4)	3.37 (4)	3.13 (4)	0.56 (3)	0.22 (3)	1.04 (3)
Ir(2A)	0.25200(5)	0.24104(4)	-0.20866(3)	4.18 (5)	3.42 (4)	3.37 (4)	1.27 (4)	0.46 (3)	1.31 (3)
Ir(1B)	-0.24685(5)	0.24364(4)	0.35311(3)	4.18 (5)	3.09 (4)	2.91 (4)	1.03 (3)	0.42 (3)	0.71 (3)
Ir(2B)	-0.07859(5)	0.24376(4)	0.28990(3)	3.68 (4)	3.12 (4)	3.21 (4)	0.50 (3)	0.32 (3)	1.10 (3)
Cl(1A)	0.3756(4)	0.1129(4)	-0.1863(3)	8.5 (5)	12.2 (6)	7.9 (5)	4.1 (4)	1.1 (4)	4.3 (4)
Cl(2A)	0.2060(4)	0.1141(4)	-0.2462(3)	8.4 (5)	12.9 (6)	7.8 (5)	2.9 (4)	0.5 (4)	3.8 (4)
Cl(1B)	-0.2840(4)	0.1163(4)	0.3123(3)	7.9 (4)	11.4 (5)	7.2 (4)	1.6 (4)	1.0 (3)	3.4 (4)
Cl(2B)	-0.1243(5)	0.1168(4)	0.2554(3)	10.1 (5)	12.1 (6)	8.0 (5)	4.3 (5)	2.0 (4)	3.5 (4)
P(1A)	0.4776(3)	0.2210(3)	-0.2533(2)	4.5 (3)	4.0 (3)	4.0 (3)	1.2 (2)	0.8 (2)	1.4 (2)
P(2A)	0.3049(3)	0.2242(2)	-0.3126(2)	5.0 (3)	3.5 (3)	3.3 (3)	0.8 (2)	0.1 (2)	1.1 (2)
P(3A)	0.3587(3)	0.2256(2)	-0.0558(2)	4.7 (3)	3.2 (3)	3.4 (3)	0.8 (2)	0.3 (2)	1.2 (2)
P(4A)	0.1841(3)	0.2241(3)	-0.1161(2)	3.7 (3)	4.0 (3)	3.9 (3)	0.7 (2)	0.6 (2)	1.1 (2)
P(1B)	-0.3161(3)	0.2327(2)	0.2535(2)	4.0 (3)	2.0 (2)	3.4 (3)	0.8 (2)	0.8 (2)	1.1 (2)
P(2A)	-0.1487(3)	0.2255(2)	0.1871(2)	4.8 (3)	3.1 (3)	3.4 (3)	0.9 (2)	0.5 (2)	1.0 (2)
P(3B)	-0.1894(3)	0.2265(2)	0.4462(2)	4.9 (3)	3.2 (3)	3.3 (3)	0.8 (2)	0.6 (2)	1.2 (2)
P(4B)	-0.0182(3)	0.2297(2)	0.3825(2)	3.9 (3)	2.2 (2)	3.6 (3)	0.1 (2)	0.1 (2)	0.6 (2)

[a] Estimated standard deviations in this and other tables are given in parentheses and correspond to the least significant digits.

[b] The thermal parameters have been multiplied by 10^2. The thermal ellipsoid is given by $\exp[-2\pi^2(U_{11}a^{*2}h^2 + U_{22}b^{*2}k^2 + U_{33}c^{*2}\ell^2 + 2U_{12}a^*b^*hk + 2U_{13}a^*c^*h\ell + 2U_{23}b^*c^*k\ell)]$.

(continued...)

Table 19 (continued)

b) Isotropic Atoms

Atom	x	y	z	$B(\AA^2)^a$	Atom	x	y	z	$B(\AA^2)$
O(1A)	0.4829(9)	0.3987(7)	-0.1133(6)	4.7(3)	O(1B)	-0.1806(9)	0.4013(7)	0.4035(7)	5.0(3)
O(2A)	0.3072(9)	0.3977(8)	-0.1577(7)	5.5(3)	O(2B)	-0.0274(9)	0.4038(7)	0.3325(6)	4.9(3)
O(3A)	0.6620(12)	0.3383(10	-0.0951(9)	8.0(5)	O(3B)	-0.3622(10)	0.3470(8)	0.4830(8)	6.1(4)
O(4A)	0.1647(10)	0.3377(8)	-0.2919(8)	6.2(4)	O(4B)	0.2090(11)	0.2309(9)	0.1944(8)	6.1(4)
O(5A)	0.6936(12)	0.2289(10	-0.0395(9)	8.2(5)	O(5B)	-0.5572(10)	0.1177(8)	0.4224(7)	7.2(4)
O(6A)	-0.0308(10)	0.2311(8)	-0.3220(8)	6.2(4)	O(6B)	0.1525(10)	0.3379(8)	0.3184(7)	5.7(3)
O(7A)	0.5783(11)	0.3383(9)	-0.0128(8)	6.1(4)	O(7B)	-0.3970(10)	0.3391(8)	0.3807(7)	6.0(4)
O(8A)	0.0908(10)	0.3392(8)	-0.2037(8)	6.1(4)	O(8B)	0.1091(9)	0.3460(7)	0.2223(7)	4.9(3)
O(9A)	0.6487(10)	0.1113(8)	-0.0863(7)	5.9(3)	O(9B)	-0.5425(11)	0.2338(9)	0.4368(8)	7.0(4)
O(10A)	-0.0674(9)	0.1137(8)	-0.3459(7)	5.5(3)	O(10B)	0.1398(9)	0.1153(7)	0.1443(7)	5.3(3)
C(1A)	0.4577(12)	0.3378(10)	-0.1273(9)	3.4(4)	C(1B)	-0.2060(12)	0.3403(10)	0.3818(9)	3.5(4)
C(2A)	0.2867(12)	0.3375(11)	-0.1787(9)	4.0(4)	C(2B)	-0.0478(12)	0.3414(10)	0.3169(9)	3.6(4)
C(3A)	0.3869(11)	0.1783(9)	-0.3169(8)	3.0(3)	C(3B)	-0.2664(11)	0.1848(9)	0.1865(8)	3.2(4)
C(4A)	0.2406(11)	0.1791(9)	-0.0781(8)	3.1(3)	C(4B)	-0.1035(11)	0.1842(9)	0.4225(9)	3.5(4)
C(5A)	0.5384(13)	0.2380(10)	-0.1041(9)	4.0(4)	C(5B)	-0.3651(11)	0.2410(9)	0.3930(8)	3.1(3)
C(6A)	0.1339(12)	0.2383(10)	-0.2533(9)	3.5(4)	C(6B)	0.0406(11)	0.2410(9)	0.2492(8)	2.8(3)
C(7A)	0.5591(12)	0.1765(10)	-0.1097(9)	3.7(4)	C(7B)	-0.4252(12)	0.1822(10)	0.3939(9)	3.8(4)

(continued...)

Table 19 (continued)

C(8A)	0.0670(13)	0.1798(10)	-0.2816(9)	3.9(4)	C(8B)	0.0573(13)	0.1824(10)	0.2104(9)	4.0(4)
C(9A)	0.6040(15)	0.3089(12)	-0.0683(12)	5.6(5)	C(9B)	-0.3769(13)	0.3129(11)	0.4250(10)	4.2(4)
C(10A)	0.1252(14)	0.3081(11)	-0.2546(10)	4.7(4)	C(10B)	0.1059(13)	0.3121(10)	0.2659(10)	4.0(4)
C(11A)	0.6378(15)	0.1764(12)	-0.0752(11)	5.3(5)	C(11B)	-0.5099(13)	0.1848(11)	0.4212(10)	4.2(4)
C(12A)	-0.0116(13)	0.1775(11)	-0.3193(10)	4.1(4)	C(12B)	0.1409(13)	0.1816(11)	0.1831(10)	4.3(4)
C(13A)	0.6294(21)	0.4156(17)	0.0243(16)	10.1(9)	C(13B)	-0.3929(24)	0.4213(20)	0.4124(18)	12.5(11)
C(14A)	0.0960(20)	0.4155(17)	-0.1968(15)	9.7(8)	C(14B)	0.1718(17)	0.4191(14)	0.2445(13)	7.3(6)
C(15A)	0.7244(17)	0.1049(14)	-0.0514(13)	7.3(6)	C(15B)	-0.6477(17)	0.1103(13)	0.4487(12)	6.9(6)
C(16A)	-0.1479(16)	0.1093(13)	-0.3836(12)	6.3(6)	C(16B)	0.2198(16)	0.1089(13)	0.1149(12)	6.4(6)
H(1A)	0.5118	0.1329	-0.1356	4.6	H(1B)	-0.4111	0.1373	0.3801	4.8
H(2A)	0.0700	0.1356	-0.2764	4.5	H(2B)	0.0123	0.1373	0.1992	5.0

Table 20. Derived Parameters for the Rigid-Group Atoms of $[Ir_2(CH_3CO_2C{=}CHCO_2CH_3)_2Cl_2(CO)_2(DPM)_2]$.

Atom	X	Y	Z	B(Å²)	Atom	X	Y	Z	B(Å²)
C(G11A)	0.5511(9)	0.2948(7)	-0.2780(8)	4.1(4)	C(G31A)	0.3566(9)	0.3013(7)	-0.3426(7)	4.2(4)
C(G12A)	0.6037(11)	0.3562(9)	-0.2306	7.6(6)	C(G32A)	0.3899(11)	0.3703(9)	-0.2981(5)	6.5(6)
C(G13A)	0.6605(11)	0.4103(8)	-0.2495(8)	10.5(5)	C(G33A)	0.4327(11)	0.4270(6)	-0.3202(8)	9.1(8)
C(G14A)	0.6647(10)	0.4031(8)	-0.3150(10)	7.7(7)	C(G34A)	0.4422(10)	0.4145(8)	-0.3868(9)	7.1(6)
C(G15A)	0.6121(11)	0.3417(10)	-0.3632(6)	6.5(6)	C(G35A)	0.4090(11)	0.3455(9)	-0.4312(6)	6.3(6)
C(G16A)	0.5553(10)	0.2876(7)	-0.3443(7)	6.9(6)	C(G36A)	0.3661(10)	0.2889(6)	-0.4091(7)	6.7(6)
C(G11B)	-0.3244(10)	0.3100(6)	0.2343(7)	3.2(4)	C(G31B)	-0.1366(9)	0.3010(6)	0.1551(6)	3.2(4)
C(G12B)	-0.3607(8)	0.3758(8)	0.2616(7)	5.5(5)	C(G32B)	-0.0646(8)	0.3620(7)	0.1772(6)	5.5(5)
C(G13B)	-0.2672(10)	0.4360(6)	0.2469(8)	6.9(6)	C(G33B)	-0.0536(8)	0.4168(6)	0.1496(7)	5.7(5)
C(G14B)	-0.3375(13)	0.4304(8)	0.2049(1)	7.4(6)	C(G34B)	-0.1148(11)	0.4106(7)	0.1001(7)	6.1(5)
C(G15B)	-0.4013(10)	0.3646(11)	0.1777(8)	11.6(11)	C(G35B)	-0.1868(9)	0.3496(9)	0.0780(6)	7.3(6)
C(G16B)	-0.3947(9)	0.3044(8)	0.1924(8)	8.6(8)	C(G36B)	-0.1978(7)	0.2948(6)	0.1056(7)	5.6(5)
C(G21A)	0.5416(9)	0.1567(7)	-0.2698(7)	4.3(4)	C(G41A)	0.2232(8)	0.1615(7)	-0.3803(6)	3.8(4)
C(G22A)	0.5029(7)	0.0834(7)	-0.3003(7)	5.0(5)	C(G42A)	0.2144(9)	0.0882(8)	-0.4008(7)	5.6(5)
C(G23A)	0.5537(10)	0.0364(5)	-0.3113(7)	6.4(6)	C(G43A)	0.1534(11)	0.0415(6)	-0.4533(8)	6.9(6)
C(G24A)	0.6433(9)	0.0627(8)	-0.2918(8)	6.4(6)	C(G44A)	0.1011(9)	0.0680(9)	-0.4852(7)	7.1(6)
C(G25A)	0.6820(7)	0.1360(8)	-0.2613(8)	6.2(6)	C(G45A)	0.1099(10)	0.1413(9)	-0.4648(8)	8.3(8)
C(G26A)	0.6312(9)	0.1830(6)	-0.2503(7)	5.6(5)	C(G46A)	0.1709(10)	0.1880(6)	-0.4123(8)	6.2(6)
C(G21B)	-0.4272(7)	0.1714(6)	0.2360(7)	3.9(4)	C(G41B)	-0.1197(8)	0.1620(6)	0.1181(5)	3.4(4)
C(G22B)	-0.4448(8)	0.0984(7)	0.2022(7)	4.4(4)	C(G42B)	-0.1537(8)	0.0886(7)	0.1076(6)	4.4(4)
C(G23B)	-0.5305(10)	0.0534(5)	0.1910(7)	6.5(6)	C(G43B)	-0.1287(9)	0.0397(5)	0.0560(7)	5.7(5)
C(G24B)	-0.5986(7)	0.0814(8)	0.2136(8)	6.8(6)	C(G44B)	-0.0697(10)	0.0641(7)	0.0150(6)	5.8(5)
C(G25B)	-0.5811(8)	0.1544(8)	0.2475(8)	6.9(6)	C(G45B)	-0.0357(9)	0.1376(8)	0.0255(6)	6.0(6)
C(G26B)	-0.4954(10)	0.1994(6)	0.2586(7)	5.2(5)	C(G46B)	-0.0607(8)	0.1865(5)	0.0771(7)	4.4(4)
C(G51A)	0.3621(9)	0.2994(7)	0.0194(5)	3.8(4)	C(G71A)	0.1691(9)	0.2982(7)	-0.0489(6)	3.4(4)
C(G52A)	0.3859(10)	0.3699(8)	0.0185(6)	6.9(6)	C(G72A)	0.1695(10)	0.3626(8)	-0.0583(6)	6.7(6)
C(G53A)	0.3915(11)	0.4262(6)	0.0762(1)	8.5(7)	C(G73A)	0.1526(11)	0.4170(6)	-0.0074(9)	8.1(7)
C(G54A)	0.3734(11)	0.4121(7)	0.1348(7)	6.9(6)	C(G14A)	0.1351(10)	0.4070(8)	0.0529(7)	6.6(6)
C(G55A)	0.3496(10)	0.3416(9)	0.1357(5)	5.7(5)	C(G75A)	0.1347(11)	0.3426(9)	0.0623(6)	7.8(7)
C(G56A)	0.3439(9)	0.2853(6)	0.0781(7)	5.6(5)	C(G76A)	0.1517(10)	0.2881(7)	0.0114(8)	6.6(6)
C(G51B)	-0.1456(8)	0.3015(6)	0.5213(5)	3.5(4)	C(G71B)	0.0484(8)	0.3058(6)	0.4491(6)	3.6(4)
C(G52B)	-0.1680(8)	0.3650(7)	0.5332(6)	4.4(4)	C(G72B)	0.0369(9)	0.3732(8)	0.4595(7)	5.5(5)
C(G53B)	-0.1339(10)	0.4218(6)	0.5909(7)	5.9(5)	C(G73B)	0.0851(10)	0.4317(6)	0.5118(8)	6.3(6)
C(G54B)	-0.0774(10)	0.4151(7)	0.6366(6)	6.4(6)	C(G74B)	0.1448(10)	0.4228(7)	0.5537(6)	6.3(6)
C(G55B)	-0.0550(9)	0.3516(8)	0.6247(6)	7.0(6)	C(G75B)	0.1563(9)	0.3555(9)	0.5433(7)	9.0(8)
C(G56B)	-0.0891(9)	0.2948(6)	0.5670(7)	5.4(5)	C(G76B)	0.1081(10)	0.2969(7)	0.4910(8)	5.9(5)
C(G61A)	0.3929(8)	0.1630(6)	-0.0246(6)	3.2(3)	C(G81A)	0.0767(7)	0.1624(7)	-0.1373(7)	3.7(4)
C(G62A)	0.3505(7)	0.0895(7)	-0.0477(6)	5.4(5)	C(G82A)	0.0599(8)	0.0886(7)	-0.1512(7)	4.8(5)
C(G63A)	0.3777(9)	0.0430(5)	-0.0224(7)	5.5(5)	C(G83A)	-0.0259(10)	0.0437(5)	-0.1666(7)	6.0(5)
C(G64A)	0.4474(10)	0.0699(8)	0.0266(7)	6.0(5)	C(G84A)	-0.0948(7)	0.0725(8)	-0.1681(8)	6.7(6)
C(G65A)	0.4899(8)	0.1434(8)	0.0502(6)	8.0(7)	C(G85A)	-0.0780(8)	0.1463(9)	-0.1542(8)	7.2(6)
C(G66A)	0.4626(8)	0.1900(5)	0.0249(7)	5.3(5)	C(G86A)	0.0077(10)	0.1912(6)	-0.1388(8)	6.3(6)
C(G61B)	-0.2643(8)	0.1630(6)	0.4778(6)	3.4(4)	C(G81B)	0.0491(8)	0.1680(6)	0.3637(7)	3.6(4)
C(G62B)	-0.2836(9)	0.0893(7)	0.4664(5)	4.4(4)	C(G82B)	0.0118(7)	0.0953(7)	0.3550(7)	4.5(4)
C(G63B)	-0.3427(9)	0.0415(5)	0.4709(7)	5.7(5)	C(G83B)	0.0632(10)	0.0488(5)	0.3399(7)	6.0(5)
C(G64B)	-0.3825(9)	0.0673(7)	0.5268(7)	6.3(6)	C(G84B)	0.1519(9)	0.0749(8)	0.3335(8)	7.0(6)
C(G65B)	-0.3633(10)	0.1410(8)	0.5581(6)	6.5(6)	C(G85B)	0.1891(7)	0.1476(8)	0.3422(8)	6.3(6)
C(G66B)	-0.3042(9)	0.1888(5)	0.5336(6)	5.1(5)	C(G86B)	0.1377(9)	0.1942(6)	0.3573(7)	6.1(5)

Rigid Group Parameters

Ring 1A	0.6079(7)	0.3490(6)	-0.3969(6)	2.11(3)	1.94(1)	-1.28(3)
Ring 2A	-0.3310(7)	0.3702(6)	0.2196(5)	1.768(11)	2.618(10)	-0.243(11)
Ring 3A	0.5924(6)	0.1097(5)	-0.2808(4)	-1.044(9)	-2.794(9)	-0.235(9)
Ring 4A	-0.5129(6)	0.1264(5)	0.2248(4)	0.382(10)	-2.604(9)	-3.062(10)
Ring 5A	0.3994(6)	0.3579(6)	-0.3647(5)	2.73(3)	1.956(9)	-1.68(3)
Ring 6A	-0.1257(6)	0.3558(5)	0.1276(4)	1.722(10)	2.593(9)	-0.511(10)
Ring 7A	0.1622(6)	0.1148(6)	-0.4328(5)	0.280(9)	3.072(9)	-2.361(9)
Ring 8A	-0.0947(6)	0.1131(5)	0.0665(4)	-0.671(9)	2.817(8)	-0.977(9)
Ring 1B	0.3677(6)	0.3558(5)	0.0771(5)	2.822(12)	-2.580(9)	1.461(11)
Ring 2B	-0.1115(6)	0.3583(5)	0.5790(4)	-2.602(9)	-2.904(8)	2.157(9)
Ring 3B	0.4202(6)	0.1165(5)	0.0013(4)	-1.010(10)	-2.567(8)	0.419(10)
Ring 4B	-0.3234(6)	0.1151(5)	0.5023(4)	0.200(12)	-2.288(8)	2.435(13)
Ring 5B	0.1521(6)	0.3526(6)	0.0020(5)	3.000(13)	-2.494(9)	1.296(12)
Ring 6B	0.0966(6)	0.3643(5)	0.5014(5)	-2.661(10)	-2.919(9)	2.320(9)
Ring 7B	-0.0091(6)	0.1175(5)	-0.1527(4)	0.340(9)	-3.001(9)	-3.010(9)
Ring 8B	0.1005(6)	0.1215(5)	0.3486(4)	-0.925(8)	3.079(9)	-0.284(9)

a) X_c, Y_c, and Z_c are the fractional coordinates of the centroid of the rigid group.

b) The rigid group orientation angles phi, theta and rho (radians) are the angles by which the rigid body is rotated with respect to a set of axes x,y,z. See: La Placa, S.J.; Ibers, J.A. Acta Crystallogr., 1965, 18, 511.

Table 21. Derived Hydrogen Positions for [$Ir_2(CH_3CO_2C{=}CHCO_2CH_3)_2Cl_2(CO)_2(DPM)_2$].

atom	x	y	z	B(Å^2)	atom	x	y	z	B(Å^2)
H1C3A	0.4102	0.1738	-0.3576	4.0	H26A	0.6579	0.2329	-0.2308	6.4
H1C3B	-0.2780	0.1379	0.1891	4.0	H22B	-0.3973	0.0784	0.1878	5.1
H2C3A	0.3592	0.1318	-0.3139	4.0	H23B	-0.5414	0.0024	0.1679	6.8
H2C3B	-0.2976	0.1825	0.1472	4.0	H24B	-0.6568	0.0496	0.2038	7.4
H1C4A	0.2329	0.1321	-0.1107	4.0	H25B	-0.6281	0.1726	0.2596	8.3
H1C4B	-0.0763	0.1826	0.4626	4.0	H26B	-0.4840	0.2486	0.2795	6.4
H2C4A	0.2121	0.1731	-0.0420	4.0	H32A	0.3843	0.3799	-0.2531	7.3
H2C4B	-0.1293	0.1363	0.3952	4.0	H33A	0.4562	0.4748	-0.2909	10.0
H12A	0.6025	0.3626	-0.1849	7.8	H34A	0.4724	0.4531	-0.4030	7.8
H13A	0.6985	0.4528	-0.2174	11.0	H35A	0.4167	0.3367	-0.4773	7.6
H14A	0.7047	0.4399	-0.3292	8.4	H36A	0.3448	0.2418	-0.4395	7.5
H15A	0.6149	0.3368	-0.4085	7.6	H32B	-0.0225	0.3660	0.2101	6.4
H16A	0.5189	0.2466	-0.3760	8.1	H33B	-0.0040	0.4581	0.1637	6.5
H12B	-0.2124	0.3792	0.2911	6.6	H34B	-0.1074	0.4481	0.0808	7.3
H13B	-0.2218	0.4809	0.2664	8.0	H35B	-0.2293	0.3458	0.0443	8.0
H14B	-0.3396	0.4725	0.1960	8.0	H36B	-0.2478	0.2537	0.0907	6.2
H15B	-0.4480	0.3624	0.1501	13.6	H42A	0.2498	0.0695	-0.3797	6.1
H16B	-0.4386	0.2607	0.1748	9.7	H43A	0.1472	-0.0089	-0.4680	7.9
H22A	0.4417	0.0651	-0.3139	5.7	H44A	0.0592	0.0358	-0.5217	7.7
H23A	0.5273	-0.0139	-0.3328	7.3	H45A	0.0738	0.1591	-0.4869	8.9
H24A	0.6782	0.0305	-0.3006	7.4	H46A	0.1764	0.2375	-0.3986	7.3
H25A	0.7435	0.1539	-0.2497	7.3	H42B	-0.1943	0.0715	0.1347	5.3
H43B	-0.1526	-0.0107	0.0478	6.3	H65B	-0.3906	0.1580	0.5961	7.5
H44B	-0.0535	0.0305	-0.0212	6.6	H66B	-0.2914	0.2388	0.5549	6.5
H45B	0.0039	0.1541	-0.0033	6.8	H72A	0.1806	0.3696	-0.0989	7.6
H46B	-0.0378	0.2363	0.0836	5.4	H73A	0.1521	0.4610	-0.0129	9.5
H52A	0.3990	0.3807	-0.0201	8.1	H74A	0.1232	0.4438	0.0885	7.4
H53A	0.4088	0.4751	0.0773	9.6	H75A	0.1226	0.3352	0.1039	8.5
H54A	0.3779	0.4508	0.1756	7.7	H76A	0.1511	0.2438	0.0179	7.3
H55A	0.3370	0.3319	0.1765	6.7	H72B	-0.0036	0.3790	0.4307	6.7
H56A	0.3272	0.2375	0.0791	6.4	H73B	0.0756	0.4778	0.5193	7.1
H52B	-0.2086	0.3691	0.5034	6.2	H74B	0.1754	0.4636	0.5909	7.3
H53B	-0.1504	0.4651	0.6000	6.4	H75B	0.1960	0.3508	0.5739	9.7
H54B	-0.0526	0.4551	0.6758	6.5	H76B	0.1168	0.2520	0.4853	6.7
H55B	-0.0128	0.3491	0.6550	8.9	H82A	0.1069	0.0686	-0.1492	5.8
H56B	-0.0710	0.2531	0.5584	5.8	H83A	-0.0373	-0.0074	-0.1747	6.8
H62A	0.3028	0.0712	-0.0809	5.1	H84A	-0.1537	0.0407	-0.1779	7.3
H63A	0.3488	-0.0071	-0.0384	7.0	H85A	-0.1259	0.1646	-0.1554	8.0
H64A	0.4663	0.0382	0.0438	7.2	H86A	0.0183	0.2406	-0.1299	7.0
H65A	0.5380	0.1618	0.0835	8.0	H82B	-0.0498	0.0776	0.3509	5.0
H66A	0.4920	0.2401	0.0410	6.4	H83B	0.0361	-0.0012	0.3345	6.6
H62B	-0.2552	0.0716	0.4087	5.1	H84B	0.1856	0.0422	0.3245	7.4
H63B	-0.3544	-0.0092	0.4499	6.8	H85B	0.2492	0.1644	0.3391	7.7
H64B	-0.4221	0.0341	0.5436	7.2	H86B	0.1633	0.2432	0.3635	7.0

Table 22. Selected Distances (Å) in $[Ir_2(CH_3CO_2C{=}CHCO_2CH_3)_2Cl_2(CO)_2(DPM)_2]$.

Bonding Distances

	Dimer A	Dimer B		Dimer A	Dimer B
Ir(1)-Ir(2)	3.0128(9)	3.0216(9)	C(12)-0(6)	1.24(2)	1.22(2)
Ir(1)-Cl(1)	2.372(7)	2.371(7)	C(9)-0(7)	1.29(2)	1.30(2)
Ir(2)-Cl(2)	2.362(8)	2.364(8)	C(10)-0(8)	1.30(2)	1.32(2)
Ir(1)-P(1)	2.342(5)	2.320(5)	C(11)-0(9)	1.34(2)	1.38(2)
Ir(1)-P(3)	2.353(5)	2.355(5)	C(12)-0(10)	1.31(2)	1.35(2)
Ir(2)-P(2)	2.354(5)	2.346(5)	C(13)-0(7)	1.52(3)	1.59(3)
Ir(2)-P(4)	2.345(5)	2.335(5)	C(14)-0(8)	1.50(3)	1.48(3)
Ir(1)-C(1)	1.82(2)	1.80(2)	C(15)-0(9)	1.45(3)	1.54(3)
Ir(2)-C(2)	1.80(2)	1.82(2)	C(16)-0(10)	1.48(3)	1.45(3)
Ir(1)-C(5)	2.10(2)	2.08(2)	P(1)-C(3)	1.81(2)	1.80(2)
Ir(2)-C(6)	2.09(2)	2.11(2)	P(2)-C(3)	1.80(2)	1.83(2)
C(1)-0(1)	1.14(2)	1.14(2)	P(3)-C(4)	1.84(2)	1.81(2)
C(2)-0(2)	1.12(2)	1.16(2)	P(4)-C(4)	1.80(2)	1.81(2)
C(5)-C(7)	1.36(2)	1.32(2)	P(2)-C(G11)	1.86(2)	1.79(2)
C(6)-C(8)	1.33(2)	1.33(2)	P(1)-C(G21)	1.84(2)	1.82(1)
C(5)-C(9)	1.50(3)	1.48(2)	P(2)-C(G31)	1.87(2)	1.84(2)
C(6)-C(10)	1.48(3)	1.47(2)	P(2)-C(G41)	1.83(1)	1.81(1)
C(7)-C(11)	1.45(3)	1.49(3)	P(3)-C(G51)	1.83(1)	1.82(1)
C(8)-C(12)	1.47(3)	1.46(3)	P(3)-C(G61)	1.82(2)	1.81(1)
C(9)-0(3)	1.21(2)	1.21(2)	P(4)-C(G71)	1.82(1)	1.81(1)
C(10)-0(4)	1.22(2)	1.23(2)	P(4)-C(G81)	1.78(1)	1.83(2)
C(11)-0(5)	1.22(2)	1.21(2)			

Non-Bonding Distances

	Dimer A	Dimer B
P(1)-P(2)	3.057(8)	3.061(7)
P(3)-P(4)	3.056(8)	3.061(7)
H(1)-Cl(1)	2.30	2.43
H(2)-Cl(2)	2.45	2.50
Cl(1)-Cl(2)	3.00(1)	2.98(1)
C(1)-C(2)	2.94(3)	2.89(3)
0(1)-0(2)	2.95(2)	2.89(2)

Table 23. Selected Angles (Deg) in $[Ir_2(CH_3CO_2C{=}CHCO_2CH_3)_2Cl_2(CO)_2(DPM)_2]$.

	Dimer A	Dimer B
P(1)-Ir(1)-Ir(2)	90.7(1)	89.7(1)
P(3)-Ir(1)-Ir(2)	90.2(1)	91.4(1)
P(2)-Ir(2)-Ir(1)	90.4(1)	91.2(1)
P(4)-Ir(2)-Ir(1)	90.9(1)	89.6(1)
P(1)-Ir(1)-P(3)	163.4(2)	167.1(1)
P(2)-Ir(2)-P(4)	164.5(2)	165.2(2)
Cl(1)-Ir(1)-Ir(2)	89.8(2)	89.7(2)
Cl(2)-Ir(2)-Ir(1)	89.9(2)	89.3(2)
P(1)-Ir(1)-Cl(1)	82.2(2)	83.2(2)
P(3)-Ir(1)-Cl(1)	82.2(2)	84.0(2)
P(2)-Ir(2)-Cl(2)	82.3(2)	83.0(2)
P(4)-Ir(2)-Cl(2)	82.3(2)	82.2(2)
P(1)-Ir(1)-C(1)	95.6(6)	96.6(6)
P(3)-Ir(1)-C(1)	99.9(6)	96.3(6)
P(2)-Ir(2)-C(2)	98.7(6)	96.3(6)
P(4)-Ir(2)-C(2)	96.7(6)	98.5(6)
P(1)-Ir(1)-C(5)	93.2(5)	88.4(5)
P(3)-Ir(1)-C(5)	85.7(5)	90.3(5)
P(2)-Ir(2)-C(6)	87.3(5)	91.3(5)
P(4)-Ir(2)-C(6)	91.0(5)	87.5(5)
Cl(1)-Ir(1)-C(1)	176.7(6)	177.0(6)
Cl(2)-Ir(2)-C(2)	179.0(6)	177.8(6)
Cl(1)-Ir(1)-C(5)	89.2(5)	89.0(5)
Cl(2)-Ir(2)-C(6)	91.9(8)	89.2(5)
C(1)-Ir(1)-C(5)	93.5(8)	94.1(7)
C(2)-Ir(2)-C(6)	91.9(8)	92.9(7)
C(1)-Ir(1)-Ir(2)	91.9(8)	92.9(7)
C(2)-Ir(1)-Ir(2)	87.7(6)	87.3(6)
C(5)-Ir(1)-(Ir(2)	175.8(5)	177.8(5)
C(6)-Ir(2)-Ir(1)	177.3(5)	176.9(5)
Ir(1)-C(1)-O(1)	177(2)	176(2)
Ir(2)-C(2)-O(2)	177(2)	178(2)
Ir(1)-C(5)-C(7)	124(1)	125(1)
Ir(2)-C(6)-C(8)	126(1)	125(1)
Ir(1)-C(5)-C(9)	117(1)	114(1)
Ir(2)-C(6)-C(10)	116(1)	113(1)
C(7)-C(5)-C(9)	119(2)	121(2)
C(8)-C(6)-C(10)	117(2)	121(2)
C(5)-C(7)-C(11)	122(2)	122(2)
C(6)-C(8)-C(12)	125(2)	124(2)
C(5)-C(7)-H(1)	112	119
C(6)-C(8)-H(2)	117	119
C(11)-C(7)-H(1)	125	120
C(12)-C(8)-H(2)	117	117
C(5)-C(9)-O(3)	122(2)	127(2)
C(6)-C(10)-O(4)	121(2)	121(2)
C(5)-C(9)-O(7)	110(3)	110(2)
C(6)-C(10)-O(8)	112(2)	116(2)
C(7)-C(11)-O(5)	126(2)	130(2)
C(8)-C(12)-O(6)	125(2)	128(2)
C(7)-C(11)-O(9)	115(2)	116(2)
C(8)-C(12)-O(10)	110(2)	112(2)

	Dimer A	Dimer B
O(3)-C(9)-O(7)	126(2)	123(2)
O(4)-C(10)-O(8	125(2)	123(2)
O(5)-C(11)-O(9)	119(2)	120(2)
O(6)-C(12)-O(10)	119(2)	119(2)
C(9)-O(7)-C(13)	117(2)	111(2)
C(10)-O(8)-C(14)	114(2)	113(2)
C(11)-O(9)-C(15)	119(2)	117(2)
C(12)-O(10)-C(16)	117(2)	117(2)
P(1)-C(3)-P(2)	116(1)	115(1)
P(3)-C(3)-P(4)	114(1)	115(1)
Ir(1)-P(1)-C(3)	109.3(6)	110.0(6)
Ir(1)-P(1)-C(G11)	122.5(4)	121.3(4)
Ir(1)-P(1)-C(G21)	113.3(5)	113.3(5)
Ir(2)-P(2)-C(3)	108.7(6)	108.9(6)
Ir(2)-P(2)-C(G31)	122.0(4)	120.6(3)
Ir(2)-P(2)-C(G41)	113.5(4)	115.6(4)
Ir(1)-P(3)-C(4)	109.0(6)	108.6(6)
Ir(1)-P(3)-C(G51)	124.5(4)	121.2(4)
Ir(1)-P(3)-C(G61)	113.9(4)	115.2(4)
Ir(2)-P(4)-C(4)	109.6(6)	110.3(6)
Ir(2)-P(4)-C(G71)	122.5(5)	121.9(5)
Ir(2)-P(4)-C(G81)	112.4(5)	114.0(4)
C(G11)-P(1)-C(G21)	100.9(7)	104.9(6)
C(G11)-P(1)-C(3)	105.6(8)	105.6(8)
C(G21)-P(1)-C(3)	103.5(7)	99.36
C(G31)-P(2)-C(G41)	104.2(6)	100.3(6)
C(G31)-P(2)-C(3)	104.3(2)	106.7(8)
C(G41)-P(2)-C(3)	102.0(6)	103.1(6)
C(G51)-P(3)-C(G61)	102.1(6)	101.1(5)
C(G51)-P(3)-C(4)	103.5(7)	106.8(6)
C(G61)-P(3)-C(4)	101.0(7)	102.1(7)
C(G71)-P(4)-C(G81)	103.0(6)	103.1(6)
C(G71)-P(4)-C(4)	105.1(7)	104.0(6)
C(G81)-P(4)-C(4)	102.2(7)	101.1(8)
P(1)-C(G11)-C(G12)	102.3(6)	120.0(7)
P(1)-C(G11)-C(G16)	119.7(5)	120.1(6)
P(1)-C(G21)-C(G22)	121.9(5)	122.0(5)
P(1)-C(G21)-C(G26)	118.2(5)	118.0(4)
P(2)-C(G31)-C(G32)	120.2(6)	120.7(7)
P(2)-C(G31)-C(G36)	119.7(5)	119.2(5)
P(2)-C(G41)-C(G42)	120.7(6)	119.9(5)
P(2)-C(G41)-C(G46)	119.3(5)	120.1(4)
P(3)-C(G51)-C(G52)	120.0(6)	120.8(5)
P(3)-C(G51)-C(G56)	120.0(5)	119.2(5)
P(3)-C(G61)-C(G62)	121.2(6)	121.0(5)
P(3)-C(G2)-C(G66)	119.8(5)	119.0(5)
P(4)-C(G71)-C(G72)	120.9(6)	119.2(6)
P(4)-C(G71)-C(G76)	119.0(6)	120.8(5)
P(4)-C(G81)-C(G82)	123.2(6)	120.4(5)
P(4)-C(G81)-C(G86)	116.9(5)	119.6(5)

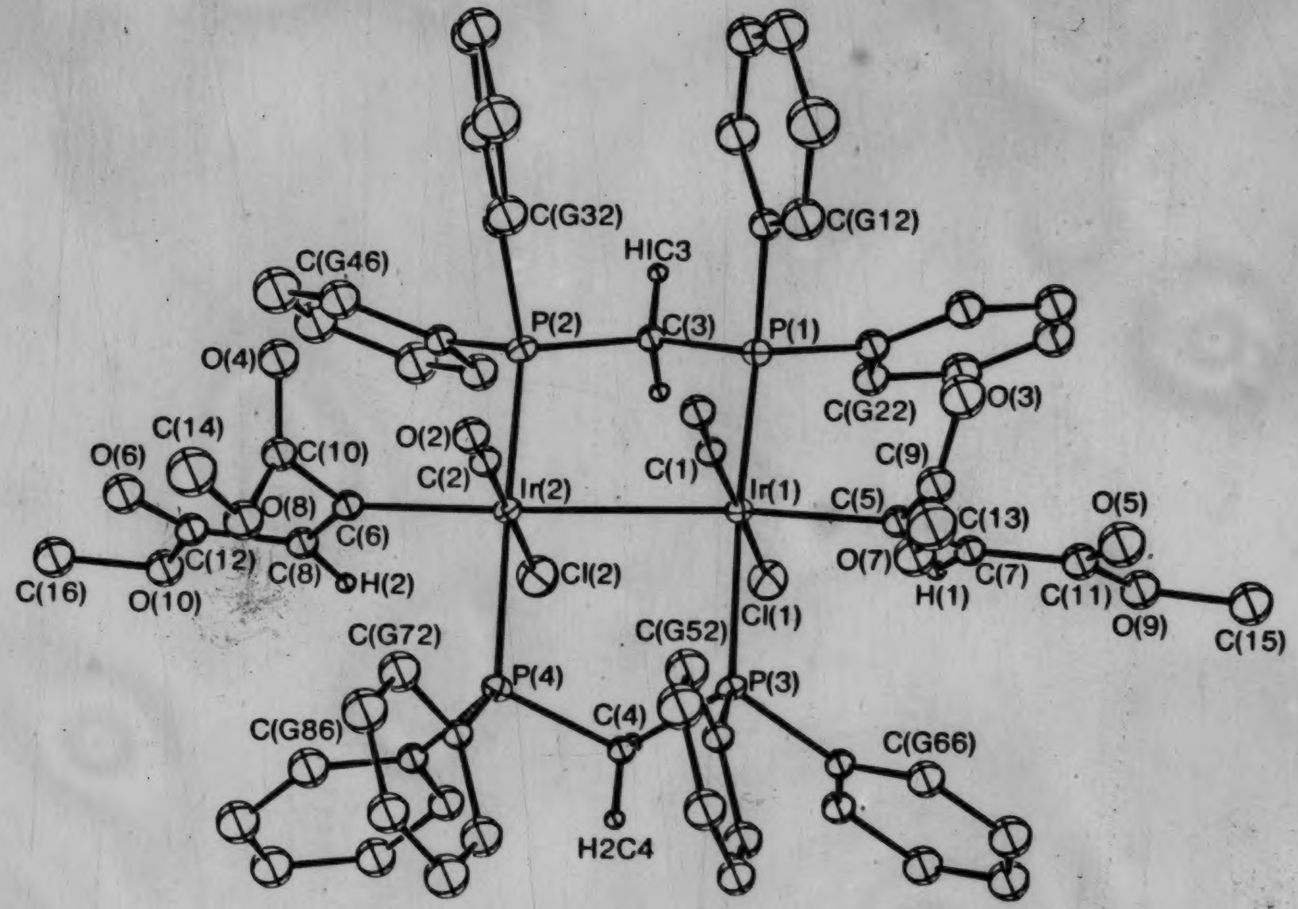
C(G32)
C(G12)
HIC3
C(G46)
P(2)
C(3)
P(1)
O(4)
C(G22)
O(3)
C(14)
C(9)
O(2)
C(10)
O(6)
C(2)
C(1)
Ir(2)
Ir(1)
C(5)
O(5)
O(8)
C(13)
C(6)
O(7)
C(12)
C(7)
C(8)
H(2)
Cl(2)
H(1)
C(11)
C(16)
O(10)
Cl(1)
O(9)
C(15)
C(G72)
C(G52)
P(4)
P(3)
C(4)
C(G86)
C(G66)
H2C4

Figure 7. Perspective view of 21, [$Ir_2(CH_3CO_2C{=}CHCO_2CH_3)Cl_2(CO)_2(DPM)_2$] (Dimer A). Thermal ellipsoids are drawn at the 15% level except for the methylene hydrogens which are drawn artificially small. Phenyl hydrogens have the same number as their attached carbon atoms.

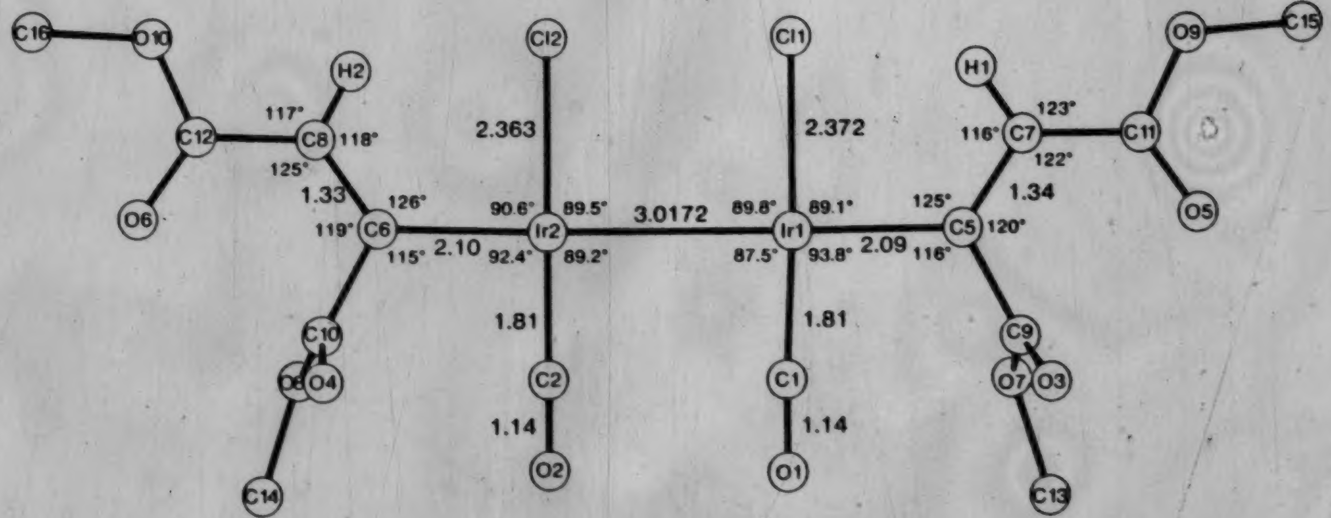
C16
O10
C12
O6
H2
C8
117°
118°
125°
1.33
126°
119°
C6
115°
2.10
C10
O8
O4
C14
Cl2
2.363
90.6°
89.5°
Ir2
92.4°
89.2°
1.81
C2
1.14
O2
3.0172
Cl1
2.372
89.8°
89.1°
Ir1
87.5°
93.8°
1.81
C1
1.14
O1
2.09
125°
C5
120°
116°
1.34
H1
116°
C7
123°
122°
C11
O9
C15
O5
C9
O7
O3
C13

Figure 8. Representation of the inner coordination sphere of the complex in the plane of the metal atoms and metallated olefin ligands. Some relevant average bond lenths and angles of the two dimers are shown.

occupied by the two trans phosphorus atoms, a carbonyl group, a chloride ligand, a metallated olefin and the Ir-Ir bond. The major distortion from octahedral geometry about each metal occurs in the P-Ir-P angles which are ca. 165.1° rather than 180° with all of the phosphorus atoms bent slightly towards the Cl ligands. This bending seems to arise in order to relieve some of the severe steric crowding in the complex. Each molecule possesses approximate C_{2v} geometry with a pseudo-mirror plane running perpendicular to the Ir-Ir bond (see Figure 8).

The iridium-iridium distances of 3.0129(10)Å and 3.0216(9)Å are extremely long and fall outside the range normally associated with Ir-Ir single bonds in analogous Ir-DPM systems (range 2.779(1)-2.893(2)Å)[151,166,173]. However, electron counting rules require a formal metal-metal bond otherwise each metal would have a 17 electron configuration. The long metal-metal separation is undoubtedly a result of the steric crowding about the Ir atoms. Bringing the metals closer together would result in highly unfavourable interactions between the two chlorine atoms and the two carbonyl groups. These distances are already rather short, at ca. 2.99 Å and 2.92 Å, respectively. In a somewhat analogous complex, $[Ir_2Cl_4(CO)_2(DPM)_2]$, which also has pseudo-octahedral Ir centres and cis Cl ligands, the metal-metal distance has a more typical value of 2.786(1) Å[166]. However, in this case the molecule is twisted about the Ir-Ir bond by ca. 27.7° such that the ligands on one metal are staggered with respect to those on the other metal, reducing the unfavourable contacts and allowing a normal metal-metal interaction. In the present complex both halves of the molecule are almost exactly eclipsed. It seems that staggering about the two metals is not possible owing to the unfavourable contacts that would result between the metallated olefins and the DPM phenyl groups. In another crowded binuclear complex containing pseudo-octahedral metal centres, $[Rh_2(CN^tBu)_4(\mu\text{-}CF_3C_2CF_3)(DPM)_2][PF_6]_2$,[44] the molecule is found to be twisted about the Rh-Rh axis by ca. 20.3° and the Rh-Rh distance is still very long (2.9653(6) Å) although the complex again has a metal-metal bond.

The Ir-Cl distances and the parameters involving the carbonyl ligands are all normal and compare well with values previously reported.[151,166,173]

As can be seen in Figures 7 and 8, the alkyne molecules have inserted into the Ir-H bonds in a cis configuration forming two metal-alkenyl linkages with the two CO_2CH_3 groups lying in the same side of the C=C bond. The C=C distances (av. 1.34 Å) are typical of carbon-carbon double bonds and the angles about these carbon atoms are all close to 120° (see Table 23), consistent with sp^2

hybridization. The Ir-C(olefin) distances (av. 2.10 Å) are normal and compare well with similar values involving σ-bonded carbon atoms[190,191]. Within each of the metallated olefin groups, one CO_2CH_3 group lies in the metal-olefin plane while the other is essentially perpendicular to it, again likely a result of intramolecular non-bonded contacts. As a result, the C=O fragment of one of the CO_2CH_3 groups is coplanar with the olefin linkage and could in principle be conjugated with it. This does appear to occur as the bond lengths indicate no significant difference betweeen the two CO_2CH_3 groups of each metallated olefin. All of the bond lengths and angles associated with the olefin atoms are unexceptional and similar to those observed in other structures.[66,173] One feature of note is that the severe crowding around the metals leads to rather short olefinic hydrogen-chlorine contacts of *ca*. 2.42 Å.

Discusssion of Results

Placing an atmosphere of H_2 over a solution of *trans*-$[IrCl(CO)(DPM)]_2$, **3**, produces an immediate reaction as evidenced by a rapid colour change from purple to yellow. The new compound **17** which is isolated from this solution displays two distinct terminal carbonyl bands (2012, 1972

cm^{-1}) and two terminal hydride bands (2222, 2091 cm^{-1}) in the infrared spectrum while analyses indicate the presence of two chlorines per dimer. Based on this information, **17** is formulated to have the structure shown below in the solid state. This geometry is analogous to that

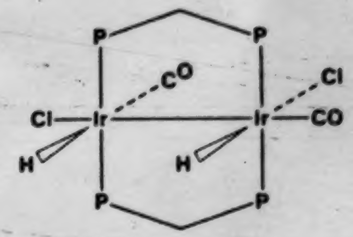

(17)

postulated for the products of the reaction of **3** with alkynes, and confirmed by an X-ray structure of the DMA adduct (see Chapter 3). Evidence that the two hydride ligands are not on the same metal comes from selective phosphorus decoupled ^1H NMR experiments (vide infra). The conversion of **3** to **17** can readily be reversed by gently warming the solution under N_2 for several minutes suggesting that the two hydride ligands are mutually cis.

Using mononuclear octahedral bisphosphine iridium hydrides as a basis for comparison, the carbonyl and iridium-hydride stretches of **17** can be assigned. In mononuclear systems, the Ir-H stretch is generally observed in the range 2100-2000 cm^{-1} when the H ligand is trans to a

CO, but when the hydride is trans to a ligand such as a halide, the Ir-H stretch occurs between 2240-2180 cm^{-1}.[192] A similar trend holds for the carbonyl stretches; when the CO is trans to a hydride ligand, ν(CO) occurs at ca. 1980 cm^{-1}, and when the carbonyl is trans to a chloride ligand, the stretch is observed at ca. 2025 cm^{-1}.[192] Using this information, the carbonyl stretch at 1972 cm^{-1} is assigned to the CO group opposite the hydride ligand, while the band at 2012 cm^{-1} is assigned to CO opposite the Ir-Ir bond. Similarly, the Ir-H stretch at 2222 cm^{-1} would appear to arise from the hydride ligand opposite the chloro ligand, while the stretch at 2091 cm^{-1} is assigned to the hydride ligand opposite the carbonyl group. The observed intensities of these bands are also consistent with this argument (see Table 17); in particular, the occurrence of vibrational coupling between the mutually trans H and CO ligands results in lowering of the ν(CO) band intensity and an increase in the ν(Ir-H) intensity[192]. Attempts to confirm these assignments by preparing the deuterated analogue of **17** were unsuccessful due to large amounts of D_2 required to isolate **17** as a solid. Examination of the solution I.R. spectrum also proved inconclusive due to the complex nature of **17** in solution (vide infra). The assignment of the carbonyl bands in also consistent with those of the aforementioned alkyne adduct [$Ir_2Cl_2(CO)_2$(μ-DMA)$(DPM)_2$] where ν(CO) trans to the metal-metal bond occurred at 2023 cm^{-1} while that trans to the coordinated alkyne moiety appeared at 1999 cm^{-1}.

In solution, **17** displays complex behaviour. At room temperature, $^{31}P\{^1H\}$ NMR spectra show only two broad featureless peaks at *ca*. δ -1 and -8 ppm. When the temperature is lowered to -40°C, the pattern sharpens into two pseudo-triplets at δ -1.4, -8.6 ppm and a small singlet at δ -5.20 ppm. Further lowering of the temperature to about -60°C causes the downfield pseudo-triplet and the singlet to collapse into the baseline while the upfield pseudo-triplet remains unchanged. By -100°C a new signal has reemerged underneath the upfield signal and results in the formation of an AA'BB' pattern centred at δ -7.7 ppm. This last pattern is very analogous to that observed for [$Ir_2Cl_2(CO)_2$(μ-DMA)$(DPM)_2$] at all temperatures (see Chapter 3). These observations can best be explained in terms of the set of equilibria shown in Scheme I. The low temperature limiting spectrum (-100°C) arises from structures XVII and XXI which are identical and represent **17** as it occurs in the solid state. As the temperature is raised, chloride dissociation becomes significant allowing the equilibrium between XVIII, XIX and XX to occur. The low temperature limiting spectrum for this equilibrium

SCHEME I

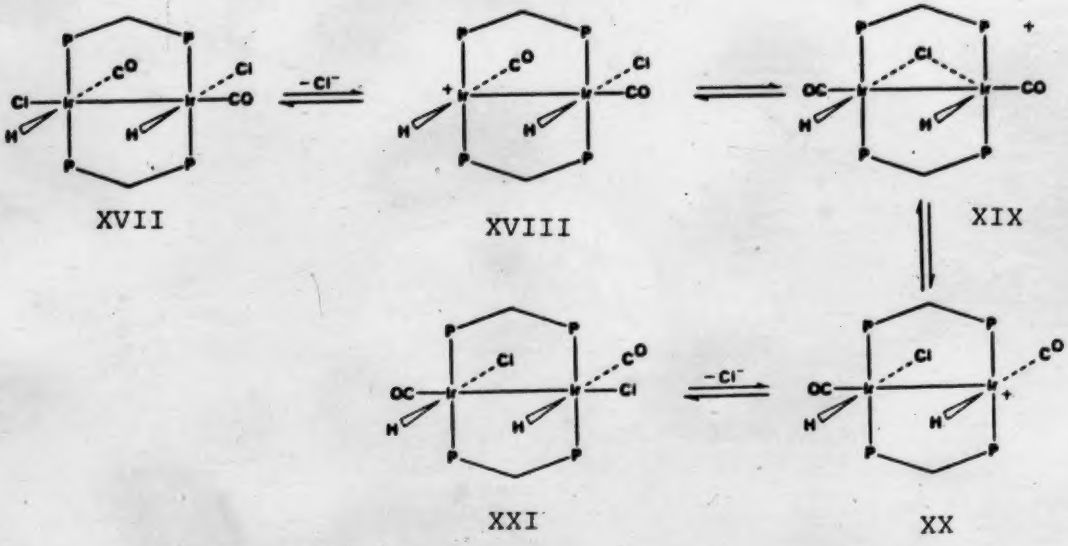

occurs at -40°C where the equivalent structures XVIII and XX give rise to the pair of pseudo-triplets and XIX gives rise to the singlet. A similar equilibrium was observed for $[Ir_2Cl(CO)_2(\mu\text{-DMA})(DPM)_2][BF_4]$ which was prepared by the abstraction of chloride ion from $[Ir_2Cl_2(CO)_2(\mu\text{-DMA})(DPM)_2]$ (see Chapter 3). The ^1H NMR data also support this scheme. At room temperature only two broad peaks are observed in the hydride region. Lowering the temperature to -80°C produces two large triplets arising from the two inequivalent hydrides in XVIII and XX, and one small triplet arising from the symmetrical chloro-bridged intermediate XIX (see Table 17). Unfortunately, the low temperature limiting spectrum could not be obtained. Selective ^1H - ^{31}P decoupling experiments show that the ^1H triplet at -5.76 ppm is coupled to the ^{31}P resonance at -8.6 ppm while the triplet at -14.86 ppm is coupled to the ^{31}P resonance at -1.4 ppm, confirming that there is one hydride on each side of the dimer.

The cationic A-frame complex, $[Ir_2(CO)_2(\mu\text{-}Cl)(DPM)_2]$-$[BF_4]$, **5**, also reacts rapidly with hydrogen to give a very pale yellow solution containing a single species **18**. The ^1H NMR spectrum indicates that **18** is a tetrahydride resulting from the coordination of two molecules of hydrogen to **5** (see Table 17). The ^1H and ^{31}P NMR spectra also indicate that **18** is fluxional in solution. The low temperature limiting ^1H spectrum shows four distinct terminal hydride resonances, three of which broaden and collapse into the baseline as the temperature is raised while the fourth resonance, that which is most upfield, remains sharp. No limiting spectrum could be obtained in the $^{31}P\{^1H\}$ NMR spectra but the room temperature spectrum displays an AA'BB' pattern suggesting that the time averaged geometry of **18** is unsymmetrical. Placing D_2 above solutions of **18** has no affect on the ^1H NMR spectrum after 15 min ruling out H_2 loss as a step in the fluxional process. It is not clear from this information what the structure of **18** is or what processes are involved in the fluxional behaviour.

When a solution of **18** is refluxed in THF for 20 min a new species, **19**, is formed in quantitative yield. The ^{1}H NMR and I.R. spectra indicate that this species is a dicarbonyl dihydride species formed by the loss of one molecule of H_2 from **18**. Adding H_2 to a solution of **19** readily regenerates **18**. Based on the above data and on the $^{31}P\{^{1}H\}$ spectra, which show a symmetrical species over all temperatures, there are two possible structures for **19**, which cannot be readily distinguished by spectroscopy alone. These structure are shown below. Structure XXII appears to be correct based on the observation that prolonged refluxing of solutions of **19** fails to result in any H_2 loss, suggesting that the hydride ligands are not mutually cis. XXII is also consistent with the X-ray structure of the alkyne-inserted adduct **21** (vide infra). On the other hand, the reaction of **17** with $AgBF_4$ to produce

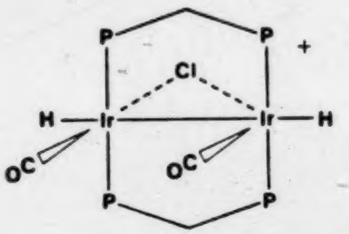

XXII

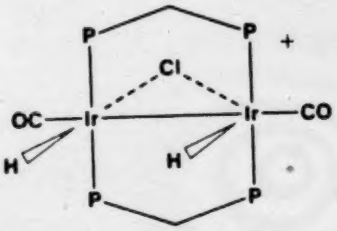

XXIII

19 would seem to favour structure XXIII (see Experimental); however it is possible that some rearrangement has occurred after chloride abstraction from **17**. Since complexes **19** and **18** are related by the respective gain and loss of H_2, some ligand rearrangement must have occurred in the initial formation of **18** from the reaction of **5** with H_2 if XXII is the correct structure for **19**. Simple addition of two equivalents of H_2 to **5** without some rearrangement cannot produce a species which would generate XXII upon H_2 loss.

Compound **17** reacts quantitatively with one equivalent of DMA to give rise to a new product **20**. The ^1H NMR spectrum of **20** shows one hydride resonance at δ -8.89 ppm and singlet at δ 3.85 ppm, each integrating as one hydrogen (see Table 17). Similarly, the I.R. spectrum shows only one ν(Ir-H) band in addition to new ν(C=O) and ν(C=C) bands of the DMA ligand (see Table 17). This spectroscopic information, coupled with the observation of a $^{31}P\{^1H\}$ pattern typical of an unsymmetrical species, suggests the structure shown below for **20** in which the alkyne has inserted into one of the Ir-H bonds of **17**. Although compound **17** is coordinatively saturated in the solid state and so would not be expected to react further, Cl^- dissociation from one iridium centre occurs in solution yielding the unsaturated cationic intermediate XVIII, as pointed out earlier in Scheme I. Coordination of the alkyne at this metal, followed by insertion into the Ir-H bond and Cl^- recoordination would yield **20** as shown in Scheme II.

SCHEME II

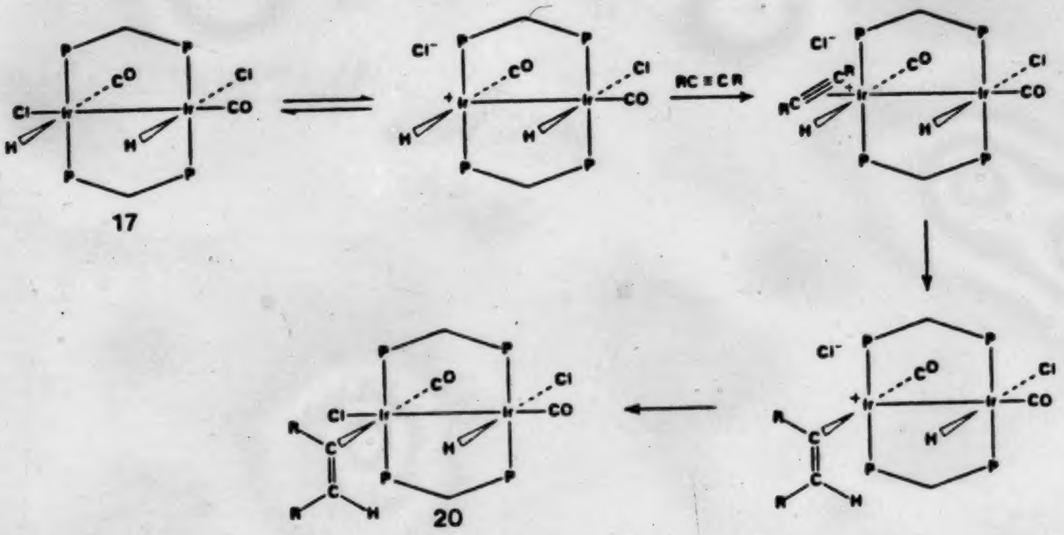

Attempts to induce further reaction between the metallated olefin and the remaining hydride ligand have been unsuccessful. In order for further reaction to occur it is apparent that an open coordination site and the concomitant coordinative unsaturation must be generated at the metal having the hydride ligand, either by loss of chloride ion or carbon monoxide. The removal of chloride ion by the reaction of **20** with $AgBF_4$ has led only to the isolation of **21** in low yield (< 30% after workup). The formation of **21** from **20** indicates that at some point alkyne loss, rearrangement and subsequent alkyne insertion into the second Ir-H bond has occurred. The alternative method of producing an open coordination site, involving removal of a carbonyl group from **20** has also proven unsuccessful; refluxing **20** in CH_2Cl_2 for 2 h had no effect. Other means of CO removal such as reaction with Me_3NO warrant investigation. It is possible that olefin insertion into the second Ir-H bond is inhibited by steric interactions involving the metallated olefin and DPM phenyl rings. Attempts to obtain suitable crystals of **20** in order to determine its X-ray structure have been unsuccessful to date.

Compound **19** also reacts with DMA. However in contrast to compound **17**, at least a two-fold excess must be used and the reaction does not proceed to one product. Within 16 h after the reaction is initiated, the $^{31}P\{^1H\}$ NMR spectrum shows that **19** has been completely consumed and three new species have been formed. This NMR spectrum consists of a complex multiplet (δ -12.5, -16.5 ppm) and two singlets at δ -13.6, -17.6 ppm in the approximate ratio 4.5:2.1:1. A ^1H NMR spectrum of this mixture shows no hydride resonances while the region from 3 to 6 ppm is very complex. An I.R. spectrum shows carbonyl bands at 2019, 2024, 1987, and 1947 cm^{-1} and a broad BF_4^- band at 1050 cm^{-1}. By means of column chromatography, the major species of the mixture, **21**, was separated in ca. 50% yield. ^{1}H NMR and I.R. spectra indicate that **21** is a di-inserted product which no longer contains BF_4^-. This is confirmed by elemental analysis and an X-ray structure determination which showed it to have the geometry as in Figure 7. Although **21** is symmetrical in the solid state, in solution the ends of the dimer are no longer equivalent as evidenced by the ^{1}H and $^{31}P\{^1H\}$ NMR spectra. This is likely due to chloride dissociation in solution which occurs in order to relieve some of the steric crowding in the molecule. Consistent with this proposal is the observed increase in the carbonyl bands by ca. 15 cm^{-1} upon going from solid to solution. Although solutions of **21** are nonconducting in CH_2Cl_2, this is not unusual and has been observed to occur in other compounds with halide counterions due to ion pairing.[165]

Complex **21** is isolated as a neutral dichloride species whereas the parent compound **19** is a cationic monochloride, posing a question as to the source of the second chloride ion. The source appears to be the CH_2Cl_2 solvent rather than disproportion of the cationic precursor, since **21** is observed in the NMR spectra to form in greater than 50% yield. Further evidence for this comes from the observation that the reaction does not proceed by an identical route when performed in acetone.[166] The reaction likely proceeds by the initial formation of a cationic di-inserted species $[Ir_2(CH_3CO_2C{=}CHCO_2CH_3)_2(CO)_2(\mu\text{-}Cl)(DPM)_2][BF_4]$ which subsequently abstracts chloride ion from the solvent. It is possible that it is this complex which gives rise to one of the singlets observed in the $^{31}P\{^1H\}$ NMR of the original reaction mixture. Further studies using solvents other than CH_2Cl_2 would be useful in clarifying this matter.

Since **21** appears to dissociate Cl^- in solution, it might be expected that with the resulting coordinative unsaturation it could further react with hydrogen and subsequently complete the hydrogenation cycle. However, this does not occur and compound **21** is recovered unchanged after stirring under H_2 for 48 h. This suggests that either the ion pairing between the complex and Cl^- ion is too strong or that the resultant cationic complex is unreactive towards H_2.

Conclusions

The binuclear complexes trans-$[IrCl(CO)(DPM)]_2$ (**3**) and $[Ir(CO)_2(\mu\text{-}Cl)(DPM)_2][BF_4]$ (**5**) have been shown to react rapidly with hydrogen under mild conditions. The reaction of 5 initially produces a tetrahydride species which can be converted into a dihydride upon refluxing under N_2. This latter species reacts with excess DMA to give a product in which alkyne insertion into each Ir-H bond has occurred. In this case, the two ends of the dimer appear to act independently and the reaction proceeds much as it would with two mononuclear species. It is not clear how this relates (if at all) to the catalytic hydrogenation of alkynes by the rhodium analogue, $[Rh_2(CO)_2(\mu\text{-}Cl)(DPM)_2]^+$, since the product of the double alkyne insertion could not be induced to react further with H_2 to give either an intermediate dihydrido dialkenyl complex such as $[IrH_2(CH_3CO_2C{=}CHCO_2CH_3)_2(CO)_2(\mu\text{-}Cl)(DPM)_2]^+$ or the olefin product. However, it may be that it is the initial tetrahydride species **18** which is analogous to the catalytically important species in the rhodium-catalyzed cycle. Further studies are needed to characterize this tetrahydride species and to investigate its subsequent chemistry with unsaturated substrates.

In constrast, the reaction of 3 with H_2 produces a dihydride species which subsequently reacts with only one equivalent of DMA. Spectroscopic evidence shows that the alkyne has inserted into only one of the Ir-H bonds. Although this insertion occurs at only one metal centre, we can forsee how the second metal can become involved through

π-coordination of the metallated olefin moiety to the second metal and subsequent hydrogen transfer to the olefin to form a dimetallated alkyl group which then reductively eliminates as the olefin. Attempts to induce the second hydrogen transfer and subsequent reductive elimination have not yet met with success in the complex studied. It is not clear whether this is due to the steric bulk of the phosphine and alkyne groups or whether it is a function of the low lability of the chloro or carbon monoxide ligands, failing to generate the required coordinative unsaturation. Further studies are needed to clarify this.

CHAPTER 5

Hydroxy and Hydrido-Bridged Binuclear Complexes of Iridium as Models for Water-Gas Shift Catalysts and the Structure of One Model Catalyst Precursor, $[Ir_2(CO)_2(\mu\text{-}OH\cdot Cl)(Ph_2PCH_2PPh_2)_2]$.

Introduction

As mentioned in Chapter I, metal hydrides are implicated in a variety of catalytic processes. The preceding chapter examined their involvement in the hydrogenation of unsaturated organic substrates; in this chapter the role of metal hydrides in the water-gas shift (WGS) reaction is considered. The WGS reaction, shown in equation 4 is an industrially important process for

$$CO + H_2O \rightleftarrows CO_2 + H_2 \qquad (4)$$

increasing the H_2/CO ratio of synthesis gas.[192,194] At the present time this reaction utilizes heterogeneous catalysts (usually metal oxides) at high temperatures.[193] However, there has been increasing interest of late in the use of homogeneous catalysts which are active at lower temperatures[35,57,117,195-205] where the above equilibrium is more favourable.[206,207] Most of these systems are thought to proceed by steps similar to those outlined below. Of relevance to this thesis is the recent study

$$[M\text{-}CO]^{n+} + H_2O \rightarrow [MCOOH]^{(n-1)+} + H^+ \qquad (5)$$

$$[MCOOH]^{(n-1)+} \rightarrow MH^{(n-1)+} + CO_2 \qquad (6)$$

$$[MH]^{(n-1)+} + H^+ \rightarrow [M]^{n+} + H_2 \qquad (7)$$

$$[M]^{n+} + CO \rightarrow [M\text{-}CO]^{n+} \qquad (8)$$

in which the binuclear DPM hydride $[Rh_2(CO)_2(\mu\text{-}H)(\mu\text{-}CO)(DPM)_2]^+$ [35] was shown to be a catalyst in the WGS reaction. The catalytic cycle was thought to be as shown below in Scheme III. However the formate species, when independently synthesized, was shown to be catalytically inactive. Also of relevance to the present work is the study by Yoshida and co-workers, utilizing mononuclear rhodium phosphine complexes,[205] which elegantly demonstrated the involvement of both metal hydrides and metal hydroxides in the catalytic cycle.

The following study was undertaken with two goals in mind: 1) to use Ir-DPM complexes in an attempt to model

SCHEME III

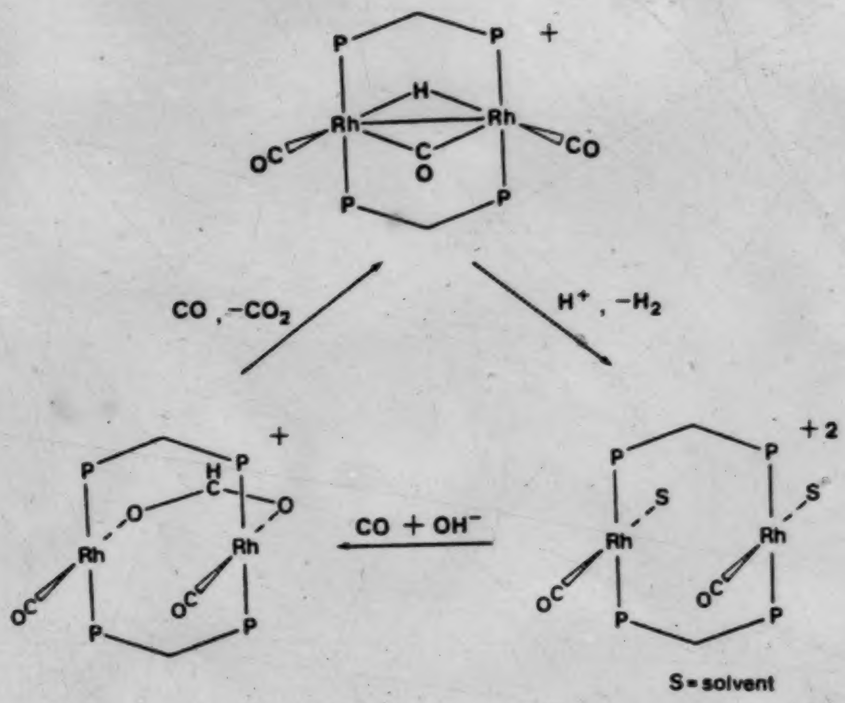
CO , −CO$_2$
H$^+$, −H$_2$
CO + OH$^-$
S = solvent

and elucidate the mechanism of catalysis by $[Rh_2(CO)_2(\mu\text{-}H)\text{-}(\mu\text{-}CO)(DPM)_2]^+$ and 2) to examine the possible role of binuclear hydroxides in the catalytic cycle.

Experimental Section

The general experimental conditions and techniques are given in Chapter Two. $[Rh_2(CO)_2(\mu\text{-}H)(\mu\text{-}CO)(DPM)_2]^+$ and $[Rh_2(CO)_2(\mu\text{-}OH)_2(DPM)_2]^+$ were prepared according to the published procedures.[57,208] The catalytic runs, using $[Rh_2(CO)_2(\mu\text{-}OH)(DPM)_2][BF_4]$ and $[Rh_2(CO)_2(\mu\text{-}H)(\mu\text{-}CO)(DPM)_2][BF_4]$ as catalyst precursors, were typically done using 75 mg of compound in a mixture of 20 mL 2-propanol and 2 mL H_2O in a 100 mL flask. The vessel was charged with 1 atm of CO and heated to 80°C. The gases, which were dried by passing them through a column of P_2O_5, were sampled into evacuated vessels and analyzed by mass spectrometry; the quantity of CO_2 was calculated based on a comparison with a known amount of Ar added to the reaction vessel at the beginning of the reaction and on the relative sensitivities of Ar and CO_2 taken from a 50:50 mixture of the two gases. A blank done under identical conditions, except that no catalyst was added, showed that no CO_2 was present.

Preparation of Compounds:

a) $[Ir_2(CO)_2(\mu\text{-}OH\cdot Cl)(DPM)_2]$ (22).

To a slurry of 200 mg (0.156 mmol) $[IrCl(CO)(DPM)]_2$ in THF was added 1.0 mL of a solution of *ca.* 2 M aqueous NaOH. Over a period of ½ h, the solution colour changed from purple to dark orange accompanied by the appearance of a bright orange solid. The solution was then taken to dryness in vacuo. To the resulting orange residue was added 10 mL of degassed H_2O and 20 mL of CH_2Cl_2 and the resulting mixture was stirred for 30 min. The two layers were allowed to separate and the orange CH_2Cl_2 layer was removed and filtered under nitrogen. The volume of the filtrate was reduced to *ca.* 10 mL under an N_2 flow and then 30 mL of Et_2O was added. This resulted in the precipitation of a finely divided light orange powder. (150 mg, 76% yield). Compound 1 was determined to be a non-electrolyte in CH_2Cl_2 solutions ($\Lambda(10^{-3}$ M) $< 0.5\ \Omega^{-1}$ cm^2 $mole^{-1}$).[170] Spectroscopic parameters for this and all subsequent products are given in Tables 24 and 25.
Anal. Calcd for $Ir_2ClP_4O_3C_{52}H_{45}$: C, 49.50%; H, 3.59%; Cl, 2.81%. Found: C, 49.73%; H, 3.61%; Cl, 2.76%.

b) $[Ir_2(CO)_2(\mu\text{-}OH)(DPM)_2][BF_4]$ (23).

To a solution of 100 mg (0.079 mmol) of **22** in 10 mL of CH_2Cl_2 was added 1 equivalent (11.4 μL) of $HBF_4 \cdot Et_2O$ which produced an immediate darkening of the original orange solution. The addition of 30 mL of Et_2O resulted in the precipitation of an orange microcrystalline solid (95 mg, 92% yield). Conductivity measurements on a CH_2Cl_2 solution of this solid indicated that it was a 1:1 electrolyte (Λ (10^{-3}M) = 41.8 Ω^{-1} cm^2 mole^{-1}).

Anal. Calcd for $Ir_2P_4F_4O_3C_{52}BH_{45}$: C, 47.56%; H, 3.45%; Cl, 0.0%. Found: C, 47.57%; H, 3.87%; Cl, 0.0%.

c) $[Ir_2(CO)_4(DPM)_2] \cdot CH_2Cl_2$ (24).

A CH_2Cl_2 solution of **22** (100 mg, 0.079 mmol, in 10 mL) was stirred under an atmosphere of CO for 30 min during which time the colour changed from orange to bright yellow. 30 mL of Et_2O, saturated with carbon monoxide, was added to the solution which was then stored at -15°C overnight. During this time bright yellow crystals of **24** appeared. This solid was determined to be very susceptible to CO loss and was stored in a sealed flask under a CO atmosphere. The yield was 95 mg, 90%. Solutions of **24** in CH_2Cl_2 were non-conducting (Λ(10^{-3}M) < 0.5 Ω^{-1} cm^2 mole^{-1}). Anal. Calcd for $Ir_2Cl_2P_4O_4C_{55}H_{46}$: C, 48.93%; H, 3.43%. Found: C, 49.01%; H, 3.39%. The presence of and the amounts of solvent molecules were verified by ^{1}H NMR for this and other complexes.

d) $[Ir_2(CO)_2(\mu\text{-}CO)(DPM)_2]$ (**25**).

Dinitrogen was bubbled through a CH_2Cl_2 solution of **24** (100 mg, 0.079 mmol, in 10 mL) for 10 min during which time the solution changed colour from bright yellow to dark golden yellow. The solution was taken to dryness under an N_2 stream leaving a dark yellow-brown residue. Recrystallization of this solid from THF/Et_2O produced a golden yellow finely divided powder. (85 mg, 87% yield). Compound **25** was determined to be a non-electrolyte in CH_2Cl_2 solutions (Λ (10^{-3} M) < 0.5 Ω^{-1} cm^2 mole^{-1}). Anal. Calcd for $Ir_2P_4O_3C_{53}H_{44}$: C, 51.45%; H, 3.58%; Cl, 0.00%. Found: C, 51.42%; H, 3.80%; Cl, 0.05%.

e) $[Ir_2(CO)_2(\mu\text{-}H)(\mu\text{-}CO)(DPM)_2][BF_4]$ (**26**).

Method A. A solution of $[Ir_2(CO)_2(\mu\text{-}OH)(DPM)_2][BF_4]$ in CH_2Cl_2 (100 mg, 0.076 mmol. in 10 mL) was stirred under an atmosphere of carbon monoxide for 30 min during which time the solution changed colour from red-orange to yellow-orange. The solution was taken to dryness under an N_2 stream leaving a dark red residue. Recrystallization from CH_2Cl_2/Et_2O gave either a red orange or a dark red-purple crystalline solid (90 mg, 89% yield) (see discussion). A

CH_2Cl_2 solution of this solid indicated that **26** was 1:1 electrolyte (Λ (10^{-3}M) = 45.7 Ω^{-1} cm^2 mole^{-1}).
Anal. Calcd for $Ir_2P_4F_4O_3C_{55}BH_{45}$: C, 48.04%; H, 3.42%.
Found C, 47.72%; H, 3.59%.

Method B. To a solution of $[Ir_2(CO)_2(\mu\text{-}CO)(DPM)_2]$ (25) in CH_2Cl_2 (100 mg in 10 mL) was added 1 equivalent (11.6 μL) of $HBF_4{\cdot}Et_2O$. The solution immediately changed colour from golden yellow to dark red. 30 mL of Et_2O was added and resulted in the precipitation of a dark red crystalline material which was identical in all of its spectroscopic properties to that isolated from Method A.

f) $[Ir_2(H)(CO)_2(\mu\text{-}H)(\mu\text{-}CO)(DPM)_2][BF_4]_2$ (27).

To a solution of $[Ir_2(CO)_2(\mu\text{-}H)(\mu\text{-}CO)(DPM)_2][BF_4]$ in CH_2Cl_2 (100 mg, 0.075 mmol, in 10 mL) was added one equivalent of $HBF_4{\cdot}Et_2O$ (10.8 μL) whereupon the solution immediately changed colour from dark red to bright yellow. The solution volume was reduced to *ca.* 5 mL under a N_2 stream. The addition of 15 mL of hexanes caused the precipitation of a golden yellow, extremely moisture sensitive solid (85 mg, 80% yield). Conductivity measurements in CH_2Cl_2 gave Λ(10^{-3}M) = 41.9 Ω^{-1} cm^2 mole^{-1}.
Anal. Calcd for $Ir_2P_4F_8O_3C_{53}B_2H_{46}$: C, 45.06%; H, 3.28%.
Found: C, 45.05%; H, 3.23%.

g) $[Ir_2(CO)_4(\mu\text{-}H)_2(DPM)_2][BF_4]_2$ (**29**).

A solution of **27** (100 mg 0.070 mmol, in 10 mL of CH_2Cl_2) was stirred under an atmosphere of carbon monoxide. Within 5 min the solution colour had changed from yellow to almost colourless pale yellow. The addition of 30 mL of Et_2O resulted in the precipitation of a white solid. The solid was redissolved in 5 mL of CH_2Cl_2 and filtered under carbon monoxide. 10 mL of hexanes was added to the filtrate and the solution was stored under a CO atmosphere at -15°C overnight during which time **29** precipitated as a white microcrystalline solid (90 mg, 89% yield). A CH_2Cl_2 solution of this solid gave a molar conductivity of $\Lambda(10^{-3}) = 37.3\ \Omega^{-1}\ cm^2\ mole^{-1}$. Anal. Calcd for $Ir_2P_4F_8O_4C_{54}B_2H_{46}$: C, 45.10%; H, 3.22%. Found: C, 42.58%; H, 3.30%. Due to the rapid rate of decomposition of 29, no better analysis could be obtained.

h) $[Ir_2(CO)_4(\mu\text{-}CO)(DPM)_2][BF_4]_2\cdot(CH_3)_2CO$ (**30**).

To a solution of $[Ir_2Cl(CO)_3(\mu\text{-}CO)(DPM)_2][Cl]$ in CH_2Cl_2 under CO (297 mg, 0.222 mmol, in 10 mL) was added dropwise a solution of two equivalents of $AgBF_4$ (86.7 mg) dissolved in 5 ml THF. No change was observed until more than half of the solution had been added after which point the solution darkened rapidly and a light yellow precipitate appeared. The solution was stirred under CO for 30 min and then 30 mL Et_2O was added to induce complete precipitation. The supernatant was removed and the solid was dried under a CO stream. The residue was redissolved in 15 mL of acetone and filtered under a CO atmosphere giving a pale yellow solution. The addition of 50 mL of Et_2O resulted in the precipitation of a white microcrystalline solid (250 mg, 78% yield). Conductivity measurements in acetone indicated that **30** was a 2:1 electrolyte[209] ($\Lambda(10^{-3}M) = 238.6\ \Omega^{-1}\ cm^2\ mole^{-1}$). Anal. Calcd for $Ir_2P_4F_8O_6C_{58}B_2H_{50}$: C, 48.04%; H, 3.42%. Found: C, 47.72%; H, 3.59%.

i) $[Ir_2(CO)_2(CH_3CN)_2(\mu\text{-}CO)(DPM)_2][BF_4]_2$ (31).

A slurry of **30** was prepared by adding 10 mL of CH_2Cl_2 to 250 mg (0.174 mmol) of the solid. 2 mL of dry CH_3CN was then added resulting in immediate gas evolution and the formation of a clear pale yellow solution. The system was then purged with N_2 for 15 min during which time a white microcrystalline solid began to form. Stirring was discontinued after 2h and the reaction flask was then placed in the freezer at -15°C overnight during which time a large amount of white precipite appeared. Complete precipitation was induced by the addition of 30 mL Et_2O. This solid was collected and washed twice with 10 mL portions of Et_2O and dried under an N_2 stream. (210 mg, 82% yield). Conductivity measurements of 30 in CH_3CN showed it to be a 2:1 electrolyte ($\Lambda(10^{-3}M) = 229.4\ \Omega^{-1}\ cm^2\ mole^{-1}$).

Anal. Calcd for $Ir_2P_4F_8O_3N_2C_{57}B_2H_{50}$: C, 45.86%; H, 3.37%; N, 1.88%. Found: C, 45.02%; H; 3.40%; N, 1.80%.

j) $[Ir_2(H)_2(CO)_3(DPM)_2][BF_4]_2$ (28).

An atmosphere of H_2 was placed over a slurry of 200 mg of 31 in 10 mL CH_2Cl_2 and the resulting mixture stirred vigorously. After 20 min all of the solid had dissolved producing a clear light yellow solution. The excess hydrogen was then removed by purging the solution with N_2 for 15 min eventually producing a darker yellow solution. 30 mL of hexanes was added and resulted in the precipitation of a white microcrystalline solid. The mother liquor was removed and the resulting solid dried initially under a N_2 stream and finally under vacuo for 2 h. Typical isolated yields of this highly moisture sensitive compound were 80-90%. Conductivity measurements on 28 in CH_2Cl_2 gave $\Lambda(10^{-3}M) = 40.7\ \Omega^{-1}cm^2\ mole^{-1}$.

Anal. Calcd for $Ir_2P_4F_8O_3C_{56}B_2H_{46}$: C, 45.06%; H, 3.28%. Found: C, 44.98%; H, 3.31%.

Table 24. Infrared Spectral Data for the Compounds of Chapter Five.[a,b]

	Compound	solid[c]	solution[d]
22	$[Ir_2(CO)_2(\mu\text{-}OH{\cdot}Cl)(DPM)_2]$	1904(m), 1882(vs)	1889(vs,br)
23	$[Ir_2(CO)_2(\mu\text{-}OH)(DPM)_2][BF_4]$	1959(vs), 1943(vs), 3498(w)[e]	1956(vs), 1935(vs)
24	$[Ir_2(CO)_4(DPM)_2]$	1991(s), 1982(vs), 1974(vs), 1922(s), 1886(s)	1990(vs), 1977(vs,br), 1928(vs), 1895(s,br)
25	$[Ir_2(CO)_2(\mu\text{-}CO)(DPM)_2]$	1950(s), 1936(vs), 1857(s)	1996(m), 1955(vs), 1929(vs), 1878(s)
26	$[Ir_2(CO)_2(\mu\text{-}H)(\mu\text{-}CO)(DPM)_2][BF_4]$	1979(m), 1967(vs), 1826(vs)(red) 1979(m), 1967(vs), 1850(s)(orange)	1971(vs,br), 1849(s)
27	$[Ir_2(H)(CO)_2(\mu\text{-}H)(\mu\text{-}CO)(DPM)_2][BF_4]_2$	2046(vs), 1961(m), 1833(m), 2108(m)[f]	2060(vs), 1969(w), 1837(s), 2115(s)[f]
28	$[Ir_2(H)_2(CO)_3(DPM)_2][BF_4]_2$	2068(m), 2031(vs), 2136(w)[f], 1957(w)[f]	2070(s), 2034(vs)
29	$[Ir_2(CO)_4(\mu\text{-}H)_2(DPM)_2][BF_4]_2$	2080(s), 2061(m), 2038(m), 2017(w)	2085(s), 2060(m)
30	$[Ir_2(CO)_4(\mu\text{-}CO)(DPM)_2][BF_4]_2$	2091(s), 2069(vs), 2019(s), 2026(vs), 1792(s)	h
31	$[Ir_2(CO)_2(CH_3CN)_2(\mu\text{-}CO)(DPM)_2][BF_4]_2$	2005(s), 1980(vs), 1731(s), 2284(w)[g], 2312(w)[g]	h

a) Abbreviations: vs = very strong, s = strong, m = medium, w = weak, br = broad

b) All frequencies are carbonyl stretches unless otherwise noted

c) Nujol mull

d) CH_2Cl_2 solution

e) ν(OH)

f) ν(Ir-H)

g) ν(CN)

h) insoluble

Table 25. NMR Spectral Data for the Compounds of Chapter Five.[a]

	Compound	${}^{31}P\{{}^{1}H\}$, ppm[b]	${}^{1}H$, ppm[c]
22	$[Ir_2(CO)_2(\mu\text{-}OH{\cdot}Cl)(DPM)_2]$	11.1(s)	7.74-7.13 (m,40 H), 4.05 (q, ${}^{1}H$, ${}^{2}J_{P-H}$ = 3.5 Hz), 4.4 (vbr., 2H) 2.8 (vbr, 2H)
23	$[Ir_2(CO)_2(\mu\text{-}OH)(DPM)_2][BF_4]$	13.7(s)	7.77-7.21 (m,40 H), 4.19 (m, 2H), 3.32 (m, 2H), 2.03 (q. ${}^{1}H$, ${}^{2}J_{P-H}$ = 3.1 Hz)
24	$[Ir_2(CO)_4(DPM)_2]$	-22.8(s)	7.30-7.06 (m, 40 H), 4.83 (vbr. 4 H)
25	$[Ir_2(CO)_2(\mu\text{-}CO)(DPM)_2]$	- 3.6(s)	7.46-7.20 (m, 40 H), 4.92 (s, 4H)
26	$[Ir_2(CO)_2(\mu\text{-}H)(\mu\text{-}CO)(DPM)_2][BF_4]$	+ 9.1(s)	7.49-7.30 (m, 40 H), 3.87 (s, br, 4 H), -9.44 (q, ${}^{1}H$, ${}^{2}J_{P-H}$ = 9.4 Hz)
27	$[Ir_2(H)(CO)_2(\mu\text{-}H)(\mu\text{-}CO)(DPM)_2][BF_4]_2$	14.4(m), -2.9(m)	7.71-7.25 (m, 40 H), 4.59 (m ,br, 4 H), -7.11 (m, br, ${}^{1}H$), -13.19 (td, ${}^{1}H$, ${}^{2}J_{P-H}$ = 10.5 Hz, ${}^{2}J_{H-H}$ = 1.6 Hz)
28	$[Ir_2(H)_2(CO)_3(DPM)_2][BF_4]_2$	-12.3(m), -17.7(m)	7.56-7.32 (m, 40H), 5.68 (m, 2H), 4.90 (m, 2H), -9.83 (t, 1 H, ${}^{2}J_{P-H}$ = 7.9 Hz), -17.42 (t, 1 H, ${}^{2}J_{P-H}$ = 11.2 Hz)
29	$[Ir_2(CO)_4(\mu\text{-}H)_2(DPM)_2][BF_4]_2$	-18.8(s)	7.53-7.47 (m, 40 H), 5.34 (vbr, 4H), -9.66 (q, 2H ${}^{2}J_{P-H}$ = 5.1 Hz)
30	$[Ir_2(CO)_4(\mu\text{-}CO)(DPM)_2][BF_4]_2$	-15.3(s)	7.77-7.45 (m, 40 H), 5.84 (q, 4H, ${}^{2}J_{P-H}$ = 4.8 Hz)
31	$[Ir_2(CO)_2(CH_3CH_2)_2(\mu\text{-}CO)(DPM)_2][BF_4]_2$	- 7.5(s)	7.67-7.22 (m, 40 H), 4.19 (m, 2H), 3.35 (m, 2H), 1.27 (m, 6H)[d]

a) Abbreviations used: s = singlet, t = triplet, td = triplet of doublets, q = quintet, m = multiplet, br = broad, vbr = very broad

b) vs 85% H_3PO_4, -40°C

c) in CD_2Cl_2 at +25°C

d) in d_6 acetone

Reaction of **30** with $NMe_4OH \cdot 5H_2O$.

To a solution of **30** in acetone (265 mg in 10 mL) was added 1 equivalent of $NMe_4OH \cdot 5H_2O$ (32.7 mg) in 1 mL of degassed H_2O. The solution colour immediately changed from pale yellow to bright yellow and a bright yellow solid precipitated. The colour then rapidly faded to dull yellow-orange and the precipitate began to redissolve. Concentrating the solution under an N_2 stream caused it to turn bright red. The solution was taken to dryness in vacuo leaving a bright red residue. This solid was redissolved in CH_2Cl_2, filtered under N_2, and precipitated by the addition of Et_2O resulting in a bright red microcrystalline product. Spectroscopic examination showed this solid to be $[Ir_2(CO)_2(\mu\text{-}H)(\mu\text{-}CO)(DPM)_2][BF_4]$ (**26**).

Reaction of **31** with $NMe_4OH \cdot 5H_2O$.

To a solution of **31** in acetonitrile (55 mg in 5 mL) was added 1 equivalent of $NMe_4OH \cdot 5H_2O$ (6.5 mg) in 1 mL of degassed H_2O. The solution colour immediately changed from yellow to orange. The solvent was removed in vacuo leaving a dark orange powder. This was then redissolved in CH_2Cl_2 and filtered under N_2. Addition of 30 mL ether resulted in the precipiation of an orange solid which was shown by spectroscopic means to be a mixture of **23** and **26** (ratio ~3:1).

Reaction of **31** with NaO_2CH.

To a solution of **31** in acetonitrile (150 mg in 5 mL) was added 1 equivalent of NaO_2CH (6.8 mg) in 1 mL acetonitrile. Over a period of 1 h the solution colour changed from yellow to bright red and coincided with the appearance of a red solid. The solution was taken to dryness under vacuum and then redissolved in CH_2Cl_2 giving a bright red solution which was filtered under N_2. Addition of 30 mL ether resulted in the precipitation of a bright red solid which was shown by I.R. and NMR (^1H, ^{31}P) spectroscopy to be $[Ir_2(CO)_2(\mu\text{-}H)(\mu\text{-}CO)(DPM)_2][BF_4]$ (**26**).

Reaction of **31** with NaOMe.

To a solution of **31** in acetonitrile (225 mg in 5 ML) was added 1 equivalent of NaOMe (8.0 mg) in 1 mL MeOH which had been freshly distilled from magnesium turnings. The solution immediately changed from yellow to bright red. This was taken to dryness under vacuo and then redissolved in CH_2Cl_2 giving a bright red solution which was filtered under N_2. Addition of 30 mL ether resulted in the precipitation of a bright red solid which was shown by means of I.R. and NMR (^1H and ^{31}P) spectroscopy to be **26**.

X-ray Data Collection

An orange crystal of $[Ir_2(CO)_2(\mu\text{-}OH{\cdot}Cl)(DPM)_2]$, obtained by the slow diffusion of diethyl ether into a saturated CH_2Cl_2 solution of the complex, was mounted in a glass capillary under N_2. Preliminary film data showed that the crystal belonged to the orthorhombic system, with systematic absences (h00: h = odd, 0k0: k = odd, 00l: l = odd) consistent with the space group $P2_12_12_1$. Accurate cell parameters were obtained from a least-squares refinement of the setting angles of 23 reflections, in the range $15.0 < 2\theta < 28.2°$, which were accurately centred on an Enraf-Nonius CAD-4 diffractometer using MoKα radiation. See Table 26 for pertinent crystal and data collection details.

Intensity data were collected on a CAD-4 diffractometer in the bisecting mode and employing the ω-2θ scan technique up to $2\theta = 50.0°$ with graphite monochromated MoKα radiation. Backgrounds were scanned for 25% of the peak width on either end of the peak scan. The intensities of three standard reflections were measured every 1 h of exposure to assess possible crystal decomposition. No significant decay of these standards was observed over the course of the data collection, so no correction was applied to the data. 4781 unique reflections were measured and

Table 26. Summary of Crystal Data and Details of Intensity Collection for $[Ir_2(CO)_2(\mu\text{-}OH\cdot Cl)(DPM)_2]$.

cmpd	$[Ir_2(CO)_2(\mu\text{-}OH.Cl)(DPM)_2]$
fw	1261.66
formula	$Ir_2ClP_4O_3C_{52}H_{45}$
space group	$P2_12_12_1$
Z	4
Cell parameters	a = 14.752(2)Å b = 25.572(4)Å c = 13.765(3)Å V = 5158.73 $Å^3$
ρ(calcd), g/cm^3	1.624
temp, °C	22
radiation	MoKα (λ 0.71069Å) graphite monochromated
receiving, aperture, mm	2.00 + 0.500 tan(θ) wide x 4.0 high, 173 from crystal
take off angle, deg	2.55
scan speed, deg/min	variable from 10.058 and 1.804
scan width, deg	0.75 + 0.350 tan(θ) in ω
2θ limits, deg	$3.0 < 2\theta < 50.0$
μ, cm^{-1}	52.414
range in abs corr factors (as applied to Fo^2)	0.406 - 0.504
crystal shape	orthorhombic prism with faces of the form {120}, {011}, and {021}
unique data collected	4781

Table 26 (continued)

unique data used ($F_o^2 > 3\sigma(F_o^2)$)	2650
final no. of parameters refined	223
error in observation of unit weight	1.516
R	0.043
R_w	0.065

processed in the usual way using a value of 0.04 for p[153]; of these 2650 had $Fo^2 > 3\sigma(Fo^2)$ and were used in subsequent calculations. Absorption corrections were applied to the data by using Gaussian integration.[154]

Structure Solution and Refinement

The structure was solved in the space group $P2_12_12_1$ with the use of a Patterson map to locate the two independent Ir atoms. Subsequent refinements and differences Fourier syntheses led to location of all remaining nonhydrogen atoms. Atomic scattering factors were taken from Cromer and Waber's tabulation [155] for all atoms except hydrogen, for which the values of Stewart et al. were used.[156] Anomalous dispersion terms for Ir, Cl and P were included in F_c.[157] All phenyl ring carbon atoms were refined as rigid groups having D_{6h} symmetry, C-C distances of 1.392 A and independent isotropic thermal parameters. All hydrogen atoms, except that of the bridging OH•Cl unit, were input as fixed contributions; their idealized positions were calculated after each cycle of refinement from the geometries of their attached carbon atoms using a C-H distance of 0.95 A. These hydrogen atoms were assigned isotropic thermal parameters of 1 A^2 greater than the B (or equivalent isotropic B) of their attached carbon atom.

A difference Fourier map phased on all of the non-hydrogen atoms and using a $\sin\theta/\lambda$ cutoff value of 0.35 $Å^{-1}$ revealed the hydrogen atom of the bridging OH•Cl unit as the largest peak. Attempted refinement of this hydrogen (H(1)) resulted in slow divergence of its thermal parameter. In subsequent refinements this atom was given a fixed thermal parameter and position and was not refined. All other non-hydrogen atoms were refined anisotropically.

The final model with 223 parameters refined converged to $R = 0.043$ and $R_w = 0.065$.[158] On the final difference Fourier map the 20 highest peaks (1.75 - 0.54 $Å^{-3}$) were in the vicinities of the phenyl groups, and the Ir and P atoms. A typical carbon atom on earlier syntheses had a peak intensity of about 3.5 $Å^{-3}$.

Refinement of the structure as the other enantiomer resulted in higher residuals ($R = 0.054$ and $R_w = 0.076$) and slightly larger thermal parameters for all atoms suggesting that the original choice was the correct one.

The final positional parameters of the individual non-hydrogen atoms and the phenyl groups are given in Tables 27 and 28, respectively. The derived hydrogen parameters are given in Table 29. A listing of observed and calculated structure amplitudes used in the refinements is available.[159]

Table 27. Positional and Thermal Parameters for the Non-group Atoms of $[Ir_2(CO)_2(\mu\text{-}OH\cdot Cl)(DPM)_2]$.

a) Anisotropic Atoms.

Atom	x^a	y	z	$U_{11}{}^b$	U_{22}	U_{33}	U_{12}	U_{13}	U_{23}
Ir(1)	0.06260(9)	0.17389(6)	0.26839(9)	3.07(8)	3.71(9)	3.41(8)	-0.21(8)	-0.08(7)	-0.03(7)
Ir(2)	-0.04077(8)	0.12183(5)	0.09339(9)	2.95(7)	3.64(8)	3.75(8)	-0.38(8)	-0.11(7)	-0.25(7)
Cl(1)	-0.1266(6)	0.2867(4)	0.1301(7)	5.2(6)	4.6(6)	8.7(7)	0.8(5)	-0.1(6)	1.2(6)
P(1)	-0.0725(6)	0.1709(4)	0.3532(6)	4.3(6)	3.6(6)	3.8(5)	-0.3(6)	0.7(5)	0.0(5)
P(2)	-0.1769(6)	0.1300(4)	0.1768(6)	2.7(5)	4.9(7)	4.0(6)	-0.8(5)	-0.3(4)	1.3(5)
P(3)	0.1937(6)	0.1796(4)	0.1769(6)	3.3(5)	2.7(6)	3.7(5)	0.0(5)	-0.3(4)	0.0(6)
P(4)	0.0980(5)	0.1193(4)	0.0130(6)	2.9(5)	4.2(6)	3.5(5)	0.5(5)	0.0(4)	-0.9(5)
O(1)	0.157(2)	0.159(1)	0.456(2)	6(2)	16(3)	7(2)	-4(2)	-2(2)	2(2)
O(2)	-0.090(2)	0.016(1)	0.019(2)	10(2)	7(2)	9(2)	-5(2)	-1(2)	-3(2)
O(3)	-0.001(1)	0.1946(7)	0.140(1)	5(1)	2(1)	6(1)	-1(1)	1(1)	-2(1)
C(1)	0.119(3)	0.163(2)	0.379(3)	8(3)	7(3)	7(3)	-6(3)	5(2)	-4(3)
C(2)	-0.069(2)	0.054(2)	0.048(3)	3(2)	14(5)	7(3)	-4(3)	3(2)	-7(3)
C(3)	-0.173(2)	0.176(1)	0.273(3)	4(2)	4(2)	6(2)	0(2)	3(2)	2(2)
C(4)	0.172(2)	0.173(1)	0.048(2)	5(2)	3(2)	3(2)	2(2)	2(2)	1(2)

(continued...)

Table 27 (continued)

b) Isotropic Atoms

Atom	x[a]	y	z	$B(\AA^2)$
H(1)	-0.0529	0.2191	0.1429	4.0

---

[a] Estimated standard deviations in this and other tables are given in parentheses and correspond to the least significant digits.

[b] The thermal parameters have been multiplied by 10^2. The thermal ellipsoid is given by $\exp[-2\pi^2(U_{11}a^{*2}h^2 + U_{22}b^{*2}k^2 + U_{33}c^{*2}\ell^2 + 2U_{12}a^*b^*hk + 2U_{13}a^*c^*h\ell + 2U_{23}b^*c^*k\ell)]$.

Table 28. Derived Parameters for the Rigid Groups of $[Ir_2(OH \cdot Cl)(CO)_2(DPM)_2]$.

Atom	x	y	z	B, Å²	Atom	x	y	z	B, Å²
C(11)	-0.0914(16)	0.1128(8)	0.4271(15)	3.0(7)	C(51)	0.2488(16)	0.2442(8)	0.1058(19)	3.8(8)
C(12)	-0.1710(14)	0.1097(8)	0.4810(18)	4.9(9)	C(52)	0.3100(17)	0.2617(9)	0.1162(14)	5.3(10)
C(13)	-0.1887(14)	0.0656(11)	0.5371(16)	5.6(10)	C(53)	0.3546(15)	0.3091(10)	0.1291(17)	4.9(9)
C(14)	-0.1368(18)	0.0246(8)	0.5392(16)	4.6(9)	C(54)	0.3381(18)	0.3390(8)	0.2116(21)	6.0(10)
C(15)	-0.0473(12)	0.0276(8)	0.4853(18)	5.4(9)	C(55)	0.2769(20)	0.3215(11)	0.2813(16)	8.8(13)
C(16)	-0.0296(12)	0.0717(10)	0.4292(15)	5.0(9)	C(56)	0.2323(15)	0.2741(11)	0.2684(16)	5.5(9)
C(21)	-0.0854(17)	0.2230(9)	0.4413(19)	4.2(8)	C(61)	0.2845(14)	0.1323(8)	0.2004(17)	2.5(7)
C(22)	-0.1237(16)	0.2702(12)	0.4122(15)	6.4(10)	C(62)	0.2696(13)	0.0907(10)	0.2636(16)	5.4(9)
C(23)	-0.1283(17)	0.3119(8)	0.4769(24)	6.8(11)	C(63)	0.3374(18)	0.0538(8)	0.2790(16)	5.5(9)
C(24)	-0.0947(20)	0.3064(11)	0.5708(21)	8.0(13)	C(64)	0.4200(15)	0.0584(9)	0.2311(19)	5.6(9)
C(25)	-0.0564(19)	0.2593(13)	0.5999(15)	9.8(14)	C(65)	0.4349(13)	0.0999(10)	0.1678(18)	6.6(10)
C(26)	-0.0517(17)	0.2176(9)	0.5351(22)	8.3(12)	C(66)	0.3672(17)	0.1369(8)	0.1525(15)	5.9(10)
C(31)	-0.2720(13)	0.1512(9)	0.1108(17)	2.8(7)	C(71)	0.0900(15)	0.1232(10)	-0.1203(11)	3.6(7)
C(32)	-0.2922(17)	0.1233(8)	0.0267(19)	5.9(10)	C(72)	0.0396(14)	0.0849(8)	-0.1675(15)	4.0(8)
C(33)	-0.3667(19)	0.1374(11)	-0.0295(15)	11.3(17)	C(73)	0.0329(14)	0.0852(8)	-0.2683(16)	4.5(8)
C(34)	-0.4209(14)	0.1793(11)	-0.0017(17)	5.0(9)	C(74)	0.0767(18)	0.1237(10)	-0.3220(11)	5.6(9)
C(35)	-0.4006(16)	0.2071(8)	0.0824(19)	6.0(10)	C(75)	0.1272(16)	0.1620(8)	-0.2748(18)	6.1(10)
C(36)	-0.3262(17)	0.1931(9)	0.1386(14)	4.4(9)	C(76)	0.1338(14)	0.1618(8)	-0.1740(19)	5.5(10)
C(41)	-0.2227(15)	0.0710(7)	0.2329(15)	2.9(6)	C(81)	0.1683(17)	0.0599(9)	0.0292(21)	3.3(8)
C(42)	-0.3110(14)	0.0710(8)	0.2682(17)	4.5(8)	C(82)	0.2424(20)	0.0532(11)	-0.0320(17)	6.7(11)
C(43)	-0.3459(13)	0.0265(11)	0.3128(17)	6.5(11)	C(83)	0.2957(16)	0.0085(14)	-0.0245(22)	10.6(17)
C(44)	-0.2924(19)	-0.0180(8)	0.3222(17)	6.0(10)	C(84)	0.2748(21)	-0.0295(10)	0.0443(27)	8.3(14)
C(45)	-0.2041(18)	-0.0180(7)	0.2869(18)	6.5(11)	C(85)	0.2007(24)	-0.0228(11)	0.1055(11)	9.7(15)
C(46)	-0.1692(12)	0.0265(9)	0.2423(16)	3.7(7)	C(86)	0.1475(17)	0.0219(13)	0.0979(19)	9.0(14)

Rigid Group Parameters

	X_c	Y_c	Z_c	phi	theta	rho
Group 1	-0.1091(11)	0.0687(6)	0.4832(10)	-2.006(15)	2.841(14)	0.620(14)
Group 2	-0.0900(11)	0.2647(8)	0.5060(14)	-2.474(23)	-2.363(18)	2.022(23)
Group 3	-0.3464(11)	0.1652(7)	0.0546(11)	0.274(20)	-2.448(16)	-2.33(19)
Group 4	-0.2576(11)	0.0265(6)	0.2776(10)	-2.069(15)	2.993(15)	0.463(14)
Group 5	0.2935(11)	0.2916(7)	0.1987(12)	1.302(33)	-2.087(15)	0.261(32)
Group 6	0.3523(11)	0.0953(6)	0.2157(10)	-0.884(20)	2.454(15)	0.198(18)
Group 7	0.0834(9)	0.1235(6)	-0.2212(11)	-0.616(13)	3.105(15)	-1.631(15)
Group 8	0.2216(13)	0.0152(8)	0.0367(14)	2.090(32)	-2.305(17)	3.030(29)

[a] X_c, Y_c, and Z_c, are the fractional coordinates of the centroid of the rigid group. The rigid group orientation angles phi, theta and rho have been defined before: La Placa, S.J.; Ibers, J.A. Acta Crystallogr., 1965, 18, 511.

Table 29. Derived Hydrogen Positions for $[Ir_2(CO)_2(\mu\text{-}OH\cdot Cl)(DPM)_2]$.

Atom	x	y	z	B(Å²)	Atom	x	y	z	B(Å²)
H(1C3)	-0.2256	0.1716	0.3118	4.0	H(45)	-0.1667	-0.0483	0.2949	7.5
H(2C3)	-0.1734	0.2102	0.2454	4.0	H(46)	-0.1085	0.0268	0.2200	4.5
H(1C4)	0.1447	0.2047	0.0263	4.0	H(52)	0.3204	0.2420	0.0598	6.4
H(2C4)	0.2283	0.1685	0.0163	4.0	H(53)	0.3963	0.3215	0.0819	6.3
H(12)	-0.2135	0.1373	0.4793	5.8	H(54)	0.3696	0.3714	0.2215	6.9
H(13)	-0.2423	0.0636	0.5753	7.1	H(55)	0.2670	0.3418	0.3390	9.7
H(14)	-0.1376	-0.0051	0.5799	6.0	H(56)	0.1911	0.2623	0.3169	6.7
H(15)	-0.0041	-0.0001	0.4885	6.0	H(62)	0.2130	0.0867	0.2949	5.9
H(16)	0.0247	0.0736	0.3925	6.0	H(63)	0.3268	0.0244	0.3206	6.5
H(22)	-0.1442	0.2746	0.3467	7.0	H(64)	0.4665	0.0326	0.2415	6.5
H(23)	-0.1540	0.3446	0.4559	7.6	H(65)	0.4924	0.1031	0.1365	7.5
H(24)	-0.1004	0.3351	0.6150	8.8	H(66)	0.3786	0.1654	0.1108	6.6
H(25)	-0.0370	0.2556	0.6649	10.6	H(72)	0.0087	0.0588	-0.1313	5.0
H(26)	-0.0272	0.1856	0.5557	9.0	H(73)	-0.0015	0.0585	-0.3011	5.6
H(32)	-0.2555	0.0942	0.0083	7.4	H(74)	0.0732	0.1228	-0.3918	6.1
H(33)	-0.3811	0.1172	-0.0864	11.2	H(75)	0.1581	0.1874	-0.3129	6.7
H(34)	-0.4728	0.1876	-0.0401	6.4	H(76)	0.1683	0.1877	-0.1431	6.5
H(35)	-0.4389	0.2350	0.1007	6.6	H(82)	0.2581	0.0789	-0.0791	6.5
H(36)	-0.3133	0.2120	0.1954	5.2	H(83)	0.3468	0.0033	-0.0660	10.1
H(42)	-0.3479	0.1011	0.2631	5.5	H(84)	0.3104	-0.0606	0.0491	9.2
H(43)	-0.4061	0.0260	0.3380	7.1	H(85)	0.1851	-0.0491	0.1513	10.6
H(44)	-0.3155	-0.0486	0.3538	7.0	H(86)	0.0964	0.0265	0.1382	9.6

Description of Structure

As shown in Figure 9, $[Ir_2(CO)_2(\mu\text{-}OH\cdot Cl)(DPM)_2]$ displays an "A-frame" type structure in which the apical site is occupied by the bridging OH•Cl moiety with the two terminal carbonyl groups almost trans to the iridium-oxygen bonds. The bridging DPM ligands are coordinated in mutually trans positions, essentially perpendicular to the Ir-O-Ir plane, much as is observed in other DPM-bridged complexes. As such, the overall geometry closely resembles that of other "A-frames" [58,61] and is especially close to that of the rhodium analogue, $[Rh_2(CO)_2(\mu\text{-}OH\cdot Cl)(DPM)_2]$.[208]

The relatively long Ir(1)-Ir(2) separation of 3·148(2)Å (see Table 30) suggests that there is no formal metal-metal bond. This distance is significantly longer than those observed in similar compounds containing Ir-Ir single bonds (range 2.779(1)-2.893(2)Å),[151,166,173] and is also longer than the intraligand P-P distances (*ca*. 3.07Å) in the compound, suggesting a lack of attraction between the metals. The absence of a formal metal-metal bond is also consistent with conventional electron counting techniques which give each Ir atom a 16-electron configuration.

Certainly the most interesting aspect of the structure is the presence of the bridging OH•Cl moiety. This group

Table 30. Selected Distances (Å) in $[Ir_2(CO)_2(\mu\text{-}OH\cdot Cl)(DPM)_2]$.

Bonding Distances

Ir(1)-O(3)	2.07(2)	P(1)-C(3)	1.85(3)
Ir(2)-O(3)	2.06(2)	P(2)-C(3)	1.78(4)
Ir(1)-C(1)	1.75(5)	P(3)-C(4)	1.81(3)
Ir(2)-C(2)	1.89(5)	P(4)-C(4)	1.82(4)
Ir(1)-P(1)	2.312(9)	P(1)-C(11)	1.82(2)
Ir(1)-P(3)	2.313(9)	P(1)-C(21)	1.81(3)
Ir(2)-P(2)	2.323(9)	P(2)-C(31)	1.76(2)
Ir(2)-P(4)	2.330(8)	P(2)-C(41)	1.83(2)
O(3)-H(1)	0.99	P(3)-C(51)	1.85(2)
Cl(1)-H(1)	2.13	P(3)-C(61)	1.84(2)
C(1)-O(1)	1.21(4)	P(4)-C(71)	1.84(2)
C(2)-O(2)	1.10(4)	P(4)-C(81)	1.85(3)

Non-Bonded Distances

Ir(1)-Ir(2)	3.148(2)	O(2)-H(72)	2.75
P(1)-P(2)	3.06(1)	O(2)-H(44)	2.79
P(3)-P(4)	3.08(1)	O(3)-H(1C4)	2.67
Cl(1)-H(2C3)	2.58	C(1)-H(62)	2.67
O(1)-H(74)	2.61	C(1)-H(16)	2.69
O(1)-H(84)	2.87	C(2)-H(46)	2.55
O(3)-Cl(1)	3.10(2)	C(2)-H(72)	2.72
O(2)-H(43)	2.71		

Table 31. Selected Angles (deg) in [$Ir_2(CO)_2(\mu$-OH·Cl)$(DPM)_2$].

a) Bond Angles

O(3)-Ir(1)-C(1)	174.0(14)	Ir(2)-O(3)-H(1)	111	Ir(2)-P(4)-C(71)	114.6(7)	P(1)-C(21)-C(26)	120.7(10)
O(3)-Ir(1)-P(1)	92.8(6)	Ir(1)-C(1)-O(1)	176(4)	Ir(2)-P(4)-C(81)	117.3(8)	P(2)-C(31)-C(32)	116.3(10)
O(3)-Ir(1)-P(3)	84.1(6)	Ir(2)-C(2)-O(2)	176(4)	C(3)-P(1)-C(11)	105.6(12)	P(2)-C(31)-C(36)	123.7(9)
C(1)-Ir(1)-P(1)	87.9(11)	O(3)-H(1)-Cl(1)	163	C(3)-P(1)-C(21)	105.1(13)	P(2)-C(41)-C(42)	119.7(9)
C(1)-Ir(1)-P(3)	95.0(12)	Ir(1)-P(1)-C(3)	112.8(10)	C(3)-P(2)-C(31)	102.0(12)	P(2)-C(41)-C(46)	120.3(9)
P(1)-Ir(1)-P(3)	176.8(3)	Ir(2)-P(2)-C(3)	113.6(10)	C(3)-P(2)-C(41)	104.2(12)	P(3)-C(51)-C(52)	121.9(10)
O(3)-Ir(2)-C(2)	175.9(12)	Ir(1)-P(3)-C(4)	112.3(11)	C(4)-P(3)-C(51)	103.0(13)	P(3)-C(51)-C(56)	118.0(11)
O(3)-Ir(2)-P(2)	90.7(6)	Ir(2)-P(4)-C(4)	112.2(10)	C(4)-P(3)-C(61)	104.0(13)	P(3)-C(61)-C(62)	119.9(9)
O(3)-Ir(2)-P(4)	85.5(6)	Ir(1)-P(1)-C(11)	116.2(7)	C(4)-P(4)-C(71)	105.3(12)	P(3)-C(61)-C(66)	120.1(9)
C(2)-Ir(2)-P(2)	93.3(10)	Ir(1)-P(1)-C(21)	113.9(8)	C(4)-P(4)-C(81)	104.6(13)	P(4)-C(71)-C(72)	117.5(9)
C(2)-Ir(2)-P(4)	90.5(10)	Ir(2)-P(2)-C(31)	117.6(7)	P(1)-C(11)-C(12)	118.2(9)	P(4)-C(71)-C(76)	122.6(10)
P(2)-Ir(2)-P(4)	176.2(4)	Ir(2)-P(2)-C(41)	117.1(7)	P(1)-C(11)-C(16)	121.8(9)	P(4)-C(81)-C(82)	118.0(12)
Ir(2)-O(3)-Ir(2)	99.4(8)	Ir(1)-P(3)-C(51)	112.9(7)	P(1)-C(21)-C(22)	119.2(10)	P(4)-C(81)-C(86)	122.1(12)
Ir(1)-O(3)-H(1)	119	Ir(1)-P(3)-C(61)	118.3(7)				

b) Torsion Angles

P(1)-Ir(1)-Ir(2)-P(2)	6.6(3)	P(1)-Ir(1)-Ir(2)-P(4)	176.0(3)
P(3)-Ir(1)-Ir(2)-P(4)	6.7(3)	P(3)-Ir(1)-Ir(2)-P(2)	170.7(3)

can be most logically considered as a bridging hydroxide ligand having the chloride anion hydrogen-bonded to it, although this is not the only interpretation, as will be discussed later. The hydrogen atom of the hydroxy group did not refine well, even though it was clearly defined on difference Fourier maps. Its observed and unrefined position yields an approximately linear O(3)-H(1)-Cl angle of _ca._ 163° and short O(3)-H(1) and H(1)-Cl contacts of 0·99 and 2·13Å, respectively, suggesting the presence of hydrogen bonding involving O(3), H(1) and Cl. Furthermore, the O(3)-Cl distance of 3·10(2)Å is shorter than a normal van der Waals contact of between 3.20 and 3.40Å again suggestive of hydrogen bonding. All parameters are in agreement with those found in other hydrogen-bonded systems.[210] The strength of this O-H-Cl interaction is further evidenced by the failure of the chloride ion to dissociate in solution (vide infra). It also can be seen that the chloride ion is interacting with one of the DPM methylene hydrogens resulting in a Cl-H(2C3) contact (_ca._ 2.58Å) which is again less than the van der Waals distance. The OH·Cl moiety is symmetrically bonded to both metals, with Ir-O distances of 2.07(2) and 2.06(2)Å and an Ir(1)-O(3)-Ir(2) angle of 99.4(8)°; these values compare rather well with those in the rhodium analogue.[208] As Figure 10 shows the hydrogen atom of the hydroxy group lies

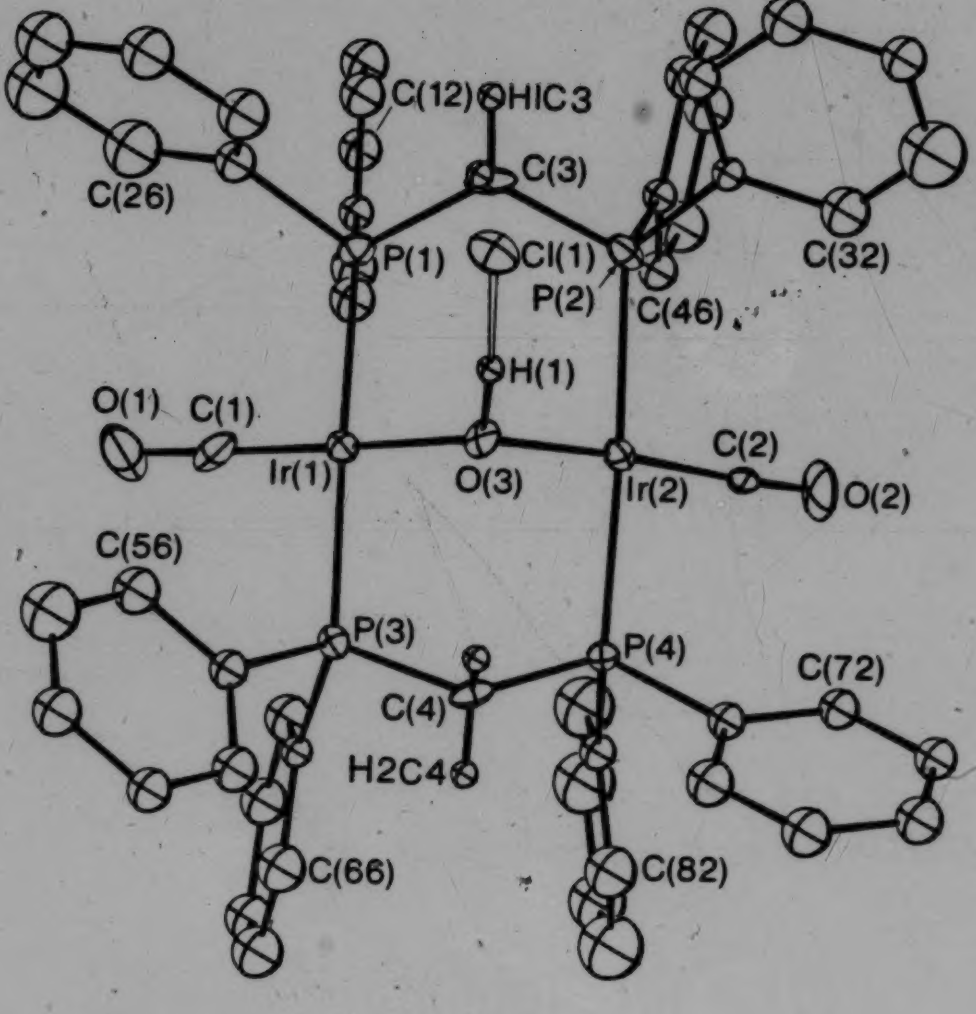
C(12)
HIC3
C(3)
C(26)
P(1)
Cl(1)
P(2)
C(46)
C(32)
H(1)
O(1)
C(1)
Ir(1)
O(3)
Ir(2)
C(2)
O(2)
C(56)
P(3)
P(4)
C(72)
C(4)
H2C4
C(66)
C(82)

Figure 9. Perspective view of $[Ir_2(CO)_2(\mu\text{-}OH \cdot Cl)(DPM)_2]$, showing the numbering scheme. The numbering on the phenyl carbon atoms starts at the carbon atom bonded to phosphorus and increases sequentially around the ring. Twenty percent ellipsoids are shown.

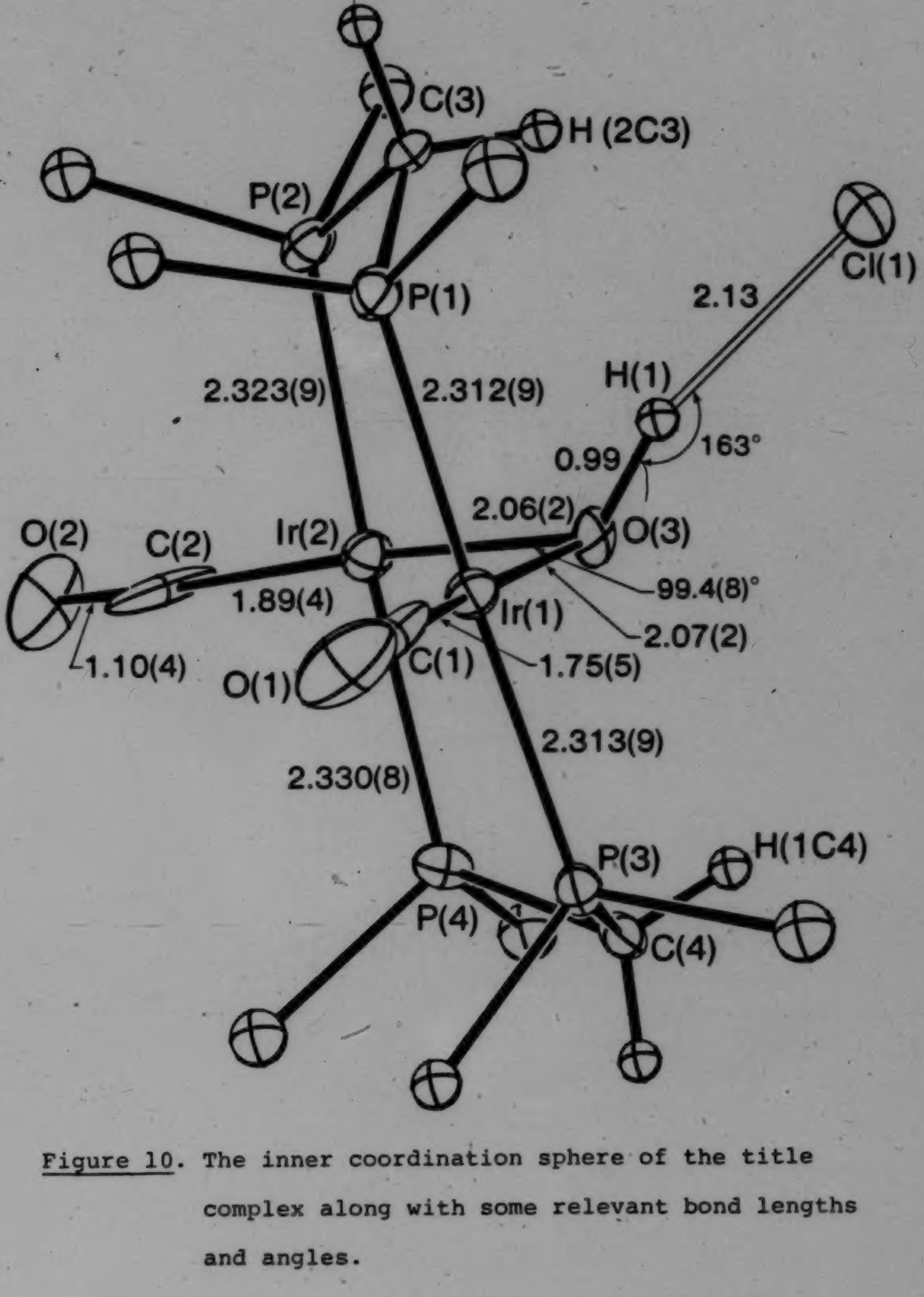
C(3)
H (2C3)
P(2)
Cl(1)
P(1)
2.13
2.323(9)
2.312(9)
H(1)
163°
0.99
2.06(2)
O(3)
O(2)
C(2)
Ir(2)
99.4(8)°
1.89(4)
Ir(1)
2.07(2)
1.10(4)
C(1)
1.75(5)
O(1)
2.313(9)
2.330(8)
H(1C4)
P(3)
P(4)
C(4)

Figure 10. The inner coordination sphere of the title complex along with some relevant bond lengths and angles.

well above the Ir(1)-Ir(2)-O(3) plane (by ca. 0.67 Å), suggesting sp^3 hybridization of the oxygen atom.

Within the DPM framework the parameters are unexceptional (see Tables 30 and 31) and are similar to those found in related structures. Both DPM methylene groups are folded towards the bridging OH•Cl group allowing the phenyl rings to occupy the relatively open positions on the opposite side of the complex. This orientation also allows the previously described interaction between the methylene protons and the chloride ion to occur. As is also shown in Figure 10 the $Ir_2(DPM)_2$ framework is skewed somewhat, with P-Ir-Ir-P torsion angles of ca. 6.5° (see Table 31). However, this slight degree of skewing is not unusual. The carbonyl groups are also quite normal and are essentially trans to the Ir-O bonds leading to a rather undistorted "A-frame" geometry.

Results and Discussion

(a) Preparation and Characterization of Compounds.

The studies of Yoshida and coworkers on catalysis of the WGS reaction by mononuclear rhodium phosphine complexes demonstrated the involvement of metal hydroxides in the catalytic cycle, part of which is outlined in equations 9-12 below.[205] In this system, it was proposed that

$$[Rh(OH)(CO)(PR_3)_2] \underset{}{\overset{S}{\rightleftharpoons}} [Rh(CO)(S)(PR_3)_2][OH] \quad (9)$$

S = solvent

$$[Rh(CO)(S)(PR_3)_2][OH] \rightleftharpoons [Rh(CO)_2(PR_3)_2][OH] \quad (10)$$

$$[Rh(CO)_2(PR_3)_2][OH] \rightleftharpoons [Rh(CO)(CO_2H)(PR_3)_2] \quad (11)$$

$$[Rh(CO)(CO_2H)(PR_3)_2] \rightleftharpoons [RhH(CO)(PR_3)_2] \quad (12)$$

hydroxide ion first dissociates from the complex and subsequently attacks an electrophilic CO ligand. We were interested in developing complexes related to $[Rh(OH)(CO)(PR_3)_2]$, in which as many ligands as possible could be actively involved in the reaction of interest (in this case the WGS reaction) and therefore set out to synthesize a binuclear iridium analogue of the above hydroxide, namely trans-$[Ir(OH)(CO)(DPM)]_2$. We had observed the following equilibrium in solution, involving the closely related chloro species (XXIV) (see Chapter 2), and reasoned that

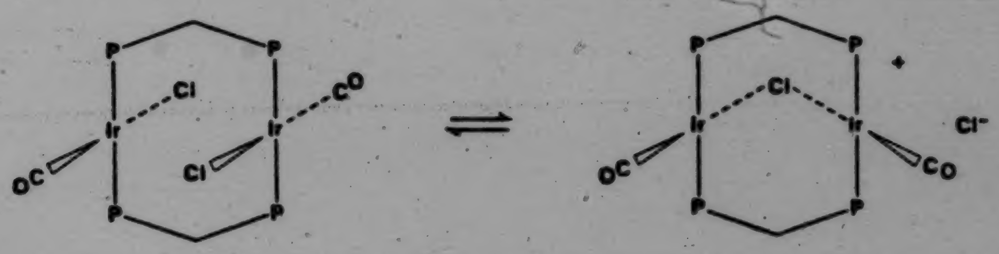

XXIV

XXV

the hydroxide complex might behave similarly. Such reversible hydroxide ion dissociation would parallel that shown in eqn. 9 for the mononuclear system suggesting the potential for catalysis of the WGS reaction by these binuclear complexes. However, the reaction between trans-$[IrCl(CO)(DPM)]_2$ and excess NaOH does not yield a dihydroxy analogue of species XXIV as was anticipated. Instead, compound **22**, which analyzes as $[Ir_2Cl(OH)(CO)_2(DPM)_2]$, is obtained. This species, shown by its $^{31}P\{^1H\}$ NMR spectrum to be symmetrical on the NMR time scale, has two rather low carbonyl stretches at 1904 and 1882 cm^{-1} and is a non-electrolyte in CH_2Cl_2. Although no stretch attributable to an O-H moiety was obvious in the I.R. spectrum, careful examination of the ^1H NMR spectrum showed a broad quintet at δ 4.85 due to the hydroxide hydrogen atom coupled to four phosphorus nuclei. As discussed earlier, the X-ray structure determination clearly established the structure shown below for this compound, in which the bridging hydroxide group is hydrogen bonded to the chloride ion. It seems, based on the lack of conductivity and on the similarities in the solution and solid I.R. spectra, that the chloride ion remains hydrogen bound in CH_2Cl_2 solution. The hydrogen bonding involving the hydroxide group accounts for our failure to observe the O-H stretch in the region normally associated with a free OH moiety.

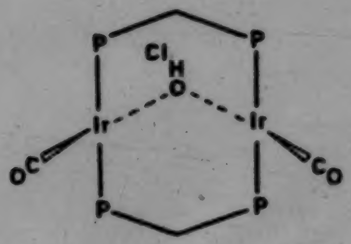

(22)

In the ^1H NMR spectrum of **22** the resonances for the DPM methylene protons are rather broad and unresolved with one being shifted downfield from what is usually observed, suggesting that the interaction between the chloride ion and the methylene group, which was observed in the X-ray structure, persists in solution. Since there are only two methylene resonances in the ^1H NMR spectrum and since the $^{31}P\{^1H\}$ resonance appears as a singlet down to -40°C, a rapid fluxional process must be occurring which transfers the chloride ion from one methylene group to the other as shown below.

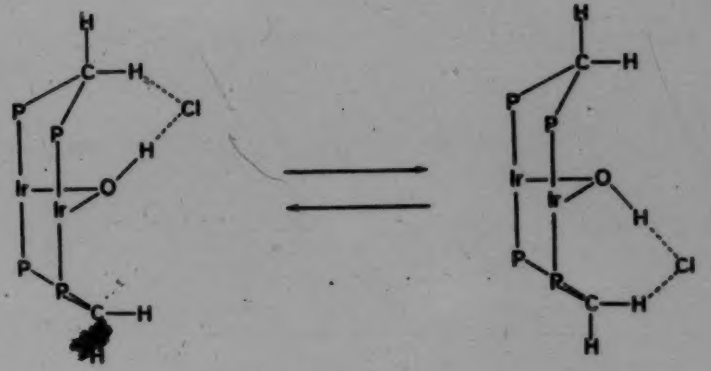

Although complex **22** can be viewed as containing a bridging hydroxide group with a hydrogen-bound chloride ion, an alternate viewpoint is to consider it as a bridging oxide complex with a hydrogen-bound HCl molecule. This latter view is not totally unreasonable since a comparison of the carbonyl stretches in **22** with those in the analogous sulfide-bridged complex, $[Ir_2(CO)_2(\mu\text{-}S)(DPM)_2]$,[151] (1918, 1902 cm^{-1}) indicates that they are very similar.

Treatment of compound **22** with one equivalent of $HBF_4 \cdot Et_2O$ results in the formation of $[Ir_2(CO)_2(\mu\text{-}OH)(DPM)_2][BF_4]$ (**23**), presumably through loss of HCl (although no attempt was made to detect this). The O-H stretch for the bridging hydroxide group in **23** appears as a weak band at 3498 cm^{-1}, and the ^1H NMR resonance appears as a quintet at δ 2.6 ppm with $^3J_{P-H} = 3.1$ Hz. The carbonyl bands in the I.R. spectrum, although still quite low (1959, 1943 cm^{-1}), are higher than in the parent compound **22**, reflecting the positive charge of compound **23**. All of the spectroscopic parameters (see Tables 24 and 25) are consistent with compound **23** having an "A-frame" geometry like compound **22**, but without the chloride ion. Another route for the preparation of **23** from **22** by reaction with Ag^+ does yield **23** in ca. 70% yield; unfortunately other products are also produced which appear to contain coordinated Ag^+, as suggested by the observation of long-range Ag-P coupling in the $^{31}P\{^1H\}$ NMR spectra ($J_{P-Ag} \simeq 10$ Hz). Owing to the difficulties in separating these Ag-containing impurities from **23**, the reaction of **22** with acid is the route of choice. Silver adducts of these binuclear iridium complexes have been obtained by the direct reaction of **25** with $AgBF_4$.[166]

The reactions of compounds **22** and **23** with CO take two rather different, although related routes. When a CH_2Cl_2 solution of **22** is treated with an atmosphere of CO (under ambient conditions) the solution changes from dark orange to bright yellow after about 20 min. From this solution, a new compound **24** can be isolated in 90% yield as bright yellow crystals. This solid displays five bands in the carbonyl region of the I.R. spectrum (see Table 24). Elemental analyses of these crystals shows the presence of two chlorine atoms per dimer, however ^1H NMR spectra clearly show that these chlorines are due to CH_2Cl_2 of solvation. Furthermore, recrystallization of this solid from THF/ether yields **24** with no CH_2Cl_2 appearing in the ^1H NMR spectra and with no chlorine detected in the elemental analyses. Apart from the resonances due to the DPM phenyl and methylene protons no other resonances appear between 15 and -40 ppm in the ^1H NMR spectrum. Compound **24** is very susceptible to CO loss, such that flushing the solution with N_2 causes it to darken, and a new compound **25** can be isolated as a golden yellow solid. This species is observed to be symmetrical in the $^{31}P\{^1H\}$ NMR spectrum (between 25 and -60°C), has three carbonyl bands in the I.R. spectrum of the solid at 1950, 1936 and 1857 cm^{-1} and contains no chlorine, as indicated by elemental analyses. The rhodium analogue of 25 has been reported and was suggested to have the "A-frame" structure shown for XXVI, with no metal-metal bond. This structure for 25 (and also for the Rh dimer) is rejected on the basis of the I.R.

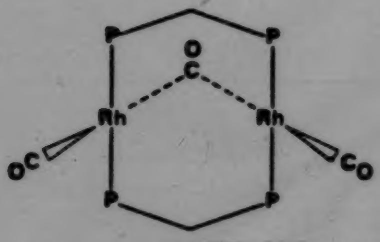

XXVI

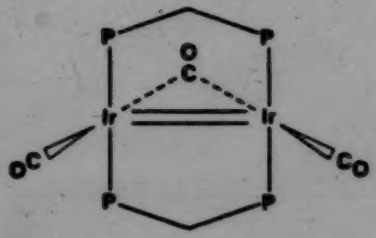

XXVII

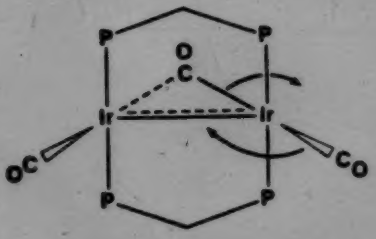

XXVIII

stretch for the bridging carbonyl group. It would be expected that a species like XXVI would have a much lower carbonyl stretch (< ca. 1720 cm^{-1}) as has been observed in all reliably characterized complexes of this type[42,66,74,211]. Based on the spectroscopic evidence we favour a metal-metal bonded structure for 25. One possibility is the doubly bonded structure XXVII which would give both metals 18-electron configurations. However, the observation of only one DPM methylene resonance, instead of the usual two, in the ^{1}H NMR spectrum at room temperature suggests that a fluxional process is occurring which equilibrates both faces of the dimer. This could occur by interchange of a terminal CO with the bridging one as indicated in structure XXVIII. Evidence for a non-static structure also comes from the solution I.R. spectrum which shows four strong carbonyl bands between 1994 and 1878 cm^{-1} as opposed to only three in the I.R. of the solid. Further studies are needed to characterize **25** more fully in solution and in the solid state.

Although compound **24** displays five carbonyl stretches in the I.R. spectrum, ranging from 1886 to 1991 cm^{-1}, we believe that it is only a tetracarbonyl species. A symmetrical pentacarbonyl species would, of necessity, have one bridging carbonyl group and no Ir-Ir bond, in order to avoid exceeding an 18-electron configuration at each metal. Such a bridging carbonyl would be expected, as noted previously, to have a carbonyl stretch far lower than the range observed. The NMR spectra of **24** suggest that it too is fluxional in solution. In the ^{31}P{^{1}H} spectrum only a sharp singlet appears at room temperature which broadens and begins to coalesce into the baseline by -40°C (the low temperature limiting spectrum could not be obtained). Similarly, the fluxional process results in the ^{1}H resonance of the DPM methylene protons appearing as a broad singlet at room temperature. It seems therefore, that **24** exists in solution as a mixture of rapidly interconverting tetracarbonyl isomers, more than one of which also occur in the solid state. A similar situation was observed for $Fe_3(CO)_{12}$.[212] It is also significant that in the reversible transformation of **25** to **24** by the slow stepwise addition of CO, no other species is observed, supporting our contention that we are observing a conversion between tricarbonyl and tetracarbonyl species.

The formation of the Ir(O) complexes **24** and **25** from **22** is novel; in particular it should be noted that this does not occur with the analogous Rh species[208]. One possibly is that this reaction proceeds via a metallocarboxylic acid intermediate as shown in SCHEME IV. If the chloride ion remains hydrogen bonded, as shown, then expulsion of CO_2

SCHEME IV

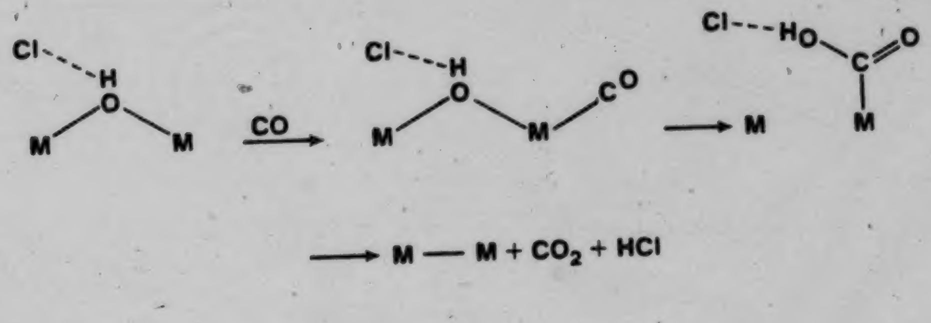

and HCl, leaving the Ir(O) complex, is readily understood. The reaction as outlined raises an interesting point regarding the mechanism of formation of the metallocarboxylic acid intermediate. Usually, such species are considered to result from nucleophilic attack on a coordinated carbonyl ligand by free OH^-. However, there has been at least one reference to an intramolecular transfer of OH^- from a metal to a coordinated CO ligand[213] and we suggest that this may be possible in the present reaction, as will be discussed later. Attempts to observe intermediates in the above reaction in the $^{31}P\{^1H\}$ NMR spectra, at -80°C, using stoichiometric amounts of CO were unsuccessful; only compounds **22** and **25** were observed.

The corresponding reaction of compound **23** with excess CO also proceeds readily at room temperature resulting in the eventual production of a yellow-orange solution. Upon reducing the volume of this solution under N_2, a dark red colour appears from which a red-purple solid, **26**, can be isolated. This species displays three carbonyl bands in the I.R. spectrum at 1981, 1967 and 1826 cm^{-1} and shows a quintet in the ^1H NMR spectrum at δ -9.44 ppm ($^2J_{PH}$ = 9.5 Hz). Based on this information and the observation of a singlet in the $^{31}P\{^1H\}$ NMR spectrum, **26** can be formulated as $[Ir_2(CO)_2(\mu\text{-}H)(\mu\text{-}CO)(DPM)_2]^+$ as shown below. Compound **26** can actually be isolated in two different forms in the solid state: the aforementioned red-purple solid, **26a**, and

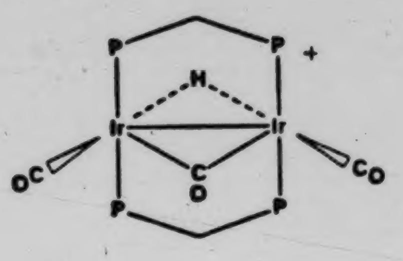

(26)

a dark orange form, **26b**. These two solids differ only in the position of their bridging carbonyl and BF_4^- stretches in the I.R. (see Table 24). This is most likely due to slight conformational differences in the solid state, since in solution both have identical spectroscopic properties. There appears to be no systematic method for obtaining one or the other form and **26** is often isolated as a mixture of the two. An X-ray study has been carried out on the dark orange form and confirms the structure as shown above.[214]

The initial pale yellow-orange colour which develops when **23** is treated with excess CO is likely due to the formation of a cationic tetra- or pentacarbonyl hydride since this species and the accompanying colour can be regenerated upon reacting a solution of **26** with CO. We have not been able to characterize this compound (other than by $^{31}P\{^1H\}$ NMR, where it appears as a singlet at δ -10.5 ppm at -40°C) owing to the ease with which it loses CO and reverts to **26** unless kept under CO pressures of greater than 1 atmosphere.

In the slow stepwise addition of CO to compound **23** at -40°C, a minor species is observed at intermediate times together with compounds **23** and **26**. This intermediate is observed as a singlet at δ 15.6 in the $^{31}P\{^1H\}$ NMR spectrum and its appearance is accompanied by the growth of two new I.R. bands at 3687 and 1604 cm^{-1}. It may be that this intermediate is a metallocarboxylic acid complex since the I.R. bands agree well with those previously reported for such species [215-218]. No other features in the carbonyl region of the I.R. spectra prove to be helpful in assigning a structure to this intermediate since these spectra are dominated by bands due to compounds **23** and **26**. We were also unable to observe the M-C(O)OH proton in the ^1H NMR spectrum. CO_2-loss from this metallocarboxylic intermediate could occur by β-hydride transfer to the metals yielding compound **26**. Although this spectroscopic evidence above is not consistent with a formate intermediate, one cannot be ruled out since the reaction of $[Ir_2(CO)_2(CH_3CN)_2(\mu\text{-}CO)(DPM)_2][BF_4]$ with sodium formate yields compound **5** as the only observed product (see Experimental section). When the transformation of **23** to **26** is carried out in deuterated solvents no evidence of deuterium incorporation into **26** is observed indicating that the hydrido ligand in **26** does originate from the hydroxy group in **23**.

Compound **26** can also be formed by the protonation of **25** with one equivalent of $HBF_4.Et_2O$, however the reverse deprotonation has not been effected; even the strong base 1,8-bis(dimethylamino)naphthalene[219] leaves **26** unchanged.

The analogous rhodium hydride complex, $[Rh_2(CO)_2(\mu\text{-}H)(\mu\text{-}CO)(DPM)_2]^+$, was found to be a catalyst in the WGS reaction, under relatively mild conditions,[35] however, none of the intermediates in the reaction was clearly characterized. With the iridium analogue we seemed to have an opportunity to examine in detail a model system for this reaction and thereby learn more about the steps involved. The reaction of $[Ir_2(CO)_2(\mu\text{-}OH)(DPM)_2]^+$ with CO accomplishes one of these steps, namely the oxidation of CO to CO_2. The other important step, the generation of H_2, was accomplished in the Rh system through the reaction $[Rh_2(CO)_2(\mu\text{-}H)(\mu\text{-}CO)(DPM)_2]^+$ with strong acid giving an uncharacterized dicationic rhodium complex.[35] We find that compound **26** also reacts with the strong acid, $HBF_4.Et_2O$, but in this case H_2 is not produced and we instead isolate the dihydride $[Ir_2H(CO)_2(\mu\text{-}H)(\mu\text{-}CO)(DPM)_2][BF_4]_2$. The I.R. spectrum of **27** (see Table 24) shows an Ir-H stretch at 2108 cm^{-1} and carbonyl bands at 2046, 1961 and 1833 cm^{-1}. The $^{31}P\{^1H\}$ NMR spectrum (see Table 25) indicates that the species is unsymmetrical and the ^1H NMR spectrum shows two high field resonances, integrating as 1 hydrogen each. The highfield resonance at δ -13.2 ppm appears as a sharp triplet of doublets ($^{1}J_{P-H}$ = 10.5 Hz, $^{2}J_{H-H}$ = 1.6 Hz) corresponding to a terminal hydride coupled to two adjacent phosphorus nuclei and to another hydrogen, while the downfield resonance at -7.1 ppm appears as a broad unresolved peak. It is probable that the latter resonance is due to the bridging hydride which is coupled to two pairs of chemically inequivalent P nuclei and to the terminal hydride. Our failure to resolve this resonance into its expected triplet of triplets of doublets is not surprising given the probable similar magnitudes of the coupling constants. Two structures are possible for this diprotonated species as shown. We suggest that compound **27** has structure XXX, owing to its failure to reductively eliminate H_2 vide infra). Although the H-H coupling

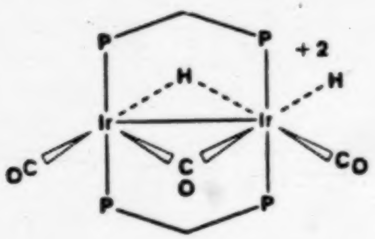

XXIX

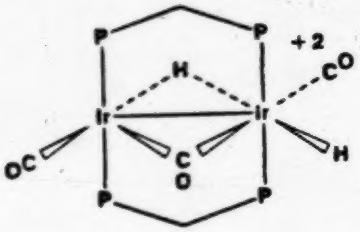

XXX

observed is rather small for what might be expected for trans hydride ligands,[220] we have observed similarly small coupling constants for $[Ir_2H(CO)_2(\mu\text{-}H)_2(DPM)_2]^+$ (see

Chapter 6). It appears, based on the facile loss of H_2, that protonation of the rhodium analogue[35] yields structure XXIX. Such a notion is consistent with the structural differences between **26** and $[Rh_2(CO)_2(\mu\text{-}H)(\mu\text{-}CO)(DPM)_2]^+$. In the rhodium compound the (μ-H)-Rh-CO angle is much greater than the (μ-CO)-Rh-CO angle (155(4)° vs. 114.6(9)°)[35] favouring proton addition cis to the bridging hydride, whereas in compound **26** the corresponding angles between the bridging CO and the terminal ones are ca. 120.0°.[214] It is also significant that in the solid state structure of **26** four phenyl groups block the sites adjacent to the bridging hydride ligand whereas in the rhodium analogue it is the sites adjacent to the carbonyl ligand which are blocked. Although we recognize that these are solid state comparisons, the solid state differences do parallel the observed differences in the chemistry of these two species and therefore appear to be significant.

Upon standing in solution for about one week **27** rearranges to a new compound **28** in which the two hydride and three carbonyl ligands are now all terminal (see Tables 24 and 25). The $^{31}P\{^1H\}$ NMR spectrum indicate that the molecule is still unsymmetrical, making structures XXXI to XXXIII, shown below, the most likely possibilities. Of these we favour XXXI since **28** can also be obtained by the rapid reaction of $[Ir_2(CO)_2(MeCN)_2(\mu\text{-}CO)(DPM)_2]^{2+}$ (**31**) with H_2. We have demonstrated that a similar side-by-side

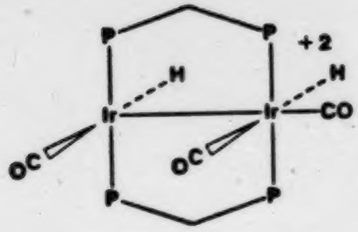

XXXI

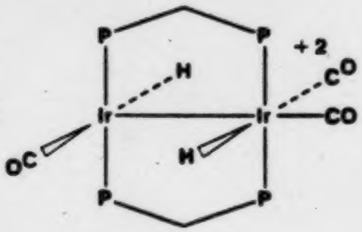

XXXII

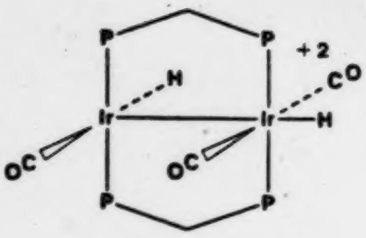

XXXIII

arrangement of hydrides, as shown in XXXI, occurs upon the reaction of $[IrCl(CO)(DPM)]_2$ with H_2 (see Chapter 4). Structure XXXI is also more consistent with the oxidative addition of H_2 occurring in a concerted manner leading to a cis hydride complex. Significantly, no evidence of **27** is observed in the reaction of **31** with H_2, further suggesting a trans arrangement of hydrides for **27**.

The isomerization of **27** to **28** undoubtedly occurs by a deprotonation and reprotonation step with compound **26** as the intermediate. It seems that protonation of **26** gives **27** as the kinetic product, having structure XXX, which then rearranges to the thermodynamically favoured species **28**, having structure XXXI. When weaker acids, such as trifluoracetic acid, are used to protonate **26** an excess must be used and **28** is formed instead of **27**. The more facile rearrangement with the stronger conjugate base is in agreement with a deprotonation mechanism for the isomerization. It should be noted that compounds **27** and **28** are readily deprotonated by weak bases such as acetone and water to rapidly regenerate compound **26**.

The conductivity measurements for compounds **27** and **28** (and also of **29**) are too low for normal 2:1 electrolytes, however the spectral and chemical information leaves no doubt concerning their stoichiometries. For example, compound **31**, shown to be a normal 2:1 electrolyte, reacts with H_2 to yield **28**, and as will be explained, **31** can ultimately be regenerated from **28**. We conclude that the low conductivity measurements are due to ion pairing in the solvent having a low dielectric constant. Unfortunately, solvents which would reduce the amount of ion pairing also result in deprotonation of these dihydrides and so cannot be used.

Attempts to induce H_2 loss from either **27** or **28** by refluxing in CH_2Cl_2 for up to 4 h failed and only starting materials were recovered. However, H_2 loss can be induced by two routes, first by the addition of CO and second by refluxing in acetonitrile. It had been observed that the reaction of $[Ir_2(H)_4(CO)_2(DPM)_2]$ with CO leads to H_2 elimination and the formation of compound **24** (see Chapter 6) suggesting that a similar process might be possible with compounds **27** and **28**. When either **27** or **28** are stirred under an atmosphere of CO an immediate reaction occurs producing a pale yellow solution, from which a white solid (**29**) can be isolated. The I.R. spectrum of **29** shows carbonyl bands at 2080, 2061, 2038 and 2017 cm^{-1} and the ^1H

NMR spectrum shows a high field quintet, ($^2J_{P-H}$ = 5.1 Hz) integrating as two protons, for the two bridging hydrogens. Based on these data and on the $^{31}P\{^1H\}$ NMR spectrum which shows a singlet we propose the following structure for **29**. Heating this species in CH_2Cl_2 regenerates only **27**, again suggesting the trans hydride geometry (XXIX) for this latter species; loss of a terminal carbonyl group in **29** would readily yield **27** by moving one H to a terminal site and one terminal carbonyl to the vacated bridging position. Significantly, since **29** is formed from the reaction of both **27** and **28** with CO, this suggests that the reaction involves more than simple CO addition. It is possible that CO addition results in the labilization of one of the hydride ligands resulting in proton loss and the formation of a common intermediate $[Ir_2(H)(CO)_4(DPM)_2][BF_4]$ which can subsequently reprotonate to give **29**. Support for this comes from the observation that the reaction of **26** with acid under a CO atmosphere leads directly to **29**.

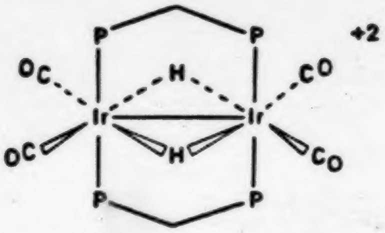

29

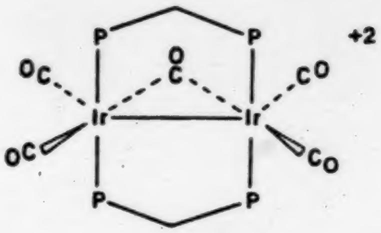

30

Although the major product from the reaction of **27** with CO is still a hydride, another product is observed in about 10% yield. This was subsequently identified as $[Ir_2(CO)_4(\mu\text{-}CO)(DPM)_2][BF_4]_2$, **30**, which was prepared independently from the reaction of $[Ir_2Cl(CO)_3(\mu\text{-}CO)(DPM)_2][Cl]$ with two equivalents of $AgBF_4$ under a CO atmosphere (see Experimental Section). The infrared spectrum of **30** shows four terminal and one bridging carbonyl bands indicating that compound **30** probably has the structure shown above in which the geometry is similar to that observed for $[Ir_2Cl_2(CO)_2(\mu\text{-}CO)(DPM)_2]$ (see Chapter 2).

The production of some **30** from the reaction of **27** and **28** with CO shows that reductive elimination of H_2 has occurred. This further supports a mechanism involving proton loss and recoordination for the formation of **29** from **27** and **28**. Although most of the proton recoordination occurs opposite the bridging proton, some must occur cis to it to allow the reductive elimination of H_2. Compound **29** also converts to **30**, albeit very slowly, when left under an atmosphere of CO for up to two weeks. Again a deprotonation-reprotonation mechanism is implicated, however, in this case both the bridging hydride ligands appear to be more strongly bound than the terminal hydrides in **27** and **28**, judging by the very slow formation of **30**.

H_2 removal from **28** can also be partially effected by heating in acetonitrile for ca. twenty or more minutes, yielding the tricarbonyl species $[Ir_2(CO)_2(CH_3CN)_2(\mu\text{-}CO)(DPM)_2]^{2+}$ (**31**). This latter product can also be prepared in high yield by the reaction of **30** with acetonitrile (see Experimental section) and has carbonyl bands in the I.R. spectrum at 2005, 1980 and 1731 cm^{-1} and bands due to the acetonitrile ligands at 2312 and 2284 cm^{-1}. Based on these data and on $^{31}P\{^1H\}$ NMR spectrum which indicates that **31** is symmetric, the following two structures are possible. Although differentiation of these two species based on the available data is not possible, the low stretch for the bridging carbonyl group may suggest that it is trans to the better σ-donor acetonitriles rather than the π-accepting

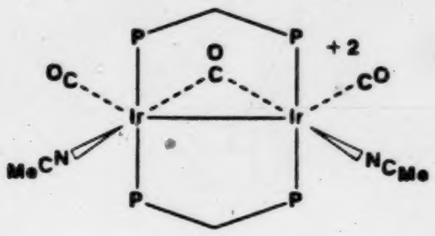

XXXIV

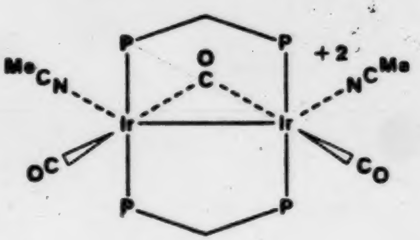

XXXV

carbonyls. Although this hydride-free product is obtained readily in refluxing acetonitrile, it is obtained as only a minor product (ca. 10% yield); the other products have not been identified and their number increases with increased reflux time.

Both compounds **30** and **31** react with hydroxide ion. The reaction of **30** with one equivalent of $NMe_4OH \cdot 5H_2O$ results in the formation of only compound **26**. This reaction probably occurs by OH^- attack at one of the carbonyl ligands resulting in the formation of a metallocarboxylic acid species. The high carbonyl stretches for the terminal carbonyls in the dicationic species **30** suggest that these groups will be susceptible to nucleophilic attack. Direct attack at the metals is less likely since both metals have 18-electron configurations and CO dissociation would first have to occur. Subsequent loss of CO_2 from the metallocarboxylic intermediate, via β-hydride transfer to the metals, would then yield a tetracarbonyl hydride complex which after CO loss would yield **26** (vide infra).

Reaction of **31** with OH^- also occurs readily but based on the products obtained, appears to proceed by a different route. In this reaction, both compounds **23** and **26** are obtained, in the ratio of 3:1, respectively. Futhermore, if the reaction vessel is flushed with N_2 during the course of the reaction this ratio changes to 5:1. This information suggests that in this case OH^- attack does not occur directly at a carbonyl group since this would be expected to yield, after CO_2 loss, the hydride $[Ir_2(CO)_2(\mu\text{-}H)(DPM)_2]^+$, which is not observed. The observation of the hydroxy bridged species **23** indicates that OH^- attack occurs at the metals at some stage of the reaction. It seems likely that the reaction of **31** with OH^- occurs with coordination of the hydroxide ligand at the metals, accompanied by acetonitrile loss to give $[Ir_2(CO)_2(\mu\text{-}OH)(\mu\text{-}CO)(DPM)_2]^+$ (XXXVI), a short-lived intermediate which is not observed. This proposed intermediate is very similar to the previously characterized chloro-bridged species, $[Ir_2(CO)_2(\mu\text{-}Cl)(\mu\text{-}CO)(DPM)_2]^+$, and CO-loss from this species would yield one of the observed products, **23**. It is expected that CO-loss from XXXVI would be quite facile since, as described previously, when the stepwise addition of CO to **23**, is monitored, such a tricarbonyl intermediate is never observed. The other product in the reaction of **31** with hydroxide ion, **26**, could arise by several routes, although it is clear that based on its reduced yield when the solution is flushed with N_2, additional CO is required for its formation. One possibility is that CO lost from XXXVI can be picked up by compound **31** to give either **30** or a dicationic tetracarbonyl species and that subsequent nucleophilic attack by OH^- at one of the carbonyl groups yields **26** after CO_2 loss. However, XXXVI may itself be an intermediate in the production of **26**; it could coordinate additional CO lost by other molecules of XXXVI and after intramolecular hydroxide migration to a carbonyl group could yield a metallocarboxylic acid intermediate, which though loss of CO_2 would yield **26**. Although such an intramolecular pathway has not often been proposed, it cannot be ruled out as a viable pathway.

Consistent with the attack of the OH^- at the metal is the observation that the reaction of **31** with methoxide ion does not yield a methoxycarbonyl species but instead gives **26** in essentially quantitative yield. Again, it seems that methoxide attack at the metals occurs to yield an intermediate, $[Ir_2(CO)_2(OMe)(\mu\text{-}CO)(DPM)_2]^+$, which then β-hydride eliminates to give **26**.

(b) Water Gas Shift Catalysis.

We have demonstrated in the foregoing chemistry that the hydroxy-bridged species **23** presents a useful model for WGS catalysis. These reactions are summarized in scheme V, depicting the conversion of CO and H_2O (OH^- + H^+) to CO_2 and H_2. In the present system the model catalyst precursor is $[Ir_2(CO)_2(\mu\text{-}OH)(DPM)_2]^+$, however the involvement of the hydride-bridged species $[Ir_2(CO)_2(\mu\text{-}H)(\mu\text{-}CO)(DPM)_2]^+$ in this cycle suggests that the chemistry may be applicable to the catalytic cycle reported by Eisenberg and coworkers which utilized the analogous rhodium hydride $[Rh_2(CO)_2(\mu\text{-}H)(\mu\text{-}CO)(DPM)_2]^+$ as the catalyst precursor.[35] Although

SCHEME V

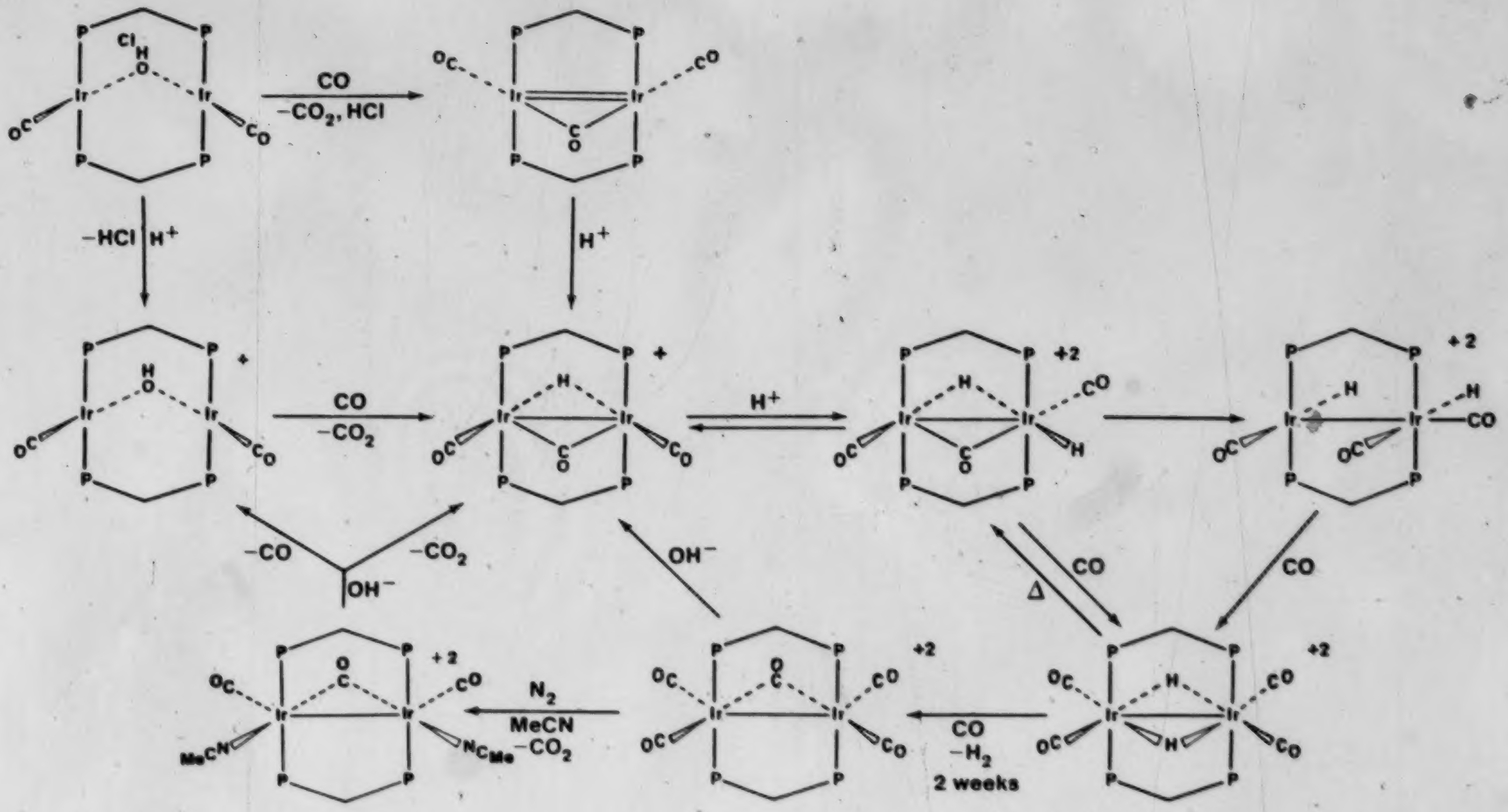
CO
−CO$_2$, HCl
−HCl
H$^+$
H$^+$
CO
−CO$_2$
H$^+$
−CO
−CO$_2$
OH$^-$
OH$^-$
CO
Δ
CO
N$_2$
MeCN
−CO$_2$
CO
−H$_2$
2 weeks
+
+
+2
+2
+2
+2
+ 2

detailed kinetic studies on this system have not been carried out, parallel comparative runs using $[Rh_2(CO)_2(\mu\text{-}OH)(DPM)_2]^+$ and $[Rh_2(CO)_2(\mu\text{-}H)(\mu\text{-}CO)(DPM)_2]^+$ as catalyst precursors, under the conditions studied by Eisenberg and coworkers (see Experimental Section), show that the two have equivalent turnover rates after a 48 h period (turnover rate ≈ 0·15 equiv. CO_2/h). Furthermore, I.R. spectra run on the solid isolated from the catalytic reaction involving the hydroxy-bridged species indicates that the major species present is the hydrido-bridged tricarbonyl cation.

The question then remains as to how well this iridium system models the rhodium-catalyzed reactions. This study does show the possible involvement of hydroxy-bridged species in a catalytic cycle and it is possible that such a cycle, involving metal-coordinated hydroxide ion is feasible as a catalytic pathway. However, it is likely that this is not the most important pathway. Instead, it is felt that nucleophilic attack by free OH^- on a coordinated CO ligand in a dicationic intermediate is a more favourable route. In the iridium cycle, the species involved was a dicationic pentacarbonyl complex (see Scheme V). Whether or not such a species actually exists with rhodium or whether the catalytically active rhodium species is a tetra or tricarbonyl analogue is not known, but in such dicationic species, the carbonyl ligands should be very susceptible to nucleophilic attack by OH^-.

It was noted in the study of the Rh system[35] that the addition of such salts as LiCl to the reaction mixture improved the turnover rate. Based on the observed hydrogen bonding between Cl^- and the bridging OH group in both the iridium species, $[Ir_2(CO)_2(\mu\text{-}OH{\cdot}Cl)(DPM)_2]$ and the rhodium analogue,[208] we initially considered that such species could offer an explanation for the observed rate enhancement upon Cl^- addition. However, it has been found that $[Rh_2(CO)_2(\mu\text{-}OH{\cdot}Cl)(DPM)_2]$ is not an active catalyst.[166,208] Under the conditions studied, this species is converted into trans-$[RhCl(CO)(DPM)]_2$ and $[Rh_2(CO)_2(\mu\text{-}Cl)(DPM)]^+$ both of which are catalytically inactive. This further suggests that the important steps in the catalytic cycle do not involve metal-bound hydroxides.

Nevertheless, this study indicates that these iridium systems can function as useful models for active rhodium catalysts. Further studies are necessary to illucidate the steps in the above WGS catalysis with emphasis on isolating and characterizing the proposed metallocarboxylic acid intermediates. Of special interest is the nature of the binding modes of such groups in the presence of a second metal centre.

CHAPTER 6

The Preparation and Characterization of Some DPM-Bridged Iridium Polyhydride Complexes and the Structure of $[Ir_2(H)(CO)_2(\mu\text{-}H)_2(DPM)_2][Cl]\cdot1.2CH_2Cl_2$

Introduction

One of the aims of this thesis was to prepare a series of DPM-bridged binuclear Ir hydrides with the eventual goal of using them to model catalytic systems. One approach, used in Chapter 4, involves the direct reaction of H_2 with metal complexes and has obvious relevance to catalytic processes which utilize H_2 as a reactant. Another approach, which forms the basis of this chapter, uses borohydride reagents to replace inactive ligands such as Cl^- by the more catalytically active hydrido ligand. The strategy of this latter approach is to prepare complexes in which as many of the ligands are chemically active. It was decided to try and prepare complexes such as $[IrH(CO)(DPM)]_2$, a binuclear iridium analogue of $[RhH(CO)(PPh_3)_2]$, the catalytically active species in olefin hydrogenation and hydroformulation reactions.[20-24] This chapter describes the results of this study.

Preparation of Compounds

a) $[Ir_2(H)_4(CO)_2(DPM)_2]$ (**32**).

An atmosphere of hydrogen was placed over a slurry of trans-$[IrCl(CO)(DPM)]_2$, **3**, (200 mg, 0.159 mmol) and $NaBH_4$ (25 mg, 0.661 mmol). The mixture was stirred for 24 h during which time all of **3** was consumed and a bright yellow solution was formed. 500 µl of degassed water was then added to the mixture to destroy the excess borohydride, resulting in significant gas evolution. When this subsided (ca. 30 sec) the solution was taken to dryness under vacuum resulting in the isolation of a bright yellow powder. The solid was redissolved in THF (10 mL) and was then filtered under nitrogen, yielding a clear bright yellow solution. 20 mL of hexanes was added, the volume reduced to 10 mL under vacuum and the solution stored overnight at -15°C. This yielded **32** as a yellow microcrystalline product in about 75% yield. Spectroscopic parameters for this and all subsequent compounds are given in Table 32. When dissolved in CH_2Cl_2, compound **32** proved to be non-conducting ($\Lambda(10^{-3}M) = 4.0\ \Omega^{-1}\ cm^2\ mole^{-1}$).[170] Anal. Calcd for $Ir_2P_4O_2C_{52}H_{48}$: C, 51.48%; H, 3.99%. Found: C, 51.61%; H, 4.08%.

b) $[Ir_2(H)_5(CO)_2(DPM)_2][BF_4] \cdot \frac{1}{2} CH_2Cl_2$ (**33**).

Method A. To a solution of **32** in CH_2Cl_2 under an atmosphere of hydrogen (150 mg, 0.124 mmol in 10 mL) was added one equivalent of $HBF_4 \cdot Et_2O$ (17.8 µl, 0.124 mmol) causing an immediate colour change to pale yellow. 30 mL of dry Et_2O was then added and the solution volume reduced to 15 mL under a rapid stream of H_2 causing the precipitation of **33** as a white microcrystalline solid in ca. 85% yield. Compound **33** was determined to be a non-electrolyte in CH_2Cl_2 solutions ($\Lambda(10^{-3}M) = 4.6\ \Omega^{-1}\ cm^2\ mole^{-1}$).

Anal. Calcd for $Ir_2ClP_4F_4O_2C_{52.5}BH_{50}$: C, 46.52%; H, 3.72%; Cl, 2.61%. Found: C, 46.88%; H, 3.76%; Cl, 2.09%. The presence of and amount of solvent molecules was confirmed by ^1H NMR for this and other compounds.

Method B. An atmosphere of hydrogen was placed over a solution of $[Ir_2(CO)_2(\mu\text{-}H)(\mu\text{-}CO)(DPM)_2][BF_4]$ (**26**) in CH_2Cl_2 (200 mg, 0.151 mmol in 10 mL) and the resulting mixture stirred for 16 h, during which time the solution changed colour from intense red to light yellow. The addition of 30 mL Et_2O followed by reduction of the volume to 15 mL under a rapid stream of hydrogen resulted in the precipitation of a white solid which was shown to be identical in all respects to that isolated by Method A.

c) $[Ir_2(H)(CO)_2(\mu\text{-}H)_2(DPM)_2][BF_4]\cdot CH_2Cl_2$ (**35a**).

Method A. To a solution of **32** in CH_2Cl_2 under an atmosphere of nitrogen (150 mg, 0.124 mmol in 10 mL) was added one equivalent of $HBF_4\cdot Et_2O$ (17.8 µl, 0.124 mmol) causing the solution colour to change to light yellow. The solution was then stirred for 24 h under a very slow nitrogen stream during which time the colour deepened to golden yellow. The volume was reduced to 5 mL under nitrogen and then 25 mL of Et_2O was added causing the precipitation of a golden yellow solid in 90% yield. Compound **35a** proved to be a 1:1 electrolyte in CH_2Cl_2 ($\Lambda(10^{-3}M) = 45.7\ \Omega^{-1}\ cm^2\ mole^{-1}$).

Anal. Calcd for $Ir_2Cl_2P_4F_4O_2C_{53}BH_{49}$: C, 45.99%; H, 3.57%; Cl, 5.12%. Found: C, 45.60%; H, 3.59%; Cl, 5.09%.

Method B To a solution of **32** in CH_2Cl_2 (150 mg, 0.124 mmol in 5 mL) was added dropwise one equivalent of $Ph_3C^+BF_4^-$ (37.3 mg, 0.124 mmol) in 2 mL CH_2Cl_2 which produced a rapid colour change from bright yellow to dark golden-yellow. After 30 min, the solution volume was reduced to 5 mL under an N_2 flow and the addition of 25 mL of Et_2O resulted in the precipitation of a golden yellow solid which was identical in all its properties to that prepared by Method A.

d) $[Ir_2(H)(CO)_2(\mu\text{-}H)_2(DPM)_2][Cl].2CH_2Cl_2$ **(35b)**.

Anhydrous HCl was bubbled into a solution of **32** in CH_2Cl_2 (150 mg, 0.124 mmol in 10 mL) under an N_2 atmosphere until the colour changed from bright yellow to pale yellow (~ 30 sec) indicating the formation of $[Ir_2(H)_3(CO)_2\text{-}(\mu\text{-}H)_2(DPM)_2][Cl]$. The HCl was then shut off and the solution stirred for 16 h during which time the colour darkened to golden brown. 10 mL of Et_2O was then added and the resulting mixture stored at -10°C for 16 h. This resulted in the precipitation of **35b** as golden yellow prisms which were subsequently collected and dried under an N_2 stream. Typical yields were 45%. Compound **35b** proved to be weakly conducting in CH_2Cl_2 ($\Lambda(10^{-3}M) = 10.4\ \Omega^{-1}\ cm^2\ mole^{-1}$).

Anal. Calcd for $Ir_2Cl_5P_4O_2C_{54}H_{51}$: C, 45.75%; H, 3.63%; Cl, 12.51%. Found: C, 45.82%; H, 3.65%; Cl, 12.48%.

e) $[Ir_2(H)(CO)_2(\mu\text{-}H)_2(DPM)_2][OMe]$ **(35c)**.

To a solution of **32** in CH_2Cl_2 (150 mg, 0.124 mmol in 10 mL) under a N_2 atmosphere was added 2 mL of dry MeOH. N_2 was then rapidly bubbled through the solution (ca. mL min^{-1}) resulting in a colour change from yellow to orange. The solvent was then removed under vacuum leaving a dark orange precipitate. This solid was then recrystallized from CH_2Cl_2/Et_2O giving **35c** as a yelow orange powder. Typical yields were 80%. Compound **35c** proved to be weakly conducting in $CH_2Cl_2(\Lambda(10^{-3}M) = 11.7\ \Omega^{-1}\ cm^2\ mole^{-1})$.

f) $[Ir_2(H)_4(CO)_2(DPM)_2][BF_4]_2$ (**36**).

To a solution of **35a** in CH_2Cl_2 (150 mg, 0.108 mmol in 10 mL) was added an excess of $HBF_4 \cdot EtO$ (45.0 µl, 0.313 mmol) under a slow N_2 stream which caused the immediate precipitation of a white solid. Complete precipitation was induced by the addition of 20 mL of Et_2O. The solid was collected and washed with a further 10 mL portion of Et_2O and finally dried in vacuo for 2 h. The lack of solubility of the compound in most common solvents and its tendency to deprotonate in others such as acetone precluded its complete characterization in solution. Typical isolated yields were about 90%.

Anal. Calcd for $Ir_2P_4F_8O_2C_{52}B_2H_{48}$: C, 45.04%; H, 3.41%.
Found: C, 45.12%; H, 3.32%.

Reaction of $[Ir_2(H)(CO)_2(\mu\text{-}H)_2(DPM)_2][BF_4]$ (**35a**) with $NaBH_4$.

A suspension of **35a** (150 mg, 0.108 mmol) and $NaBH_4$ (25 mg, 0.661 mmol) in 10 mL THF was stirred for 24 h during which time the solid dissolved and a bright yellow solution formed. 500 µl of degassed water was then added to the solution to destroy the excess borohydride and the solution

Table 32. Spectral Data for the Compounds of Chapter Six.[a]

Compound	Infrared cm^{-1}		NMR	
	solid[b]	solution[c]	$^{31}P\{^1H\}$ δ, ppm[d]	^1H δ, ppm
32 $[Ir_2(H)_4(CO)_2(DPM)_2]$	1933(vs), 1890(vs)[e] 2076(m), 2107(w)[f]	1944(vs,br), 1899(s)[e] 2061(m,br), 2110(br,sh)[f]	-3.4 (sing)	7.56-7.05(mult, 40 H), 5.84(mult, 2H), 4.07 (mult, 2H) -10.94(br, 2H), -11.39(br, 2H)
33 $[Ir_2(H)_3(CO)_2(\mu-H)_2(DPM)_2][BF_4]$	2008(vs), 2027(vs)[e] 2119(w), 2157(w), 2017(m)[f]	g		
34 $[Ir_2(H)_2(CO)_2(\mu-H)_2(DPM)_2]$		g	-6.6 (sing)	7.65-7.33(mult, 40 H), 4.96(sing, br,4H), -10.46 (quin,br,2H $^2J_{P-H}$ ~ 12 Hz), -13.42(br,2H)
35a $[Ir_2(H)(CO)_2(\mu-H)_2(DPM)_2][BF_4]$	1946(vs), 1955(vs)[e] 2052(s)[f]	1966(br, vs)[e] 2059(s)[f]	13.4, -1.4(mult)	7.77-7.23(mult, 40 H), 5.21(mult, 2H), 4.12 (mult, 2H), -10.08(mult, 1H), -10.15(mult, 1H), -11.03(dtr, 1H, $^2J_{P-H}$ = 14.1 , $^2J_{H-H}$ = 1.2 Hz)
36 $[Ir_2(H)_2(CO)_2(\mu-H)_2(DPM)_2][BF_4]_2$	2071(vs)[e] 2022(w)[f]	2084(vs)[e] 2039(w)[f]	9.0 (sing)	h

a) Abbreviations used: w = weak, m = medium, s = strong, vs = very strong, br = broad, sing = singlet, mult = multiplet, quin = quintet, dtr = doublet of triplets

b) Nujol mull on KBr disk

c) CH_2Cl_2 solution in NaCl cells

d) vs 85% H_3PO_4, -40°C

e) ν(CO)

f) ν(Ir-H)

g) Reacts with I.R. plates

h) Owing to the limited solubility only the phenyl resonances were discernible.

was taken to dryness in vacuo leaving a bright yellow powder. The solid was redissolved in THF and filtered under N_2 yielding a bright yellow solution. The addition of 30 mL of hexanes followed by concentration of the solution under vacuum resulted in the precipitation of a yellow microcrystalline product which was identical to **32** in all of its spectroscopic properties.

Attempted reactions of $[Ir_2(H)_4(CO)_2(DPM)_2]$ (**32**) and $[Ir_2(H)(CO)_2(\mu\text{-}H)_2(DPM)_2][BF_4]$ (**35a**) with Bases.

To a solution of **32** in CH_2Cl_2 (150 mg, 0.116 mmol in 10 mL) was added an excess of proton sponge[219] (75.0 mg, 0.350 mmol) in 2 mL CH_2Cl_2. The solution was allowed to stir for 24 h with no apparent change. Both $^{31}P\{^1H\}$ NMR and I.R. spectra after this time showed only starting material indicating that no reaction had occurred. Similar results were obtained with **35a**. No change in solutions of **32** and **35a** occurred when NEt_3 was used as the base.

Reaction of $[Ir_2(H)_2(CO)_2(\mu\text{-}H)_2(DPM)_2][BF_4]_2$ (**36**) with Proton Sponge.[219]

To a suspension of **36** (150 mg, 0.108 mmol) in 10 mL CH_2Cl_2 was added a solution of one equivalent of proton sponge (23.1 mg 0.108 mmol) in 2 mL CH_2Cl_2. A rapid reaction occurred as evidenced by the dissolution of the solid and the formation of a dark yellow solution. Addition of ether to this solution resulted in the precipitation of a golden yellow solid which was shown to be **35a** based on its infrared and $^{31}P\{^1H\}$ NMR spectra.

X-ray Data Collection

Suitable X-ray diffraction quality crystals of $[Ir_2(H)(CO)_2(\mu\text{-}H)_2(DPM)_2][Cl]$ (**35b**) were obtained after several days by the slow diffusion of ether into a CH_2Cl_2 solution containing a mixture of $[Ir_2(H)_4(CO)_2(DPM)_2]$ (**32**) and anhydrous HCl under an N_2 atmosphere. These crystals proved to be indistinguishable from samples of the BF_4^- salt **35a** in all spectroscopic properties except for the absence of a BF_4^- band in the I.R. spectrum. Several crystals were mounted in thin walled glass capillaries under nitrogen to minimize decomposition. Unit cell parameters were obtained from a least-squares refinement of the setting angles of 25 reflections in the range $13.0° < 2\theta < 22.0°$ which were accurately centred on an Enraf-Nonius CAD4 diffractometer using MoKα radiation. Since four crystals were used for data collection, the cell parameters reported are those from the best crystal; all others gave similar values. The systematic absences ($h0\ell$: $h + \ell$ = odd, $0k0$: k = odd) were consistent with the space group $P2_1/n$.

Intensity data were collected on a CAD4 diffractometer in the bisecting mode employing the ω-2θ scan technique up to $2\theta = 50.00°$ with graphite monochromated MoKα radiation. Backgrounds were scanned for 25% of the peak width on either end of the peak scan. The crystals proved to be susceptible to slow decomposition in the X-ray beam as evidenced by the decline in the intensities of three standard reflections monitored every 1 h of exposure time. When these standards dropped to 75% of their original intensity, data collection was stopped and a new crystal was used. Attempts to collect data at low temperature (-40°C) were unsuccessful since the decomposition was not slowed significantly and crystal movement in the cold stream caused additional difficulties. In all, four different crystals were employed to collect the data. A linear decomposition correction was applied to the data from each crystal. 9461 unique reflections were measured and processed in the usual way using a value of 0.04 for p;[153] of these 3543 were considered to be observed and were used in subsequent calculations. Absorption corrections were applied to the data by using Gaussian integration.[154] See Table 33 for pertinent crystal data and details of data collection.

Table 33. Summary of Crystal Data and Details of Intensity Collection for $[Ir_2(H)(CO)_2(\mu\text{-}H)_2(DPM)_2][Cl]\cdot 1.2CH_2Cl_2$

compd	$[Ir_2(H)(CO)_2(\mu\text{-}H)_2(DPM)_2][Cl]\cdot 1.2\ CH_2Cl_2$
f_ω	1349.59
formula	$Ir_2Cl_{3.4}P_4O_2C_{58.2}H_{49.4}$
cell parameters	a = 12.794(4) Å b = 20.468(5) Å c = 20.433(8) Å β= 91.58(4)°
d(calcd), g/cm^3	1.654
space group	$P2_1/n$
temp, °C	22
radiation (λ, Å)	graphite-monochromated Mo Kα (0.71069)
receiving aperture, mm	2.00 + (0.500 tan θ) wide x 4.0 high, 173 from crystal
take off angle, deg	3.05
scan speed, deg/min	variable between 10.06 and 0.91
scan width, deg	0.75 + (0.347 tan θ) in ω
2θ limits, deg	0.20° < 2θ < 50.00°
no. of unique collcd	9461 (+h, +k, ±ℓ)
no. of unique data used ($F_o^2 > 3\sigma(F_o^2)$)	3543
range of transmission factors	0.3535-0.7423
final no. of parameters refined	241
error in obsern of unit weight	2.367
R	0.080
R_ω	0.102

Structure Solution and Refinement

The structure was solved in the space group $P2_1/n$ using standard Patterson and Fourier techniques. All non-hydrogen atoms were ultimately located. In the full-matrix least-squares refinements, the data from each crystal were independently scaled. Atomic scattering factors were taken from Cromer and Waber's tabulation[155] for all atoms except hydrogen, for which the values of Stewart et al[156] were used. Anomalous dispersion terms[157] for Ir, Cl, and P were included in F_c. The carbon atoms of the phenyl rings were refined as rigid groups having D_{6h} symmetry, C-C distances of 1.392 Å and independent isotropic thermal parameters. All hydrogen atoms of the DPM ligands were located and included as fixed contributions but were not refined. Their idealized positions were calculated from the geometries about their attached carbon atoms using C-H distances of 0.95 Å. Hydrogen atoms were assigned isotropic thermal parameters of 1 $Å^2$ greater than the isotropic thermal parameter (or equivalent isotropic thermal parameter of anisotropic atoms) of their attached carbons. Attempts to locate the hydride ligands using standard techniques were unsuccessful. The C and O atoms of the carbonyl groups did not refine well anisotropically and so were left isotropic.

Although the analyses indicated the presence of two CH_2Cl_2 solvent molecules in the asymmetric unit, only ca. 1.2 CH_2Cl_2's were located. Each molecule refined to an occupancy of 0.6 suggesting the disorder of two molecules over three sites, each with an occupancy of ca. 2/3. A third area of smeared out electron density was located in the cell near the two other partial occupancy CH_2Cl_2 molecules but attempts to fit this density to one or more CH_2Cl_2 orientations failed, therefore this density was left unaccounted for. The hydrogen atoms of the solvent molecules were not included owing to the large thermal parameters of the carbon atoms.

The final model in the space group $P2_1/n$ with 241 parameters refined converged to $R = 0.080$ and $R_\omega = 0.102$.[158] In the final difference Fourier map, the 20 highest residuals (1.4 - 0.4 e/Å^3) were in the vicinity of the solvent molecules and the Ir atoms. A typical carbon on an earlier synthesis had an electron density of 4.0 e/Å^3. The parameters for the individual, non-hydrogen atoms and those of the groups are given in Table 34 and 35, respectively. The derived hydrogen parameters are listed in Table 36. A listing of the observed and calculated structure amplitudes is available.[159]

Table 34. Positional and Thermal Parameters of the Nongroup Atoms of $[Ir_2(H)(CO)_2(\mu\text{-}H)_2(DPM)_2][Cl]\cdot 1.2CH_2Cl_2$.

a) Anisotropic Atoms.

Atom	x	y	z	U_{11}[b]	U_{22}	U_{33}	U_{12}	U_{13}	U_{23}
Ir(1)	0.0633(1)	0.30591(7)	0.20873(7)	3.11(8)	4.5(2)	4.1(1)	0.25(7)	0.22(7)	0.74(8)
Ir(2)	0.0582(1)	0.18299(6)	0.14266(7)	3.06(8)	4.6(2)	3.31(9)	0.04(7)	0.14(6)	0.79(8)
Cl(1)	-0.4333(8)	0.1977(6)	0.2644(6)	5.2(6)	10.0(8)	7.9(8)	0.5(6)	0.9(6)	-2.4(7)
Cl(2)[c]	0.040(2)	0.120(2)	0.362(1)	14(2)	27(3)	7(2)	10(2)	-5(1)	-6(2)
Cl(3)	0.240(3)	0.152(2)	0.343(1)	25(4)	23(3)	9(2)	-10(3)	-3(2)	5(2)
Cl(4)	0.512(2)	0.068(2)	0.439(2)	14(3)	44(6)	13(3)	-8(3)	-3(2)	4(4)
Cl(5)	0.471(6)	0.007(3)	0.354(3)	42(9)	29(6)	17(5)	7(6)	18(6)	2(4)
P(1)	0.2423(7)	0.3199(5)	0.1958(5)	3.1(5)	5.4(6)	4.2(6)	0.3(4)	0.7(4)	0.9(5)
P(2)	0.2318(6)	0.1953(5)	0.1178(4)	3.2(5)	5.8(6)	3.3(5)	0.1(5)	0.1(4)	0.1(5)
P(3)	-0.1183(6)	0.3028(4)	0.2143(4)	3.1(5)	4.4(6)	2.8(5)	0.1(4)	0.5(4)	0.8(4)
P(4)	-0.1099(7)	0.1626(4)	0.1753(5)	2.7(5)	4.3(5)	3.7(6)	0.1(4)	0.7(4)	0.5(4)
C(3)	0.305(2)	0.242(2)	0.182(2)	2(2)	6(2)	2(2)	1(1)	0(1)	-1(2)
C(4)	-0.157(3)	0.221(2)	0.234(2)	7(2)	5(2)	1(2)	-2(2)	0(2)	0(2)

---

[a] Estimated standard deviations in this and other tables are given in parentheses and correspond to the least significant digits.

[b] The thermal parameters have been multiplied by 10^2. The thermal ellipsoid is given by $\exp[-2\pi^2(U_{11}a^{*2}h^2 + U_{22}b^{*2}k^2 + U_{33}c^{*2}\ell^2 + 2U_{12}a^*b^*hk + 2U_{13}a^*c^*h\ell + 2U_{23}b^*c^*k\ell)]$.

(continued...)

Table 34 (continued)

b) Isotropic Atoms

Atom	x	y	z	$B(\AA^2)^a$	Atom	x	y	z	$B(\AA^2)$
O(1)	0.080(2)	0.322(1)	0.356(2)	9.0(7)	C(2)	0.047(3)	0.117(2)	0.078(2)	4.3(9)
O(2)	0.042(2)	0.074(1)	0.049(1)	6.3(7)	C(5)	0.151(5)	0.095(3)	0.312(4)	7.7(2)
C(1)	0.079(3)	0.324(2)	0.300(2)	7.3(9)	C(6)	0.474(6)	0.097(4)	0.367(4)	8.6(2)

Table 35. Derived Parameters for the Rigid Groups of $[Ir_2(H)(CO)_2(\mu\text{-}H)(DPM)_2][Cl]$.

atom	x	y	z	B, $Å^2$	atom	x	y	z	B, $Å^2$
C(11)	0.314(2)	0.351(1)	0.267(1)	3.5(7)	C(51)	-0.196(2)	0.329(1)	0.144(1)	3.6(7)
C(12)	0.288(2)	0.414(1)	0.287(1)	4.0(8)	C(52)	-0.152(2)	0.367(1)	0.095(1)	6.3(10)
C(13)	0.332(2)	0.4384(9)	0.345(1)	4.8(8)	C(53)	-0.212(2)	0.385(1)	0.040(1)	8.8(14)
C(14)	0.402(2)	0.400(1)	0.383(1)	8.7(14)	C(54)	-0.316(2)	0.365(1)	0.034(1)	7.3(12)
C(15)	0.427(2)	0.338(1)	0.362(1)	5.1(9)	C(55)	-0.360(2)	0.327(1)	0.084(1)	5.7(10)
C(16)	0.383(2)	0.3133(8)	0.304(1)	4.8(8)	C(56)	-0.300(2)	0.309(1)	0.137(1)	4.3(8)
C(21)	0.285(2)	0.376(1)	0.134(1)	3.2(7)	C(61)	-0.170(2)	0.354(1)	0.278(1)	2.6(6)
C(22)	).390(2)	0.395(1)	0.134(1)	5.4(9)	C(62)	-0.128(2)	0.416(1)	0.288(1)	4.6(9)
C(23)	0.426(2)	0.435(1)	0.085(1)	7.3(11)	C(63)	-0.167(2)	0.4566(8)	0.335(1)	4.8(9)
C(24)	0.357(2)	0.456(1)	0.035(1)	5.7(10)	C(64)	-0.250(2)	0.436(1)	0.373(1)	5.0(9)
C(25)	0.253(2)	0.437(1)	0.035(1)	8.5(13)	C(65)	-0.292(2)	0.374(1)	0.363(1)	5.0(9)
C(26)	0.217(1)	0.397(1)	0.084(1)	5.3(9)	C(66)	-0.252(2)	0.3328(8)	0.316(1)	4.4(8)
C(31)	0.263(2)	0.234(1)	0.039(1)	4.0(8)	C(71)	-0.211(1)	0.159(1)	0.111(1)	2.7(6)
C(32)	0.364(2)	0.248(1)	0.020(1)	5.6(10)	C(72)	-0.187(1)	0.180(1)	0.048(1)	4.4(8)
C(33)	0.381(2)	0.281(1)	-0.038(1)	7.7(12)	C(73)	-0.263(2)	0.179(1)	-0.0019(9)	5.9(10)
C(34)	0.296(3)	0.300(1)	-0.078(1)	5.1(9)	C(74)	-0.364(2)	0.157(1)	0.011(1)	4.3(10)
C(35)	0.195(2)	0.287(1)	-0.059(1)	9.2(15)	C(75)	-0.388(1)	0.136(1)	0.073(1)	4.4(8)
C(36)	0.178(2)	0.254(1)	0.000(1)	5.5(10)	C(76)	-0.312(2)	0.137(1)	0.1232(9)	3.5(7)
C(41)	0.307(2)	0.1208(9)	0.111(1)	3.6(7)	C(81)	-0.126(2)	0.0871(9)	0.225(1)	4.1(8)
C(42)	0.360(2)	0.095(1)	0.1655(9)	4.0(8)	C(82)	-0.200(2)	0.0826(9)	0.273(1)	4.1(8)
C(43)	0.411(2)	0.035(1)	0.161(1)	3.7(7)	C(83)	-0.208(2)	0.026(1)	0.310(1)	4.9(9)
C(44)	0.410(2)	0.0014(9)	0.101(1)	4.3(8)	C(84)	-0.140(2)	-0.0261(9)	0.299(1)	4.4(8)
C(45)	0.357(2)	0.028(1)	0.047(1)	6.8(11)	C(85)	-0.066(2)	-0.0215(9)	0.251(1)	4.2(8)
C(46)	0.306(2)	0.087(1)	0.052(1)	4.9(9)	C(86)	-0.0585(2)	0.035(1)	0.214(1)	4.7(8)

Rigid Group Parameters

	X_c[a]	Y_c	Z_c	phi[b]	theta	rho
ring 1	0.3578(12)	0.3759(8)	0.3246(9)	-2.61(1)	-3.02(1)	2.13(2)
ring 2	0.3212(14)	0.4161(8)	0.0847(9)	1.55(2)	2.73(2)	-0.93(2)
ring 3	0.2796(15)	0.2674(8)	-0.0195(10)	1.52(2)	2.99(2)	-1.06(2)
ring 4	0.3587(11)	0.0611(7)	0.1062(8)	1.78(5)	1.87(2)	-2.85(5)
ring 5	-0.2562(14)	0.3469(8)	0.0888(9)	2.14(2)	-2.75(2)	-1.03(2)
ring 6	-0.2100(12)	0.3947(7)	0.3256(8)	2.39(1)	-2.88(1)	0.83(1)
ring 7	-0.2877(11)	0.1600(7)	0.0607(8)	2.07(2)	-2.43(2)	-1.24(2)
ring 8	-0.1330(12)	0.0305(7)	0.2621(8)	-2.06(2)	2.59(1)	0.70(2)

[a] X_c, Y_c, and Z_c are the fractional coordinates of the centroid of the rigid group.

[b] The rigid group orientation angles (radians) have been defined previously: La Placa, S.J.; Ibers, J.A. Acta Crystallogr. 1965, 18, 511.

Table 36. Derived Hydrogen Positions for $[Ir_2(H)(CO)_2(\mu\text{-}H)_2(DPM)_2][Cl]\cdot 1.2CH_2Cl_2$

Atom	x	y	z	$B(\AA^2)$	Atom	x	y	z	$B(\AA^2)$
H(1C3)	0.3739	0.2491	0.1696	4.0	H(45)	0.3562	0.0048	0.0064	6.9
H2(C3)	0.3043	0.2179	0.2221	4.0	H(46)	0.2699	0.1052	0.0147	4.9
H(1C4)	-0.1443	0.2120	0.2771	4.0	H(52)	-0.0818	0.3809	0.0995	6.3
H(2C4)	-0.2394	0.2226	0.2297	4.0	H(53)	-0.1827	0.4110	0.0069	8.7
H(12)	0.2408	0.4398	0.2620	4.0	H(54)	-0.3571	0.3770	-0.0038	7.2
H(13)	0.3145	0.4810	0.3598	4.8	H(55)	-0.4306	0.3129	0.0779	5.7
H(14)	0.4314	0.4170	0.4224	8.6	H(56)	-0.3297	0.2828	0.1705	4.3
H(15)	0.4746	0.3118	0.3872	5.2	H(62)	-0.0716	0.4302	0.2618	4.6
H(16)	0.4009	0.2706	0.2894	4.8	H(63)	-0.1383	0.4988	0.3423	4.8
H(22)	0.4366	0.3804	0.1680	5.5	H(64)	-0.2767	0.4634	0.4060	5.0
H(23)	0.4968	0.4483	0.0849	7.3	H(65)	-0.3484	0.3592	0.3892	5.0
H(24)	0.3813	0.4840	0.0014	5.7	H(66)	-0.2817	0.2906	0.3087	4.4
H(25)	0.2056	0.4518	0.0012	8.4	H(72)	-0.1184	0.1943	0.0393	4.5
H(26)	0.1454	0.3839	0.0843	5.3	H(73)	-0.2468	0.1934	-0.0446	6.0
H(32)	0.4222	0.2353	0.0470	5.5	H(74)	-0.4161	0.1571	-0.0234	4.3
H(33)	0.4502	0.2906	-0.0513	7.7	H(75)	-0.4570	0.1217	0.0819	4.5
H(34)	0.3076	0.3228	-0.1180	5.1	H(76)	-0.3286	0.1226	0.1658	3.5
H(35)	0.1370	0.2997	-0.0864	9.2	H(82)	-0.2461	0.1181	0.2802	4.1
H(36)	0.1090	0.2444	0.0119	5.5	H(83)	-0.2583	0.0229	0.3431	5.0
H(42)	0.3610	0.1174	0.2060	4.1	H(84)	-0.1452	-0.0648	0.3250	4.4
H(43)	0.4473	0.0170	0.1977	3.7	H(85)	-0.0199	-0.0573	0.2440	4.2
H(44)	0.4448	-0.0394	0.0979	4.3	H(86)	-0.0077	0.0379	0.1811	4.6

Table 37. Selected Distances (Å) in $[Ir_2(H)(CO)_2(\mu\text{-}H)_2(DPM)_2][Cl]$.[a]

Bond Distances

Ir(1)-Ir(2)	2.855(2)	P(2)-C(3)	1.85(3)
Ir(1)-C(1)	1.91(4)	P(3)-C(4)	1.79(3)
Ir(1)-P(1)	2.331(9)	P(4)-C(4)	1.82(4)
Ir(1)-P(3)	2.330(8)	P(1)-C(11)	1.81(2)
Ir(2)-C(2)	1.90(4)	P(1)-C(21)	1.80(2)
Ir(2)-P(2)	2.306(9)	P(2)-C(31)	1.85(2)
Ir(2)-P(4)	2.307(9)	P(2)-C(41)	1.81(2)
Cl(1)-H(2C4)	2.65	P(3)-C(51)	1.81(2)
C(1)-O(1)	1.15(4)	P(3)-C(61)	1.81(2)
C(2)-O(2)	1.05(4)	P(4)-C(71)	1.83(2)
P(1)-C(3)	1.82(3)	P(4)-C(81)	1.86(2)

Nonbonded Distances

P(1)-P(3)	3.01(1)	C(2)-H(72)	2.74
P(2)-P(4)	2.98(1)	C(2)-H(86)	2.76
O(1)-H(74)[b]	2.49	O(2)-H(86)	2.89

a) Interatomic distances and angles for the CH_2Cl_2 solvent molecules are listed in the supplementary data.

b) Molecule at $-\frac{1}{2} + x$, $\frac{1}{2} - y$, $-\frac{1}{2} + z$

Table 38. Selected Angles (deg) in $[Ir_2(H)(CO)_2(\mu\text{-}H)_2(DPM)_2][Cl]$.

Ir(2)-Ir(1)-C(1)	129.2(12)	Ir(1)-P(1)-C(3)	110.4(10)	C(3)-P(2)-C(31)	106.2(12)	P(1)-C(21)-C(22)	119.1(11)
Ir(2)_Ir(1)-P(1)	93.7(2)	Ir(2)-P(2)-C(3)	111.9(10)	C(3)-P(2)-C(41)	103.0(12)	P(1)-C(21)-C(26)	120.8(10)
Ir(2)-Ir(1)-P(3)	89.4(2)	Ir(1)-P(3)-C(4)	108.8(12)	C(4)-P(3)-C(51)	107.8(13)	P(2)-C(31)-C(32)	123.3(11)
P(1)-Ir(1)-C(1)	90.7(12)	Ir(2)-P(4)-C(4)	113.8(11)	C(4)-P(3)-C(61)	105.4(12)	P(2)-C(31)-C(36)	116.6(11)
P(3)-Ir(1)-C(1)	91.9(12)	Ir(1)-P(1)-C(11)	115.6(7)	C(4)-P(4)-C(71)	105.4(12)	P(2)-C(41)-C(42)	120.7(9)
P(1)-Ir(1)-P(3)	173.4(3)	Ir(1)-P(1)-C(21)	118.5(8)	C(4)-P(4)-C(81)	98.2(12)	P(2)-C(41)-C(46)	119.2(10)
Ir(1)-Ir(2)-C(2)	163.6(12)	Ir(2)-P(2)-C(31)	118.0(8)	C(11)-P(1)-C(21)	100.1(10)	P(3)-C(51)-C(52)	120.8(10)
Ir(1)-Ir(2)-P(2)	89.9(2)	Ir(2)-P(2)-C(41)	116.4(6)	C(31)-P(2)-C(41)	99.8(11)	P(3)-C(51)-C(56)	119.2(10)
Ir(1)-Ir(2)-P(4)	91.9(2)	Ir(1)-P(3)-C(51)	118.7(7)	C(51)-P(3)-C(61)	101.2(10)	P(3)-C(61)-C(62)	118.8(9)
P(2)-Ir(2)-C(2)	88.9(12)	Ir(1)-P(3)-C(61)	114.0(7)	C(71)-P(4)-C(81)	105.7(9)	P(3)-C(61)-C(66)	121.3(8)
P(4)-Ir(2)-C(2)	90.9(12)	Ir(2)-P(4)-C(71)	116.7(6)	P(1)-C(3)-P(2)	110.3(4)	P(4)-C(71)-C(72)	118.5(8)
P(2)-Ir(2)-P(4)	174.1(3)	Ir(2)-P(4)-C(81)	115.0(7)	P(2)-C(4)-P(4)	111.2(4)	P(4)-C(71)-C(76)	121.5(8)
Ir(1)-C(1)-O(1)	166(4)	C(3)-P(1)-C(11)	103.0(12)	P(1)-C(11)-C(12)	117.0(10)	P(4)-C(81)-C(82)	121.8(9)
Ir(2)-C(2)-O(2)	170(4)	C(3)-P(1)-C(21)	107.8(12)	P(1)-C(11)-C(16)	122.6(9)	P(4)-C(81)-C(86)	118.2(10)

Description of Structure

Attempts to obtain X-ray suitable crystals of compound **35** as the BF_4^- salt proved unsuccessful, however it was isolated in crystalline form with a chloride counterion from the reaction of **32** with HCl. The asymmetric unit of the unit cell contains one molecule of **35b** along with two unexceptional partial occupancy (0.6) CH_2Cl_2 solvent molecules. There are no unusual contacts involving the solvent molecules. The chloride counterion is hydrogen bonded to one of the DPM methylene hydrogens of the dimer (vide infra).

The complex cation, shown in Figure 11 together with the hydrogen-bound chloride ion, appears as a rather typical DPM-bridged complex.[173] Both DPM ligands bridge the two metals in essentially mutually trans positions about the metals and the orientations of the phenyl groups are such as to minimize non-bonded contacts with the ligands in the equatorial plane. Therefore, four phenyl groups (2,3,5 and 7) are thrust into the relatively vacant positions on the side of the complex opposite the carbonyl group C(1)O(1) (see Figure 11).

Although the hydride ligands were not crystallographically located, their approximate positions are obvious based on the positions of the other ligands in the

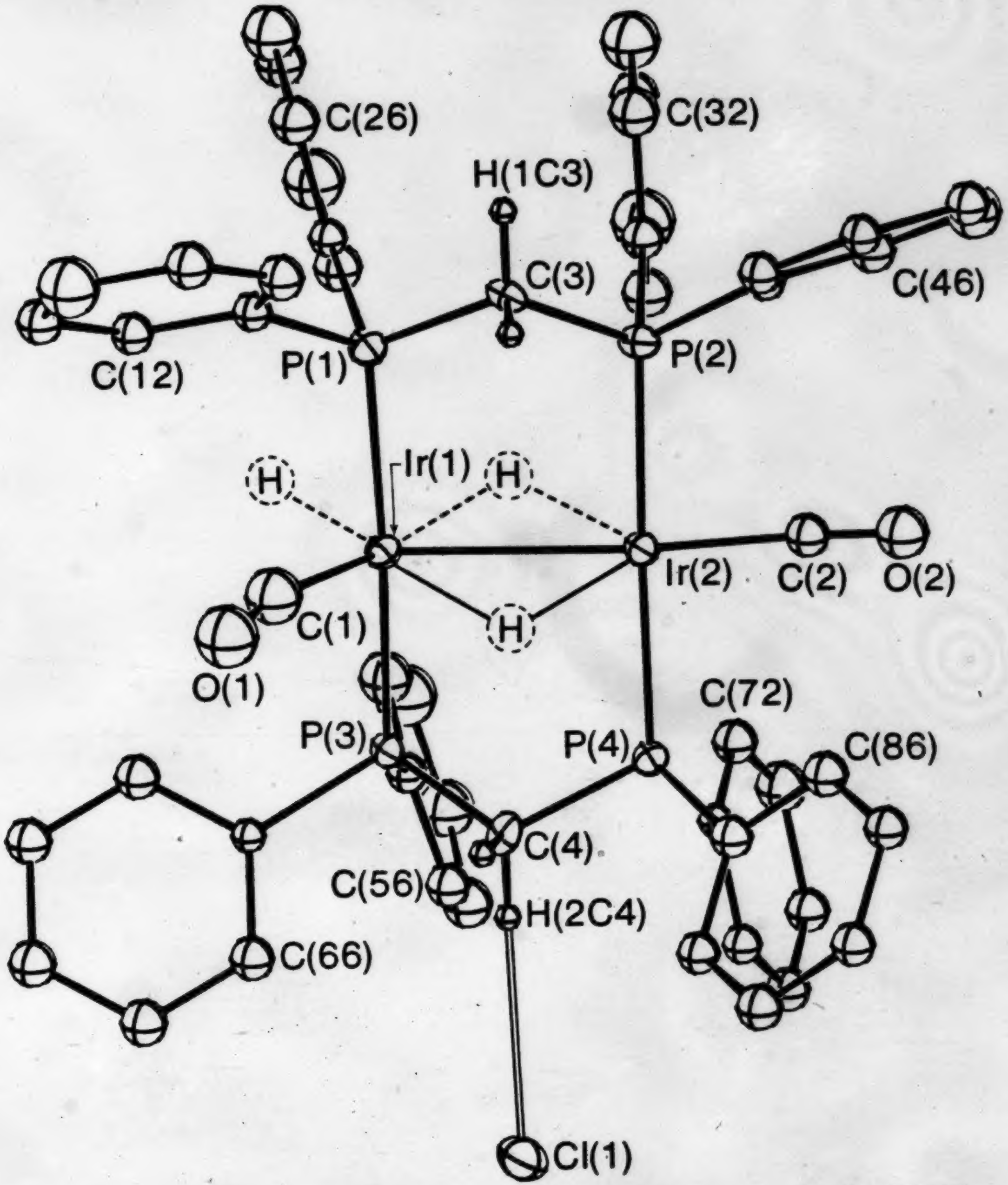

C(26)
C(32)
H(1C3)
C(3)
C(46)
C(12)
P(1)
P(2)
Ir(1)
H
H
Ir(2)
C(2)
O(2)
C(1)
H
O(1)
C(72)
P(3)
P(4)
C(86)
C(4)
C(56)
H(2C4)
C(66)
Cl(1)

Figure 11. Perspective view of $[Ir_2H(CO)_2(\mu\text{-}H)_2(DPM)_2][Cl]$. Hydrido ligands, which were not located, are shown in their idealized positions. Thermal ellipsoids are drawn at the 20% level except for methylene hydrogens which are drawn artificially small. Phenyl hydrogens have the same number as their attached carbon atoms.

structure and on the spectroscopic data observed for 35. The ^{1}H NMR spectrum clearly indicates that two hydride ligands bridge the metals (probably on opposite faces of the complex) while another is terminal (vide infra). Location of the terminal hydride ligand becomes obvious upon examining the geometries about each metal. The carbonyl group C(2)O(2) is almost linearly disposed along the Ir-Ir bond (Ir(1)-Ir(2)-C(2)angle = 163.6 (12)°) whereas group C(1)O(1) is bent away from this vector forming and Ir(2)-Ir(1)-C(1) angle of 129.2(11)°, leaving a conspicuously vacant coordination site on Ir(1), adjacent to C(1). Clearly the terminal hydride ligand must occupy this coordination site as diagrammed below.

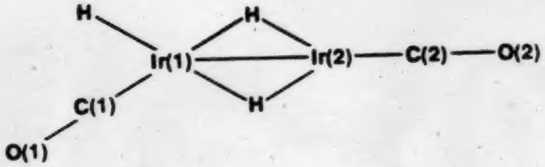

The resulting coordination geometries about each metal differ significantly. If the formal metal-metal bond is ignored, the geometry about Ir(1) is pseudo-octahedral whereas that about Ir(2) more closely approximates a trigonal bipyramid. Although the metal-phosphorus distances are normal they can be grouped into two pairs, with those on Ir(1) (av. 2.331(9)Å) being slightly longer than those on Ir(2) (av. 2.307(9)Å). This difference is consistent with the different coordination numbers of the metals. It has previously been observed in similar cases that the longer metal-phosphorus distances are associated with the metal having the higher coordination number.[165,174] The carbonyl geometries are normal; the slight bend in these groups, (166(4)° and 169(4)°) is not unusual and most probably results from non-bonded contacts involving the phenyl groups 7 and 8 (see Figure 11 and Table 38). Similar bending of the carbonyl groups was observed in the two independent molecules of [$Rh_2Cl_2(CO)$-$(C_2S_4)(DPM)_2$] and again short non-bonded phenyl contacts were responsible.[67]

The Ir-Ir separation (2.855(2)Å) is normal for a single bond and is consistent with the range of values observed for other Ir-Ir bonded DPM-bridged systems.[151,166,173] This metal-metal distance is significantly shorter than the intraligand P...P separation (average 3.00(1)Å) indicating compression along the Ir-Ir axis and mutual attraction of the metals.

As noted earlier, the chloride ion is hydrogen bound to H(2C4) of one of the DPM ligands, at a distance of approximately 2.7 Å. This contact is somewhat uncertain since the hydrogen atom was included in the idealized position for an unperturbed CH_2 group, at 0.95 Å from carbon, and was not refined; nevertheless it indicates a substantial interaction. We have previously observed hydrogen bonding between DPM methylene protons and chloride ligands in $[Ir_2(CO)_2(\mu\text{-}OH{\cdot}Cl)(DPM)_2]$ (see Chapter 4) so this in itself is not surprising. However, what is surprising is that the chloride ion does not coordinate to one of the metal centres in this cationic complex; presumably this reflects the inertness of the metals in **35** towards attack by nucleophiles.

Results and Discussion

The reaction of trans-$[IrCl(CO)(DPM)]_2$ (**3**) with an excess of $NaBH_4$ under H_2 gives rise to a new compound **32** with the formula $[Ir_2(H)_4(CO)_2(DPM)_2]$. The highfield region of the ^1H NMR spectrum shows only two featureless peaks which could in principle arise from either bridging or terminal hydrides. However, the fact that both peaks have identical shapes and integrate as two hydrogens each, combined with the observation of terminal Ir-H stretches at 2076 and 2107 cm^{-1} in the infrared spectrum suggests that all of the hydride ligands are terminal. The $^{31}P\{^1H\}$ NMR spectrum shows only a singlet over the temperature range +25 to -60°C, indicative of a symmetrical species. Based on this information, two structures are possible for 3 as shown below. Structure XXXVII, in which the carbonyls are mutually cis, has C_{2v} symmetry, while XXXVIII, where the carbonyls are trans, has C_{2h} symmetry. Structure XXXVII

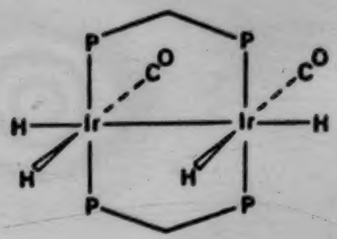

XXXVII

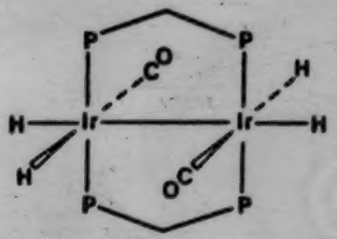

XXXVIII

would appear to be the correct choice based on the observation of two ν(CO) bands in the infrared spectrum and two DPM methylene resonances in the room temperature ^{1}H NMR spectrum; for structure XXXVIII only one methylene resonance would be expected (see Chapter 2). However, based on the reaction of 32 with trityl cation (vide infra), XXXVIII cannot be ruled out. The lack of resolution of the hydride signals is possibly due to our inability to resolve the various phosphine-hydride ($^2J_{P-H}$ and $^3J_{P-H}$) and hydride-hydride couplings. Lowering the temperature to -80°C produced no noticeable effect on the peak shapes, arguing against a fluxional process being responsible for the broadness.

A dihydrogen atmosphere is not necessary for the synthesis of **32** from **3** and $NaBH_4$. If the reaction is performed under N_2, **32** is still the major product formed, but the yield is slightly lower and the reaction times longer. If, however, the reaction is done under a CO atmosphere, the only product observed after 24 h is the previously characterized Ir(0) compound, $[Ir_2(CO)_4(DPM)_2]$. This latter product can also be formed by allowing a solution of **32** to stir under CO for 12 h. Similarly, adding H_2 to $[Ir_2(CO)_4(DPM)]_2$ gives **32** after 12 h. Attempts at using single hydride sources such as $LiB(C_2H_5)_3H$ were unsuccessful and led only to mixtures of unidentified products as determined by $^{31}P\{^1H\}$ NMR.

The formation of **32** from the reaction of trans-$[IrCl(CO)(DPM)]_2$ with $NaBH_4$ is in contrast to initial reports of the equivalent reaction with the Rh analogue where no hydride species were observed and only the Rh(0) compound $[Rh_2(CO)_2(DPM)_2]$ was isolated.[35] However, a more recent report suggests that when the reaction is performed under H_2, some hydride-containing products are formed.[221]

The reaction of **32** with $HBF_4 \cdot Et_2O$ under an H_2 atmosphere leads to the isolation of a white solid **33** which displays three terminal Ir-H stretches, two terminal carbonyl bands and a broad BF_4^- band at 1050 cm^{-1} in the infrared spectrum (see Table 32). Based on this information and on the solution properties of **33** (vide infra), the most probable structure for **33** is the proton addition product shown below. In solution under H_2, this

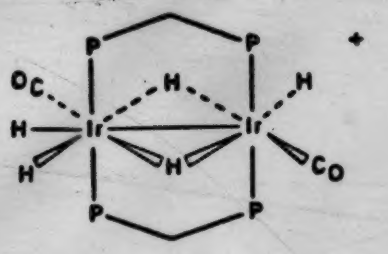

33

species shows a singlet in the $^{31}P\{^1H\}$ NMR spectrum (+25 to -60°C) and only two hydride resonances, each integrating as two protons, in the ^1H NMR spectrum. One of these hydride resonances appears as a quintet while the other appears as a featureless peak much as was observed for compound **32**. This information, along with the observation of only one DPM methylene resonance in the ^1H NMR, is inconsistent with the formulation drawn for **33** and suggests the existence of a new compound **34** in solution whose possible structure is shown below. It appears that when the pentahydride **33** is dissolved in CH_2Cl_2, proton dissociation occurs resulting in the formation of the neutral tetrahydride **34**. Attempts to obtain an I.R. spectrum of this solution were unsuccessful due to apparent reaction of the free acid

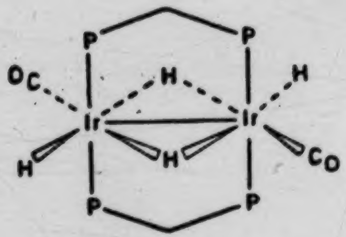

34

and/or the complex with the I.R. cells. When ether is added to this solution, compound **33** is again isolated. This suggests the existence of an equilibrium between **33** and **34** in solution as shown in equation 13. The isolation of only the cationic species **33** from solution is likely a result of

$$[Ir_2(H)_2(CO)_2(\mu\text{-}H)_2(DPM)_2] + H^+ \rightleftharpoons [Ir_2(H)_3(CO)_2(\mu\text{-}H)_2(DPM)_2]^+ \qquad (13)$$

its lower solubility. This equilibrium can also be confirmed by the addition of a large excess (ca. 200 x) of acid to **32**. In addition to the original singlet due to **34**, the $^{31}P\{^1H\}$ NMR spectrum shows a new complex pattern at δ -2.0 and -10.4 ppm which likely corresponds to the unsymmetrical species **33**. Attempts to monitor the same process in the ^1H NMR spectra have been unsuccessful since the hydride resonances due to **32**, **33**, **34**, and **35**, the last of which is generated by H_2 loss from **33** (vide infra), all occur in the same region, making the assignment of peaks difficult. It is clear that the reaction of **32** with acid to give the equilibrium mixture of **33** and **34** involves only one equivalent of acid; monitoring the $^{31}P\{^{1}H\}$ NMR spectra during the stepwise addition of $HBF_4 \cdot Et_2O$ to **3** shows signals due to both **32** and **34** in the appropriate ratio until exactly one equivalent of acid has been added, at which point only the signal due to **34** is observed. Allowing any of the intermediate mixtures to stand for several hours produces no change in the ratio of **32** and **34**.

Acids other than $HBF_4 \cdot Et_2O$ can be used to accomplish the protonation of **32**. Both HCl and MeOH, when added to solutions of **32**, produce **34** as observed in the $^{31}P\{^{1}H\}$ NMR. However, excess acid must be used in both cases (see Experimental).

If the reaction of **32** with $HBF_4 \cdot Et_2O$ is performed under an atmosphere of nitrogen instead of hydrogen, the solution begins to darken after several minutes and a new complex pattern typical of an unsymmetrical species appears in the $^{31}P\{^{1}H\}$ NMR spectrum. After stirring overnight, only this latter pattern is observed. The reaction can actually be accelerated by slowly bubbling N_2 through the solution. Adding ether to the solution leads to the isolation of a golden yellow solid, **35**, whose solution and solid spectroscopic parameters (see Table 32) indicate that it is the cationic trihydride shown below. Confirmation of

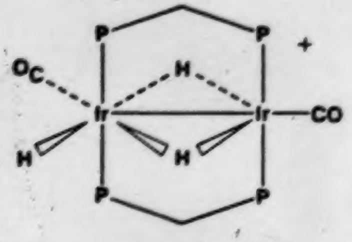

(35)

this comes from the crystal structure determination of this compound with a chloride counterion (**35b**) (see Figure 11). Compound **35** is undoubtedly generated via H_2 loss from **33** since placing a solution of **35** under hydrogen rapidly regenerates **34** (actually an equilibrium mixture of **33** and **34**) as identified by $^{31}P\{^1H\}$ NMR.

Compound **35** can also be produced by H^--abstraction from **32** using trityl cation (see Experimental) and conversely reaction of **35** with sodium borohyride regenerates **32** as the only observed product. These observations suggest that the actual geometry for **32** is XXXVIII (C_{2h} geometry) and not XXXVII. However, the reaction of **32** with trityl cation may not proceed by a simple route. Evidence for this comes from an experiment in which less than one equivalent of trityl cation (0.9:1) was added to **32** and the reaction monitored by $^{31}P\{^1H\}$ NMR spectroscopy. After 30 min the spectrum showed a small peak at -6.6 ppm due to compound **34** in addition to the signal due to **35**. Significantly, no signal due to **32** was observed. This suggests that **34** is an intermediate in the transformation of **32** to **35**. It is clear that hydride abstraction from **34** should lead directly to **35** but the question remains as to how **34** arises from **32**. Further evidence for a complex reaction pathway comes from the observation that strong base such as proton sponge[219] reduces the rate of formation of **35** from **32** drastically (several hours *vs.* ~ 20 min). A $^{31}P\{^1H\}$ NMR spectrum of this mixture showed signals due to **32**, **34**, and **35**. It is not clear at this point what processes are involved in the formation of **35** from **32** and further studies are needed.

A spin saturation transfer experiment performed by irradiating the terminal hydride resonance in the ^1H NMR spectrum of **35** indicates that it and one of the bridging hyrides are undergoing site exchange. The other bridging hydride signal remains unchanged. This observation can be rationalized in terms of the process shown below. This interchange is slow on the NMR timescale since both the $^{31}P\{^1H\}$ and ^1H NMR spectra are sharp at room temperature and no averaging of the signals due to Ha and Hb is observed.

Acids other than $HBF_4 \cdot Et_2O$ can be used to produce **35**; the use of HCl yields **35** with a Cl^- counterion (**35b**) while MeOH gives **35** with an OMe^- counterion (**35c**). In the latter

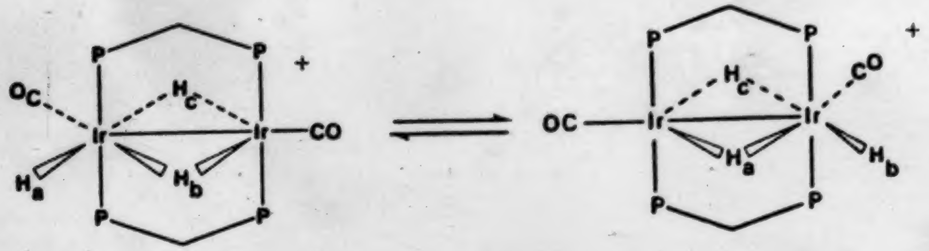

case, large excesses (2 mL) and a rapid N_2 stream must be used. The solid and solution properties of these compounds are identical to those of the BF_4^- salt apart from a downfield shift of one of the DPM methylene resonances (from 4.12 to 4.97 ppm) for the Cl^- and OMe^- species, consistent with the occurrence of hydrogen bonding between these counterions and one of methylene hydrogens as was observed in the structure of the chloride adduct (see Figure 11). Furthermore, the conductivity measurements for these compounds are very low compared to normal 1:1 electrolytes[170] suggesting significant association of the anion with the complex cation. It is somewhat surprising that with neither Cl^- nor OMe^- anions is there any evidence of anion coordination to the unsaturated Ir centre.

Attempts at deprotonating **35** to give a neutral dihyride have been unsuccessful. The addition of nitrogen bases such as NEt_3 or proton sponge[219] produces no change in the $^{31}P\{^1H\}$ NMR spectra even when used in large excess

(~ 200 x). Successful deprotonation of these complexes might be accomplished by using more powerful reagents such as ${}^tBuLi$.

The reaction of **32** with a three-fold excess of $HBF_4 \cdot Et_2O$ under N_2 results in the precipitation of a highly insoluble white compound **36**. Monitoring the addition of acid by ${}^{31}P\{{}^1H\}$ NMR spectroscopy shows the appearance of a new singlet at δ 9.0 ppm in addition to the peak due to **32**. Complex **36** is also formed rapidly upon reaction of **35** with one equivalent $HBF_4 \cdot Et_2O$. Based on the ${}^{31}P\{{}^1H\}$ NMR and infrared data, the latter of which shows one terminal CO band and one terminal Ir-H band, **36** probably has the structure shown below. Unfortunately, **36** is very insoluble in most solvents and deprotonates in acetone and other weakly basic solvents (see below) precluding its further

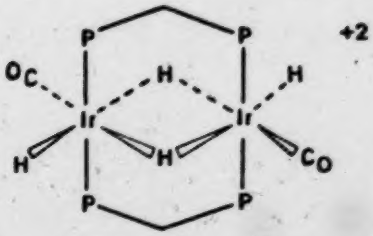

(36)

characterization in solution. It is likely that the reaction of **32** with excess acid proceeds through compound **33**, which loses H_2 to give **35**, which is then subsequently protonated to produce **36**. That **36** is a simple adduct formed from H^+ addition to **35** and does not involve H_2 loss can be shown by the reaction of **36** with one equivalent of strong base which rapidly regenerates **35**, as observed by $^{31}P\{^1H\}$ NMR. Strong bases are not needed to effect the deprotonation of **36**; even the addition of 2 mL of acetone results in significant deprotonation of **36** after several minutes (~ 50% by infrared) and after 1 hour only **35** is observed.

In contrast to the reaction of **32** with acids, weaker acids such as HCl and MeOH do not react with **35** to produce **36**. Only the powerful protonating agent $HBF_4 \cdot Et_2O$, when used in excess, results in the formation of **36**.

Summary

The reaction of trans-$[IrCl(CO)(DPM)]_2$ (3) with $NaBH_4$ in THF yields the tetrahydride complex $[Ir_2(H)_4(CO)_2(DPM)_2]$ in which all hydrido ligands are terminally bound. From this product a series of cationic binuclear polyhydrides, ranging from trihydrides to pentahydrides, can be prepared; all of these cationic species have two bridging hydride ligands with the remaining hydride ligands terminally bound. These results are in apparent contrast to the analogous borohydride reaction with trans-$[RhCl(CO)(DPM)]_2$

in which hydrido species are very labile and are apparently only observed under an H_2 atmosphere [221]. In the absence of H_2 the Rh(O) dimer $[Rh(CO)(DPM)]_2$ is produced instead[35]. Such a difference between the Rh and Ir chemistry is in agreement with the known greater lability of second row metal hydrides compared to their third row counterparts. Whether the iridium chemistry reported here effectively models the rhodium chemistry or whether the rhodium chemistry is limited to simple metathesis under H_2 to give $[RhH(CO)(DPM)]_2$ is not known. However, it is clear that with iridium the simple metathesis product $[IrH(CO)(DPM)]_2$ is not observed, and attempts at obtaining it have so far been unsuccessful.

The reaction of $[Ir_2(CO)_2(\mu\text{-}H)(\mu\text{-}CO)(DPM)_2][BF_4]$ (**26**) with H_2 to give an equilibrium mixture of $[Ir_2(H)_3(CO)_2(\mu\text{-}H)_2(DPM)_2][BF_4]$ (**33**) and $[Ir_2(H)_2(CO)_2(\mu\text{-}H)_2(DPM)_2]$ (**34**) has obvious relevance to the reported hydrogenation of acetylenes and olefins by the Rh analogue of **26**.[35] Although no intermediate species were reported in these Rh-catalyzed reactions, it is possible that species analogous to **33**, **34**, and also $[Ir_2(H)(CO)_2(\mu\text{-}H)_2(DPM)_2][BF_4]$ (**35**), the last of which is formed by H_2 loss from **33**, are analogous to the catalytically actives species in these hydrogenations. With these ideas in mind the chemistry of these hydrides with unsaturated organic substrates such as olefins and acetylenes should be examined, in hopes of gaining information on the natures of intermediates in reactions catalyzed by polynuclear complexes, and on the involvement of the adjacent metal centres in such reactions.

CHAPTER 7

Conclusions

As stated in Chapter One, the aims of the studies in this thesis were two-fold: to prepare binuclear Ir-DPM compounds analogous to those known for Rh, and to examine these compounds as model systems for the Rh chemistry with the emphasis on examining the role of DPM-bridged binuclear hydrides in catalysis. The results of these studies suggest that to a certain extent, both of these objectives have been met.

The similarities and differences between the Rh and Ir chemistry is best displayed in Chapter Two. Although with both Rh and Ir binuclear DPM-bridged complexes are prepared by essentially the same route, the final products differ significantly. With Rh, the reaction of $[RhCl(C_8H_{14})_2]_2$ with DPM and CO leads to the neutral dicarbonyl complex $[RhCl(CO)(DPM)]_2$. In contrast, starting with $[IrCl(C_8H_{14})_2]_2$, the product isolated is the cationic tetracarbonyl complex $[Ir_2Cl(CO)_3(\mu\text{-}CO)(DPM)_2][Cl]$. Refluxing solutions of this product results in carbonyl loss yielding first $[Ir_2Cl_2(CO)_2(\mu\text{-}CO)(DPM)_2]$ and finally $[IrCl(CO)(DPM)]_2$. This different behaviour is a reflection of the greater basicity of Ir versus Rh which results in a greater tendency to coordinate π-acid ligands and bind them more strongly. This is also reflected in the reactions of these compounds with alkynes. With both Ir and Rh, alkynes react to give complexes in which the alkyne bridges the two metals as a cis-dimetallated olefin. However, with Rh, only alkynes such as DMA and HFB which have strong electron-withdrawing substituents react to give isolable products. With Ir, this is not a necessary requirement, as evidenced by the reaction of $[IrCl(CO)(DPM)]_2$ with acetylene. The lower value of ν(C=C) in the Ir complexes also indicates that the bridging alkyne ligands are also more strongly bound than in their Rh analogues. These studies show that despite the obvious similarities between the Rh and Ir chemistry, differences do exist and care should be taken in drawing analogies between the two.

It can be seen that a key feature of this Ir-DPM chemistry is the ability of the Ir complexes to form stable adducts with certain reactants when none are observed with Rh. This has obvious uses in modelling the catalytic processes observed with Rh. An example of this is the reaction of $[IrCl(CO)(DPM)]_2$ and $[Ir_2(CO)_2(\mu\text{-}Cl)(DPM)_2]$-$[BF_4]$ with H_2. Although no reaction is observed with the Rh analogues, it must occur since these Rh complexes are known to hydrogenate alkynes.[34,35] By isolating discrete

Ir-hydrogen adducts and subsequently studying their reactions with alkynes it was possible to suggest some possible intermediates in the Rh system. Unfortunately, it is not clear from these studies what effect, if any, the two metal centres have on each other or whether they act independently. This work suggests that further studies are warranted especially to examine the effect of different conditions and different alkynes.

Another reaction where Ir-DPM complexes provided a useful model was for the catalysis of the water gas shift reaction by $[Rh_2(CO)_2(\mu\text{-}H)(\mu\text{-}CO)(DPM)_2]^+$. Using such complexes it was possible to demonstrate an alternative mechanism from that originally proposed.[35] Of significance was the observed involvement of the bridging hydroxide complex $[Ir_2(CO)_2(\mu\text{-}OH)(DPM)_2]^+$ in the model catalytic cycle. The unique reactivity displayed by this complex is likely a direct result of the cooperative interaction of the two metal centres and suggests further studies be carried on complexes of this sort.

The preparation of binuclear Ir-DPM hydrides as outlined in Chapter Six has obvious relevance to the hydrogenation of alkynes and olefins by $[Rh_2(CO)_2(\mu\text{-}H)(\mu\text{-}CO)(DPM)_2]^+$.[35] The next logical step, having isolated these hydrides, is to examine their reaction with unsaturated organic molecules such as alkynes. It is likely that a study of this sort will shed some light on the mechanism of the Rh catalysis.

References and Footnotes

1. Muetterties, E.L. (Editor) "Transition Metal Hydrides" Marcel Dekker, Inc., New York, 1971.
2. Bau, R. (Editor) "Transition Metal Hydrides" Amer. Chem. Soc. Adv. Chem. Ser., Vol. 167, 1978.
3. Collman, J.P.; Hegedus, L.S. "Principles and Applications of Organotransition Metal Chemistry" University Science Books, Mill Valley, California, 1980, Chapters 6, 7 and 8 and references therein.
4. Ewens, R.V.G.; Lister, M.W. Trans. Faraday Soc. 1939, **35**, 681.
5. Hieber, W. Die Chemie 1942, **55**, 24.
6. Cotton, F.A.; Wilkinson, G. Chem. Ind. (London) 1956, 1305.
7. Cotton, F.A. J. Am. Chem. Soc. 1958, **80**, 4425.
8. La Placa, S.J.; Ibers, J.A. J. Am. Chem. Soc. 1963, **85**, 3501.
9. Teller, R.G.; Bau, R. Structure and Bonding 1981, **44**, 1.
10. Mason, R.; Mingos, D.M.P. J. Organomet. Chem. 1973, **50**, 53.
11. Hieber, W.; Hübel, W. Z. Elektrochem. 1953, **57**, 235.

12. Schwartz, J.; Labinger, J.A. Angew. Chem. Int. Ed. Engl. 1976, 15, 333.

13. Schunn, R.W. in reference 1., p. 239, and references therein.

14. Woodward, R.B.; Hoffmann, R. Angew. Chem. Int. Ed. Engl. 1969, **8**, 781.

15. Osborn, J.A.; Jardine, F.H.; Young J.F.; Wilkinson, G. J. Chem. Soc. (A) 1966, 1711.

16. Tolman, C.A.; Meakin, P.Z.; Lindner, D.L.; Jesson, J.P. J. Am. Chem. Soc. 1972, **94**, 3240.

17. Halpern, J. Trans. Am. Crystallogr. Assoc. 1978, **14**, 59.

18. Halpern, J.; Okamoto, T.; Zakhariev, A. J. Mol. Cat. 1976, **2**, 65.

19. Halpern, J. Inorg. Chim. Acta 1981, **50**, 11.

20. Paulik, F.E. Catal. Rev. 1972, **6**, 49.

21. James, B.R. "Homogeneous Hydrogenation" Wiley, 1974, p. 250.

22. Cotton, F.A.; Wilkinson, G. "Advanced Inorganic Chemistry", 4th Edn., Wiley-Interscience, New York, 1980, p. 1271.

23. Orchin, M. Adv. Catalysis 1966, **16**, 1.

24. Pruett, R.L. Adv. Organomet. Chem. 1979, **17**, 1.

25. Laine, R.M. J. Am. Chem. Soc. 1978, **100**, 6451, 6527.

26. Muetterties, E.L.; Krause, M.J. Angew. Chem. Int. Ed. Engl. 1983, 22, 135 and references therein.

27. Johnson, B.F.G. (Editor) "Transition Metal Clusters" Wiley, New York, 1980.

28. Chisholm, M.H. (Editor) "Reactivity of Metal-Metal Bonds" American Chemical Society, Washington, D.C., 1981.

29. Chisholm, M.H.; Cotton, F.A. Acc. Chem. Res. 1978, 11, 356.

30. Fox, J.R.; Gladfelter, W.L.; Geoffroy, G.L. Inorg. Chem. 1980, 19, 2574.

31. Breen, M.J.; Geoffroy, G.L. Organometallics 1982, 1, 1437.

32. Olmstead, M.M.; Guimerans, R.R.; Farr, J.P.; Balch, A.L. Inorg. Chim. Acta 1983, 75, 199.

33. Puddephatt, R.J. Chem. Soc. Rev. 1982, 12, 99.

34. Sanger, A.R. Prepr. - Can. Symp. Catal. 6th 1979, 37.

35. Kubiak, C.P.; Woodcock, C.; Eisenberg, R. Inorg. Chem. 1982, 21, 2119.

36. Band, E.; Bruker, C.F.; Muetterties, E.L.; Pretzer, W.R.; Rhodin, T.N. Chem. Rev. 1979, 79, 91.

37. Hieber, W.; Kummer, R. Chem. Ber. 1967, 100, 148.

38. Mague, J.T.; Mitchener, J.P. Inorg. Chem. 1969, 8, 119.

39. Cowie, M.; Mague, J.T.; Sanger, A.R. J. Am. Chem. Soc. 1978, **100**, 3628.

40. Mague, J.T.; Sanger, A.R. Inorg. Chem. 1979, **18**, 2060.

41. Mague, J.T.; DeVries, S.H. Inorg. Chem. 1980, **19**, 3743.

42. Mague, J.T.; DeVries, S.H. Inorg. Chem. 1982, **21**, 1632.

43. Mague, J.T. Inorg. Chem. 1983, **22**, 45.

44. Mague, J.T. Inorg. Chem. **1983**, **22**, 1158.

45. Sanger, A.R. J. Chem. Soc., Chem. Commun. 1975, 893.

46. Sanger, A.R. J. Chem. Soc., Dalton Trans. 1977, 120.

47. Sanger, A.R. J. Chem. Soc., Dalton Trans. 1977, 1971.

48. Cowie, M.; Dwight, S.K.; Sanger, A.R. Inorg. Chim. Acta 1978, **31**, L407.

49. Sanger, A.R. J. Chem. Soc., Dalton Trans. 1981, 228.

50. Sanger, A.R. Can. J. Chem. 1982, **60**, 1363.

51. Balch, A.L. J. Am. Chem. Soc. 1976, **98**, 8049.

52. Balch, A.L.; Tulyathan, B. Inorg. Chem. 1977, **16**, 2840.

53. Balch, A.L.; Labadie, J.W.; Delker, G. Inorg. Chem. 1979, **18**, 1224.

54. Olmstead, M.M.; Lindsay, C.H.; Benner, L.S.; Balch, A.L. J. Organomet. Chem. 1979, **179**, 289.

55. Balch, A.L.; Benner, L.S. Inorg. Synth. 1982, **21**, 47.

56. Kubiak, C.P.; Eisenberg, R. J. Am. Chem. Soc. 1977, **99**, 6129.

57. Kubiak, C.P.; Eisenberg, R. J. Am. Chem. Soc. 1980, **2**, 3637.

58. Kubiak, C.P.; Eisenberg, R. Inorg. Chem. 1980, **19**, 2726.

59. Woodcock, C.; Eisenberg, R. Organometallics 1982, **1**, 886.

60. Cowie, M. Inorg. Chem. 1979, **18**, 286.

61. Cowie, M.; Dwight, S.K. Inorg. Chem. 1979, **18**, 2700.

62. Cowie, M.; Dwight, S.K. Inorg. Chem. 1980, **19**, 209.

63. Cowie, M.; Dwight, S.K. Inorg. Chem. 1980, **19**, 2500.

64. Cowie, M.; Dwight, S.K. Inorg. Chem. 1980, **19**, 2508.

65. Cowie, M.; Dwight, S.K. J. Organomet. Chem. 1980, **198**, C20.

66. (a) Cowie M.; Southern, T.G. J. Organomet. Chem. 1980, **193**, C46.
(b) Cowie, M.; Southern, T.G. Inorg. Chem. 1982, **21**, 246.

67. Cowie, M.; Dwight, S.K. J. Organomet. Chem. 1981, **214**, 233.

68. Cowie, M.; Dickson, R.S. Inorg. Chem. 1981, **20**, 2682.

69. McKeer, I.R.; Cowie, M. Inorg. Chim. Acta 1982, **65**, L107.

70. Yaneff, P.V.; Powell, J. J. Organomet. Chem. 1979, **179**, 101.

71. Van der Ploeg, A.F.M.J.; Van Koten, G. Inorg. Chim. Acta 1981, **51**, 225.

72. Fryzuk, M.D. Inorg. Chim. Acta 1981, **54**, L265.

73. Fordyce, W.A.: Crosby, G.A. J. Am. Chem. Soc. 1982, **104**, 985.

74. (a) Colton, R.; McCormick, M.J.; Pannan, C.D. J. Chem. Soc., Chem. Commun. 1977, 823.
(b) Colton, R.; McCormick, M.J.; Pannan, C.D. Aust. J. Chem. 1978, **31**,1425.

75. Holloway, R.G.; Penfold, B.R.; Colton, R.; McCormick, M.J. J. Chem. Soc., Chem. Commun. 1976, 485.

76. Olmstead, M.M.; Hope, H.; Benner, L.S.; Balch, A.L. J. Am. Chem. Soc. 1977, **99**, 5502.

77. Benner, L.S.; Balch, A.L.; J. Am. Chem. Soc. 1978, **100**, 6099.

78. Benner, L.S.; Olmstead, M.M.; Hope, H.; Balch, A.L. J. Organomet. Chem. 1978, **153**, C31.

79. Balch, A.L.; Benner, L.S.; Olmstead, M.M. Inorg. Chem. 1979, **18**, 2996.

80. Brant, P.; Benner, L.S.; Balch, A.L. Inorg. Chem. 1979, **18**, 3422.

81. Olmstead, M.M.; Benner, L.S.; Hope, H.; Balch, A.L. Inorg. Chim. Acta 1979, **32**, 193.

82. Lindsay, C.H.; Benner, L.S.; Balch, A.L. Inorg. Chem. 1980, 19, 3503.

83. Lindsay, C.H.; Balch, A.L. Inorg. Chem. 1981, 20, 2267.

84. Balch, A.L.; Hunt, C.T.; Lee, C.-L.; Olmstead, M.M.; Farr, J.P. J. Am. Chem. Soc. 1981, 103, 3764.

85. Lee, C.-L.; Hunt, C.T.; Balch, A.L. Inorg. Chem. 1981, 20, 2498.

86. Olmstead, M.M.; Farr, J.P.; Balch, A.L. Inorg. Chim. Acta 1981, 52, 47.

87. Hunt, C.T.; Balch, A.L. Inorg. Chem. 1982, 21, 1242.

88. Hunt, C.T.; Balch, A.L. Inorg. Chem. 1982, 21, 1641.

89. Lee, C.-L.; Hunt, C.T.; Balch, A.L. Organometallics 1982, 1, 824.

90. Rattray, A.D.; Sutton, D. Inorg. Chim. Acta 1978, 27, L85.

91. Taylor, S.T.; Maitlis, P.M. J. Am. Chem. Soc. 1978, 100, 4700.

92. Hughes, J.G.; Robson, R. Inorg. Chim. Acta 1979, 35, 87.

93. Grossel, M.C.; Brown, M.P.; Nelson, C.D.; Yavari, A.; Kallas, E.; Moulding, R.P.; Seddon, K.R. J. Organomet. Chem. 1982, 232, C13.

94. Appleton, T.G.; Bennett, M.A.; Tomkins, I.B. J. Chem. Soc., Dalton Trans. 1976, 439.

95. Brown, M.P.; Puddephatt, R.J.; Rashidi, M. Inorg. Chim. Acta 1976, **19**, L33.

96. Brown, M.P.; Puddephatt, R.J.; Rashidi, M.; Seddon, K.R. Inorg. Chim. Acta 1977, **23**, L27.

97. Brown, M.P.; Puddephatt, R.J.; Rashidi, M.; Manojlovic-Muir, Lj.; Muir, K.W.; Solomun, T.; Seddon, K.R. Inorg. Chim. Acta 1977, **23**, L33.

98. Brown, M.P.; Puddephatt, R.J.; Rashidi, M.; Seddon, K.R. J. Chem. Soc., Dalton Trans. 1977, 951.

99. Brown, M.P.; Puddephatt, R.J.; Rashidi, M.; Seddon, K.R. J. Chem. Soc., Dalton Trans. 1978, 516.

100. Brown, M.P.; Fisher, J.R.; Franklin, S.J.; Puddephatt, R.J.; Seddon, K.R. J. Organomet. Chem. 1978, **161**, C46.

101. Brown, M.P.; Puddephatt, R.J.; Rashidi, M.; Seddon, K.R. J. Chem. Soc., Dalton Trans. 1978, 1540.

102. Brown, M.P.; Fisher, J.R.; Franklin, S.J.; Puddephatt, R.J.; Seddon, K.R J. Chem. Soc., Chem. Commun. 1978, 749.

103. Brown, M.P.; Fisher, J.R.; Puddephatt, R.J.; Seddon, K.R. Inorg. Chem. 1979, **18**, 2808.

104. Brown, M.P.; Franklin, S.J.; Puddephatt, R.J.; Thomson, M.A.; Seddon, K.R. J. Organomet. Chem. 1979, **178**, 281.

105. Brown, M.P.; Fisher, J.R.; Manojlovic-Muir, Lj.; Muir, K.W.; Puddephatt, R.J.; Thomason, M.A.; Seddon, K.R. J. Chem. Soc., Chem. Commun. 1979, 931.

106. Brown, M.P.; Cooper, S.J.; Puddephatt, R.J.; Thomson, M.A.; Seddon, K.R. J. Chem. Soc., Chem. Commun. 1979, 1117.

107. Brown, M.P.; Fisher, J.R.; Mills, A.J.; Puddephatt, R.J.; Thomson, M.A. Inorg. Chim. Acta 1980, **44**, 271.

108. Brown, M.P.; Cooper, S.J.; Frew, A.A.; Manojlovic-Muir, Lj.; Muir, K.W.; Puddephatt, R.J.; Thomson, M.A. J. Organomet. Chem. 1980, **198**, C33.

109. Cooper, S.J.; Brown, M.P.; Puddephatt, R.J. Inorg. Chem. 1981, **20**, 1374.

110. Brown, M.P.; Cooper, S.J.; Frew, A.A.; Manojlovic-Muir, Lj.; Muir, K.W.; Puddephatt, R.J.; Seddon, K.R.; Thomson, M.A. Inorg. Chem. 1981, **20**, 1500.

111. Bancroft, G.M.; Chan, T.; Puddephatt, R.J.; Brown, M.P. Inorg. Chim. Acta 1981, **53**, L119.

112. Puddephatt, R.J.; Thomson, M.A.; Manojlovic-Muir, Lj.; Muir, K.W.; Frew, A.A.; Brown, M.P. J. Chem. Soc., Chem. Commun. 1981, 805.

113. Brown, M.P.; Fisher, J.R.; Hill, R.H.; Puddephatt, R.J.; Seddon, K.R. Inorg. Chem. 1981, **20**, 3516.

114. Brown, M.P.; Fisher, J.R.; Franklin, S.J.; Puddephatt, R.J.; Thomson, M.A. Adv. Chem. Ser. 1982, **196**, 231.

115. Brown, M.P.; Cooper, S.J.; Frew, A.A.; Manojlovic-Muir, Lj.; Muir, K.W.; Puddephatt, R.J.; Thomson, M.A. J. Chem. Soc., Dalton Trans. 1982, 299.

116. Azam, K.A.; Brown, M.P.; Cooper, S.J.; Puddephatt, R.J. Organometallics 1982, **1**, 1183.

117. Fisher, J.R.; Mills, A.J.; Sumner, S.; Brown, M.P.; Thomson, M.A.; Puddephatt, R.J.; Frew, A.A.; Manojlovic-Muir, Lj.; Muir, K.W. Organometallics 1982, **1**, 1421.

118. Azam, K.A.; Puddephatt, R.J.; Brown, M.P.; Yavari, A. J. Organomet. Chem. 1982, **234**, C31.

119. Puddephatt, R.J.; Azam, K.A.; Hill, R.H.; Brown, M.P.; Nelson, C.D.; Moulding, R.P.; Seddon, K.R.; Grossel, M.C. J. Am. Chem. Soc. 1983, **105**, 5642.

120. Hill, R.H.; Puddephatt, R.J. Inorg. Chim. Acta 1981, **54**, L277.

121. Puddephatt, R.J.; Thomson, M.A. Inorg. Chem. 1982, **21**, 725.

122. Azam, K.A.; Frew, A.A.; Manojlovic-Muir, Lj.; Muir, K.W.; Puddephatt, R.J. J. Chem. Soc., Chem. Commun. 1982, 614.

123. Hill, R.H.; DeMayo, P.; Puddephatt, R.J. Inorg. Chem. 1982, **21**, 3642.

124. Puddephatt, R.J.; Thomson, M.A. J. Organomet. Chem. 1982, **238**, 231.

125. Azam, K.A.; Puddephatt, R.J. Organometallics 1983, **2**, 1396.

126. Hill, R.H.; Puddephatt, R.J. Organometallics 1983, **2**, 1472.

127. Hill, R.H.; Puddephatt, R.J. J. Am. Chem. Soc. 1983, **105**, 5797.

128. Grossel, M.C.; Moulding, R.P.; Seddon, K.R. Inorg. Chim. Acta 1982, **64**, L275.

129. Grossel, M.C.; Moulding, R.P.; Seddon, K.R. J. Organomet. Chem. 1983, **247**, C32.

130. Manojlovic-Muir, Lj.; Muir, K.W.; Solomun, T. Acta Crystallogr., Sect. B 1979, **B35**, 1237.

131. Manojlovic-Muir, Lj.; Muir, K.W.; Solomun, T. J. Organomet. Chem. 1979, **179**, 479.

132. Frew, A.A.; Manojlovic-Muir, Lj.; Muir, K.W. J. Chem. Soc., Chem. Commun. 1980, 624.

133. Manojlovic-Muir, Lj.; Muir, K.W. J. Chem. Soc., Chem. Commun. 1982, 1155.

134. Chin, C.-S.; Sennett, M.S.; Wier, P.J.; Vaska, L. Inorg. Chim. Acta 1978, **31**, L443.

135. Anderson, G.K.; Clark, H.C.; Davies, J.A. J. Organomet. Chem. 1981, 210, 135.

136. Cameron, T.S.; Gardner, P.A.; Grundy, K.R. J. Organomet. Chem. 1981, 212, C19.

137. Morris, R.H.; Foley, H.C.; Targos, T.S.; Geoffroy, G.L. J. Am. Chem. Soc. 1981, 103, 7337.

138. Geoffroy, G.L. ACS Symp. Ser. 1982, 198, 347.

139. Pringle, P.G.; Shaw, B.L. J. Chem. Soc., Chem. Commun. 1982, 581.

140. McDonald, W.S.; Pringle, P.G.; Shaw, B.L. J. Chem. Soc., Chem. Commun. 1982, 861.

141. McEwan, D.M.; Pringle, P.G.; Shaw, B.L. J. Chem. Soc., Chem. Commun. 1982, 1240.

142. Blagg, A.; Hutton, A.T.; Pringle, P.G.; Shaw, B.L. Inorg. Chim. Acta 1983, 76, L265.

143. Pringle, P.G.; Shaw, B.L. J. Chem. Soc., Chem. Commun. 1982, 81.

144. Pringle, P.G.; Shaw, B.L. J. Chem. Soc., Dalton Trans. 1983, 889.

145. McEwan, D.M.; Pringle, P.G.; Shaw, B.L. J. Chem. Soc., Chem. Commun. 1982, 859.

146. Pringle, P.G.; Shaw, B.L. J. Chem. Soc., Chem. Commun. 1982, 956.

147. Pringle, P.G.; Shaw, B.L. J. Chem. Soc., Chem. Commun. 1982, 1313.

148. Langrick, C.R.; Pringle, P.G.; Shaw, B.L. Inorg. Chim. Acta 1983, 76, L263.

149. Cooper, G.R.; Hutton, A.T.; McEwan, D.M.; Pringle, P.G.; Shaw, B.L. Inorg. Chim. Acta 1983, 76, L267.

150. Mague, J.T.; Sanger, A.R. Inorg. Chem. 1979, 18, 2060.

151. Eisenberg, R.; Kubiak, C.P.; Woodcock, C. Inorg. Chem 1980, 19, 2733.

152. Herde, J.L.; Lambert, J.C.; Senott, C.V. Inorg. Synth. 1974, 15, 28.

153. Doedens, R.J.; Ibers, J.A. Inorg. Chem. 1967, 6, 204.

154. Besides local programs, the following were used in solution and refinement of the structure: BUCILS, structure factor and refinement program; FASTFO, a modified version of FORDAP, fourier summation program by R.J. Dellaca; ORFFE for calculating bond lengths, angles and associated deviations by W. Busing and H.A. Levy; ORTEP, plotting program by C.K. Johnson; EAC, empirical absorption program by A.C.T. North, D.C. Phillips and F.S. Mathews from the Enraf-Nonius Structure Determination Package by B.A. Frenz.

155. Cromer, D.T.; Waber, J.T. "International Tables for Crystallography"; Kynoch Press: Birmingham, England, 1974, Vol. IV, Table 2.2A.

156. Stewart, R.F.; Davidson, E.R.; Simpson, W.T. *J. Chem. Phys*. 1965, **42**, 3175.

157. Cromer, D.T.; Liberman, D.J. *J. Chem. Phys*. 1970, 53, 1891.

158. $R = \Sigma||Fo|-|Fc||/\Sigma|Fo|$; $Rw = [\Sigma w(|Fo|-|Fc|)^2/\Sigma wFo^2]^{1/2}$

159. A listing of the observed and calculated structure amplitudes and other supplementary material is available from Dr. M. Cowie, Department of Chemistry, University of Alberta, Edmonton, Alberta, Canada T6G 2G2.

160. Peterson, S.W.; Reis, A.H. *Ann. N.Y. Acad. Sci*. 1978, **313**, 560 and references therein.

161. Balch, A.L., private communication.

162. Cowie, M.; Dwight, S.K. *Inorg. Chem*. 1981, 20, 1534.

163. Mague, J.T. *Inorg. Chem*. 1969, 8, 1975.

164. Sanger, A.R. *J. Chem. Soc., Dalton Trans*. 1977, 1971.

165. Sutherland, B.R.; Cowie, M. *Inorg. Chem*. 1984, **23**, 1290.

166. Cowie, M.; Sutherland, B.R., unpublished results.

167. The observed density and the measured cell parameters in fact yield z = 2.21. This discrepancy probably results from the poorly determined cell parameters derived from film measurements; it may also be true that there is solvent of crystallization.

168. Hodgson, K.O.; Raymong, K.N. Inorg. Chem. 1972, 11, 171 and references therein.

169. Bird, P.H.; Fraser, A.R.; Hall, D.N. Inorg. Chem. 1981, **20**, 2682.

170. Typically a 1:1 electrolyte, such as $[Rh_2(CO)_2(\mu\text{-}Cl)\text{-}(\mu\text{-}CO)(DPM)_2][BF_4]$, gives a value of ca. 45 Ω^{-1} cm^2 $mole^{-1}$.

171. The cell reduction was performed by using a modification of TRACER II by S.L. Lawson. See: Lawson, S.L.; Jacobsen, R.A. "The Reduced Cell and Its Crystallographic Applications", Ames Laboratory Report IS-1141; USAEC: Iowa State University, Ames, Iowa, April 1965.

172. Besides local programs, the following were used in solution and refinement of the structure: FORDAP, the Fourier summation program by A. Zelkin; SFLS-5, structure factors and least-squares refinement by C.J. Prewitt; ORFFE, for calculating bond length, angles and associated standard deviations by W. Busing and H.A. Levy; ORTEP, plotting program by C.K. Johnson; AGNOST, the Northwestern University absorption program which includes Coppens-Leiseriwitz-Rabinowitz logic for Gaussian integration.

173. See the other chapters in this thesis.

174. Gibson, J.A.E.; Cowie, M. Organometallics 1984, **3**, 722.

175. Farr, J.P.; Olmstead, M.M.; Balch, A.L. Inorg. Chem 1983, **22**, 1229 and references therein.

176. Cowie, M.; Dickson, R.S.; Hames, B.W. Organometallics, 1984, in press.

177. Boag, N.M.; Green, M.; Howard, J.A.K.; Spencer, J.L.; Stansfield, R.F.D.; Thomas, M.D.O.; Stone, F.G.A.; Woodward, P. J. Chem. Soc., Dalton Trans. 1980, 2182.

178. Restivo, R.J.; Ferguson, G.F.; Ng, T.W.; Carty, A.J. Inorg. Chem. 1977, **16**, 172.

179. Dickson, R.S.; Pain, G.N. J. Chem. Soc. Chem. Commun. 1979, 297.

180. Jarvis, A.C.; Kemmitt, R.D.W.; Russell, D.R.; Tucker, P.A. J. Organomet. Chem. 1978, **159**, 341.

181. Kosower, E.M.; "An Introduction to Physical Organic Chemistry", Wiley, New York, 1968, p 49.

182. Mague, J.T., private communication.

183. Similar spectra have previously been analyzed, and have been shown to be consistent with the spin system proposed. See: Gibson, J.A.E. and Cowie M., Organometallics 1984, **3**, 722.

184. Hoffman, D.M.; Hoffmann, R. Inorg. Chem. 1981, **20**, 3543.

185. Hoffman, D.M.; Hoffmann, R.; Fisel, C.R. *J. Am. Chem. Soc*. 1982, **104**, 3858.

186. Brown, M.P.; Keith, A.N.; Manojlovic-Muir, Lj.; Muir, K.W.; Puddephatt, R.J.; Seddon, K.R. *Inorg. Chim. Acta* 1979, **34**, L223.

187. Cowie, M.; Dickson, R.S., unpublished results.

188. Fryzuk, M.D.; Jones, T.; Einstein, F.W.B. *Organometallics* 1984, **2**, 185.

189. Lewis, J. *Gazz. Chem. Italiana*, 1979, **109**, 27.

190. Diversi, P.; Ingrosso, G.; Lucharini, A.; Porzio, W.; Zucchi, M. *Inorg. Chem*., 1980, **19**, 3590.

191. Crabtree, R.H.; Quirk, J.M.; Felkin, H.; Fillebeen-Khan, T.; Pascard, C. *J. Organomet. Chem*., 1980, **187**, C32.

192. Kaesz, H.D.; Saillant, R.B. *Chem. Rev*. 1972, **72**, 231.

193. "Catalyst Handbook", Springer-Verlag, West Berlin, 1970, Chapters 5 and 6.

194. Storch, H.H., Golumbic, N.; Anderson, R.B. "The Fischer-Tropsch and Related Syntheses", Wiley, New York, 1951.

195. Laine, R.M.; Rinker, R.G.; Ford, P.C. *J. Am. Chem. Soc*. 1977, **99**, 252.

196. Kang, H.C.; Maudlin, C.; Cole, T.; Slegeir, W.; Cann, K.; Pettit, R. *J. Am. Chem. Soc*., 1977, **99**, 8323.

197. Cheng, C.-H., Hendriksen, D.E.; Eisenberg, R. *J. Am. Chem. Soc.*, 1977, **99**, 2791.

198. King, R.B.; Fraier, C.C.; Hanes, R.M.; King, A.D., *J. Am. Chem. Soc.*, 1977, **100**, 2925.

199. Ungermann, C.; Landis, V.; Maya, S.A.; Cohen, H.; Walker, H.; Pearson, R.G.; Rinker, R.G.; Ford, P.C. *J. Am. Chem. Soc.*, 1979, **101**, 5922

200. Ryan, R.C.; Wileman, G.M.; Dalsanto, M.P.; Pittman, C.U. *J. Mol. Catal.*, 1979, **5**, 319.

201. King, A.D.; King, R.B.; Yang, D.B. *J. Am. Chem. Soc.*, 1980, **102**, 1028.

202. Baker, E.C.; Hendriksen, D.E.; Eisenberg, R. *J. Am. Chem. Soc.*, 1980, **102**, 1020.

203. Cheng, C.-H.; Eisenberg, R. *J. Am. Chem. Soc.*., 1978, **100**, 5968.

204. Yoshida, T.; Ueda, Y.; Otsuka, S. *J. Am. Chem. Soc.*, 1978, **100**, 3941.

205. Yoshida, T.; Okana, T.; Ueda, Y.; Otsuka, S. *J. Am. Chem. Soc.*, 1981, **103**, 3411.

206. Kassel, L.S. *J. Am. Chem. Soc.*, 1934, **56**, 1838.

207. K for eqn (1) = 1.45 x 10^3 at 127°C and 26.9 at 327°C, from ref. 16.

208. Grundy, K.R., private communication.

209. Geary, W.J. *Coord. Chem. Rev.*, 1971, **7**, 81.

210. Vinogradov, S.N.; Linnell, R.H. "Hydrogen Bonding"; Van Nostrand. Reinhold, New York, 1971.

211. Brown, M.R.; Keith, A.N.; Manojlovic-Muir, Lj.; Muir, K.W.; Puddphatt, R.J.; Seddon, K.R. *Inorg. Chim. Acta*, 1979, **34**, L223.

212. Cotton, F.A.; Hunter, D.L. *Inorg. Chim. Acta*, 1974, **11**, L9.

213. Appleton, T.G.; Bennett, M.A. *J. Organometal. Chem.*, 1973, **55**, C88.

214. Cowie, M.; Sutherland, B.R., manuscript in preparation. At the present time the structure has refined to R = 0.031, R_ω = 0.043 and the bridging hydride ligand has been located.

215. Sweet, J.R.; Graham, W.A.G. *Organometallics*, 1982, **1**, 982.

216. Catellani, M.; Halpern, J. *Inorg. Chem.*, 1980, **19**, 982.

217. Grice, N.; Kao, S.C.; Pettit, R. *J. Am. Chem. Soc.*, 1979, **101**, 1627.

218. Deeming, A.J.; Shaw, B.L. *J. Chem. Soc. A*, 1969, 443.

219. [1,8-bis(dimethylamino)naphthalene] = Proton Sponge.

220. Typical coupling on Ir-phosphine hydrides beteen cis hydrides fall in the range 2-5 Hz but in all cases the hydrides are on the same metal. See Guilmet, E.; Masisonnat, A.; Poilblanc, R *Organometallics*, 1983, **2**, 1123.

221. Woodcock, C.; Eisenberg, R. "Abstracts of Papers", 186th National Meeting of the American Chemical Society, Washingtin, D.C., Aug. 1983, INOR 253.

APPENDIX I

Solvents and Drying Agents

$(CH_3)_2CO$	$CaSO_4$
CH_3CN	CaH_2
CH_2Cl_2	P_2O_5
THF	Na/benzophenone
CH_3OH	Mg turnings
Et_2O	molecular sieves
C_6H_6	Na/K
C_7H_8	Na/K